CALIFORNIA INSTITUTE OF TECHNOLOGY

EARTHQUAKE ENGINEERING RESEARCH LABORATORY

STRUCTURAL CONTROL USING REGENERATIVE FORCE ACTUATION NETWORKS

THESIS BY

JEFFREY T. SCRUGGS

REPORT NO. EERL 2004-09

PASADENA, CALIFORNIA
JUNE 2004

(DEFENDED MAY 24, 2004)

STRUCTURAL CONTROL USING REGENERATIVE FORCE ACTUATION NETWORKS

Thesis by

Jeffrey T. Scruggs

In Partial Fulfillment of the Requirements for the

degree of

Doctor of Philosophy

CALIFORNIA INSTITUTE OF TECHNOLOGY

Pasadena, California

2004

(Defended May 24, 2004)

Acknowledgments

I have been very fortunate to have Prof. Iwan as my advisor. Throughout the course of this work, he has given me an extraordinary amount of freedom to pursue my own ideas (and make my own mistakes), and would often wait patiently while I tinkered with esoteric proofs and fine details. He has been extremely enthusiastic and supportive concerning this research, and I have learned a great deal through our frequent interactions. I hope that we can continue our collaboration for many years to come.

I have had the pleasure of interacting with many other faculty members at Caltech. I would especially like to thank Prof. Beck for the countless discussions regarding this research. His comments, ideas, and suggestions have made a strong imprint on this work, and on my plans for future investigations. I would also like to thank Profs. Middlebrook, Murray, Hall, Caughey, and Bhattacharya for their time and thoughts. Additional thanks go to Profs. Murray, Beck, and Hall for serving on my committee. Their comments and suggestions have significantly improved the quality of this thesis, both in terms of its content and presentation.

I would like to thank Prof. Kobori, Dr. Miyamura, Dr. Ikeda, and all others at Kajima Corporation for their time and hospitality during my visit with them earlier this year, and for their interest in this research. I would also like to thank Prof. Iemura at Kyoto University for inviting me to visit and discuss my work with him and his department.

I have made many friends at Caltech, and they have had a significant positive impact on the quality of my life over these past five years. Special thanks go to Prashant Purohit, Arash Yavari, Judy Mitrani, Swaminathan Krishnan, Michel Tanguay, Andy Guyader, and John Chevillet. I would also like to express my gratitude to Bill and Mary Elise Klug for their hospitality and generosity over the years.

I want to give my deepest thanks to my parents and sisters, who have been unrelenting in their support for all my academic pursuits, even though I have been rather unreliable when it comes to returning their calls and keeping in touch.

This research was made possible, in part, through a graduate fellowship provided by Betty and Gordon Moore. I am extremely grateful and honored to have received this funding.

Abstract

A Regenerative Force Actuation (RFA) Network consists of multiple electromechanical forcing devices distributed throughout a structural system and actuated in such a way as to reduce the response of the structure when subject to an excitation. The associated electronics of the devices are connected together such that they are capable of sharing electrical power with each other. This makes it possible for some devices to extract mechanical energy from the structure, while others re-inject a portion of that energy back into the structure at other locations. The forcing capability of an RFA network is constrained only by the requirement that in the aggregate the total network must always dissipate energy.

The electromechanical currents generated by RFA networks must be controlled to create the desired structural forces. This control is facilitated by the alternation of a multitude of power-electronic transistor switches in the electrical network. In this study, a sliding-mode switching controller is proposed for realizing zero-error force command tracking. It is shown that parameter uncertainty is a critical issue for force commands which require the network to operate near its optimum transmissive efficiency.

RFA networks can be used to create velocity-proportional damping forces in structures. However, unlike traditional structural damping, RFA networks have the ability to create non-local and asymmetric damping forces. It is shown that this more generalized damping capability can lead to significant improvements in the forced response of a structure, as compared with traditional linear damping.

RFA networks may also be used for feedback control. In this context, the forcing capability of the RFA network is constrained by its physical limitations. In this study, a systematic method of nonlinear control design called "Damping-Reference" control is proposed, which guarantees a certain level of quadratic performance for the structural response. Variants of the control law synthesis are proposed for quadratic regulation, stochastic control, and $\mathcal{H}_\infty$ control contexts.

These ideas are illustrated in the context of earthquake engineering through a simulation example, involving a three-story structure with a two-actuator RFA network installed. In this example, it is shown that the "power sharing" nature of the RFA network has a significant influence on the response.

Table of Contents

Frequently-Used Symbols

$\mathbf{A}$	:	State derivative matrix for Nominal System Model
$\mathbf{B}_a$	:	Acceleration input matrix for Nominal System Model
$\mathbf{B}_u$	:	Force input matrix for Nominal System Model
$\mathbf{C}_c$	:	Size parameter matrix for $S(\mathbf{v})$.
C_S	:	Capacitance of DC bus
D_k	:	Switch position for actuator k
D_R	:	Switch position for dissipative interface
$\mathbf{D}$	:	Switch position matrix $[D_1 \ldots D_m \;\; D_R]^T$
J	:	Structural control system performance measure
K_{fk}	:	Actuator proportionality constant: $f_{ek} = K_{fk} i_k$
$\mathbf{K}_f$	:	$diag\{K_{f1} \ldots K_{fm}\}$
K_v	:	Design parameter for DC bus voltage control
$\mathbf{N}$	:	Structural force input matrix
P_k	:	Power flow for actuator k
$\mathbf{Q}$	:	State weighting matrix for quadratic performance
$\mathbf{R}$	:	Force weighting matrix for quadratic performance
R_k	:	Resistance of stator coil for machine k
R_R	:	Resistance of dissipative interface
$\mathbf{S}$	:	State-force weighting matrix for quadratic performance
$S(\mathbf{v})$	:	Region of Feasible Forces, for a given velocity $\mathbf{v}$
$\mathcal{U}(\mathbf{w})$	:	Feasible forcing region for Nominal System Model, for a given state $\mathbf{w}$
V_S	:	DC bus voltage
V_{swk}	:	Switch conduction voltage for actuator k
V_{swR}	:	Switch conduction voltage for dissipative interface
$\mathbf{Z}$	:	Effective damping matrix for RFA network
a_g	:	Ground acceleration
$\mathbf{f}, f_k$	:	Force vector with $\{\mathbf{f}\}_k = f_k$ = Total force of actuator k
$\mathbf{f}_e, f_{ek}$	:	Force vector with $\{\mathbf{f}_e\}_k = f_{ek}$ = Electromech. force for actuator k
$\mathbf{f}_e^*$	:	Electromechanical force command
$\mathbf{f}_{\max}, f_{k\max}$	:	Force vector with $\{\mathbf{f}_{\max}\}_k = f_{k\max}$ = Rated force of actuator k
i_k	:	Stator current for machine k
i_R	:	Current in resistor R_R

i_{Sk}	:	Current drawn from DC bus by actuator k
i_{SR}	:	Current drawn from DC bus by dissipative interface
l_k	:	Screw lead for actuator k
m	:	Number of actuators
n	:	Structural degrees of freedom
$\mathbf{u}$, u_k	:	Normalized force vector for Nominal System Model; i.e. $\mathbf{f}_e = \mathbf{C}_c^{1/2}\mathbf{u}$
$\mathbf{v}$, v_k	:	Actuation velocity vector with $\{\mathbf{v}\}_k = v_k$
$\mathbf{x}$	:	Electrical system state vector
$\mathbf{w}$	:	Normalized structural system state vector for Nominal System Model
$\mathbf{q}$	:	Structural displacements, relative to the ground
η_k	:	Screw efficiency for actuator k
τ	:	Electrical time constant for all actuators

Chapter 1. Introduction

Growing attention in recent decades has been devoted to methods of active feedback control of buildings and bridges, to reduce their responses to earthquakes and winds. Considerable effort has been directed toward the design of force actuators for these structures, the development of sensory technology, and the synthesis of feedback control laws customized for these types of applications. The resultant body of research devoted to these subjects is rich and vast (Fujino et al. 1996; Housner et al. 1997; Soong 1990; Spencer and Sain 1997; Spencer and Nagarajaiah 2003). Feedback control affords certain advantages in the context of earthquake engineering, which motivate the continually growing interest in this field. By using externally powered electrical or hydraulic devices to apply forces to structures, active forcing systems have been shown to greatly reduce the excitation of a building during seismic events, in comparison to simpler passive systems. Part of this improvement is due to the availability of external power, and part is due to the use of sensory systems to formulate control actions based on global structural deformation characteristics.

The first commercial building equipped with an active control system, designed by the Kajima Corporation in 1989, is the Kyobashi Center, located in Tokyo (Ikeda et al. 2001). Its control actuators consist of two hydraulic active mass drivers (AMDs) on the roof of the 11-story structure. Together, the weight of these masses is approximately 1% of the structural mass. One of these AMDs suppresses the lateral motion of the structure, while a secondary AMD suppresses torsional motion. The system was designed to reduce vibrations due to moderate winds. To date, this constitutes one of only four or five times that a fully active control system has been successfully installed in a commercial building (although several more implementations have been successfully applied toward the stabilization of pylons during the erection of bridges). There are many reasons for the failure of this technology to gain a foothold in the industry, not the least of which is the associated cost. However, aside from expense, active structural control systems have two significant and fundamental disadvantages which diminish their likelihood of gaining acceptance in practice.

The most fundamental disadvantage of active control is that it in general requires an external power supply. This presents questions about both reliability and practicality. In civil engineering applications, an active control system designed to protect a building during earthquakes would only be as reliable as its power source on which it depends. But history has

shown that during earthquakes, the power grid is highly susceptible to destabilization and blackouts. On the other hand, the power demands of active control systems for large buildings are typically too large to be met with local supplies. Thus, active control systems are, by their very nature, inherently unreliable.

The second disadvantage of active control is that, by designing an actuator which may accept power from an external source, the system cannot be characterized as a "bounded-energy" system. Questions therefore quickly arise concerning the stability-robustness of such systems. Although significant effort has been put toward alleviating this problem through the application of robust control theory, the nature of model uncertainty in civil engineering structures is such that significant concerns remain unresolved.

One compromise between active and passive actuation is found in hybrid systems. These consist of a combination of active and passive systems working in tandem. Hybrid systems are more reliable, because the passive part of the actuator will still work in the absence of power. Extensive research over several decades has yielded many different designs for these systems (Soong 1990) and to date over 40 commercial buildings in Japan alone, as well as many more in China, Taiwan, and Korea have been equipped with some form of hybrid actuation (Ikeda 2004; Spencer and Nagarajaiah 2003).

Another important emerging technology in structural control concerns low-power, high-performance force actuators called *semiactive* devices (Symans and Constantinou 1999). These devices are dissipative like passive devices, but possess fast-acting variable properties which may be "tuned" in real-time to optimize the dynamic response of the structure. Despite their limitations, such devices exhibit some of the appealing traits of active systems, in that they are capable of real-time force control, although in a limited range. Also, the parameters of a semiactive device situated in one location in the structure may be controlled based on the dynamic response of the entire structure. The only power necessary for operation of semiactive systems is that which is needed for the sensors and control intelligence, and to tune the device parameters. Typically these demands are orders of magnitude below the power flow capabilities of the devices.

1.1: Semiactive Forcing Systems

A simple, but theoretical, example of a semiactive device would be the variable dashpot shown in Fig. 1.1. The actuator accepts an input parameter γ, and for different values of γ, the relationship between the actuator velocity $\dot{x}$ and the actuator force f has a different shape. The input parameter γ is formulated through some control system to be such that the resultant force f

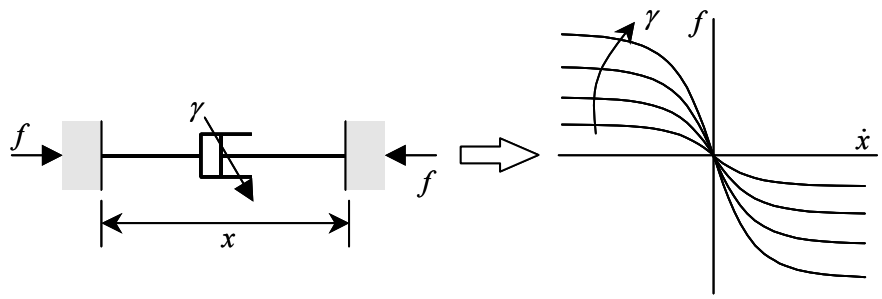

Figure 1.1: Idealized semiactive damper

will be of a desired magnitude. This parameter corresponds to some property of the device which may be modified to yield the differing curves in Fig. 1.1.

Perhaps the simplest example of a real semiactive device is the variable-orifice damper. In this case, the parameter γ represents the size of the orifice through which the viscous fluid in the damper is forced to flow, due to the motion of the piston. Theoretically, it requires no work to change the size of the orifice. Rather, the orifice size simply controls the amount of energy dissipated by the surrounding mechanical system. Therefore, if the device were ideal, there would be no power flow associated with parameter γ. In actuality, of course, there is a small amount of work associated with γ, because there will be losses in the electromechanical system which changes the orifice size, but these losses are extremely small, in comparison to the power flow of the actuator. This is a common trait of all semiactive actuators. Their control parameters do not have significant power flow associated with them. In fact, most semiactive devices, even ones which have force capabilities of over 10 tons, are capable of operating for extended periods of time using only a battery for a power supply.

Semiactive actuation has received a fair amount of attention during the last decade because of its potential for reliable, low-power structural control. There are two distinct advantages to semiactive control. The first of these is that, for a structure which is open-loop stable (i.e., stable without control), the implementation of a control system employing semiactive actuators physically cannot destabilize the structure. Thus, some questions concerning stability-robustness vanish. Secondly, semiactive actuators are unaffected by external power supply failures (as they operate on small, local, battery power) making them more reliable.

These two properties, combined, result in a highly appealing actuator for use in systems requiring extremely high reliability, such as in civil engineering applications concerning seismic response reduction. Also, these properties have made semiactive devices appealing in the area of

automotive suspensions, where they have exhibited favorable, reliable performance, while consuming negligible power.

1.1.1: Semiactive Control of Civil Structures: A Brief History

Semiactive devices were first researched in the area of vehicular suspensions over twenty-five years ago (Croila and Abdel-Hady 1991; Karnopp et al. 1974). In civil engineering, interest in these devices is a more recent phenomenon (Patten et al. 1994; Spencer 1996). There have been many different types of semiactive devices proposed for civil engineering structures. The following is a short list of some of these investigations. It is not intended to be a complete, exhaustive listing of the many contributions in this area. For more thorough surveys, see (Spencer and Nagarajaiah 2003) and (Housner et al. 1997).

- ***Variable Orifice Fluid Dampers***: In the civil engineering area, the ability of variable-orifice dampers to reduce the response of buildings subjected to seismic loads has been shown to be effective (Hrovat et al. 1983; Kurata et al. 1994; Liang et al. 1995; Mirzuno et al. 1992; Patten et al. 1994; Sack et al. 1994; Shinozuka et al. 1992; Symans and Constantinou 1996; Symans et al. 1994). These results have concerned simulation and small-scale experiments. In addition, some full-scale experiments have also been done for a building (Kamagata and Kobori 1994; Kobori et al. 1993) and for a bridge (Feng and Shinozuka 1990; Kawashima et al. 1992).

- ***Variable-Friction Dampers***: The idea behind variable-friction dampers is to control the friction force between two sliding objects by varying the pressure to the contact surface. Several different variants on this idea exist in the literature. A variable-friction device was proposed by (Akbay and Aktan 1990; Akbay and Aktan 1991) and by (Kannan et al. 1995) in which the actuator is connected rigidly to the structure, with the pressure at the friction interface being controlled actively by controlling the slippage of the device. A similar study was conducted by (Dowdell and Cherry 1994a; Dowdell and Cherry 1994b) and (Cherry 1994), who also showed, analytically, that the such devices may be employed to reduce the inter-story drifts in excited buildings. Another type of variable-friction device, a friction-controllable fluid bearing, was studied by (Feng et al. 1993) and (Yang et al. 1994). This area continues to see the proposal of new, novel devices (He et al. 2003; Nishitani et al. 2003).

- ***Controllable Tuned Liquid Dampers***: Normal tuned liquid dampers dissipate energy through the sloshing of a fluid in a tank, which is excited by the structure. The fluid, and tank, are designed such that the sloshing effect resonates near the resonant frequency of the structure. Several studies (Kareem 1994; Lou et al. 1994; Yalla and Kareem 2003; Yeh et al. 1996) have been conducted which equip these dampers which semiactive characteristics.

- ***Variable Stiffness Devices***: The idea of using a variable-orifice damper as an on/off variable-stiffness device was first proposed by (Kobori et al. 1993). Since that time these researchers, and others at the Kajima Corporation in Japan, have developed the concept into a commercially-viable technology, which has been implemented in numerous buildings over the last decade (Kobori 2003; Yamada and Kobori 2001). Various methods of structural control have been developed for these devices (Nasu et al. 2001). One particular approach (Hayen and Iwan 1994), in which the main structure is interfaced with one or more secondary structural systems.

  A device capable of continuously varying its stiffness has been proposed by (Nagarajaiah and Mate 1998). Such a device may be characterized as semiactive, because the amount of power needed to vary this stiffness can be made much lower than the overall power flow of the stiffness system. This device has been implemented in the capacity of a scale-model controllable TMD.

- ***Controllable Fluid Dampers***: Controllable fluid dampers possess fluids with properties which may be influenced by the presence of magnetic or electric fields. For these two cases, the dampers are called *magnetorheological* (MR) and *electrorheological* (ER) dampers. Rheological fluids (both kinds) were discovered in the 1940's (Rabinow 1948; Winslow 1947; Winslow 1949). When the respective fields are applied to these fluids, their behavior changes from that of a low-viscosity fluid to more of a semi-solid, visco-plastic behavior. Thus, the application of such a fluid in a damper gives the ability to actively control the effective viscosity of the damper through electrical and magnetic fields. Research on ER fluids has been quite extensive. ER fluid dampers have been shown to be quite effective in civil engineering applications, as evidenced in (Ehrgott and Masri 1992; Ehrgott and Masri 1994a; Ehrgott and Masri 1994b; Gavin et al. 1994a; Gavin et al. 1994b; Gordaninejad et al. 1994; Leitmann and Reithmeier 1993; Makris et al. 1995; Masri et al. 1995; McClamroch and Gavin 1995). Recent research in MR fluid dampers has demonstrated their use in the suppression of vibrations for civil structures, due to earthquake excitation (Dyke et al. 1996a;

Dyke et al. 1996b; Dyke et al. 1996c; Spencer et al. 1996; Spencer et al. 1997). In addition, a 20-ton MR damper, discussed in (Carlson and Spencer 1996) and (Spencer et al. 1997), demonstrates that these devices can be scaled for civil engineering applications.

Semiactive devices are beginning to be implemented in commercial applications in Japan by the Kajima Corporation. Notable among these implementations are four new buildings in the Siodome area of Tokyo, including the 38-story Siodome Tower, which have been designed with switching hydraulic dampers and feedback control systems. Also, the 54-story Mori Tower, in the Roppongi area of Tokyo, has over 350 variable-orifice dampers installed.

1.1.2: Electromechanical Dissipation

All of the semiactive devices thus far described dissipate energy through mechanical means. For instance, the variable-orifice and the controllable fluid dampers dissipate energy as liquid passes through an orifice. Likewise, the variable friction damper dissipates energy at the contact surface. However, energy may also be dissipated through electrical means. For instance, in the control of flexible structures with piezoelectric materials, research has shown that considerable reduction in vibration can be accomplished by the application of electrical RL shunt impedances across the terminals of the piezoelectric actuator (Hagood and von Flotow 1991). Such impedances store, and dissipate, electrical energy transduced by the piezoelectric material from the vibrating structure. Such ideas were expanded to a semiactive framework by allowing the resistor to be controllable in real time, with favorable results (Edberg and Bicos 1991; Hollkamp and Starchville 1994). This idea constitutes a kind of semiactive control.

For civil engineering applications, the same concept may be applied. However, because of the physical scale of civil structures, the piezoelectric materials used in lightweight, flexible aerospace structures cannot be employed. Instead an electric motor, by operating as a generator, could be used to convert mechanical to electrical energy. Then, this energy could be dissipated in an electrical network. This idea has been applied to semiactive vehicle suspension design by Karnopp (1989). Semiactive control through electrical dissipation has an advantage over mechanical methods in that such devices may also be operated as *active* devices if power is available. A semiactive device which uses an electric motor to facilitate energy dissipation may be driven as an active device by a simple switch in the circuitry to which the machine is connected. This would give such an actuator a versatility not attainable with most other semiactive devices.

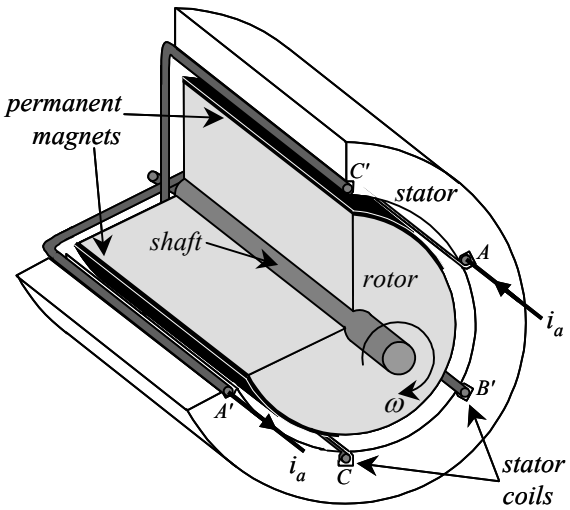

Figure 1.2: A permanent magnet brushless DC machine (cutaway)

A study by Nerves and Krishnan (1996) concluded that the optimal electromechanical actuator for use in civil structures is the permanent-magnet brushless DC (PMBDC) machine. Such a machine is shown in Fig. 1.2. Mounted to the rotor of the machine are permanent magnets which provide a rotating magnetic field as the rotor spins. The interaction of this magnetic field with the stator windings provides the avenue by which mechanical power on the machine shaft is converted to electrical power in the stator coils, and vice versa. Currently, these machines are available commercially at power ratings in excess of 20kW, placing them in the right "ballpark" for civil structure applications.

In Scruggs and Iwan (2003), these machines are used in the design of semiactive electromechanical devices for use in civil structures. A basic schematic for such a device is illustrated in Fig. 1.3. This conceptual diagram shows a rotational electric motor being used as a linear force actuator, by means of a linear-to-rotational converter consisting of a gear reduction and screw mechanism. Two electrical circuits may be connected to the motor, depending on the

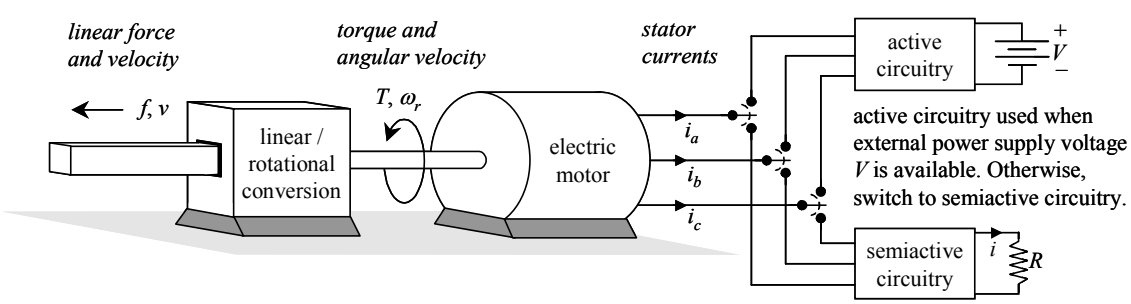

Figure 1.3: General approach for device with active/semiactive capability

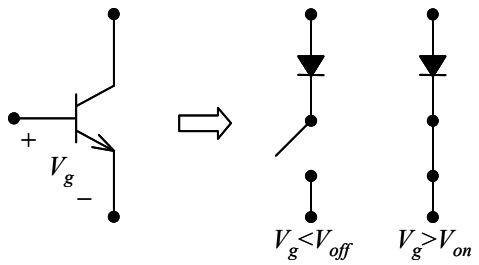

Figure 1.4: Operation of the transistor as an electrical switch

positions of three switches. The upper, “active” circuitry is connected to an external power source, and may be designed to actively drive the force actuator. When the switches are in the "down" position, the motor is connected to the "semiactive" circuitry, consisting of a network of passive components (i.e., resistors, inductors, etc.) and transistors.

In the semiactive mode of operation, the device uses the motor as a generator which converts mechanical energy to electrical energy, which in turn is dissipated in the network. By controlling the transistors in the network, this energy dissipation can be regulated, using concepts from basic power electronics (Kassakian et al. 1991). The transistors are used as “electronic switches,” as illustrated in Fig. 1.4. By proper selection of the voltage V_g, the transistor resembles a mechanical switch in parallel with a diode. As with actual mechanical switches, this mode of operation consumes very little power, even if the electric power flowing through the network is very high. As these transistor switches (together with the sensors and control intelligence) constitute the only demand for an external power source, the system is semiactive.

In Scruggs and Iwan (2003), it was shown that the performance of such an electromechanical semiactive device is competitive with that of a similar-sized magnetorheological fluid damper, and that the rotational inertia of the device actually works to the benefit of the overall system performance.

1.2: Regenerative Force Actuation

In the last decade a separate class of actuator, first formally defined by Jolly and Margolis (1997a), has been proposed for use in structural control. Called *Regenerative Force Actuation* (*RFA*), such devices are capable of two-way power flow, like active devices. However, regenerative actuators possess energetic constraints which limit their capability in a way which makes them distinct from the devices discussed thus far. Like semiactive systems, regenerative actuators have external power supply demands which are orders of magnitude below their power

flow capabilities. However, they have two characteristics which set them apart from semiactive devices:

1) *Power storage and reuse:* Semiactive devices must always remove energy from the mechanical system. By contrast, RFA systems have the capability of storing at least a fraction of the energy they remove from the mechanical system, and of re-injecting that energy back into the mechanical system at a later time.
2) *Power coupling in actuation networks:* When multiple regenerative actuators are distributed throughout a structure, they may be capable of "sharing" power with each other. For example, one device may remove energy from a mechanical system from one location, while another device simultaneously re-injects that energy back into the mechanical system at another location.

The advantage of RFA systems is that they, like their semiactive cousins, are a compromise between active and passive designs. Many of the favorable power and reliability issues of semiactive actuators extend to regenerative ones. However, regenerative actuators relax the constraints imposed on semiactive systems, giving these devices the potential to "push the envelope" for the level of performance achievable for energy-constrained control.

The concept of regenerative actuation have appeared in numerous areas of structural control, and there exist some differences as to exactly what qualifies an actuation system as "regenerative." These discrepancies arise from how the energy storage system is modeled (if it is included at all), whether multiple actuators are considered, and if so, whether they are allowed to share power. In this section, a brief synopsis of some past contributions on this subject will be presented. Then, the framework in which these devices will be considered for this study will be presented. This framework is intended to be rather general, in the sense that it applies to systems with or without energy storage, and to arbitrarily large actuation networks.

1.2.1: Past Work

Regenerative actuation is still quite new in structural control applications. It has been examined in the context of automobile suspension systems using a hydraulic regenerative actuator (Jolly and Margolis 1997b) and an electromechanical regenerative actuator (Okada et al. 1997), in small, flexible structures, with the use of a piezoelectric actuator with an inductor for energy storage (Wang et al. 1996), and in civil structures with the use of an electric machine with a battery for energy storage (Nerves and Krishnan 1996).

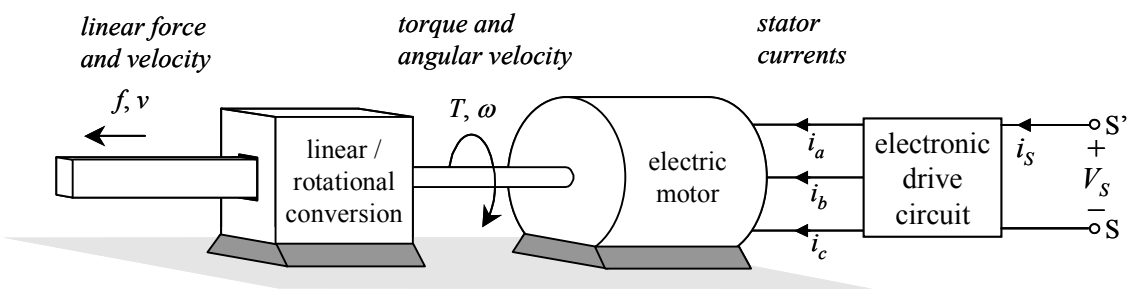

Figure 1.5: Block diagram of an actuator subsystem

In the area of vehicle suspensions, regenerative actuators are defined in (Jolly and Margolis 1997a; Jolly and Margolis 1997b) as a network of force actuators which has power-coupled capability (i.e., trait 2 above) and which possesses a single, global, ideal energy storage device. By "ideal," the implication is that this storage device possesses no dynamics, has 100% efficiency, and has no upper limit on energy capacity. In that study, both electrical and hydraulic designs are discussed. The emphasis is on steady-state disturbance rejection problems, and the energetic constraints of the devices are handled by classifying linear feedback control laws for which, in steady-state or stationary excitation, the energy stored in the power supply tends to infinity.

In civil engineering applications, regenerative actuators have received much less attention. Nerves and Krishnan (1996) conducted investigations into this subject where, as in the aforementioned suspension research, this power supply is considered to be ideal. A study conducted by Scruggs (1999) examined the implications of the fact that the energy storage system has a limited size, resulting in saturation and exhaustion of the supply system. It is also important to mention that in the civil engineering area, studies with regenerative actuators have been limited to a single device with local energy storage. The concept of power-sharing between actuators has yet to receive any significant attention.

1.2.2: A Generalized Approach

The concept of regenerative actuation can be approached as an extension of the electromechanical semiactive system discussed in the previous section. Consider again the system depicted in Fig. 1.3, slightly revised in Fig. 1.5. If terminals *S*-*S*' are connected to an energy source instead of a resistor, the system in Fig. 1.5 is capable of two-way power flow. The present study envisions the use of several such electromechanical systems (henceforth called *actuator subsystems*) as force actuators for use in structural vibration control. With the terminals *S*-*S*' of each machine subsystem connected in parallel, these subsystems are capable of sharing

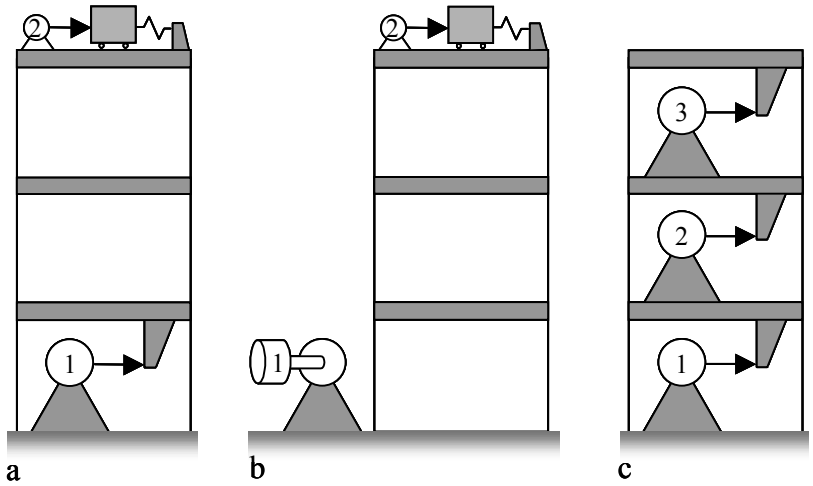

Figure 1.6: Various Applications of Regenerative Actuation

power with each other, through proper control of the electrical circuitry. Thus, the electrical energy generated by one device may be converted back into mechanical energy by another.

Remote energy storage and reuse is possible for this system. The simplest way to accomplish this is by designing one of the actuation subsystems as a flywheel drive system. Thus, the energy storage device becomes just another degree of freedom in the mechanical system to which the RFA system is connected. If an energy supply does not exist, or if it is saturated at its maximum storage level, excess electrical energy may be dissipated in a resistor bank, also connected to *S*-*S'*.

In this context, RFA systems have many potential uses in the control of civil structures. Consider, for example, the possible implementations shown in Fig. 1.6. In Fig. 1.6a, two machines are incorporated into a structure, one between the ground and first floor, and the other in the form of a mass driver on the roof. If machine 1 were operated as a generator and machine 2 as a motor, the system could deliver energy directly from the ground to the roof. Or, as shown in Fig. 1.6b, one of the two machines could be mounted on the ground and made to drive a flywheel using energy withdrawn by the second machine. In this way, machine 1 is used as an energy storage device. Yet another possible configuration is the densely-actuated structure in Fig. 1.6c. The capability of the actuators to share power allows for the structural vibration energy to flow in more complex patterns than for traditional damping systems.

1.2.3: The Ideal RFA Network

A schematic diagram of an *m*-machine RFA network is shown in Fig. 1.7. Each actuator subsystem undergoes a relative velocity v_k. The force vector is denoted by $\mathbf{f}_e = \{f_{e1}...f_{em}\}^T$

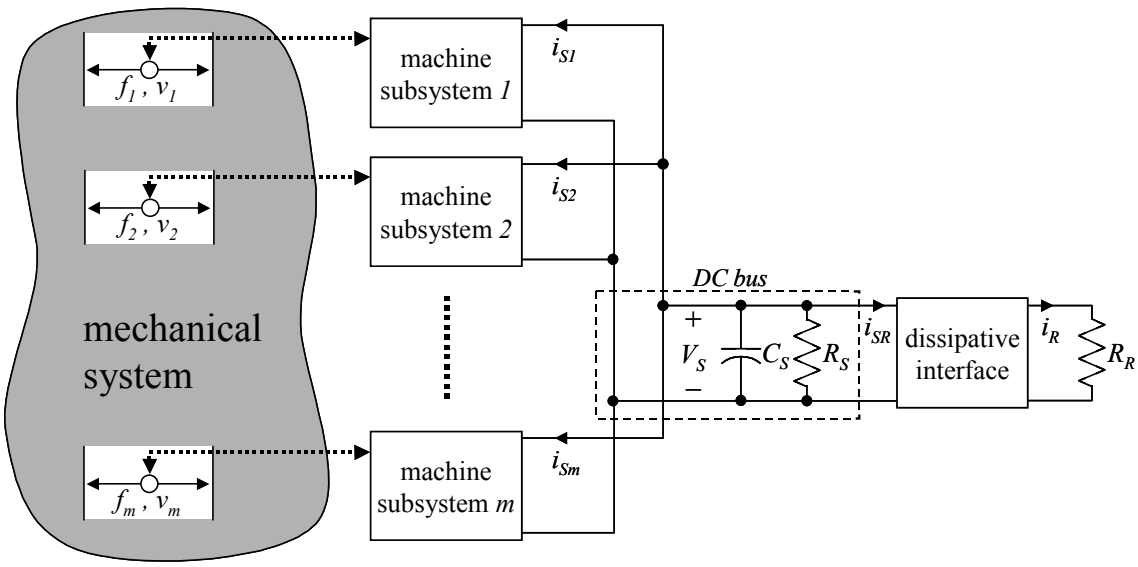

Figure 1.7: Idealized Electromechanical Regenerative Actuation System

and the corresponding relative velocity vector is $\mathbf{v} = \{v_1 ... v_m\}^T$. For each actuator, the power injected into the structure is $P_k = f_{ek} v_k$. This mechanical power is converted from an electrical power $V_S i_{Sk}$. Ideally, this power conversion would be lossless and instantaneous, with $f_{ek} v_k$ being equal to $V_S i_{Sk}$. The terminals *S-S'* of all the machines are connected in parallel, and referred to as the *DC bus*, with voltage V_S. Also connected to the DC bus is a "dissipative interface" which is used to dissipate excess electrical energy generated by the actuators. This subsystem extracts current i_{SR} from the DC bus, to produce a current i_R through resistor R_R. Ideally, the dissipative interface would be lossless and instantaneous, with $V_S i_{SR}$ equal to $i_R^2 R_R$.

As with the electromechanical semiactive device discussed in the previous section, this electrical network (i.e., inside the boxes labeled "electronic drive circuit" in Fig. 1.5 and "dissipative interface" in Fig. 1.7) is controlled by using transistors as electronic switches. Thus, ideally, control of these electronic networks consumes negligible power.

In Fig. 1.7, capacitor C_S is not intended to store any significant amount of energy, and resistor R_S is selected to be sufficiently large, such that the energy it dissipates is minimal. Therefore, in ideal steady-state operation, the aggregate power flow onto the DC bus is approximately zero, implying that

$$\sum_{k=1}^{m} i_{Sk} V_S = -i_R^2 R_R \tag{1.1}$$

This in turn implies that

$$\sum_{k=1}^{m} i_{Sk} V_S \leq 0 \tag{1.2}$$

Lossless power conversion further requires that $i_{Sk}V_S = f_{ek}v_k$ so the above leads to the ideal regenerative actuation constraint,

$$\sum_{k=1}^{m} f_{ek} v_k = \mathbf{f}_e^T \mathbf{v} \leq 0 \tag{1.3}$$

For an ideal RFA network, the above relationship is the only constraint on the forces. Of course, the power conversions in a real electromechanical system are not lossless. The electrical system also possesses significant dynamics and limitations which must be modeled. These issues constrain the system operation, producing realistic regenerative actuation constraints that are more restrictive and complex than the one in equation (1.3). However, the above discussion illustrates the general concept of regenerative actuation.

1.3: Objectives & Scope of This Study

The focus of this study concerns the design, modeling, simulation, and control of RFA networks, such as the one in Fig. 1.7, and their implementation in structural control problems pertaining to earthquake engineering. The ensuing chapters delve deeper into these concepts, following the outline below:

Ch.2: **System Modeling.** The design of a realistic RFA network, with arbitrary number of actuators and possible energy storage, is developed. This leads to a physical model for the electrical dynamics of the RFA network, in which the inputs to the system are the linear velocity vector **v**, and the positions of the electronic switches in the network.

Ch. 3: **Capabilities of RFA Systems.** The theoretical forcing capability of the designed RFA network is examined, yielding a single constraint similar to Eq. (1.3), but accounting for internal electrical losses in the network, and practical limitations on the electrical states. Implications for systems with power storage are examined, which paint a more complex picture of the energy storage capability of these systems than the "ideal" supply assumptions of previous studies.

Ch. 4: **Switching Control.** An electronic control system is designed by which the switches in the network are toggled so as to bring about zero-error tracking for an electromechanical force command $\mathbf{f}_e^*$. Robustness issues are addressed, and the final controller design is

robust to parameter uncertainties and sensory time delay. The transient characteristics of the closed-loop system are also examined.

Ch. 5: **The Structure-Actuator System.** The integration of the RFA network into a linear structural model is presented. Also, a "nominal model" of the actuator-structure system, for use in the design and analysis of the structural feedback controller, are presented. It is then shown that the RFA network may be viewed as a structural damping system, but where the damping capabilities are more general than those achievable with mechanical damping. For instance, the damping forces may be non-local, and the resultant structural damping matrix may be asymmetric. Scalar measures are defined, by which the performance of the RFA structural control system may be assessed, and these measures are used to optimize the linear damping for the RFA network.

Ch. 6: **Feedback Control Algorithms.** The development of "Clipped-Linear" feedback control is presented. This approach to controller design is common for semiactive devices, and has been shown to yield favorable performance. Here, it is extended to RFA networks, and several simple examples are given which examine its performance. Its equivalence to Lyapunov-based control system design is also discussed.

Ch 7: **A Simulation Example.** For the control system design approaches developed in Chapter 6, a numerical example is shown which exhibits the performance of an RFA network for the actuator configuration shown in Fig. 1.6a, subject to earthquake loading. The performances of several feedback controller designs are compared to each other, and to the uncontrolled case. Characteristics arising from the non-ideal network realization are illustrated.

Ch. 8: **Optimal Control.** The constraints on the RFA network result in a physical limitation on the achievable performance for the system. The derivation and study of this physical limit is useful in the design of RFA networks for particular applications. This chapter presents some ideas on the use of optimal control theory to derive this performance limit. However, there are basic questions in this analysis which remain unanswered, and consequently, the results presented here are merely preliminary.

Ch. 9: **Conclusions and Future Research.** Conclusions are drawn for this study, and the numerous avenues for future research are discussed.

It must be emphasized that this type of actuator design is fairly new, and this study is a preliminary investigation into its application to civil engineering. Therefore, the focus will be on fundamental ideas, and not on theoretical subtlety or technological nuance. It is nowhere claimed

in this analysis that the designs presented herein are optimal for a given application, or that they represent concepts which could be carried directly into practical implementation without modification or refinement. Rather, an effort was made to strike a comfortable balance between theoretical tractability and technological realism.

This study relies on simulation data to justify theoretical claims, and does not report on any laboratory study or prototype development. The reason for this is simply that the components used in the design of the system are all available commercially, and extremely detailed models for their behavior already exist. It was thus deemed more important to focus on an assessment of the general potential of these devices for use in a variety of structural control applications, rather than on a specific experimental demonstration.

Chapter 2. System Modeling

The RFA network in Fig. 1.7 is quite general. It is not stated how the electromechanical conversion is accomplished in each actuator subsystem, or how the current i_R is regulated through the dissipative interface. This chapter constitutes one description of how such an RFA network might be constructed, along with a derivation of a dynamic model of its behavior.

For each actuator in the network, the proposed design of the actuator subsystem is shown in Fig. 1.5. The linear-to-rotational conversion converts the linear force f_k to a torque T_k. The machine converts the mechanical energy to electrical energy, and vice versa. Finally, the power electronics interface the terminals of the machine with the DC bus. This system has nontrivial dynamic behavior due to dissipation, inductances in the stator coils, etc. The DC bus subsystem also has dynamics, because of its capacitance C_S. Its inputs are the currents from the machine subsystems and the dissipative interface. The dissipative interface subsystem has dynamic behavior as well, and must be controlled to properly regulate the current i_R flowing through its resistor.

The approach of this chapter is to model and discuss each subsystem in Fig. 1.7 (i.e., the actuator subsystems, DC bus, and dissipative interface) separately. For each, its hardware design will be presented, and its dynamic model derived. Then, at the end of the chapter, the dynamic description of the entire network is presented.

2.1: The Actuator Subsystems: Electromechanical Conversion

All actuator subsystems are assumed to be assembled from the same types of components; i.e., the same types of linear-to-rotational conversions, motors, etc. However, these components may have different parameters for each subsystem. As they all obey the same fundamental laws, their descriptions may be generalized. For convenience, the notation of subsystem number (i.e., f_{ek}) will be dropped (i.e., f_e) with the tacit implication that such expressions apply to all the subsystems in the network.

2.1.1: Mechanical Modeling

The mechanical interface of the machines with the structure is accomplished through linear-to-rotational conversions, related by

$$v = l\omega \tag{2.1}$$

where l, called the *lead* of the conversion, has units of m/rad. For the purposes of this analysis, the efficiency of the screw conversion will be considered the same in both directions of operation, and will be denoted by η. Other attributes of the conversion, such as backlash and axial play, are considered negligible in this analysis.

The shaft torque T is related to the linear force f through the lead and the efficiency. For convenience, define $h(T\omega)$ as

$$h(T\omega) = \begin{cases} \eta & : \quad T\omega \geq 0 \\ 1/\eta & : \quad T\omega \leq 0 \end{cases} \tag{2.2}$$

Then f can be expressed as

$$f = \frac{h(T\omega)}{l} T \tag{2.3}$$

Note that $h(T\omega)$ is equal to $h(fv)$.

For machines in the network used to excite flywheels, there is obviously no linear-to-rotational conversion. However, it will be inconvenient to continually make distinctions between linear and rotational actuators in the mechanical system. Thus, flywheels will be incorporated into the general framework by designating η=1 and choosing an arbitrary l for these subsystems. Unless otherwise stated, no distinction will be made between these and other actuator subsystems.

A cross-section schematic for a brushless DC machine is shown in Fig. 2.1. The stator of the machine is made up of copper windings surrounded by an iron core. Mounted to the rotor of the machine are permanent magnets (the heavy black lines in the figure) which provide a rotating magnetic field as the rotor spins. The interaction of this magnetic field with the stator windings provides the avenue for electromechanical power conversion, and results in an electromechanical torque T_e, applied to the shaft.

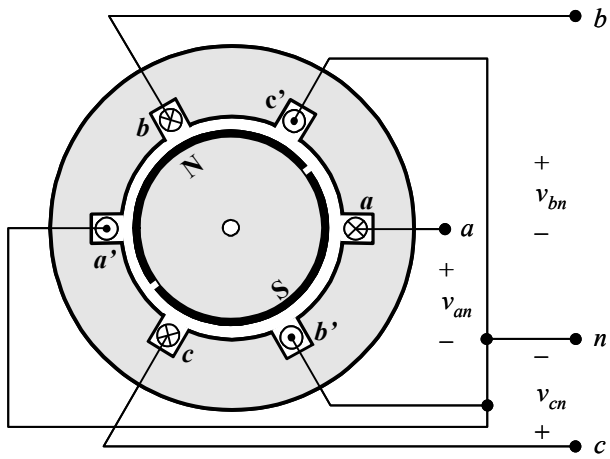

Figure 2.1: Cross-section of a BDC machine

The angular velocity of the rotor shaft is denoted by ω, and the resultant angular displacement is θ. Let the torsional viscous friction coefficient and rotational inertia of the rotor be denoted by B and J, respectively. Then, the resultant total torque T transmitted to the shaft may be expressed as

$$T = T_e - J\dot{\omega} - B\omega \,. \tag{2.4}$$

Defining f_e as

$$f_e = T_e / l \tag{2.5}$$

the mechanical dynamics of the machine can be described in terms of the linear motion variables as

$$f = h(fv)\left(f_e - \frac{J}{l^2}\dot{v} - \frac{B}{l^2}v \right). \tag{2.6}$$

In the ensuing analysis, it will be convenient to work directly with f_e rather than f, with the understanding that they are related through Eq. (2.6).

2.1.2: Electrical Modeling

Concerning the electrical dynamics, the stator of the machine is wound with three distinct coils called the *phases*, denoted as a, b, and c. At the ends of the coils for which the current is shown to flow *into* the machine are terminals, or *lines*, at which voltages may be applied. The other ends of the coils, denoted by the labels a', b', and c', are connected together at the so-called

neutral node, labeled as n. The corresponding line-to-neutral voltages applied to the terminals are v_{an}, v_{bn}, and v_{cn}.

With the stator coils connected as described, the electrical dynamics of the stator currents may be represented by the equivalent circuit shown in Fig. 2.2. For instance, the a-phase current i_a satisfies the differential equation

$$v_{an} = e_{an} + Ri_a + L\frac{di_a}{dt} \tag{2.7}$$

In the figure, R and L are the resistance and effective inductance, respectively, for each stator coil. The equivalent voltage sources e_{an}, e_{bn}, and e_{cn}, called the *back EMF* voltages, result from magnetic induction between the rotor and stator fields. These voltages are related to the mechanical dynamics of the rotor. Through its angular velocity and position, this relationship is described by the periodic, trapezoidal functions K_a, K_b, and K_c, shown in Fig. 2.3. Using these functions, e_{an} is

$$e_{an} = K_a(\theta)\omega \tag{2.8}$$

Analogous expressions follow for the b and c phases.

The electromechanical force f_e, due to the stator currents, can be found by equating the electrical power flow $i_a e_{an}+i_b e_{bn}+i_c e_{cn}$ (into the back EMF voltages) to the resultant mechanical power delivered by the actuator, equal to $f_e v$. This gives

$$\begin{aligned} f_e &= \left(i_a e_{an} + i_b e_{bn} + i_c e_{cn}\right)/v \\ &= \frac{1}{l}\left(K_a i_a + K_b i_b + K_c i_c\right) \end{aligned} \tag{2.9}$$

where K_a, K_b, and K_c become functions of linear displacement, through parameter η. With f_e thus defined, Eqs. (2.1) through (2.9) fully describe the dynamics of each actuator subsystem.

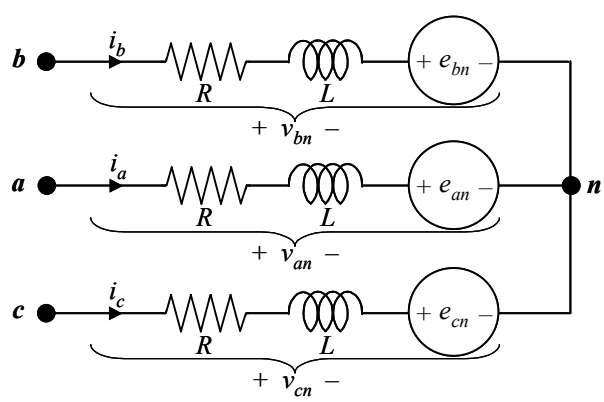

Figure 2.2: BDC equivalent circuit

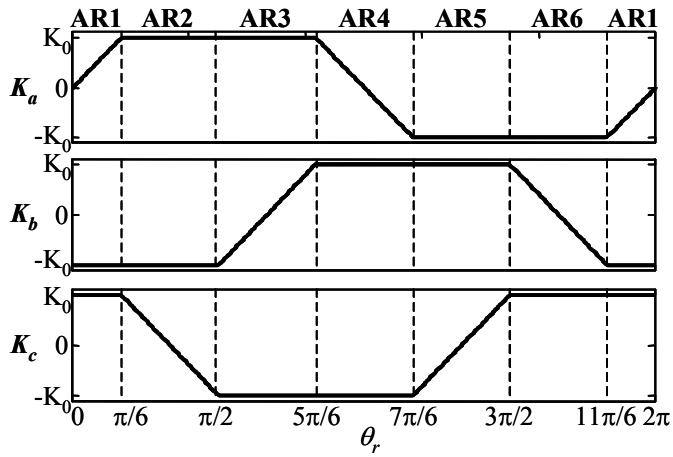

Figure 2.3: Trapezoidal back-EMF functions

2.2: The Actuator Subsystems: Electronic Conversion

The objective is to use the machine as a force actuator; i.e., to excite currents i_a, i_b, and i_c in such a way that f_e tracks some desired force f_e^*. By Eq. (2.9), this implies that the three stator currents have to be controlled to track a set of commands i_a^*, i_b^*, and i_c^* such that

$$f_e^* = \frac{1}{l}\left(K_a i_a^* + K_b i_b^* + K_c i_c^*\right) \tag{2.10}$$

However, there are three currents, and one desired force, so Eq. (2.10) is not enough to determine three unique current commands (i.e., the problem is overdetermined). Two additional, independent relations for the current commands are necessary.

One of these relations is immediate. Because the three coils connect at the neutral node n, the currents must always sum to zero. Therefore, for successful current tracking, it must always be the case that

$$i_a^* + i_b^* + i_c^* = 0 \tag{2.11}$$

The other relation arises from convenience rather than necessity. Consider again the trapezoidal back-EMF waveforms in Fig. 2.3. Define a current command i^* to be related to the three stator current commands as shown in Fig. 2.4 below. Note that this set of current commands always meets Eqs. (2.10) and (2.11). Defined as such, Eq. (2.10) becomes

$$f_e^* = K_f i^* \tag{2.12}$$

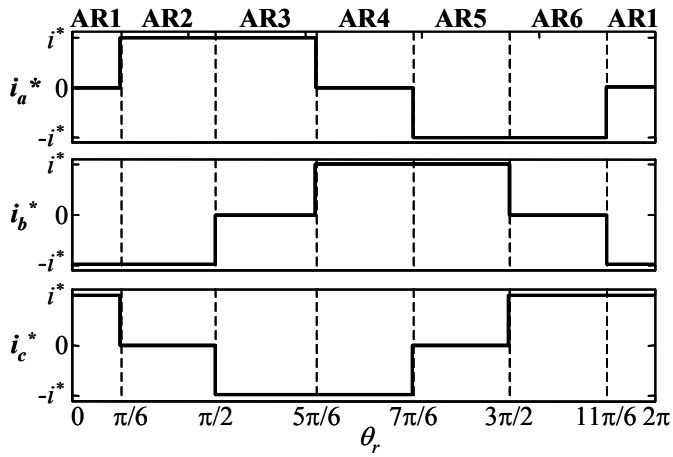

Figure 2.4: Current commands

where

$$K_f = 2K_0 / l \tag{2.13}$$

Eq. (2.12) is convenient because the relationship between f_e^* and i^* is proportional and time-invariant. Through Fig. 2.4, it determines uniquely the current commands i_a^*, i_b^*, and i_c^* as a function of f_e^*. It is also an l_∞-optimal solution to Eqs. (2.10) and (2.11) for $\{i_a^*, i_b^*, i_c^*\}$, and thus yields the maximum amount of force for a given current level.

2.2.1: Drive Circuitry

The drive circuitry is an electronic network connected to the terminals of the machine that provides the means of controlling the stator currents. It interfaces the machine terminals with the DC bus voltage V_S, as was shown in Fig. 1.5.

Terminals *a*, *b*, and *c* are connected to a six-transistor drive circuit which interfaces with V_S, as shown in Fig. 2.5. The dynamics of the circuit are influenced by the on/off switching ability of the transistors. By firing the transistors on and off, the stator currents can be raised and lowered. Thus, by proper concurrent timing of these firings, the currents can be controlled.

In order to render a tractable model for the electrical dynamics, the traits of the transistors and diodes will be approximated. The diodes are modeled by a nonzero forward conduction voltage V_D and infinite reverse breakdown voltage.

Because they are operated as electronic switches, the transistors can be approximated as in Fig. 2.6, where V_{gs} is the gate-source voltage, used to switch the transistor "on" and "off." The impedance between the gate and source is typically quite high. Thus, switching the transistor

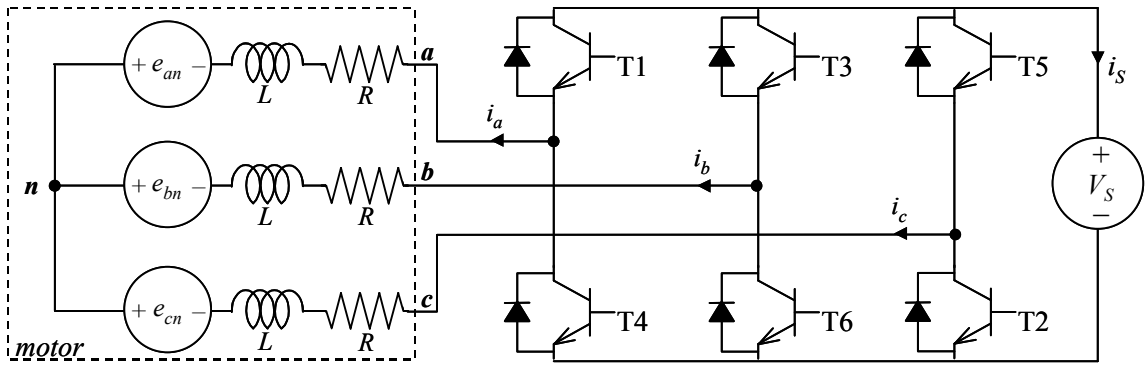

Figure 2.5: Transistor bridge

on and off requires very little current i_g, even if the current i_{ds} is quite large. As a result, the gate drive circuitry which excites the voltage V_{gs} typically consumes very little power.

Fig. 2.6 is an approximate model. Among other characteristics, it ignores dissipation which occurs as the transistor turns on and off.

With the transistor approximation in Fig. 2.6, the transistor bridge circuitry may be approximated by the switching system in Fig. 2.7.

2.2.2: H-Bridge Switching Logic

A system of control logic must be determined for these transistors in order to control the stator currents so as to track the commands illustrated in Fig. 2.4.

Consider that for any rotor angle θ in Fig. 2.4, one stator current command is always zero. Suppose that at some time t, $\theta(t) \in$ AR1. Thus, $i_a^*=0$. Under the condition that

$$V_S(\tau) > \left|K_f v(\tau)\right| \tag{2.14}$$

for $\tau>t$, the current $i_a(\tau) = 0$ is a stable equilibrium point if neither transistor T1 or T4 is activated. Thus, it is possible to achieve tracking for the zero-current phase by not firing either of its corresponding transistors.

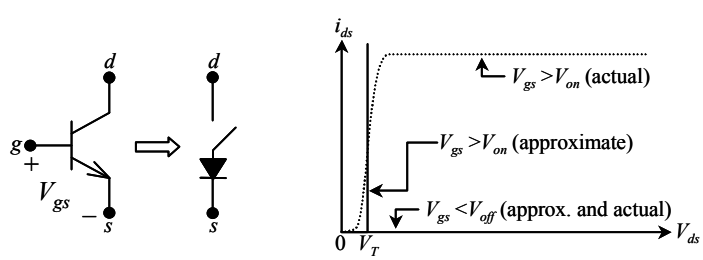

Figure 2.6: Transistor approximations

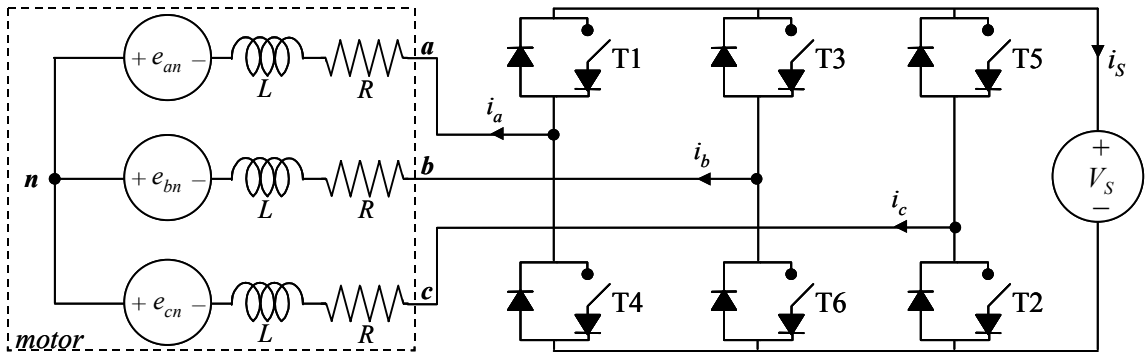

Figure 2.7: Approximate transistor bridge

If $\theta \in$AR1 for all time, the schematic in Fig. 2.5 can then be simplified by removing the *a*-phase circuitry, because it is known that $i_a = 0$. Similarly, if $\theta \in$AR4 for all time, the simplified schematic would look the same. Furthermore, for θ in any angle range for all time, the resultant schematics differ only in their transistor assignments. The schematic Fig. 2.8 could then be used to accurately model its behavior, by keeping track of which transistors T1-T6 assume the roles of $T1_S$, $T2_S$, $T3_S$, and $T4_S$ in the various angle ranges, as shown in the accompanying table. The relationships between i and the actual stator currents i_a, i_b, and i_c also differ for different angle ranges. The relationships of these three currents to i, for all six angle ranges, are the same as for the current commands shown in Fig. 2.4. The relation of i to the force f_e is therefore also the same, i.e.,

$$f_e = K_f i \tag{2.15}$$

The operation of the 6-transistor drive in Fig. 2.5 follows from this rationale. For θ in a given angle range, four of the transistors take on the roles of $T1_S$ through $T4_S$, while the other

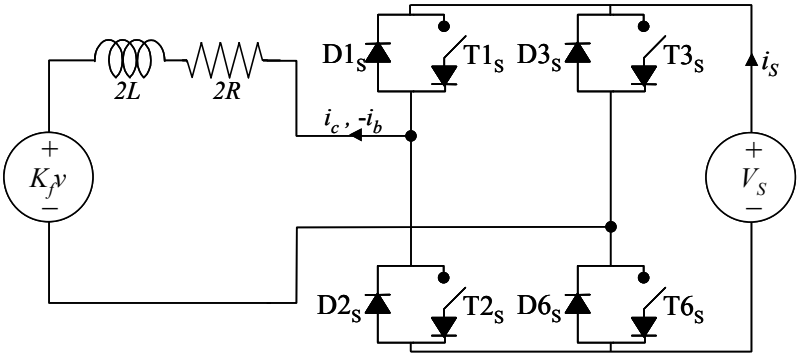

	1S	2S	3S	4S	i=
AR1	5	2	3	6	i_c , -i_b
AR2	1	4	3	6	i_a , -i_b
AR3	1	4	5	2	i_a , -i_c
AR4	3	6	5	2	i_b , -i_c
AR5	3	6	1	4	i_b , -i_a
AR6	5	2	1	4	i_c , -i_b

Figure 2.8: Simplified bridge

two (corresponding to the zero-current phase) remain switched off. When θ transits from one angle range to another, these transistor assignments change.

After such a transition, one stator coil will demagnetize (i.e., its current will drop to zero) and another one will become activated. For example, a transition from AR1 to AR2 results in i_b dropping to zero and i_a rising to i. Because of the inductance of the stator coils, this magnetization/demagnetization process is not instantaneous, but rather occurs over a brief time period following the transition. These dynamics are not reflected in Fig. 2.8, and result in a pulsation in i during the transition. This phenomenon (which is the electrical equivalent of the mechanical commutation of the rotor in a traditional DC motor) will be considered negligible in this analysis. It has been shown elsewhere that its effect is so minimal in similar applications, and its inclusion greatly complicates the dynamic system description. Thus, Fig. 2.8 will be used as the dynamic model of the actuator subsystem.

The simplified 4-transistor bridge shown in Fig. 2.8 is called an *H-Bridge*, because of its geometrical shape. This type of motor drive is very common, and there exist several variations in the methods by which transistors $T1_S$ through $T4_S$ are used to control the currents. Here, only one of these is illustrated.

Consider the case where the current i satisfies

$$V_S > \left| K_f v + 2Ri + V_{sw}\,\mathrm{sgn}(i) \right| \tag{2.16}$$

where

$$V_{sw} = V_D + V_T \tag{2.17}$$

If this inequality holds, then the circuit in Fig. 2.8 is equivalent to the one in Fig. 2.9, if the switch position S1 related to $T1_S$ and $T2_S$ by

i	S1	$T1_S$	$T2_S$
>0	1	on	off
>0	2	off	off
<0	1	off	off
<0	2	off	on

and if S2 is related to $T3_S$ and $T4_S$ by an analogous relationship.

Control of the bridge circuitry amounts to controlling the positions of switches S1 and S2. The switching logic used here is bistate, and is represented by the variable D, which can be either 1 or -1. Its relation to the switch states is

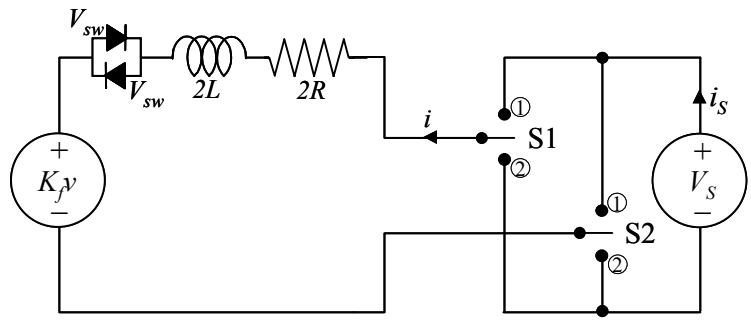

Figure 2.9: Approximate ideal-switch circuitry

$$D = \begin{cases} 1 & : \text{S1} = 1,\ \text{S2} = 2 \\ -1 & : \text{S1} = 2,\ \text{S2} = 1 \end{cases} \tag{2.18}$$

With this definition, the differential equation for the current i may be written as

$$\frac{d}{dt} i = \frac{1}{2L}\left(DV_S - K_f v - 2Ri - V_{sw}\,\mathrm{sgn}(i)\right) \tag{2.19}$$

or, using Eq. (2.15),

$$\frac{d}{dt} f_e = \frac{1}{2L}\left(K_f DV_S - K_f^2 v - 2Rf_e - K_f V_{sw}\,\mathrm{sgn}\left(f_e\right)\right) \tag{2.20}$$

If Eq. (2.16) is true, then for $D = 1$, df_e/dt is positive and for $D = -1$, it is negative. Thus, f_e can be raised or lowered through these switches, and through proper alternation of D, its value may be made to track a command f_e^*.

Eqs. (2.6) and (2.20) constitute a reasonable dynamic model for an actuator subsystem, under the assumption that V_S satisfies Eqs. (2.14) and (2.16). In developing a switching control algorithm for the RFA network, V_S must be explicitly controlled to ensure that these conditions are satisfied.

2.3: The Electrical Network

The various machines in the network are connected, both to each other and to the dissipative interface, through the voltage V_S. This is shown in Fig. 2.10, assuming the general case of m machines. This electrical bus is called a *DC link*, to imply that the voltage V_S is a DC voltage that "links" several disparate electrical systems together. DC links are common in many power electronic systems, where different parts of the system may operate at different DC voltages, or are AC subsystems. They provide an avenue for power to flow from one part of the

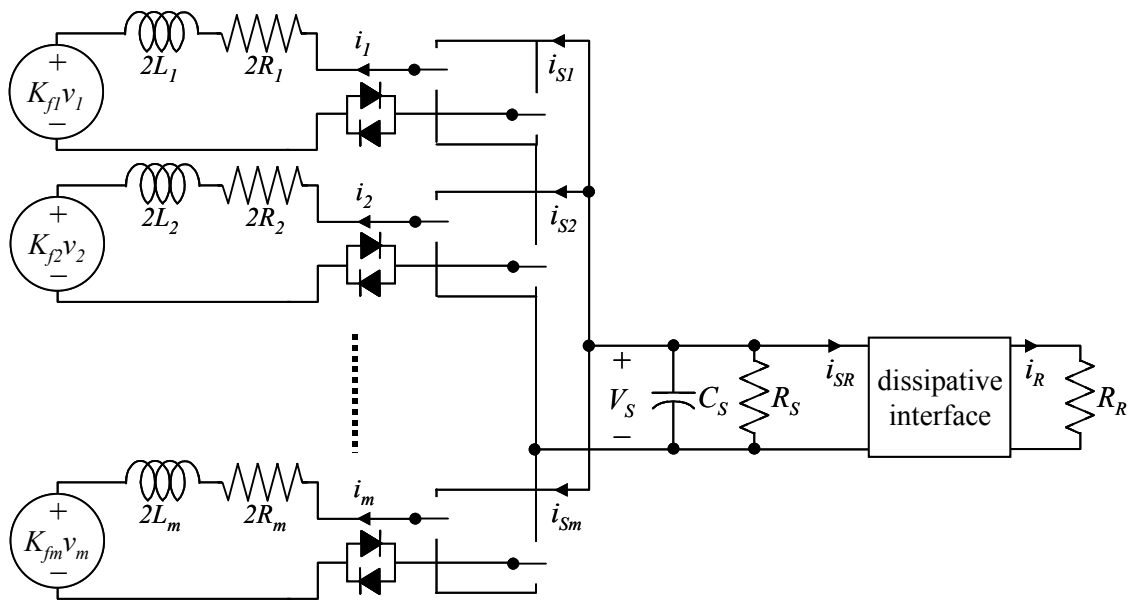

Figure 2.10: Machine interconnections

network to another. The purpose of the capacitor C_S is to filter out high-frequency voltage noise which arises due to the switching of the transistor bridges. The resistor R_S is present to provide some light damping to the dynamics of the voltage V_S. It is designed to be large, and typically dissipates much less energy than R_R.

The differential equation for V_S may be expressed as

$$\frac{d}{dt}V_S = \frac{1}{C_S}\left(-i_{S1} - \ldots - i_{Sm} - i_{SR} - \frac{1}{R_S}V_S\right) \tag{2.21}$$

Current i_{SR} is the current drawn from the DC bus by the dissipative interface. Currents i_{Sk}, $k \in \{1..m\}$, are the currents shown in the simplified schematic in Fig. 2.9, for each machine subsystem. These currents are related to the respective i_k currents through their switch position D_k, as

$$i_{Sk} = D_k i_k \tag{2.22}$$

Therefore, using Eq. (2.15), Eq. (2.21) may be rewritten in terms of the i_k currents as

$$\frac{d}{dt}V_S = \frac{1}{C_S}\left(-\frac{D_1}{K_{f1}}f_{e1} - \ldots - \frac{D_m}{K_{fm}}f_{em} - i_{SR} - \frac{1}{R_S}V_S\right) \tag{2.23}$$

The circuit for the dissipative interface is shown in Fig. 2.11a, consisting of an inductor, a transistor, a diode, and the resistor R_R. The amount of energy dissipated is controlled through the transistor. As with the transistor bridge circuitry used to control the machines, the

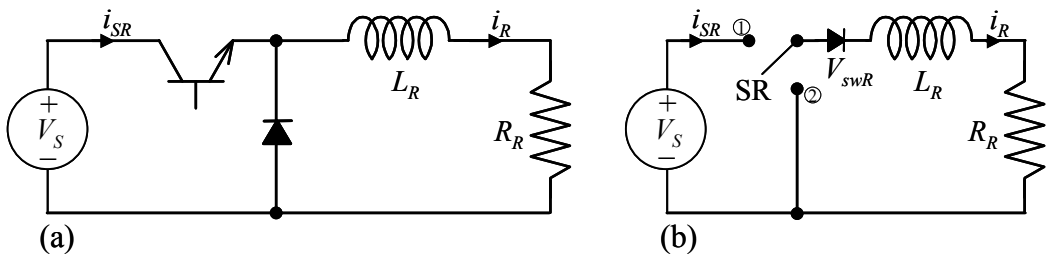

Figure 2.11: Dissipative circuitry (a) and switching approximation (b)

transistor and diode in Fig. 2.11a may be replaced by a switch. This is shown in Fig. 2.11b. For simplicity, it will be assumed that

$$V_{DR} = V_{TR} = V_{swR} \tag{2.24}$$

If the two voltages differ, the behavior of the system is not fundamentally altered, but the system description is more complicated.

To describe the behavior of the system, define the switching variable D_R to be

$$D_R = \begin{cases} 1 \ : \ \text{SR in position 1} \\ 0 \ : \ \text{SR in position 2} \end{cases} \tag{2.25}$$

Defined as such, D_R may be used to describe the differential equation for the circuit as

$$\frac{d}{dt} i_R = \frac{1}{L_R}\left(D_R V_S - R_R i_R - V_{swR}\ \mathrm{sgn}(i_R)\right) \tag{2.26}$$

For constant V_S, the value of i_R is limited by

$$i_R \in \left[0, \max\left\{0, \frac{V_S - V_{swR}}{R_R}\right\}\right] \tag{2.27}$$

Because of this, it can be concluded that $D_R = 1$ will make i_R increase, and $D_R = 0$ will make it decrease. By switching between these two states, the current can be controlled to be anything within its possible range. Furthermore, the power dissipated by the circuit is equal to $R_R i_R^2$, so by controlling the value of i_R, the dissipation by circuit may be varied.

2.4: Total Electronic System Model

2.4.1: The Electrical State Space

A description of the entire electrical network can now be expressed as a single (m+2)-order differential equation. This equation is a collection of Eqs. (2.20) for the forces $\{f_{e1}...f_{em}\}$, Eq. (2.23) for the DC bus voltage V_S, and Eq. (2.26) for the dissipative current i_R. The switches enter the equation through the D terms; i.e., D_1 through D_m for the machines, and D_R for the dissipative element.

Define the state vector **x** and switch position vector **D** as

$$\mathbf{x} = \begin{bmatrix} \mathbf{f}_e^T & i_R & V_S \end{bmatrix}^T \qquad \mathbf{D} = \begin{bmatrix} D_1 & \cdots & D_m & D_R \end{bmatrix}^T \tag{2.28}$$

Then, the differential equation can be expressed as

$$\dot{\mathbf{x}} = \mathbf{\Delta}(\mathbf{A}_H \mathbf{x} + \mathbf{A}_S(\mathbf{D})\mathbf{x} - \tilde{\mathbf{v}}_x) \tag{2.29}$$

with the following definitions

$$\mathbf{K}_f = diag(K_{f1}...K_{fm}) \;,\; \mathbf{\Delta}_f = \mathbf{K}_f^2 diag(1/2L_1...1/2L_m) \;,\; \mathbf{R}_f = diag(2R_1...2R_m)$$

$$\mathbf{K} = \begin{bmatrix} \mathbf{K}_f & \\ & \mathbf{I}_2 \end{bmatrix} \;,\; \mathbf{\Delta} = \begin{bmatrix} \mathbf{\Delta}_f & & \\ & 1/L_R & \\ & & 1/C_S \end{bmatrix} \;,\; \mathbf{R} = \begin{bmatrix} \mathbf{R}_f & & \\ & R_R & \\ & & 1/R_S \end{bmatrix}$$

$$\mathbf{A}_S(\mathbf{D}) = \mathbf{K}^{-1}\begin{bmatrix} \mathbf{0} & \mathbf{D} \\ -\mathbf{D}^T & 0 \end{bmatrix}\mathbf{K}^{-1} \;,\; \mathbf{A}_H = -\mathbf{K}^{-1}\mathbf{R}\mathbf{K}^{-1}$$

$$\mathbf{v}_{sw} = \mathbf{K}_f^{-1}[V_{sw1}\,\mathrm{sgn}(f_{e1}), \ldots, V_{swm}\,\mathrm{sgn}(f_{em})]^T \;,\; \tilde{\mathbf{v}} = \mathbf{v} + \mathbf{v}_{sw}$$

$$\tilde{\mathbf{v}}_x = \begin{bmatrix} \tilde{\mathbf{v}}^T & V_{swR}\,\mathrm{sgn}(i_R) & 0 \end{bmatrix}^T$$

The vector $\mathbf{v}_{sw}$ is determined by the direction of current flowing through the switches, and by the switch conduction voltages. Mathematically, it contributes to the system differential equation like a velocity offset.

The total forces **f** can be related to this system and the mechanical system, through Eq. (2.6). For the entire system, this equation may be represented as

$$\mathbf{f} = \mathbf{H}(\mathbf{f}, \mathbf{v})\left[\mathbf{f}_e - \mathbf{L}^{-2}\mathbf{B}_A\mathbf{v} - \mathbf{L}^{-2}\mathbf{J}_A\dot{\mathbf{v}}\right] \tag{2.30}$$

where

$$\begin{aligned} &\mathbf{H}(\mathbf{f}, \mathbf{v}) = diag\{h_1(f_1, v_1), \ldots, h_1(f_m, v_m)\} \quad &&\mathbf{L} = diag\{l_1, \ldots, l_m\} \\ &\mathbf{B}_A = diag\{B_1, \ldots, B_m\} &&\mathbf{J}_A = diag\{J_1, \ldots, J_m\} \end{aligned} \tag{2.31}$$

Note that this equation is nonlinear, because of the efficiency factors. Also, depending on how the actuators are distributed throughout the mechanical system, $d\mathbf{v}/dt$ will depend on $\mathbf{f}$ as well. Thus, a closed-form expression for Eq. (2.30) requires information about the mechanical system.

2.4.2: Electrical Time Constants

For the purposes of this analysis, the time constants of the electrical network will all be designed to be equal to τ. Thus,

$$L_k / R_k = L_R / R_R = R_S C_S = \tau \tag{2.32}$$

Note that the inductances L_k will include the inductances of the stator coils themselves, as well as supplemental inductors connected to the terminals of each machine. The value of τ should be designed to be significantly smaller than the time constants of the mechanical system, so that there is minimal coupling between electrical and mechanical dynamics. In other words, the ideal RFA network would appear to have instantaneous dynamics, from the point of view of the mechanical system.

2.4.3: Distinguishing between Linear and Rotational Actuators

As was mentioned in Section 2.1, Eq. (2.28) makes no distinction between linear actuators, and those exciting flywheels. In controlling the electronic circuitry, this distinction is, for the most part, immaterial. However, where it is necessary to distinguish between these two groups, the vectors $\mathbf{f}_{el}$ and $\mathbf{f}_l$ will refer to the linear electromechanical force vector, and total linear force vector, respectively. Similarly, the vector $\mathbf{v}_l$ will be used to refer to the vector of linear actuator velocities.

For this analysis, it will be assumed throughout that at most one flywheel exists in the network, and that this flywheel has electromechanical and total torques T_{efw} and T_{fw}, respectively, and a rotational velocity of ω_{fw}.

With these distinctions, the conventions for $\mathbf{f}_e$, $\mathbf{f}$, and $\mathbf{v}$ will be

$$\mathbf{f}_e = \begin{bmatrix} \mathbf{f}_{el} \\ T_{efw} \end{bmatrix}, \ \mathbf{f} = \begin{bmatrix} \mathbf{f}_l \\ T_{fw} \end{bmatrix}, \ \mathbf{v} = \begin{bmatrix} \mathbf{v}_l \\ \omega_{fw} \end{bmatrix} \tag{2.33}$$

Chapter 3. Capabilities of RFA Networks

The description of the system dynamics, given by Eq. (2.29), does not explicitly state which operating points (i.e. which forces $\mathbf{f}_e$ at a velocity $\mathbf{v}$) the system is capable of producing. Clearly, there are some operating points that are possible, and others that are not. Eq. (1.3) implies that, even if the network were ideal, its limitations would constrain the forces it could achieve.

In this chapter, realistic constraints on operating points for the RFA network will be derived and discussed. Indeed, they are somewhat more complicated than the ideal limitation of (1.3). In the discussion, losses in the stator resistances, losses in the switches, and the required lower bound on V_S in Eqs. (2.14) and (2.16) render a more complex picture of the system's capability.

It is important to note that the overarching focus in this chapter is *independent* of any control algorithm that might be designed to control the switch position vector $\mathbf{D}$. The limitations discussed here are intrinsic, physical limitations on the behavior of the system, resulting from the parameters of the hardware used in the design. However, this discussion may be framed in a control context, as a study to find the set of equilibrium points $\mathbf{x}^0$ for which there exists a switch control algorithm such that $\mathbf{x}$ is stable about $\mathbf{x}^0$ at a given velocity $\mathbf{v}$. This set of $\mathbf{x}^0$ in turn gives a resultant set of possible steaty-state force equilibria $\mathbf{f}_e^{\,0}$, for a given $\mathbf{v}$.

It will be assumed that $\mathbf{v}$ may be viewed as essentially constant from the point of view of the electrical system dynamics. This assumption is justified by the observation that the bandwidth of the electrical system will typically be at least an order of magnitude higher than that of the mechanical system.

3.1: Switching Equilibrium

The switch positions $\{D_1 ... D_m\}$ can be either 1 or –1, and D_R can be either 1 or 0. Thus, $\mathbf{D}$ lies in a set of 2^{m+1} possible vectors. The set of these vectors shall be referred to as $\mathcal{D}$; i.e.

$$\mathcal{D} = \left\{ \mathbf{D} \in \Re^{m+1} \mid D_{m+1} \in \{0,1\} \ , D_k \in \{-1,1\} \ , k \in \{1..m\} \right\} \tag{3.1}$$

For a switch position $\mathbf{D}$ to bring $\mathbf{x}$ to equilibrium about $\mathbf{x}^0$ at constant velocity $\mathbf{v}$, in the traditional sense, it would have to satisfy

$$\dot{\mathbf{x}}\left(\mathbf{x}^0, \mathbf{v}, \mathbf{D}\right) = \mathbf{0} \tag{3.2}$$

Using Eq. (2.29), **D** must therefore satisfy

$$\left(\mathbf{A}_H + \mathbf{A}_S(\mathbf{D})\right)\mathbf{x}^0 - \tilde{\mathbf{v}}_x = \mathbf{0} \tag{3.3}$$

For each $\mathbf{D} \in \mathcal{D}$ Eq. (3.3) has a unique solution for $\mathbf{x}^0$, because $\mathbf{A}_H + \mathbf{A}_S(\mathbf{D})$ is nonsingular. So in general, Eq. (3.2) is only possible for 2^{m+1} values of $\mathbf{x}^0$. Thus, due to the switching nature of the control input, a weaker conception of equilibrium must be used for this type of system. This issue is common to all dynamic switching systems, and there are two common approaches to its resolution.

3.1.1: Approach 1: Duty Cycle-Based Switching

Assume that each switch position goes through a cycle with period T_s. During each cycle, the switch starts at position one, toggles to position 2, and at the end of the cycle returns to position 1. Let the average of **D** over one cycle be denoted as **d**. Assuming the value of **d** changes very little from one cycle to the next, it may be viewed as a continuous function of time, i.e., $\mathbf{d}(t)$. The components of $\mathbf{d}(t)$ are called the *duty cycles* or *duty ratios* of the switches. Under the assumtion that $\mathbf{d}(t)$ varies slowly over any duration T_s, the dynamics of the system may be closely approximated by a "switch-averaged" model. This model is the same as Eq. (2.29), except that **D** is replaced with continuous-time functions $\mathbf{d}(t)$. It then becomes possible to say that, for equilibrium of the switch-averaged system, the state $\mathbf{x}^0$ must be such that there exists an admissible **d** such that

$$\left(\mathbf{A}_H + \mathbf{A}_S(\mathbf{d})\right)\mathbf{x}^0 - \tilde{\mathbf{v}}_x = \mathbf{0} \tag{3.4}$$

The admissible region for **d** is a prism in $\Re^{m+1}$ with vertices coincident with $\mathcal{D}$. This region maps to a region in $\mathbf{x}^0$ space, constituting the set of equilibria possible for the system. Further, it can be shown that all these equilibria are asymptotically stable for **v** constant.

This duty-cycle-based approach is appealing for switching systems because it allows for the control input to be viewed as a continuous signal. This, in turn, allows for the system to be linearized about an operating point, and thus for the control algorithm for **d** to be designed through linear control system theory. However, this approach is not taken in this study, for the simple reason that the switching control algorithm proposed here for RFA networks, which will be discussed in the following chapter, is based on sliding-mode control theory and does not

involve linear system analysis. However, it is acknowledged that a duty cycle-based approach to RFA network analysis and design may lead to superior switching controller designs.

3.1.2: Approach 2: Lyapunov-Based Switching

This second apporach to the analysis of equilibrium for switching systems, which will be used here, involves Lyapunov analysis. Basically, the goal is to determine the set of $\mathbf{x}^0$ values for which there exists a switching control algorithm $\mathbf{D} = \mathbf{F}(\mathbf{x})$ such that in the closed-loop system, $\mathbf{x}$ is stable about $\mathbf{x}^0$ in the Lyapunov sense. It is tentatively assumed that the switches in the network have negligible switching transition times, and that they may alternate infinitely rapidly. Consequences of physical limitations on switch operation will be addressed in the next chapter.

<u>DEFINITION</u>: (Switching Equilibrium): For the system in (2.29), let $\mathbf{v}$ be assumed constant, and let $\mathbf{D}$ be determined by a memoryless feedback law $\mathbf{D} = \mathbf{F}(\mathbf{x})$. It is assumed that $\mathbf{F} : \Re^{m+2} \mapsto \mathcal{D}$ is continuous almost everywhere in $\Re^{m+2}$. Then the system is in *switching equilibrium* about a point $\mathbf{x}^0$ if there exists a function $U : \Re^{m+2} \mapsto \Re^{+}$ such that $U(\mathbf{x})$ is a Lyapunov function; i.e.

$$U(\mathbf{x}) \geq 0 \quad , \quad \frac{dU}{dt} \leq 0 \quad , \quad \frac{dU}{dt} = 0 \Leftrightarrow \mathbf{x} = \mathbf{x}^0 \tag{3.5}$$

Such a state $\mathbf{x}^0$ will be called a *switching equilibrium point* (*s.e.p.*)

Thus, switching equilibrium is characterized by an ever-shrinking neighborhood, inside which $\mathbf{x}-\mathbf{x}^0$ must lie. Note that switching equilibrium points are always stable, by definition.

This notion of equilibrium is more relaxed than the one defined by Eq. (3.2) because it allows for discontinuities in $\mathbf{F}(\mathbf{x})$ at $\mathbf{x}^0$, thus allowing for $\dot{\mathbf{x}}$ to be discontinuous at $\mathbf{x}=\mathbf{x}^0$. In general, it is nontrivial to prove stability for feedback systems with such discontinuities because there may be sliding modes in the system dynamics on which $\mathbf{D}$ is undefined. However, it can be shown that for all $\mathbf{F}(\mathbf{x})$ functions proposed in this study, the dependency of dU/dt on D_i vanishes wherever D_i is undefined. Thus, Eq. (3.5) can be interpreted in the Lyapunov stability sense, without ambiguity.

3.2: Stability of Operating Points

Although not stated as such, some necessary conditions for $\mathbf{x}^0$ to be in switching equilibrium for a given $\mathbf{v}$ were derived in Chapter 2. Specifically, these are Eqs. (2.14), (2.16), and (2.27). If they do not hold, the transistor switches cannot be controlled to determine the signs

of the derivatives of $\mathbf{f}_e$. It is also clear that, in switching equilibrium, energy should be conserved; i.e. the aggregate amount of electrical power generated by the machines should equal the amount dissipated in the network. Mathematically, this requires that

$$\mathbf{x}^{0T}\mathbf{A}_H\mathbf{x}^0 - \mathbf{x}^{0T}\tilde{\mathbf{v}}_x = 0 \tag{3.6}$$

So, using physical arguments, Eqs. (2.14), (2.16), (2.27) and (3.6) are necessary for $\mathbf{x}^0$ to be a s.e.p. It will now be shown that these equations are also sufficient. This will be done by construction; i.e. by proposing a candidate Lyapunov function U, and showing that a switch position control law $\mathbf{F}(\mathbf{x})$ exists which yields switching equilibrium about $\mathbf{x}^0$ if it satisfies these conditions.

The state of the system $\mathbf{x}$ can be described relative to $\mathbf{x}^0$ as

$$\mathbf{x} = \mathbf{x}^0 + \delta\mathbf{x} \tag{3.7}$$

If condition (2.14) holds, then it follows from Eq. (2.29) that the dynamics of $\delta\mathbf{x}$ are governed by the equation

$$\delta\dot{\mathbf{x}} = \mathbf{\Delta}\big(\mathbf{A}_H + \mathbf{A}_S(\mathbf{D})\big)\delta\mathbf{x} + \mathbf{\Delta}\big(\mathbf{A}_H + \mathbf{A}_S(\mathbf{D})\big)\mathbf{x}_0 - \mathbf{\Delta}\tilde{\mathbf{v}}_x \tag{3.8}$$

Let the candidate Lyapunov function U be defined as

$$U = \frac{1}{2}\delta\mathbf{x}^T\mathbf{\Delta}^{-1}\delta\mathbf{x} \tag{3.9}$$

Then the derivative of U is

$$\frac{d}{dt}U = \delta\mathbf{x}^T\mathbf{\Delta}^{-1}\dot{\mathbf{x}} = \delta\mathbf{x}^T\mathbf{A}_H\delta\mathbf{x} + \delta\mathbf{x}^T\left(\big(\mathbf{A}_H + \mathbf{A}_S(\mathbf{D})\big)\mathbf{x}_0 - \tilde{\mathbf{v}}_x\right) \tag{3.10}$$

The first term on the right-hand side is quadratic, and negative-definite. It represents the damping in the system due to the resistances in the stator coils, and in resistors R_S and R_R. For $\delta\mathbf{x}$ sufficiently small, the effect of this quadratic term in the above derivative is negligible in comparison to the effect of the second term, which is linear in $\delta\mathbf{x}$. Thus, an operating point $\mathbf{x}^0$ may be held in switching equilibrium if

$$\forall\delta\mathbf{x} \in \Re^{m+2}, \exists\mathbf{D} \in \mathcal{D} \ni \delta\mathbf{x}^T\left(\big(\mathbf{A}_H + \mathbf{A}_S(\mathbf{D})\big)\mathbf{x}^0 - \tilde{\mathbf{v}}_x\right) \le 0 \tag{3.11}$$

To more easily analyze the implications of the condition in Eq. (3.11), let $\delta\mathbf{x}$ be decomposed into two vectors, as

$$\delta\mathbf{x} = \mathbf{x}^0 q_1 + \begin{bmatrix} \mathbf{I}_{m+1} \\ \mathbf{0}_{1\times m+1} \end{bmatrix} \mathbf{q}_2 \tag{3.12}$$

Note that the mapping from $\delta\mathbf{x}$ to $\{q_1,\mathbf{q}_2\}$ is invertible, so long as $V_S^0 > 0$. With $\delta\mathbf{x}$ decomposed as such, Eq. (3.11) becomes

$$\left(q_1\mathbf{x}^{0T} + \mathbf{q}_2^T\begin{bmatrix}\mathbf{I} & \mathbf{0}\end{bmatrix}\right)\left(\left(\mathbf{A}_H + \mathbf{A}_S(\mathbf{D})\right)\mathbf{x}^0 - \tilde{\mathbf{v}}_x\right) \le 0 \quad \forall q_1 \in \Re\ ,\ \ \mathbf{q}_2 \in \Re^{m+1} \tag{3.13}$$

yielding two sufficient conditions for switching equilibrium as

$$q_1\mathbf{x}^{0T}\left(\left(\mathbf{A}_H + \mathbf{A}_S(\mathbf{D})\right)\mathbf{x}^0 - \tilde{\mathbf{v}}_x\right) \le 0 \quad \forall q_1 \in \Re \tag{3.14a}$$

$$\mathbf{q}_2^T\begin{bmatrix}\mathbf{I} & \mathbf{0}\end{bmatrix}\left(\left(\mathbf{A}_H + \mathbf{A}_S(\mathbf{D})\right)\mathbf{x}^0 - \tilde{\mathbf{v}}_x\right) \le 0 \quad \forall \mathbf{q}_2 \in \Re^{m+1} \tag{3.14b}$$

Consider condition (3.14a). Recognizing that quadratic expressions are identically zero for skew matrices, it can be simplified to

$$q_1\left(\mathbf{x}^{0T}\mathbf{A}_H\mathbf{x}^0 - \mathbf{x}^{0T}\tilde{\mathbf{v}}_x\right) \le 0 \quad \forall q_1 \in \Re \tag{3.15}$$

If (3.6) holds, this expression is identically zero. Now, consider condition (3.14b). Substituting components of the vectors and matrices gives

$$\mathbf{q}_2^T\begin{bmatrix} -\dfrac{2R_1}{K_{f1}^2}f_{e1}^0 - \dfrac{V_{sw1}}{K_{f1}}\operatorname{sgn}\left(f_{e1}^0\right) - v_1 + \dfrac{D_1}{K_{f1}}V_S^0 \\ \vdots \\ -\dfrac{2R_m}{K_{fm}^2}f_{em}^0 - \dfrac{V_{swm}}{K_{fm}}\operatorname{sgn}\left(f_{em}^0\right) - v_m + \dfrac{D_m}{K_{fm}}V_S^0 \\ -R_R i_R^0 - V_{swR}\operatorname{sgn}\left(i_R^0\right) + V_S^0 D_R \end{bmatrix} \le 0 \tag{3.16}$$

For a given $\mathbf{q}_2$, there must exist a $\mathbf{D}\in\mathcal{D}$ such that its components yield an inner product in Eq. (3.16) which is less than or equal to zero. Because $\mathbf{q}_2$ is arbitrary, this requirement is satisfied if and only if

$$\max_k\left|\frac{2R_k}{K_{fk}}f_{ek}^0 + V_{swk}\operatorname{sgn}\left(f_{ek}^0\right) + K_{fk}v_k\right| \le V_S^0 \tag{3.17a}$$

$$0 \le R_R i_R^0 + V_{swR}\operatorname{sgn}\left(i_R^0\right) \le V_S^0 \tag{3.17b}$$

These equations are equivalent to (2.16) and (2.27), respectively.

Thus, (2.14), (2.16), (2.27) and (3.6) are necessary and sufficient conditions for $\mathbf{x}^0$ to be a s.e.p.

3.3: Force Capability

With the assumption that **v** may be treated as a slowly-varying parameter, we now use the analyis of the stability of operating points $\mathbf{x}^0$ from Section 3.2 to find the resultant implications for the forces $\mathbf{f}_e^0$ achievable at a given velocity **v**.

3.3.1: The Region of Feasible Forces

The *Region of Feasible Forces* is the region in $\mathbf{f}_e^0$-space of electromechanical forces for which switching equilibrium is possible at a given **v**. In this section, its mathematical expression is derived. This expression is analogous to Eq. (1.3) for the ideal RFA network.

<u>DEFINITION</u>: (Region of Feasible Forces): The *Region of Feasible Forces*, denoted $S(\mathbf{v})$, is defined as

$$S(\mathbf{v}) = \left\{ \mathbf{f}_e^0 \in \Re^m \;\middle|\; \exists\, i_R^0, V_S^0 \in \Re \text{ and } \mathbf{F} : \Re^{m+2} \mapsto \Re^{m+1} \;\ni\; \mathbf{x}^0 = \left[\mathbf{f}_e^{0T} \;\; i_R^0 \;\; V_S^0 \right]^T \text{ a s.e.p.} \right\} \quad (3.18)$$

Furthermore, its boundary is denoted as $\partial S(\mathbf{v})$.

The equations determining $S(\mathbf{v})$ are (2.14), (3.17) and (3.6). Combining Eqs. (3.17b) and (3.6) to eliminate i_R^0 gives

$$-V_S^0 \left(\frac{\max\left\{ V_S^0 - V_{swR}, 0 \right\}}{R_R} + \frac{V_S^0}{R_S} \right) \le \mathbf{f}_e^{0T} \left(\mathbf{K}_f^{-2} \mathbf{R}_f \mathbf{f}_e^0 + \tilde{\mathbf{v}} \right) \le -\frac{V_S^{02}}{R_S} \quad (3.19)$$

Combining Eqs. (3.17a) and (2.14) gives a lower bound for V_S^0 as

$$\max\left\{ \left\| \mathbf{K}_f \mathbf{v} \right\|_\infty ,\; \left\| \mathbf{K}_f \tilde{\mathbf{v}} + \mathbf{K}_f^{-1} \mathbf{R} \mathbf{f}_e^0 \right\|_\infty \right\} \le V_S^0 \quad (3.20)$$

Combining Eqs. (3.19) and (3.20) to eliminate V_S^0 gives the equation for $S(\mathbf{v})$ as

$$\mathbf{f}_e^{0T} \left(\mathbf{K}_f^{-2} \mathbf{R}_f \mathbf{f}_e^0 + \tilde{\mathbf{v}} \right) \le -\frac{1}{R_S} \max\left\{ \left\| \mathbf{K}_f \mathbf{v} \right\|_\infty^2 ,\; \left\| \mathbf{K}_f \tilde{\mathbf{v}} + \mathbf{K}_f^{-1} \mathbf{R} \mathbf{f}_e^0 \right\|_\infty^2 \right\} \quad (3.21)$$

It is useful to interpret Eq. (3.21) graphically. To do this, first define

$$\mathbf{C}_c = \mathbf{R}_f^{-1} \mathbf{K}_f^2 \quad (3.22)$$

and consider the case where $\|\mathbf{v}\| >> \|\mathbf{v}_{sw}\|$. In this case, $\mathbf{v} \approx \tilde{\mathbf{v}}$. Assuming also that R_S is extremely large, Eq. (3.21) is approximately

$$\mathbf{f}_e^{0T}\left(\mathbf{C}_c^{-1}\mathbf{f}_e^0+\mathbf{v}\right)\le 0 \tag{3.23}$$

or, by completing the square

$$\left(2\mathbf{C}_c^{-1}\mathbf{f}_e^0+\mathbf{v}\right)^T\mathbf{C}_c\left(2\mathbf{C}_c^{-1}\mathbf{f}_e^0+\mathbf{v}\right)\le \mathbf{v}^T\mathbf{C}_c\mathbf{v} \tag{3.24}$$

The region described by the expression above is an ellipsoid in $\mathbf{f}_e$-space, centered at $-\mathbf{C}_c\mathbf{v}/2$. For $m = 2$, this ellipse is shown in Fig. 3.1.

Note that the center of $S(\mathbf{v})$ increases linearly with the magnitude of the velocity vector, $\mathbf{v}$. Also of interest are its principal axes. For the jth direction, the size of the principal axis is

$$\sqrt{\sum_{k=1}^{m}\frac{K_{fj}^2\left(K_{fk}v_k\right)^2}{16R_jR_k}}$$

Thus, the dimensions of $S(\mathbf{v})$ increase linearly with velocity magnitude. Also, notice that the boundary of the operating region intersects the origin. At this intersection, the tangent to the boundary is orthogonal to $\mathbf{v}$.

Consider the case where the direction of $\mathbf{v}$ is fixed, as its magnitude is varied. For a fixed force range, plots of $\mathcal{S}(\mathbf{v})$ are shown in Fig. 3.2. As $\|\mathbf{v}\|$ becomes large, $\mathcal{S}(\mathbf{v})$ approaches the ideal plane boundary expressed by Eq. (1.3).

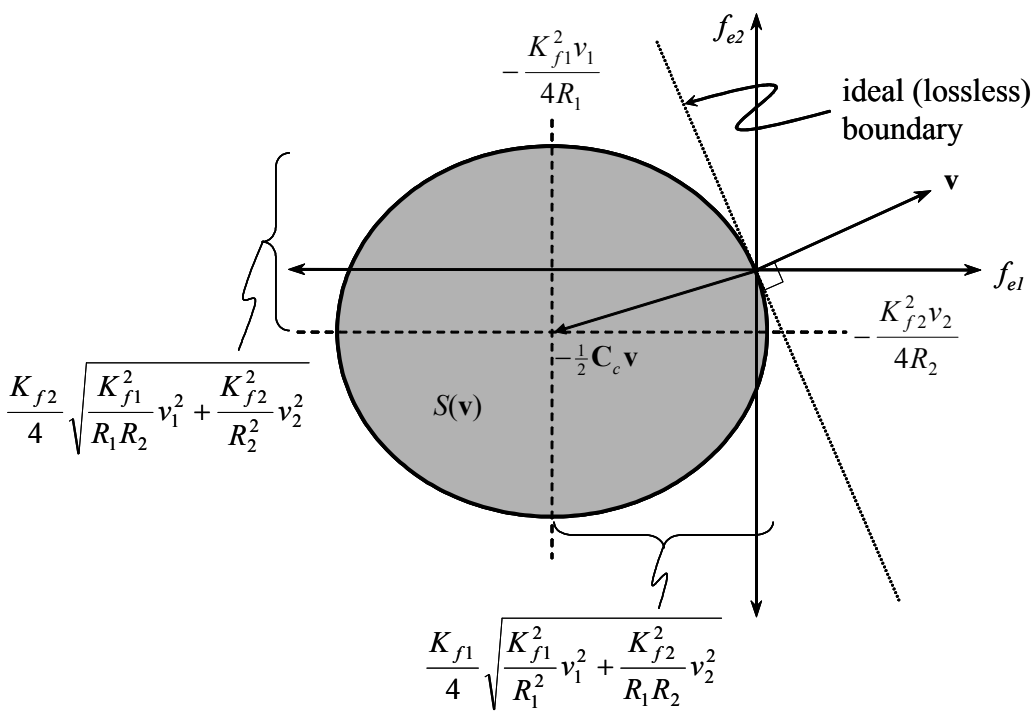

Figure 3.1: Approximate $S(\mathbf{v})$ for $m = 2$, for arbitrary velocity vector $\mathbf{v}$

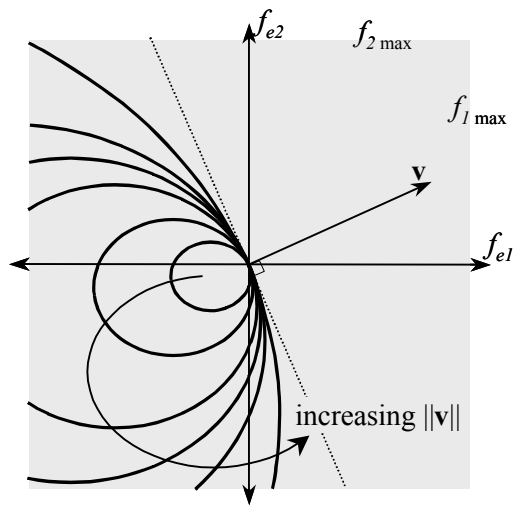

Figure 3.2: $\partial S(\mathbf{v})$ in region of interest for increasing $\|\mathbf{v}\|$

3.3.2: Secondary Attributes of the Region of Feasible Forces

To get a more realistic picture of $S(\mathbf{v})$, let R_S be finite, causing the term on the right-hand side of Eq. (3.21) to be nonzero. Assuming again that $\mathbf{v} \approx \tilde{\mathbf{v}}$, Eq. (3.21) can be conservatively approximated by

$$\mathbf{f}_e^{0T}\left(\mathbf{K}_f^{-2}\mathbf{R}_f\mathbf{f}_e^0 + \mathbf{v}\right) \le -\frac{1}{R_S}\left(\left\|\mathbf{K}_f\mathbf{v}\right\|_2^2 + \left\|\mathbf{K}_f\mathbf{v} + \mathbf{K}_f^{-1}\mathbf{R}_f\mathbf{f}_e^0\right\|_2^2\right) \tag{3.25}$$

or, equivalently,

$$\mathbf{f}_e^{0T}\left(\mathbf{I}+\boldsymbol{\Xi}\right)\left(\mathbf{C}_c^{-1}\left(\mathbf{I}+\boldsymbol{\Xi}\right)\mathbf{f}_e^0 + \boldsymbol{\Psi}\mathbf{v}\right) \le -2\mathbf{v}^T\mathbf{C}_c\boldsymbol{\Xi}\mathbf{v} \tag{3.26}$$

where

$$\begin{aligned}\boldsymbol{\Xi} &= \mathbf{R}_f / R_S \\ \boldsymbol{\Psi} &= \left(\mathbf{I}+\boldsymbol{\Xi}\right)^{-1}\left(\mathbf{I}+2\boldsymbol{\Xi}\right)\end{aligned} \tag{3.27}$$

Completing the square gives

$$\left(2\mathbf{C}_c^{-1}\left(\mathbf{I}+\boldsymbol{\Xi}\right)\mathbf{f}_e^0 + \boldsymbol{\Psi}\,\mathbf{v}\right)^T\mathbf{C}_c\left(2\mathbf{C}_c^{-1}\left(\mathbf{I}+\boldsymbol{\Xi}\right)\mathbf{f}_e^0 + \boldsymbol{\Psi}\,\mathbf{v}\right) \le \mathbf{v}^T\mathbf{C}_c\left(-8\boldsymbol{\Xi} + \boldsymbol{\Psi}^2\right)\mathbf{v} \tag{3.28}$$

For the RFA network to be effective, $R_S >> R_k$ for $k \in \{1..m\}$. Thus, it is the case that $\boldsymbol{\Xi}^2 \approx \mathbf{0}$, $\boldsymbol{\Psi} \approx \mathbf{I}+\boldsymbol{\Xi}$, and $\boldsymbol{\Psi}^2 \approx \mathbf{I}+2\boldsymbol{\Xi}$. If these approximations hold, then Eq. (3.28) may be very closely approximated by

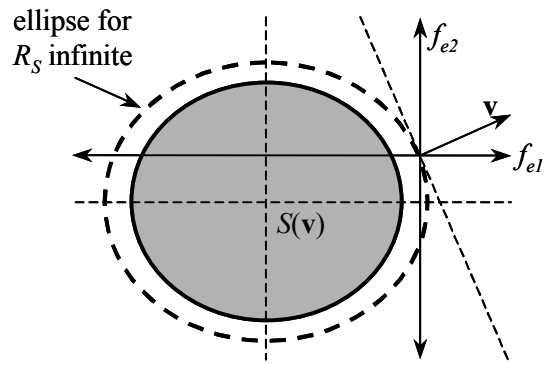

Figure 3.3: $S(\mathbf{v})$ for finite R_S

$$\left(2\mathbf{C}_c^{-1}\mathbf{f}_e^0 + \mathbf{v}\right)^T \mathbf{C}_c\left(\mathbf{I} + 2\Xi\right)\left(2\mathbf{C}_c^{-1}\mathbf{f}_e^0 + \mathbf{v}\right) \le \mathbf{v}^T\mathbf{C}_c\left(\mathbf{I} - 6\Xi\right)\mathbf{v} \tag{3.29}$$

Thus, the result of finite R_S is a slight "shrinking" of the elliptical operating region, as shown in Fig. 3.3. This shrinking approximately preserves the elliptic shape of the boundary.

Now, removing the remaining approximation, let $\mathbf{v} \ne \tilde{\mathbf{v}}$. Then Eq. (3.28) becomes

$$\left(2\mathbf{C}_c^{-1}\mathbf{f}_e^0 + \tilde{\mathbf{v}}\right)^T \mathbf{C}_c\left(\mathbf{I} + 2\Xi\right)\left(2\mathbf{C}_c^{-1}\mathbf{f}_e^0 + \tilde{\mathbf{v}}\right) \le \tilde{\mathbf{v}}^T\mathbf{C}_c\left(\mathbf{I} - 2\Xi\right)\tilde{\mathbf{v}} - 4\mathbf{v}^T\mathbf{C}_c\Xi\mathbf{v} \tag{3.30}$$

This impacts Fig. 3.3 by shifting the center of the ellipse, depending on which quadrant of $\mathbf{f}_e$-space contains the boundary point. This "shifting" phenomenon is shown in Fig. 3.4. The principal axes of these various ellipses will also be different sizes. For $\|\mathbf{v}\|$ large, this effect is subtle, but at low $\|\mathbf{v}\|$ it dominates. Most importantly, it presents a finite velocity below which $S(\mathbf{v})$ vanishes (except for the origin). This constraint on the system can be expressed as

$$\max_k \left|v_k / v_{swk}\right| \le 1 \quad \Rightarrow \quad \mathrm{S}(\mathbf{v}) = \{\mathbf{0}\} \tag{3.31}$$

where $\mathbf{v} = \{v_1 \,..\, v_m\}^T$ and $\mathbf{v}_{sw} = \{v_{sw1} \,..\, v_{swm}\}^T$. When the components of $\mathbf{v}$ just above the critical condition in Eq. (3.31), $S(\mathbf{v})$ is highly distorted. As $\|\mathbf{v}\|$ increases along a given direction, the operating region approaches its elliptical shape in Fig. 3.3.

3.3.3: Force Ratings

Each machine $k \in \{1..m\}$ has a rated current, $i_{k\,\max}$, which cannot be exceeded without resulting in thermal damage. This results in an effective force rating $f_{k\,\max}$ for each actuator. Unlike the physical limitations resulting in $S(\mathbf{v})$, the limitations arising from these force ratings are not implied by the system description in Eq. (2.29). Rather, any control intelligence which

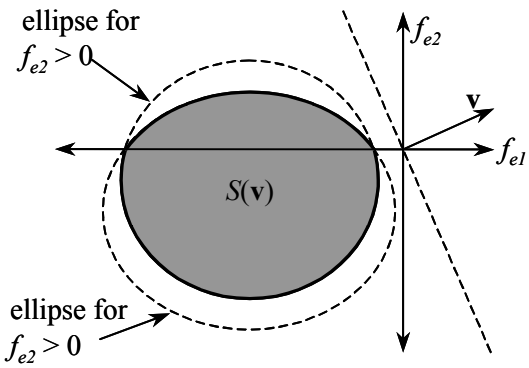

Figure 3.4: Distortion of $S(\mathbf{v})$ for low $\|\mathbf{v}\|$, due to switching losses

uses this system must explicitly impose limits on the forces which the system may be commanded to achieve.

3.4: Effect of Energy Storage on Force Capability

The concept of the Region of Feasible Forces is independent of the possible existence of flywheel energy storage in the RFA network. If a flywheel exists, it is simply treated as another degree of freedom in the mechanical system, as discussed in the previous chapter. As defined in Eq. (2.33), the linear forces $\mathbf{f}_{el}$ and $\mathbf{f}_l$ are augmented with the flywheel torques T_{efw} and T_{fw}, to obtain $\mathbf{f}_e$ and $\mathbf{f}$. Similarly, the linear velocity vector $\mathbf{v}_l$ is augmented with the flywheel rotational velocity ω_{fw} to obtain $\mathbf{v}$.

Separating the flywheel variables from the linear actuator variables in Eq. (3.24) gives

$$\left(2\mathbf{C}_{cl}^{-1}\mathbf{f}_{el}^{0}+\mathbf{v}_l\right)^T\mathbf{C}_{cl}\left(2\mathbf{C}_{cl}^{-1}\mathbf{f}_{el}^{0}+\mathbf{v}_l\right)\le\mathbf{v}_l^T\mathbf{C}_{cl}\mathbf{v}_l-\frac{8R_{fw}}{K_{tfw}^2}T_{fw}^2-4T_{fw}\omega_{fw} \tag{3.32}$$

with $\mathbf{C}_{cl}$ appropriately defined. Define the power flow P_E as

$$P_E=-\frac{2R_{fw}}{K_{tfw}^2}T_{fw}^2-T_{fw}\omega_{fw} \tag{3.33}$$

This is the electrical power generated by the flywheel minus the dissipation incurred in transmission to the rest of the network. The value of T_{fw} which maximizes P_E, subject to the condition that $|T_{fw}| \le T_{fw\max}$, is equal to

$$T_{fw}=-\max\left\{\frac{K_{tfw}^2}{4R_{fw}}\left|\omega_{fw}\right|\ ,\ T_{fw\max}\right\}\operatorname{sgn}\left(\omega_{fw}\right) \tag{3.34}$$

Defining ω_{fwc} as

$$\omega_{fwc} = \frac{4R_{fw}}{K_{tfw}^2} T_{fw\max} \tag{3.35}$$

P_E therefore has an upper bound, $P_E^{\max}$, dictated by

$$P_E^{\max} = \begin{cases} \dfrac{K_{tfw}^2}{8R_{fw}} \omega_{fw}^2 & : \quad |\omega_{fw}| \le \omega_{fwc} \\ \dfrac{K_{tfw}^2}{8R_{fw}} \omega_{fw}^2 - \dfrac{K_{tfw}^2}{8R_{fw}} \left(|\omega_{fw}| - \omega_{fwc} \right)^2 & : \quad |\omega_{fw}| \ge \omega_{fwc} \end{cases} \tag{3.36}$$

This upper bound on P_E signifies that the flywheel has a limit to how much power it can deliver to the rest of the system, which depends on the flywheel torque rating and rotational velocity.

The discussion above can be framed directly in terms of flywheel energy storage. The energy stored in the flywheel is

$$E_{fw} = \tfrac{1}{2} J_{fw} \omega_{fw}^2 \tag{3.37}$$

Define quantities τ_E and E_{fwc} as

$$\tau_E = \frac{4R_{fw} J_{fw}}{K_{tfw}^2} \quad , \quad E_{fwc} = \tfrac{1}{2} J_{fw} \omega_{fwc}^2 = \frac{T_{fw\max}^2}{2J_{fw}\tau_E^2} \tag{3.38}$$

Then $P_E^{\max}$ is

$$P_E^{\max} = \begin{cases} \dfrac{1}{\tau_E} E_{fw} & : \quad E_{fw} \le E_{fwc} \\ \dfrac{1}{\tau_E} E_{fw} - \dfrac{1}{\tau_E} \left(\sqrt{E_{fw}} - \sqrt{E_{fwc}} \right)^2 & : \quad E_{fw} \ge E_{fwc} \end{cases} \tag{3.39}$$

A graph of $P_E^{\max}$ vs. E_{fw} is shown in Fig. 3.5. This illustrates that, as E_{fw} becomes larger, the ability of the flywheel to deliver power to the DC bus becomes hampered, due to the torque rating $T_{fw\max}$.

It is interesting at this point to consider the region in $\mathbf{f}_{el}$-space of linear forces which are possible at a given linear velocity $\mathbf{v}_l$, and given an amount of energy E_{fw} stored in the flywheel. This region will be called $S_l(\mathbf{v}_l, E_{fw})$. Using Eqs. (3.39) and (3.32), an approximate expression for $S_l(\mathbf{v}_l, E_{fw})$ (which neglects switching and DC bus losses) can be found as

$$\left(2\mathbf{C}_{cl}^{-1}\mathbf{f}_{el}^0 + \mathbf{v}_l \right)^T \mathbf{C}_{cl} \left(2\mathbf{C}_{cl}^{-1}\mathbf{f}_{el}^0 + \mathbf{v}_l \right) \le \mathbf{v}_l^T \mathbf{C}_{cl} \mathbf{v}_l + P_E^{\max}\left(E_{fw} \right) \tag{3.40}$$

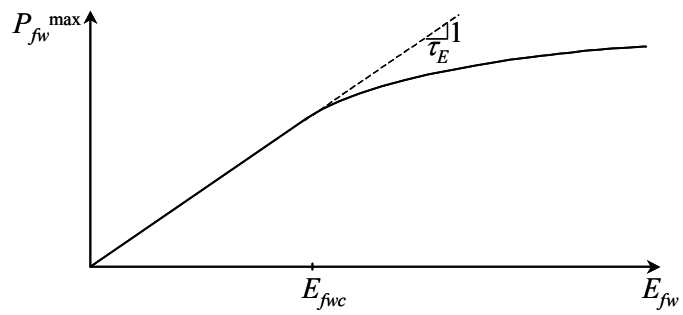

Figure 3.5: Upper bound on P_E, as a function of the flywheel energy E_{fw}

Illustrations of the boundary ∂S_l are shown in Fig. 3.6, for increasing values of E_{fw}, for the region of $\mathbf{f}_{el}$-space bounded by the maximum force ratings of the linear actuators. For all E_{fw}, S_l retains its elliptical shape, as well as its center. As E_{fw} grows, the principle axes of S_l increase uniformly, expanding the ellipsoidal region. For E_{fw} extremely large, the system becomes capable of realizing any linear force $\mathbf{f}_{el}$ within ratings.

Thus, we arrive at the expected conclusion that, with sufficient energy storage, RFA networks behave the same as fully active forcing systems. However, as stored energy increases, the transition from energy-constrained operation to fully-active operation is gradual. This is because, for energy from the flywheel to be delivered to the DC bus, some energy must be dissipated in the flywheel stator coils. There is a maximum rate at which energy can be drawn from the flywheel, above which the energy dissipated in transmission exceeds the energy extracted from the flywheel. Operation above this level effectively has *negative* efficiency, and reduces the size of S_l. Such operation is therefore undesirable.

The effect of dissipation in the switches and R_S can be incorporated into Eq. (3.40) for $S_l(\mathbf{v}_l, E_{fw})$ in a manner analogous to that of the previous section for $S(\mathbf{v})$. The most significant change resulting from this, aside from distortions to S_l similar to those for $S(\mathbf{v})$, is that the flywheel back EMF must overcome the switch conduction voltage V_{fwsw} before power delivery to the DC bus can take place. This modifies $P_E^{\max}$ to the expression

$$P_E^{\max} = \begin{cases} \dfrac{1}{\tau_E}\bar{E}_{fw} & : \quad \bar{E}_{fw} \le E_{fwc} \\ \dfrac{1}{\tau_E}\bar{E}_{fw} - \dfrac{1}{\tau_E}\left(\sqrt{\bar{E}_{fw}} - \sqrt{E_{fwc}}\right)^2 & : \quad \bar{E}_{fw} \ge E_{fwc} \end{cases} \tag{3.41}$$

where

$$\bar{E}_{fw} = \max\left\{0 \ , \ \sqrt{E_{fw}} - \sqrt{E_{swfw}}\right\}^2 \tag{3.42}$$

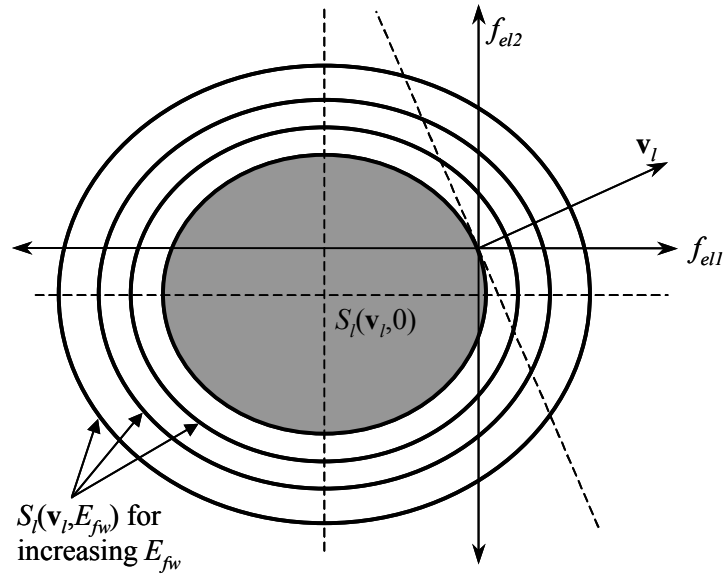

Figure 3.6: Effect of flywheel energy storage on S_l

and where E_{swfw} is the minimum stored energy necessary to overcome switching losses, i.e.,

$$E_{swfw} = \frac{J_{fw} V_{swfw}^2}{2K_{tfw}^2} \tag{3.43}$$

There is therefore a ciritcal energy that must be stored in the flywheel before it may deliver any energy to the DC bus.

3.5: A Two-Machine Example

Consider a two-machine system, with parameters listed in Table 3.1. The two machines have identical electrical properties, and identical rotational mechanical properties. The model for these machines corresponds to a particular Kollmorgen® motor, which was analyzed in (Pillay and Krishnan 1989). This machine has a power rating of about 150W, and would not be of sufficient size for a full-scale Civil Engineering application. However, its size is appropriate for application in scale-model experiments. The screw leads for the two machines are more than an order of magnitude apart. Such a configuration would be useful for an application in which machine 1 is used as an inter-story actuator (for which the velocities would be quite low) and in which machine 2 is used to excite a secondary structure, or a mass damper (for which the velocities would be significantly higher.

Table 3.1: Example Actuator Parameters

R_1, R_2	.29Ω
L_1, L_2	5.9mH
K_{t1}, K_{t2}	0.37N/A
B_1, B_2	0.0001N-m-s
J_1, J_2	0.0002265N-m-s^2
$f_{1\,\max}$	830N
$f_{2\,\max}$	276N
l_1	0.0013m/rad
l_2	0.004m/rad
η_1, η_2	0.9
V_{sw1}, V_{sw2}	1.4V
C_S	40μF
R_S	500Ω
L_R	20mH
R_R	1Ω

The electrical network was designed such that $\tau = 0.02$. The actual inductances of the stator coils are 0.365mH, and the remaining inductance being supplied externally. The switch conduction voltages V_{sw1} and V_{sw2} are equal to twice the conduction voltage of a diode.

3.5.1: Force Capability for an RFA Network with *m*=2

Figure 3.7 shows the analytical $\mathcal{OS}(\mathbf{v})$ for a given direction of **v**, and for various values of

$$\xi = \max_k \{v_k / v_{swk}\} \tag{3.44}$$

Note that the size of the regioin grows very quickly as ξ rises above its critical value. The values of v_{sw1} and v_{sw2} are 0.49 cm/s and 1.5 cm/s, respectively. It is clear that for ξ>2, the system has significant dissipative capability, and that for ξ>5, the power-sharing capability becomes very pronounced. As ξ grows further, the boundary looks similar to that of the ideal RFA network. For large values of ξ, however, the losses incurred in resistor R_S will distort the boundary as shown in Fig. 3.3. However, this effect is largely a secondary phenomenon, and has little impact on the system in the practical range of velocities for which the system is designed.

Fig. 3.7 can be interpreted from the perspective of power flow and energy. For a force $\mathbf{f}_e$ in the quadrant opposite from the one containing **v**, both actuators generate electrical energy, which is dissipated by the network. For $\mathbf{f}_e$ in one of the other two possible quadrants of the feasible force region, one actuator is generating electrical energy, which the network uses to drive the other actuator. It is operation in these regions which is not possible for passive and semiactive devices.

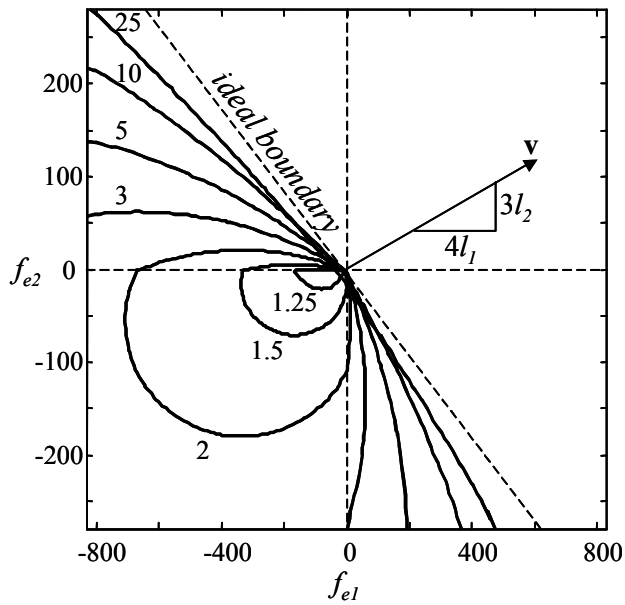

Figure 3.7: $S(\mathbf{v})$, within maximum force ranges, for various values of ξ

For different directions of **v**, the plots look similar, except that the ellipses are distorted in a different way for low **v**. Fig. 3.8 shows these boundaries for v_2=0, with v_1 growing. This plot emphasizes one of the appealing features of RFA networks. Although v_2=0, f_{e2} may still be quite large if v_1 is nonzero, and may be of either sign.

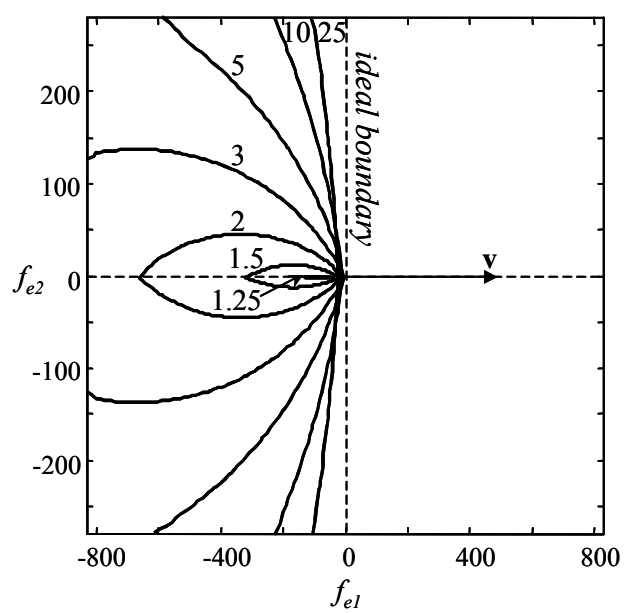

Figure 3.8: $S(\mathbf{v})$, within maximum force ranges, for various values of ξ

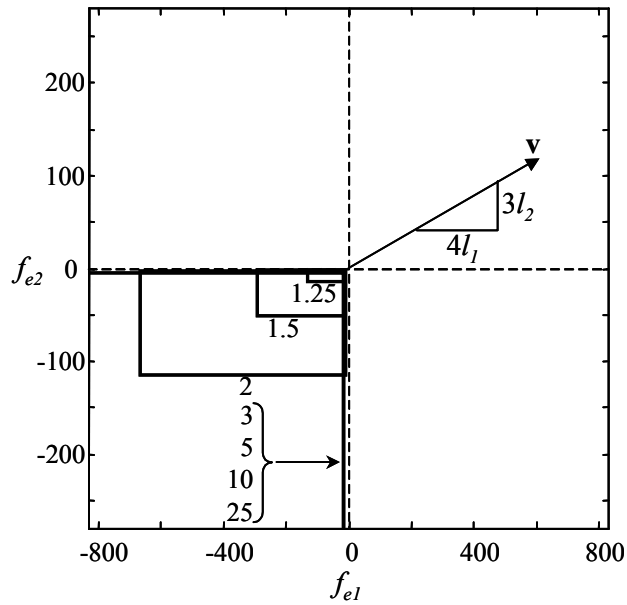

Figure 3.9: Force capability of an equivalent *m*-actuator semiactive system for various ξ

3.5.2: Comparison with a 2-Actuator Semiactive System

It is interesting to compare the forcing capability of an RFA network to that of a *m*-actuator semiactive system, constructed from the same machines and mechanical components. Such semiactive acutators were discussed in the introductory chapter. Each semiactive device can be viewed as an RFA network with only one machine. Fig. 3.9 shows the force capability of 2 such semiactive devicesA comparison between Figs. 3.7 and 3.9 illustrates the force capability which is gained by RFA devices. For ξ low, the difference is slight. For larger velocities, it is pronounced.

3.5.3: Force Capability of a Linear Actuator with Energy Storage

Consider a modified RFA network, using the machines and parameters in Table 1, but with the revision that machine 1 will now be used to drive a remote flywheel. A graph of the range of f_{e2}, for a given flywheel energy E_{fw}, may then be constructed. This is shown in Fig. 3.10. For $E_{fw}<E_{swfw}$ the flywheel energy does not affect the range of force capability of f_{e2}. As E_{fw} increases above E_{swfw}, this range expands at the upper and lower boundaries for a given v_2. Note the depenency of the force range on v_2. As v_2 increases in magnitude, the lower boundary increases as well. However, interestingly, the upper boundary becomes smaller as v_2 increases. Thus, as the velocity of the linear actuator beomes greater, its range of opposing force becomes

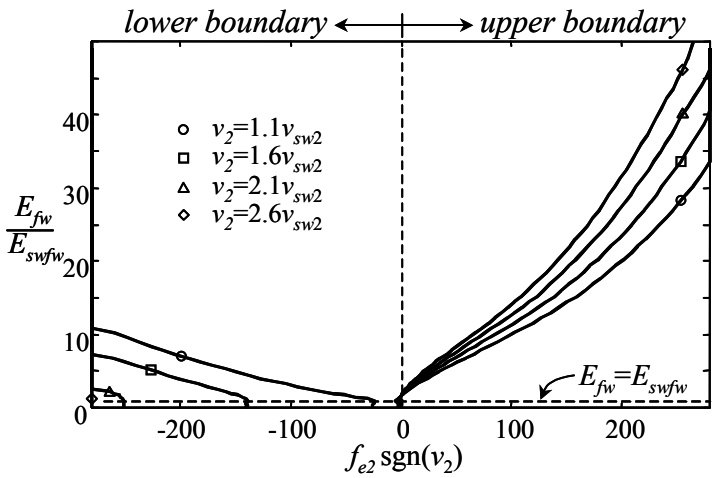

Figure 3.10: $S_l(v_2)$, within maximum force range, for increasing flywheel energy storage E_{fw}

greater while its range of contributing force becomes less. This phenomenon is not taken into account in most studies concerning actuators with ideal regenerative power supplies.

Chapter 4. Switching Control

For a given actuation velocity $\mathbf{v}$, the previous chapter characterized $S(\mathbf{v})$, the Region of Feasible Forces for the system. The approximately elliptical shape of the boundary of this region arises from losses in the electrical system. The development assumed that $\mathbf{v}$ was a slowly-varying parameter, compared to the electrical dynamics.

In this chapter, a feedback controller is developed which facilitates zero-error tracking for a force command $\mathbf{f}_e^*$, assuming $\mathbf{f}_e^* \in S(\mathbf{v})$. This controller relates the switch position vector $\mathbf{D}$ to the electrical state vector $\mathbf{x}$. Following the development of the controller, the dynamics of the closed-loop system are studied, and it is verified that the time constants associated with these dynamics are much smaller than those of the associated mechanical system, justifying the assumption that $\mathbf{v}$ is slowly varying.

The design of this controller is challenging for several reasons. Obviously, the fact that the system is nonlinear complicates the design. However, the greater challenge arises from the fact that the closed-loop performance of the system must be robust to parametric uncertainty in the electrical network. Thus, zero-error tracking is desired, even though it is assumed that the system parameters are not known precisely.

This problem is made more complicated by the fact that, because of this system uncertainty, the boundary $\partial S(\mathbf{v})$ is also uncertain. Thus, a $\mathbf{f}_e^*$ which is in the nominal (i.e., modeled) $S(\mathbf{v})$ may be outside the physical $S(\mathbf{v})$. In this circumstance, force tracking is physically impossible. The controller should be designed to be robust, such that in these circumstances, the system equilibrates to a value of $\mathbf{f}_e$ which is on the boundary of the actual $S(\mathbf{v})$, and somehow "close" to the $\mathbf{f}_e^*$ command.

As an added complication to the control system design, the switches have a maximum frequency at which they can operate. The approach taken in this chapter is to design the switching controller first without considering this constraint. Then, the controller design is modified to accommodate switching frequency limitations.

4.1: Introduction

In Section 3.2, it was shown that the following equations are necessary and sufficient conditions for a state $\mathbf{x}^0 = [\mathbf{f}_e^{0T}\ i_R^0\ V_S^0]^T$ to be a switching equilibrium point.

$$V_S^0 \geq \max\left\{ \left\|\mathbf{K}_f \mathbf{v}\right\|_\infty , \left\|\mathbf{K}_f \tilde{\mathbf{v}} + \mathbf{K}_f^{-1}\mathbf{R}\mathbf{f}_e^0\right\|_\infty \right\} \tag{4.1a}$$

$$0 \leq i_R^0 \leq \max\left\{0, \left(V_S^0 - V_{swR}\right)/R_R\right\} \tag{4.1b}$$

$$\mathbf{f}_e^{0^T}\left(\mathbf{C}_c^{-1}\mathbf{f}_e^0 + \tilde{\mathbf{v}}_f\right) + V_S^{0^2}/R_S + i_R^0\left(V_{swR} + R_R i_R^0\right) = 0 \tag{4.1c}$$

Let the vector $\mathbf{x}^* = \{\mathbf{f}_e^{*T}, i_R^*, V_S^*\}^T$ be a desired set point for the state of the system. Assuming $\mathbf{x}^*$ satisfies expressions (4.1a-c), it is a feasible operating point for the system. Define the deviation $\delta\mathbf{x}$ as

$$\delta\mathbf{x} = \mathbf{x} - \mathbf{x}^* \tag{4.2}$$

Then it is a straight forward procedure to design a switching control rule to drive $\delta\mathbf{x}$ to zero. To see this, define q_1 and $\mathbf{q}_2$ by

$$\delta\mathbf{x} = \mathbf{x}^* q_1 + \begin{bmatrix} \mathbf{I}_{m+1} \\ \mathbf{0} \end{bmatrix}\mathbf{q}_2 \quad , \quad \begin{bmatrix} \mathbf{q}_2 \\ q_1 \end{bmatrix} = \delta\mathbf{x} - \frac{\delta V_S}{V_S^*}\begin{bmatrix} \mathbf{I}_{m+1} & \mathbf{0} \\ \mathbf{0} & 0 \end{bmatrix}\mathbf{x}^* \tag{4.3}$$

Then it follows from Eq. (3.16) that the control law

$$\mathbf{D} = \mathbf{F}(\mathbf{x}) = \mathrm{Dsat}(-\mathbf{q}_2) \tag{4.4}$$

where

$$\{\mathrm{Dsat}(-\mathbf{q}_2)\}_i = \begin{cases} \mathrm{sgn}(-q_{2i}) & : i \in \{1..m\} \\ \frac{1}{2}[1 + \mathrm{sgn}(-q_{2_{m+1}})] & : i = m+1 \end{cases} \tag{4.5}$$

brings about switching equilibrium about $\mathbf{x}^*$.

It can be shown that the above approach, when implemented, equilibrates at $\mathbf{q}_2 = \mathbf{0}$ if inequalities (4.1a) and (4.1b) hold for $\mathbf{x}^*$. However, for $q_1 = 0$ in equilibrium, $\mathbf{x}^*$ must be selected such that Eq. (4.1c) holds. Because (4.1c) is an equality constraint, the set of $\mathbf{x}^*$ satisfying this equation has measure zero in $\Re^{m+2}$, and varies with system parameters. Thus, the controller in Eq. (4.4) requires perfect knowledge of the system parameters in order to accomplish its zero-error tracking objectives.

If tracking fails then q_1 is nonzero, resulting in tracking failure for all the states, including the force vector $\mathbf{f}_e$. A more appealing controller would track $\mathbf{f}_e$ and V_S in the presence of system uncertainties (if physically possible), while adjusting i_R such that the equality (4.1c) holds in equilibrium. In this chapter, a control system is proposed which does not explicitly track a commanded value of i_R. Instead, the switching controller equilibrates the system at a value of i_R^0

necessary to bring about desired behavior in $\mathbf{f}_e$ and V_S. Thus, the control system treats i_R as a "slack" variable.

4.2: Design Goals for Switching Control

Clearly, the first and most fundamental design goal for the switching controller is that $\mathbf{f}_e$ should track its command $\mathbf{f}_e^*$.

To ensure that this happens, V_S must be controlled to ensure that condition (4.1a) holds. To conservatively account for system uncertainties, the command V_S^* is assigned as

$$V_S^* = K_v \max\left\{ \left\|\mathbf{K}_f \mathbf{v}\right\|_\infty, \left\|\mathbf{K}_f \tilde{\mathbf{v}} + \mathbf{K}_f^{-1}\mathbf{R}\mathbf{f}_e^*\right\|_\infty \right\} \tag{4.6}$$

where K_v>1 is a design parameter (a typical value might be 2). However, it may not be possible for $V_S^0 = V_S^*$ in equilibrium, because the upper bound of (4.1b) for i_R^0 may not be satisfied. However, because i_R^0 is considered to be uncertain, it is impossible to explicitly enforce condition (4.1b). Recognizing that it is acceptable for $V_S^0 > V_S^*$ (i.e., it does not affect the inequality in (4.1a)), this problem can be accommodated by requiring that the switching controller yield a value of V_S^0 which has a lower bound of V_S^*, rather than requiring $V_S^0 = V_S^*$.

The fact that K_v>1 in Eq. (4.6) implies that the lower bound for V_S^0 is more conservative than condition (4.1a). Thus, the region of $\mathbf{f}_e^*$ commands for which $V_S^0 \geq V_S^*$ and $\mathbf{f}_e^0 = \mathbf{f}_e^*$ is therefore a subset of $S(\mathbf{v})$, which will be denoted as $S_{Kv}(\mathbf{v})$; i.e.,

$$S_{Kv}(\mathbf{v}) = \left\{ \mathbf{f}_e^* \in \Re^m \;\; | \;\; \mathbf{f}_e^{*T}\mathbf{C}_c^{-1}\mathbf{f}_e^* + \mathbf{f}_e^{*T}\tilde{\mathbf{v}} + V_S^{*2}\left(\mathbf{v}, \mathbf{f}_e^*\right)/R_S \leq 0 \right\} \tag{4.7}$$

Note that $S_{Kv}(\mathbf{v}) = S(\mathbf{v})$ when $K_v = 1$. Because R_S is quite large, the difference between S_{Kv} and S is typically subtle.

With these definitions, we can formally state the design goals for the feedback controller. The controller will be of the form

$$\mathbf{D} = \mathbf{F}\left(\mathbf{f}_e, V_S; \mathbf{f}_e^*, \mathbf{v}\right) \tag{4.8}$$

where $\mathbf{F}$ is a memoryless function of $\mathbf{f}_e$ and V_S, but not of i_R. Furthermore, $\mathbf{F}$ also depends on the command $\mathbf{f}_e^*$ and $\mathbf{v}$ (and therefore on V_S^* through Eq. (4.6)). The closed-loop performance of the controller must meet the following requirements:

(D1): Design requirement 1

In closed loop, $\mathbf{f}_e^0 = \mathbf{f}_e^*$ whenever $\mathbf{f}_e^* \in S_{Kv}(\mathbf{v})$.

(D2): Design requirement 2

In closed loop, $V_S^0 \geq V_S^*$ whenever $\mathbf{f}_e^* \in S_{Kv}(\mathbf{v})$.

4.3: Quasi-Lyapunov Switching Control

To restate the design goals from Section 4.2 in a more tractable way, define

$$\begin{aligned} \delta\mathbf{f}_e &= \mathbf{f}_e - \mathbf{f}_e^* \\ \delta V_S &= V_S - V_S^* \end{aligned} \tag{4.9}$$

and define the function U_1 as

$$U_1 = \frac{1}{2}\delta\mathbf{f}_e^T \mathbf{C}_c^{-1} \delta\mathbf{f}_e + \frac{1}{2R_S}\delta V_S^2 \mathrm{hvs}\left(-\delta V_S\right) \tag{4.10}$$

where hvs(.) is the Heaviside step function. Fig. 4.1 shows a contour map of U_1 in a cross section of $\{\delta\mathbf{f}_e, \delta V_S\}$-space with coordinates δV_S and $\mathbf{a}^T\delta\mathbf{f}_e$, where $\mathbf{a}$ is an arbitrary vector in $\Re^m$. The contour map looks similar for any $\mathbf{a}$. Consider that if the switch position vector $\mathbf{D}$ is related to $\delta\mathbf{f}_e$ and δV_S such that the derivative of U_1 has the property

$$\begin{aligned} &\frac{d}{dt}U_1 \leq 0 \quad , \quad \forall\{\delta\mathbf{f}_e, \delta V_S\} \in \Re^{m+1} \\ &\frac{d}{dt}U_1 = 0 \quad \Leftrightarrow \quad U_1 = 0 \end{aligned} \tag{4.11}$$

then the $\{\delta\mathbf{f}_e, \delta V_S\}$ trajectory is guaranteed to approach the set H as $t \to \infty$., where H is defined as

$$H = \left\{\{\delta\mathbf{f}_e, \delta V_S\} \in \Re^m \times \Re \mid \delta\mathbf{f}_e = \mathbf{0}, \delta V_S \geq 0\right\} \tag{4.12}$$

Thus, for large t, the system would behave approximately as if confined to H. This would result in satisfaction of design requirement D1.

A control system satisfying Eq. (4.11) would also guarantee that $\delta V_S \geq 0$ as $t \to \infty$. However, it does not guarantee that V_S stabilizes about an equilibrium V_S^0. Thus, the equilibrium condition

$$\exists \delta V_S^0 \geq 0 \quad | \quad \delta V_S(t) \to \delta V_S^0 \quad \text{as} \quad t \to \infty \tag{4.13}$$

must also be imposed on the controller.

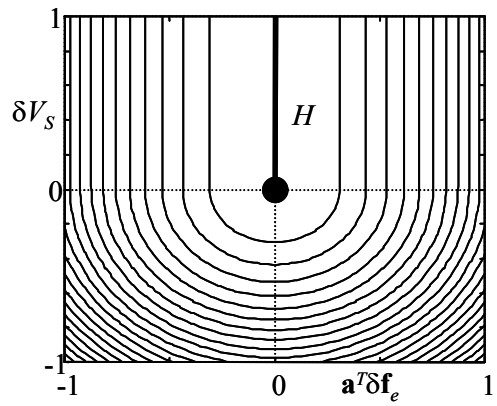

Figure 4.1: Cross section contour of U_1

The theorem below shows that it is possible to choose a feedback law **F** such that conditions (4.11) and (4.13) are true.

<u>THEOREM 4.1</u>: For any $\mathbf{f}_e^* \in S_{Kv}(\mathbf{v})$, design goals D1 and D2 are met by the feedback law

$$\mathbf{F}\left(\delta\mathbf{f}_e, \delta V_S^*\right) = \mathrm{Dsat}\left(\begin{bmatrix} -\mathbf{I} & \dfrac{\mathbf{f}_e^* u(-\delta V_S)}{V_S^*} \\ \mathbf{0} & 1 \end{bmatrix}\begin{bmatrix} \delta\mathbf{f}_e \\ \delta V_S \end{bmatrix}\right) \tag{4.14}$$

and there exists a unique $\delta V_S^0 \geq 0$ satisfying (4.13) for the closed-loop system. Furthermore,

$$\left[\delta\mathbf{f}_e(t)^T \mathbf{C}_c^{-1}\delta\mathbf{f}_e(t)\right]^{1/2} \leq e^{-t/\tau}\left[\delta\mathbf{f}_e(0)^T \mathbf{C}_c^{-1}\delta\mathbf{f}_e(0) + \delta V_S^2(0)/R_S\right]^{1/2} \quad , \ t > 0 \tag{4.15}$$

where τ is the universal electrical time constant assigned in (2.32).

proof: See Appendix A4.

Qualitatively speaking, Theorem 4.1 states that the **F** in (4.14) achieves zero-error tracking between $\mathbf{f}_e$ and $\mathbf{f}_e^*$, and equilibrates V_S at a value $V_S^0 \geq V_S^*$, with V_S^* specifically defined by Eq. (4.6). For all $\mathbf{f}_e^*$ in $S_{Kv}(\mathbf{v})$, the values of $\delta\mathbf{f}_e(t)$ decay to zero, bounded from above by (4.15).

There are subtleties concerning the performance of the switching controller in (4.14) which require some more attention. There are essentially two issues of importance.

Robustness to Uncertainty for Commands Near ∂S

Note that Eq. (4.14) does not depend explicitly on the system parameters. (Although the system parameters are needed to compute V_S^*, the conservative multiplicative factor K_v makes the

force-tracking controller insensitive to parameter uncertainty.) So the controller in Eq. (4.14) is a parameter-independent feedback controller that yields zero-error tracking if $\mathbf{f}_e^* \in S_{Kv}(\mathbf{v})$.

To assure that $\mathbf{f}_e^* \in S_{Kv}(\mathbf{v})$, knowledge of the system parameters is required. Satisfaction of this condition may be guaranteed if bounds are known on the system uncertainty, by requiring that $\mathbf{f}_e^* \in S_{Kv}(\mathbf{v})$ for any perturbations in the uncertain system parameters which lie in an admissible set. This approach, while technically valid, would restrict the force capability of the RFA system by conservatively approximating $\partial S(\mathbf{v})$. A better approach is to ensure that when $\mathbf{f}_e^* \notin S_{Kv}(\mathbf{v})$, the system naturally equilibrates to a force $\mathbf{f}_e^0$ which is somehow "close" to $\mathbf{f}_e^*$. It will be shown that the controller in Eq. (4.14) has arbitrarily bad robustness properties for $\mathbf{f}_e^* \notin S_{Kv}(\mathbf{v})$ but arbitrarily near $\partial S_{Kv}(\mathbf{v})$. The controller needs to be enhanced to be robust in such circumstances. One method for doing this is presented in Sections 4.4 and 4.5.

Switching Frequency Limitations

There is a maximum frequency at which the switches in the system may be made to operate, above which the transient behavior and the high rate of dissipation in the switches during transition become prohibitive. The controller in Eq. (4.14) does not account for this limitation. If not explicitly addressed in the design, the resultant effect of switching delay, called "chattering", can have unanticipated and highly undesirable consequences. Here, the problem is remedied in a standard way, by imposing hysteresis bands for the saturation function in Eq. (4.14). This issue is addressed in Section 4.6.

4.4: System Uncertainty and Its Consequences

Uncertainty in the system arises from several factors. The parameters of the system cannot be known precisely, and may change with time. For instance, the K_f constants for each machine may vary, depending on the machine temperature, and the amount of current it is conducting. There may also be some uncertainty in the velocities arising from measurement error and, more importantly, from the time delay between measurement and control decisions.

To formalize the discussion, a mathematical description of the system uncertainty is needed. For the purposes of this analysis, the uncertainty will be treated as a deviation in the velocity vector. Let the nominal values of $\mathbf{v}$ and $\tilde{\mathbf{v}}$ be $\mathbf{v}_0$ and $\tilde{\mathbf{v}}_0$, respectively, and assume additive uncertainty of the form

$$\begin{aligned} \mathbf{v} &= \mathbf{v}_0 + \delta\mathbf{v} \\ \tilde{\mathbf{v}} &= \tilde{\mathbf{v}}_0 + \delta\tilde{\mathbf{v}} \end{aligned} \tag{4.16}$$

where the uncertainties have some known error bound

$$\begin{aligned} |\delta\mathbf{v}| &\le \delta\mathbf{v}_{\max} \\ |\delta\tilde{\mathbf{v}}| &\le \delta\tilde{\mathbf{v}}_{\max} \end{aligned} \tag{4.17}$$

It will also be convenient to assume that the uncertainty obeys the proportional bound

$$\frac{\delta\tilde{\mathbf{v}}^T \mathbf{C}_c \delta\tilde{\mathbf{v}}}{\tilde{\mathbf{v}}_0^T \mathbf{C}_c \tilde{\mathbf{v}}_0} \le r^2 \tag{4.18}$$

Design requirements D1 and D2 assume that inequalities (4.1a) and (4.7) hold. With the bounds in inequality (4.17), condition (4.1a) may be conservatively ensured by the re-assignation of V_S^* as

$$V_S^* = K_v \max\left\{ \left\|\mathbf{K}_f\left(|\mathbf{v}| + \delta\mathbf{v}_{\max}\right)\right\|_\infty, \left\|\mathbf{K}_f\left(\left|\tilde{\mathbf{v}} + \mathbf{K}_f^{-2}\mathbf{R}_f\mathbf{f}_e^*\right| + \delta\tilde{\mathbf{v}}_{\max}\right)\right\|_\infty \right\} \tag{4.19}$$

Henceforward, V_S^* will be taken to be equal to the above, and it will consequently be assumed that condition (4.1a) always holds. Given this assumption the ensuing analysis examines the consequences of $\mathbf{f}_e^* \notin S_{Kv}(\mathbf{v})$.

4.4.1: Sensitivity of Switching Equilibrium to Uncertainty

For the closed-loop system with the controller defined in Eq. (4.14) and V_S^* defined as in Eq. (4.19), the departure of $\mathbf{f}_e^0$ from $\mathbf{f}_e^*$ can be found as a function of velocity uncertainty. It is assumed that, even if $\mathbf{f}_e^* \notin S_{Kv}(\mathbf{v})$, the condition $\mathbf{f}_e^* \in S_{Kv}(\mathbf{v}_0)$ holds; i.e., a force command is never given that the nominal system cannot realize. Given this, Theorem 4.2 below characterizes the consequences of uncertainty on the tracking error of the controller in Theorem 4.1.

<u>THEOREM 4.2</u>: If $\mathbf{f}_e^* \notin S_{Kv}(\mathbf{v})$ but $\mathbf{f}_e^* \in S_{Kv}(\mathbf{v}_0)$, and if the velocity uncertainty obeys the inequality

$$-\frac{\mathbf{f}_e^{*T}\delta\tilde{\mathbf{v}}}{\mathbf{f}_e^{*T}\tilde{\mathbf{v}}_0} < \frac{K_v - 1}{K_v} \tag{4.20}$$

then the global equilibrium for the system with the controller (4.14) is

$$\begin{aligned} \mathbf{f}_e^0 &= \left(1 + \alpha^0\right)\mathbf{f}_e^* \\ V_S^0 &= \left(1 + \alpha^0\right)V_S^* \end{aligned} \tag{4.21}$$

where

$$\alpha^0 = -\frac{\mathbf{f}_e^{*T}\mathbf{C}_c^{-1}\mathbf{f}_e^* + V_S^{*2}/R_S + \mathbf{f}_e^{*T}\tilde{\mathbf{v}}}{\mathbf{f}_e^{*T}\mathbf{C}_c^{-1}\mathbf{f}_e^* + V_S^{*2}/R_S} \geq \frac{1-K_v}{K_v} \tag{4.22}$$

proof: See Appendix A4

Consider the expression for the equilibrium value of α in Eq. (4.22). Assume that $\mathbf{f}_e^*$ is on $\partial\mathcal{S}_{Kv}(\mathbf{v}_0)$. Then Eq. (4.22) can be expressed as

$$\alpha^0 = \frac{\mathbf{f}_e^{*T}\delta\tilde{\mathbf{v}}}{\mathbf{f}_e^{*T}\tilde{\mathbf{v}}_0} \tag{4.23}$$

Using the bound in Eq. (4.18), α^0 is bounded by

$$\alpha^0 \geq -\frac{\left|\mathbf{f}_e^{*T}\delta\tilde{\mathbf{v}}\right|}{\mathbf{f}_e^{*T}\mathbf{C}_c^{-1}\mathbf{f}_e^*} \geq -r\sqrt{\frac{\tilde{\mathbf{v}}_0^T\mathbf{C}_c^{-1}\tilde{\mathbf{v}}_0}{\mathbf{f}_e^{*T}\mathbf{C}_c^{-1}\mathbf{f}_e^*}} \tag{4.24}$$

Consider force commands near the ideal regenerative boundary in $\mathbf{f}_e$-space (i.e., commands where $\mathbf{f}_e^*$ is nearly orthogonal to $\mathbf{v}$). These commands correspond to operating states where there is little dissipation in the system, and where the electrical energy generated by the actuators is nearly equal to the energy injected back into the mechanical system. This type of operation is one of the great advantages of regenerative actuation. However, for these operating points, the denominator in the above expression is small, and can be much smaller than the numerator, resulting in arbitrarily bad tracking.

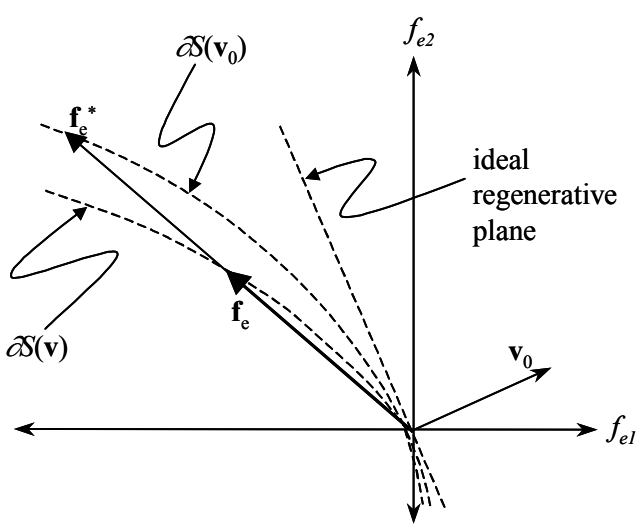

Figure 4.2: Consequences of model error on tracking

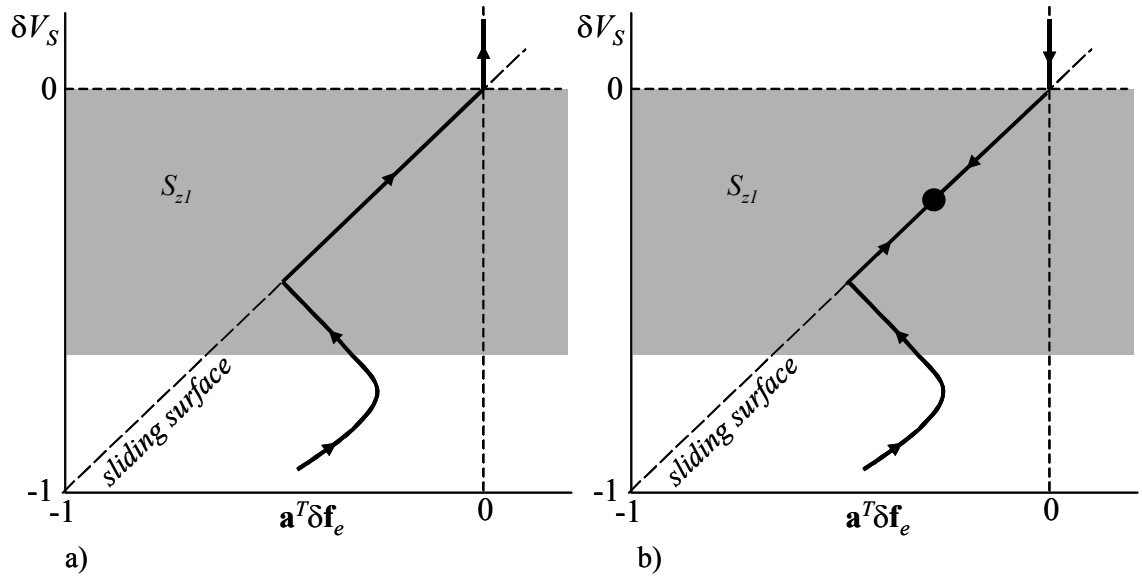

Figure 4.3: Example sliding-mode trajectories in S_{z1} without equilibrium (a) and with equilibrium (b).

In the circumstance where Eq. (4.20) is satisfied, the equilibrium vector $\delta\mathbf{f}_e^0$ is collinear with $\mathbf{f}_e^*$. Resultantly, $\mathbf{f}_e^0$ and $\mathbf{f}_e^*$ are collinear with a proportional magnitude of (α^0+1). For $\mathbf{f}_e^*$ near the ideal regenerative plane, this is illustrated in Fig. 4.2. For $\mathbf{f}_e^*$ commands arbitrarily close to the regenerative plane, tracking becomes arbitrarily bad.

4.4.2: Dynamics about Equilibrium

Consider that when δV_S<0, the control operator in Eq. (4.14) has a null space, characterized by the subspace

$$\begin{aligned} \delta\mathbf{f}_e &= \alpha\mathbf{f}_e^* \\ \delta V_S &= \alpha V_S^* \end{aligned} \tag{4.25}$$

Vector components of $\{\delta\mathbf{f}_e,\delta V_S\}$ in this subspace of $\Re^{m+1}$ do not affect the determination of **D**.

It can be shown that for a region S_{z1} defined by

$$S_{z1} = \left\{ \{\delta\mathbf{f}_e, \delta V_S\} \in \Re^{m+1} \mid \delta V_S \in \left(\frac{1-K_v}{K_v} V_S^*, 0 \right) \right\} \tag{4.26}$$

the switching controller drives the system states to this subspace, on which the dynamics exhibit a sliding mode. An example of a sliding mode is illustrated in Fig. 4.3. The idea is that the trajectory of $\{\delta\mathbf{f}_e(t),\delta V_S(t)\}$ moves in the state space so as to intersect the subspace defined by Eq. (4.25), referred to a sliding surface. The switch positions **D** are discontinuous across this surface,

so this intersection occurs in finite time. Following intersection, the trajectory of the system is confined to this subspace, until it leaves S_{z1}. During this time, the trajectory appears to "slide" on these surfaces as if constrained.

It follows that if the equilibrium of the system is inside S_{z1}, then the dynamics of the system about this equilibrium point can be described by considering the system to be constrained to the subspace defined by Eq. (4.25), thus reducing the order of the differential equation for the system from m+1 to 1. It will now be proven that if $\mathbf{f}_e^* \notin S_{Kv}(\mathbf{v})$, the equilibrium of the system lies within such a region S_{z1}, if the velocity uncertainty obeys the inequality in Eq. (4.20).

<u>THEOREM 4.3</u>: If the conditions of Theorem 4.2 are met, the switching algorithm in Eq. (4.14) produces a region S_{z1} in $\{\delta\mathbf{f}_e, \delta V_S\}$-space which includes $\{\delta\mathbf{f}_e^0, \delta V_S^0\}$, in which the trajectory of the system slides on the surface described by Eq. (4.25). On the sliding surface, the system dynamics are described through the $\alpha(t)$ coordinate in Eq. (4.25), which is governed by the differential equation

$$\dot{\alpha} = -\frac{1}{\tau}\left(\alpha - \alpha^0\right) \tag{4.27}$$

where τ is the universal electrical time constant assigned in (2.32).

proof: See Appendix A4.

It is highly desirable to have good tracking near the ideal regenerative plane. Certainly, tracking that is so bad that the equilibrium vector is not even in S_{z1} is undesirable. One simple reason for this is that it signifies that the percent error in tracking is greater than $(K_v\text{-}1)/K_v$. For a typical K_v value (say, 2) this is unacceptable. For practical reasons as well, it is important to keep the system equilibrium in S_{z1}. If the system exits S_{z1}, this signifies that the DC bus voltage has collapsed below the threshold given by condition (4.1a), which results in the failure of the transistor circuits to work properly. This modifies the dynamics of the system in undesirable ways.

What is desirable is a way of compensating for the model uncertainty to bring the system to an equilibrium point nearby, as shown in Fig. 4.4. While this would not yield zero-error tracking (which is impossible if $\mathbf{f}_e^* \notin S_{Kv}(\mathbf{v})$) it would yield much closer tracking than that of Fig. 4.2. Such a controller is presented in the next section.

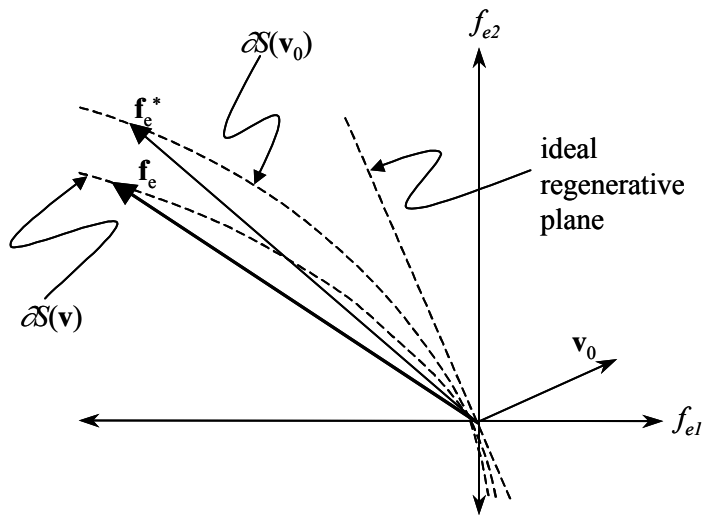

Figure 4.4: Desired compensative behavior for robust performance

4.5: Controller Redesign for Robustness

To provide some robustness to uncertainty in $\partial S_{Kv}(\mathbf{v})$, consider Fig. 4.5. Control law $\mathbf{F}$ is as in Eq. (4.14). The feedback compensator $\mathbf{F}_2$, in the outer loop, is designed to adjust $\mathbf{f}_e^*$, to get $\bar{\mathbf{f}}_e^*$, based on the tracking error α.

For the design of $\mathbf{F}_2$, it is assumed that the system is confined to its sliding surface as in Eq. (4.25). Thus, its dynamics are described by a single variable α. Strictly speaking, this is only true if α obeys the inequality in Eq. (4.22). It is assumed that in closed-loop, the compensator presented here has sufficiently good performance such that this is true. The controller is presented in the following theorem.

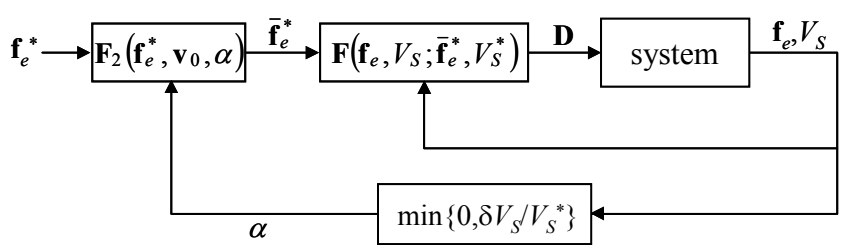

Figure 4.5: Feedback compensation for uncertainties

<u>THEOREM 4.4</u>: Let the system be constrained as in Eq. (4.25), and assume that the velocity uncertainty satisfies the upper bound in Eq. (4.18). For a given $\mathbf{f}_e^*$ and $\mathbf{v}_0$, define the function $\bar{\mathbf{f}}_e^*(\beta,\gamma)$ as

$$\bar{\mathbf{f}}_e^* = \left[(1+\beta)\frac{\tilde{\mathbf{v}}_0^T\mathbf{f}_e^*}{\tilde{\mathbf{v}}_0^T\mathbf{C}_c\tilde{\mathbf{v}}_0} + \beta\sqrt{\frac{\mathbf{f}_e^{*T}\mathbf{C}_c^{-1}\mathbf{f}_e^*}{\tilde{\mathbf{v}}_0^T\mathbf{C}_c\tilde{\mathbf{v}}_0}}\right]\mathbf{C}_c\tilde{\mathbf{v}}_0 + \gamma\left[\mathbf{I} - \frac{\mathbf{C}_c\tilde{\mathbf{v}}_0\tilde{\mathbf{v}}_0^T}{\tilde{\mathbf{v}}_0^T\mathbf{C}_c\tilde{\mathbf{v}}_0}\right]\mathbf{f}_e^* \tag{4.28}$$

where γ is related to $\beta\in[-1,0]$ through

$$\gamma = \sqrt{\frac{1-\left[\theta+(1+\theta)\beta\right]^2}{1-\theta^2}} \in [0,1] \tag{4.29}$$

with θ defined as

$$\theta = \frac{\mathbf{f}_e^{*T}\tilde{\mathbf{v}}_0}{\sqrt{\left(\mathbf{f}_e^{*T}\mathbf{C}_c^{-1}\mathbf{f}_e^*\right)\left(\tilde{\mathbf{v}}_0^T\mathbf{C}_c\tilde{\mathbf{v}}_0\right)}} \in [-1,0] \tag{4.30}$$

Then the feedback controller

$$\beta = \max\{1+\theta-r\,,0\}\min\{0,K\alpha\} \tag{4.31}$$

is stable for $K<<1$. Furthermore, the differential equation for the closed-loop system for $\alpha<0$ is

$$\dot{\alpha} = -\frac{1}{\tau}\left[\left(1+\frac{\sqrt{\left(\tilde{\mathbf{v}}_0^T\mathbf{C}_c\tilde{\mathbf{v}}_0\right)\left(\mathbf{f}_e^{*T}\mathbf{C}_c^{-1}\mathbf{f}_e^*\right)}}{\mathbf{f}_e^{*T}\mathbf{C}_c^{-1}\mathbf{f}_e^* + V_S^{*2}/R_S}qK\right)\alpha + \frac{\mathbf{f}_e^{*T}\mathbf{C}_c^{-1}\mathbf{f}_e^* + V_S^{*2}/R_S + \tau\,\mathbf{f}_e^{*T}\tilde{\mathbf{v}}}{\mathbf{f}_e^{*T}\mathbf{C}_c^{-1}\mathbf{f}_e^* + V_S^{*2}/R_S}\right] \tag{4.32}$$

where $q>0$ is

$$q = \left[(1+\Delta_1 r)(1+\theta) + \Delta_2 r\theta\sqrt{\frac{1+\theta}{1-\theta}}\right]\max\{1+\theta-r\,,0\} \tag{4.33}$$

and where Δ_1 and Δ_2 are uncertain constants with $|\Delta_1|\le 1$ and $|\Delta_2|\le 1$.

proof: See Appendix A4

The controller in Theorem 4.4 adjusts $\mathbf{f}_e^*$ by rotating the command toward the vector $-\mathbf{C}_c\tilde{\mathbf{v}}_0$, while leaving the quantity $\bar{\mathbf{f}}_e^{*T}\mathbf{C}_c^{-1}\bar{\mathbf{f}}_e^*$ constant, with the degree of adjustment being in accordance with α. This is illustrated in Fig. 4.6. This particular way of adjusting $\mathbf{f}_e^*$ is appealing because the resultant closed-loop differential equation for α is linear for all α satisfying

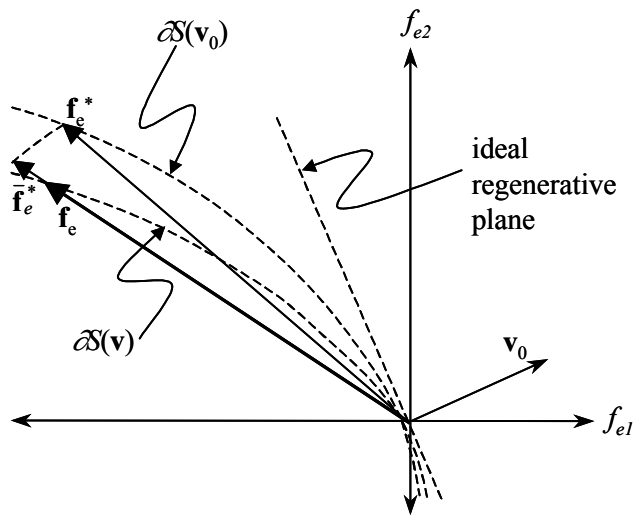

Figure 4.6: Adjustment of $\mathbf{f}_e^*$ by compensator

the inequality (4.22). It is therefore easier to make generalized statements about the tracking error and bandwidth of the closed-loop system.

Improvement in Tracking Error

Let the equilibrium points of the uncompensated and compensated systems be α^0 and $\bar{\alpha}^0$ respectively. Then, by Eq. (4.32), the two are related by

$$\bar{\alpha}^0 = \left(1 + \frac{\sqrt{\left(\tilde{\mathbf{v}}_0^T \mathbf{C}_c \tilde{\mathbf{v}}_0\right)\left(\mathbf{f}_e^{*T} \mathbf{C}_c^{-1} \mathbf{f}_e^*\right)}}{\mathbf{f}_e^{*T} \mathbf{C}_c^{-1} \mathbf{f}_e^* + V_S^{*2} / R_S} qK\right)^{-1} \alpha^0 \tag{4.34}$$

For $\mathbf{f}_e^*$ near $\partial S(\mathbf{v})$ and for R_S large,

$$\theta \approx -\frac{\mathbf{f}_e^{*T} \mathbf{C}_c^{-1} \mathbf{f}_e^* + V_S^{*2} / R_S}{\sqrt{\left(\mathbf{f}_e^{*T} \mathbf{C}_c^{-1} \mathbf{f}_e^*\right)\left(\tilde{\mathbf{v}}_0^T \mathbf{C}_c \tilde{\mathbf{v}}_0\right)}} \approx -\sqrt{\frac{\mathbf{f}_e^{*T} \mathbf{C}_c^{-1} \mathbf{f}_e^*}{\tilde{\mathbf{v}}_0^T \mathbf{C}_c \tilde{\mathbf{v}}_0}} \tag{4.35}$$

and Eq. (4.34) may therefore be approximated as

$$\bar{\alpha}^0 = \frac{1}{1 - qK/\theta} \alpha^0 \tag{4.36}$$

Note that, because $\theta < 0$, tracking of α is always improved for the compensated system. Using Eq. (4.33), with the assumption that $\Delta_1 = \Delta_2 = 0$, this improvement in tracking has a lower bound of

$$\overline{\alpha}^{0} > \frac{|\theta|}{|\theta| + K(1-r)(1+\theta)}\alpha^{0} \tag{4.37}$$

Thus, the tracking is improved for the system. Note that for θ small, this improvement can be quite significant.

Closed-Loop Transient Characteristics

From Eq. (4.32), it is clear that time constant associated with the compensated system is

$$\overline{\tau} = \left(1 + \frac{\sqrt{\left(\tilde{\mathbf{v}}_0^T \mathbf{C}_c \tilde{\mathbf{v}}_0\right)\left(\mathbf{f}_e^{*T} \mathbf{C}_c^{-1} \mathbf{f}_e^{*}\right)}}{\mathbf{f}_e^{*T} \mathbf{C}_c^{-1} \mathbf{f}_e^{*} + V_S^{*2} / R_S} qK\right)^{-1} \tau \tag{4.38}$$

For R_S large, this is approximately

$$\overline{\tau} > \left(1 + \sqrt{\frac{\tilde{\mathbf{v}}_0^T \mathbf{C}_c \tilde{\mathbf{v}}_0}{\mathbf{f}_e^{*T} \mathbf{C}_c^{-1} \mathbf{f}_e^{*}}} qK\right)^{-1} \tau \tag{4.39}$$

Thus, by the same reasoning that gave the lower bound on the tracking error,

$$\overline{\tau} > \left(1 + \theta^{-1}(1+\theta)^2 (1-r) K\right)\tau \tag{4.40}$$

Thus, for $\mathbf{f}_e^*$ small in comparison to $\mathbf{v}_0$, the bandwidth of the compensated system becomes very large. In reality, this is impractical, because this controller would require a digital implementation, and therefore be required to operate well below a sampling frequency. The value of $\overline{\tau}$ must be limited to some minimum value $\overline{\tau}_{\min}$. This limits the practical magnitude of K as a function of θ.

4.6: Switching Frequency Limitations

There is a limit to how fast switches may be made to alternate. There is also a finite delay time necessary to sense the feedback signals, process them, and produce a switch position vector **D**. However, if the switching rule in Eq. (4.14) were ideally implemented, the switches would alternate infinitely rapidly, to keep the system state precisely at its equilibrium $\mathbf{x}^0$. If the switches can only be made to alternate at a certain maximum frequency, then $\mathbf{x}(t)$ cannot be kept precisely at $\mathbf{x}^0$, but will "ripple" about this commanded value. This is illustrated in Fig. 4.7.

Usually, these switching limitations are characterized by a maximum switching frequency f_s or by its inverse, the minimum switching period, T_s. This switching period consists

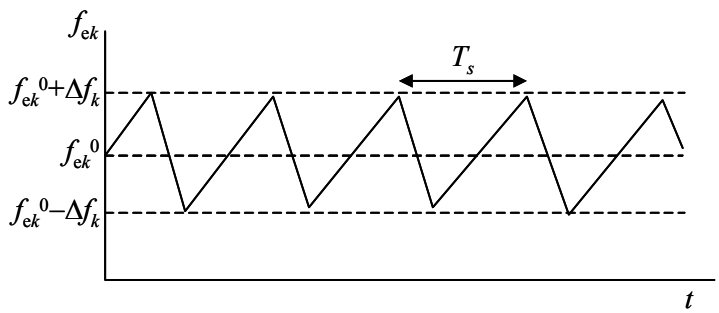

Figure 4.7: Illustration of switching noise

of the minimum time duration in which a switch may be made to alternate from position 1 to position 2, and then back again.

This lower limit on switching period, and the resultant rippling phenomenon in the closed-loop dynamics of $\mathbf{x}(t)$, is also called "chattering" and "switching noise." If not explicitly addressed, it could lead to such undesirable effects as low-frequency, nonperiodic oscillations in $\mathbf{x}(t)$. In the context of structural control, this is highly undesirable. Accepting that some ripple is unavoidable in such switching systems, the frequency content of this ripple in the $\mathbf{f}_e$ vector should be concentrated near the maximum switching frequency f_s.

4.6.1: Hysteretic Switching

This section illustrates a way of implicitly prescribing the switching frequency, using control hysteresis. There are other ways of handling the problem, such as explicit duty cycle regulation.

Define the hysteretic function hys(u,Δu) as

$$\text{hys}(u,\Delta u)=\begin{cases}1 & : u \geq \Delta u \\ \text{present value} & : -\Delta u < u < \Delta u \\ -1 & : u \leq -\Delta u\end{cases} \tag{4.41}$$

Fig. 4.8 illustrates how this function is related to its input. The hysteresis switching controller then amounts to a modification of Eq. (4.14) to

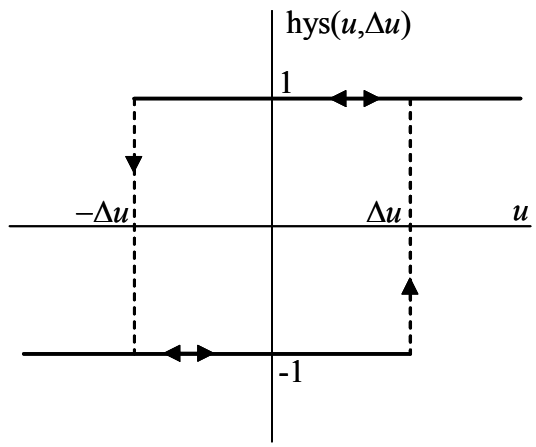

Figure 4.8: Input/output of hys(u/r)

$$\mathbf{F}\left(\delta\mathbf{f}_e, \delta V_S^*\right) = \begin{bmatrix} \text{hys}\left[-\delta f_{e1} + \dfrac{\bar{f}_{e1}^*}{V_S^*} u\left(-\delta\hat{V}_S\right)\delta\hat{V}_S\ ,\ \Delta f_1\right] \\ \vdots \\ \text{hys}\left[-\delta f_{em} + \dfrac{\bar{f}_{em}^*}{V_S^*} u\left(-\delta\hat{V}_S\right)\delta\hat{V}_S\ ,\ \Delta f_m\right] \\ \tfrac{1}{2} + \tfrac{1}{2}\text{hys}\left[\delta V_S - \Delta V_S\ ,\ \Delta V_S\right] \end{bmatrix} \tag{4.42}$$

where V_S is sent through a low-pass filter with a bandwidth well below f_s, to get the smoothed voltage $\hat{V}_S$. Note that in steady-state,

$$\delta\hat{V}_S = \hat{V}_S - V_S^* \tag{4.43}$$

is equal to αV_S^*. Thus, the value of α, for α<0, is sensed through the voltage V_S. The vector $\Delta\mathbf{f}$ contains the amplitudes of the force ripples, and the voltage ΔV_S is the magnitude of the voltage ripple.

Using the above switching logic, instead of Eq. (4.14), the various components of **x** will ripple about their equilibrium positions as discussed. The frequency of the ripple in **x**, and the neighborhood in **x**-space in which the trajectory is confined in steady state, are determined by $\Delta\mathbf{f}$ and ΔV_S. Note that as these quantities decrease, the corresponding hysteresis boxes such as the one in Fig. 4.8 get smaller and smaller. As these quantities go to zero, the controller in Eq. (4.42) becomes the one in Eq. (4.14).

Note that the hysteretic switching function for V_S has an offset, so that the DC bus voltage ripple will have a positive offset of ΔV_S, as illustrated in Fig. 4.9. The reason for this offset is that it guarantees that V_S will not violate Eq. (4.1a) during any part of its switching cycle. This becomes important for operating points with large forces, because the ripple amplitude on

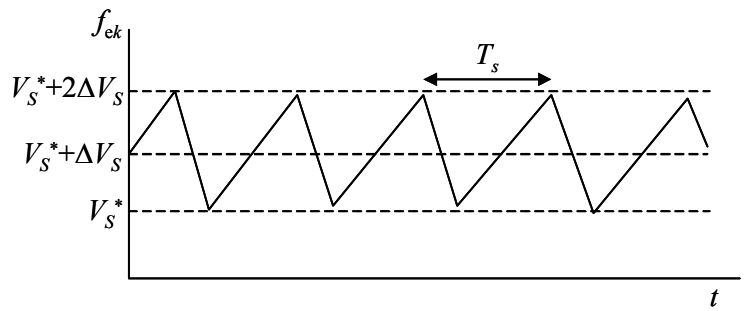

Figure 4.9: Ripple and DC offset of V_S in steady-state

the DC bus can be quite large in these cases. Because R_S is considered to be quite large, this added offset in the average value of V_S does not significantly hamper the force capability of the system.

4.6.2: Determining Appropriate Hysteresis Bands

The switching period T_s for a hysteretic function is the time that it takes for the trajectory in Fig. 4.8 to make a loop around the hysteresis box. If the value of Δu in the figure is known to be the worst-case peak amplitude for ripple at a period of T_s, then the cyclic period for the hysteresis loop has a lower bound of T_s, and thus an upper bound for the switching frequency, f_s.

To find Δf_k, the approach used here is to solve for the maximum ripple magnitude of force f_{ek}, operating over a switching period $t \in [0,T_s]$, during which the average value is

$$f_{ek}^{avg} = (1+\alpha) f_e^* \tag{4.44}$$

Assume that $f_{ek}(0)=f_{ek}(T_s)=f_{ek}^{avg}$ and assume that $D_k(0)=1$. During this period, the derivative of f_{ek} is

$$\frac{d}{dt} f_{ek} = \frac{D_k K_{fk} V_S - K_{fk}^2 \tilde{v}_k}{2L_k} - \frac{1}{\tau} f_{ek} \tag{4.45}$$

If the switching period is very short, this is approximately equal to

$$\frac{d}{dt} f_{ek} = \frac{D_k K_{fk} \hat{V}_S - K_{fk}^2 \tilde{v}_k}{2L_k} - \frac{1}{\tau} f_{ek}^{avg} \tag{4.46}$$

The boundary conditions at $t=\{0,T_s\}$ then require that D_k transition from 1 to –1 at

$$t = T_s \frac{K_{fk} \hat{V}_S + K_{fk}^2 \tilde{v}_k + 2R_k f_{ek}^{avg}}{2K_{fk} \hat{V}_S} \tag{4.47}$$

and the resultant peak amplitude of f_{ek} over the interval is thus

$$\Delta f_k = T_s \frac{\left(K_{fk}\hat{V}_S\right)^2 - \left(K_{fk}^2 \tilde{v}_k + 2R_k f_{ek}^{avg}\right)^2}{4L_k K_{fk}\hat{V}_S} \tag{4.48}$$

This is the value of the hysteresis amplitude used in the control algorithm.

For the DC bus voltage, a similar procedure could be used to find ΔV_S. However, this procedure is computationally cumbersome. An alternative approach starts with the pragmatic observation that, because R_S is very large, a large-amplitude ripple in V_S does not significantly hamper system performance, so long as V_S is consistently above V_S^* over the entire switching cycle. Thus, the approach here designates

$$\Delta V_S = 0.2V_S^* \tag{4.49}$$

This typically results in a ripple frequency for V_S which is well below f_s when $V_S > V_S^*$.

4.6.3: Summary of the Switching Controller

The overall operation of the switching controller in Fig. 4.5 consists of a number of computations. First, a command $\mathbf{f}_e^*$ must be issued, and the corresponding V_S^* must be computed. It must then be checked that $\mathbf{f}_e^* \in S_{Kv}(\mathbf{v}_0)$. The value of α is sensed through V_S, and $\mathbf{f}_e^*$ is adjusted through Eq. (4.28). Then, Eq. (4.48) is used to determine the force hysteresis bands. Finally Eq. (4.42) is used to determine each switch position.

In light of this large computational burden, it is important to note that the computations which involve high-frequency feedback quantities are limited to the hysteretic function in Eq. (4.42), which likely can be implemented using simple analog electronics. The computations for the robust controller discussed in Section 4.5 involve only parameters which vary with time constants well above T_s. This is important because the hysteresis operation must operate at an extremely high information bandwidth to be effective. Consider, as an example, a case where T_s = .05ms (i.e., f_s = 20kHz). Such a switching period is not unreasonable. For the hysteretic operation in Eq. (4.42) to work, it must be able to process information at several decades *above* this frequency.

The replacement of the switching controller in Eq. (4.42) for that in Eq. (4.14) results in a dynamic system significantly less tractable, from an analytical point of view. In the last section, some conclusions were derived concerning the ideal switching controller's stability properties, and a nonlinear compensator was developed. Here, the dynamics are more complicated, and an in-depth analysis of the exact effects of hysteretic switching on the system dynamics is not

pursued here. Rather, it will simply be taken for granted that, for small hysteresis bands, the above controller is approximately the same as the ideal one discussed in earlier sections, and that its performance should thus be very similar.

4.7: The Two-Machine Example (Revisited)

To demonstrate the performance of the controlled electrical system, simulations are performed for the two-machine system discussed at the end of the last chapter. The switching control system is fully described by parameters K_v, K, and T_s which for these examples were made equal to 2, 0.25, and 50μs, respectively.

The first example is a demonstration of the ability of the control system to stabilize, and hold in steady-state, various operating points on the boundary of $S(\mathbf{v})$. To do this, a simulation is performed which controls the system about the boundary of $S(\mathbf{v})$ for velocity vectors of common direction but varying size, as was shown in Fig. 3.7 for the theoretical case. The force command $\mathbf{f}_e^*$ is swept around the analytical boundary of $S(\mathbf{v})$, at a rate well inside the bandwidth of the closed-loop system. The commanded forces were limited to $\pm\mathbf{f}_{max}$. The simulations were done repeatedly for different velocity magnitudes, and along the same direction as in Fig. 3.7.

The results are shown in Fig. 4.10. Several important points can be ascertained from this plot. First of all, the approximate elliptical shape of the boundary can be seen, especially as $\|\mathbf{v}\|$ grows. For very small $\|\mathbf{v}\|$ the elliptical shape is distorted, due to the losses in the switches. Also, note the ripple in the force $\mathbf{f}_e$ as it tracks $\mathbf{f}_e^*$.

A second example illustrates the transient characteristics of the actuation system, with $\mathbf{v}$ as in Fig. 4.10 and with ξ=5. Simulations are performed in which the forces are brought to their commanded values, where the initial conditions for the electrical quantities are all zero. Two cases are presented; one with $\mathbf{f}_e^*$ far inside $S(\mathbf{v})$, and another with $\mathbf{f}_e^*$ just beyond the boundary of $S(\mathbf{v})$.

For the first case, the force command is

$$\mathbf{f}_e^*=[-f_{1max}\ \ -f_{2max}]^T \tag{4.50}$$

which lies far inside $S(\mathbf{v})$, as shown in Fig. 4.11. Simulation results for the force response of the closed-loop system is also shown in the figure. Several attributes of this plot deserve attention. First, note that the forces rise to their commanded values along the direction of $\mathbf{f}_e^*$, as expected, and that the system reaches switching equilibrium in finite time (about 12ms in this example). Also note that the switching ripple in the forces. The switching frequency was designed to be about 20kHz, well outside the bandwidth of the system dynamics.

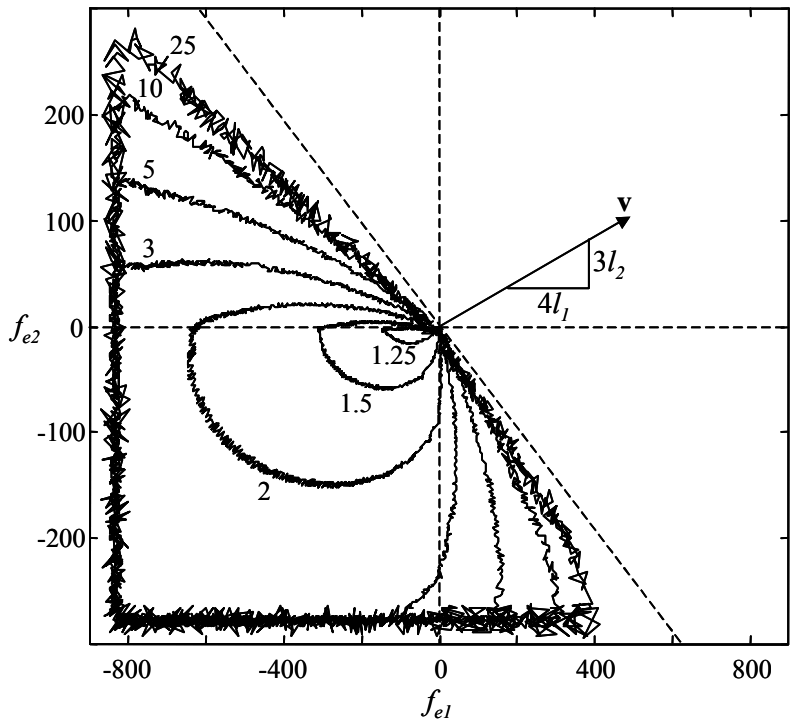

Figure 4.10: Tracings of $\mathcal{AS}_{Kv}(\mathbf{v})$ for various magnitudes of $\mathbf{v}$

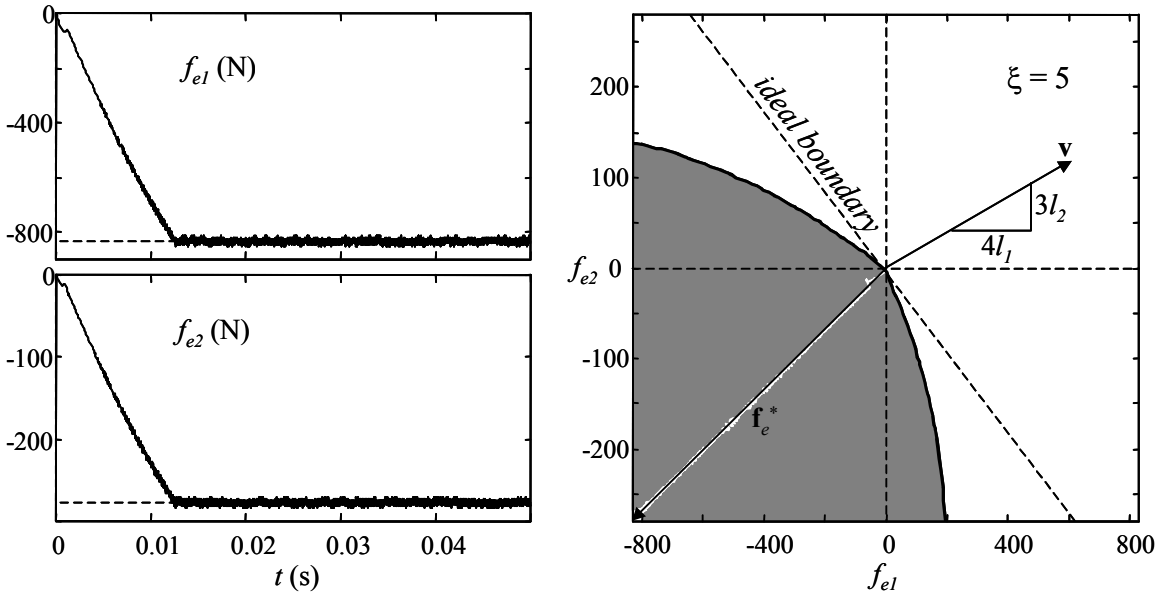

Figure 4.11: Transient response to force command (4.50)

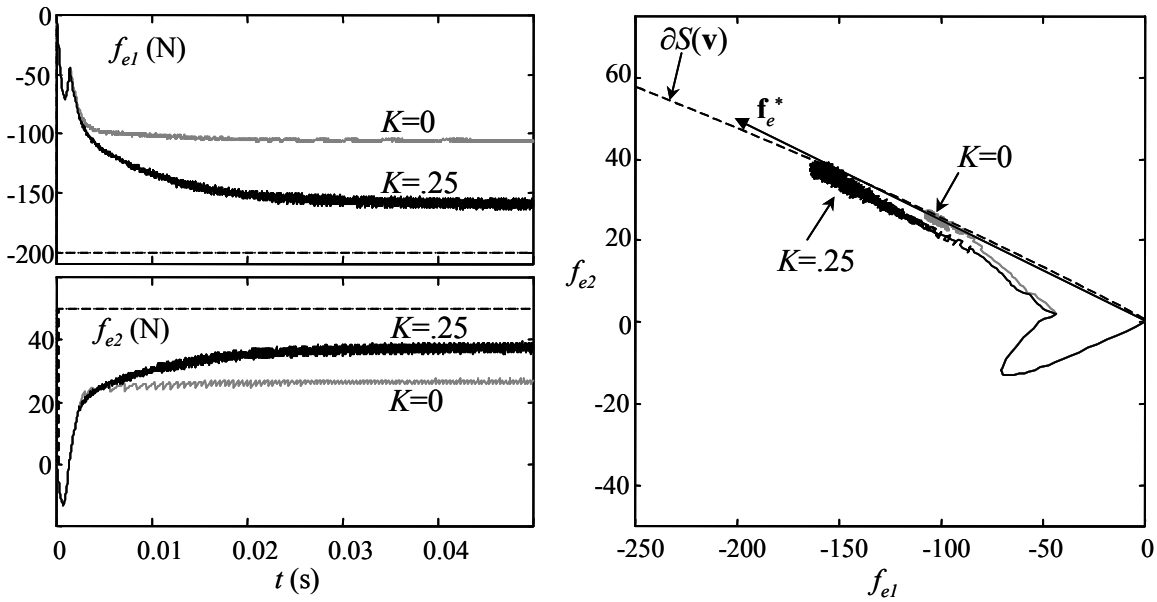

Figure 4.12: Transient response to force command (4.51), with and without the robust controller

A more interesting simulation concerns the behavior of the system when a command is issued near $\partial S(\mathbf{v})$. For this command, let

$$\mathbf{f}_e^*=[-200\text{N} , 50\text{N}]^T \tag{4.51}$$

which lies just past this boundary. The force response for the system is shown in Fig. 4.12, for two cases; K=0 and K=0.25. These simulations illustrate the value of the robust controller in the improvement of force tracking. Note that in the case of K=0, the system settles on a switching equilibrium point along the direction of $\mathbf{f}_e^*$ as predicted. This equilibrium point is around α =–0.5; near the lower boundary of the S_{z1} region. For K=0.25, the tracking error is significantly improved. With larger values of K, the responses are even better.

It is interesting to also consider the responses of V_S and i_R for this case. These signals are shown in Fig. 4.13. Note that, in both cases, i_R=0 for the duration. This is expected, because the force command is on the boundary of $S(\mathbf{v})$, and the system is therefore operating at the maximum possible efficiency. The response for V_S follows the same basic shape as that of the forces. For K=0, V_S settles at slightly above half its commanded value, whereas the switching equilibrium is significantly higher for K=0.25.

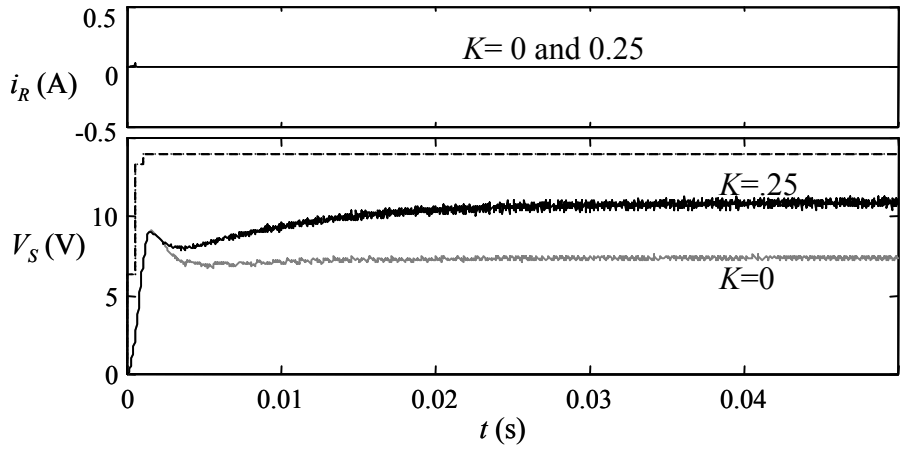

Figure 4.13: Responses of electrical quantities to force command (4.51)

Appendix A4

A4.1: The **y**-Space System Description

For the mathematical analysis of the system, it will be useful to use the coordinates $\mathbf{y}$ for the primary system, obtained through the dilation

$$\mathbf{y} = \begin{bmatrix} \mathbf{y}_f \\ y_S \end{bmatrix} = \begin{bmatrix} \mathbf{\Delta}_f^{-1/2} & \\ & C_S^{1/2} \end{bmatrix} \begin{bmatrix} \mathbf{f}_e \\ V_S \end{bmatrix} \tag{A4.1}$$

Similarly, it will be useful to refer to y_R state

$$y_R = L_R^{1/2} i_R \tag{A4.2}$$

In these coordinates, the differential equation for the primary system can be expressed as

$$\dot{\mathbf{y}} = -\frac{1}{\tau}\mathbf{y} + \mathbf{B}_v \tilde{\mathbf{s}} + \mathbf{B}_D(\mathbf{y})\mathbf{D}_f + \mathbf{B}_R y_R D_R \tag{A4.3}$$

where

$$\mathbf{B}_v = \begin{bmatrix} -\mathbf{I}_m \\ \mathbf{0}_{1\times m} \end{bmatrix}, \ \mathbf{B}_D(\mathbf{y}) = \begin{bmatrix} y_S & & \mathbf{0} \\ & \ddots & \\ \mathbf{0} & & y_S \\ -y_{f1} & \cdots & -y_{fm} \end{bmatrix} \mathbf{G}^{-1}, \ \mathbf{G} = \begin{bmatrix} \gamma_1 & & \\ & \ddots & \\ & & \gamma_m \end{bmatrix}, \ \mathbf{D}_f = \begin{bmatrix} D_1 \\ \vdots \\ D_m \end{bmatrix}, \ \mathbf{B}_R = \begin{bmatrix} 0 \\ \vdots \\ 0 \\ -1/\gamma_R \end{bmatrix}$$

and where $\mathbf{s}$ and $\tilde{\mathbf{s}}$ are the normalized velocity vectors

$$\begin{aligned} \mathbf{s} &= \mathbf{\Delta}_f^{1/2}\mathbf{v}_f \\ \tilde{\mathbf{s}} &= \mathbf{\Delta}_f^{1/2}\tilde{\mathbf{v}}_f = \mathbf{s} + \mathbf{\Delta}_f^{1/2}\mathbf{v}_{sw}(\mathbf{f}_e) \end{aligned} \tag{A4.4}$$

Note that τ is the universal time constant of the electrical system in Eq. (2.32). The γ_k terms are also time constants, with values

$$\begin{aligned} \gamma_k &= \sqrt{2L_k C_S} \\ \gamma_R &= \sqrt{L_R C_S} \end{aligned} \tag{A4.5}$$

Note that $\mathbf{B}_D(\mathbf{y})$ has the important orthogonality property

$$\mathbf{B}_D^T(\mathbf{y})\mathbf{y} = \mathbf{0} \quad , \quad \forall \mathbf{y} \in \Re^{m+1} \tag{A4.6}$$

The corresponding differential equation for y_R is

$$\dot{y}_R = -\frac{1}{\tau} y_R - \tilde{s}_{swR}\,\mathrm{sgn}(y_R) + \frac{1}{\gamma_R} D_R y_S \tag{A4.7}$$

where

$$\tilde{s}_{swR} = L_R^{-1/2} V_{swR} \tag{A4.8}$$

Commands V_S^* and $\mathbf{f}_e^*$ map to a commands y_S^* and $\mathbf{y}_f^*$, with the resultant equation for y_S^* taking the form

$$y_S^* = K_v \max\left\{ \|\mathbf{Gs}\|_\infty , \left\|\mathbf{G}\left(\tilde{\mathbf{s}} + \tfrac{1}{\tau}\mathbf{y}_f^*\right)\right\|_\infty \right\} \tag{A4.9}$$

Constraints $\mathbf{f}_e^0 \in S_{Kv}(\mathbf{v})$ and $|\mathbf{f}_e^0| \le \mathbf{f}_{\max}$ map to the constraints $\mathbf{y}_f^0 \in S_{yKv}(\mathbf{s})$ and $|\mathbf{y}_f^0| \le \mathbf{y}_{f\max}$ in the **y**-coordinates. The region $S_{yKv}(\mathbf{s})$ is described by

$$S_{yKv}(\mathbf{s}) = \left\{ \mathbf{y}_f^* \in \Re^m \mid \mathbf{y}_f^{*T}\mathbf{y}_f^* + \mathbf{y}_S^{*2} + \tau\,\mathbf{y}_f^{*T}\tilde{\mathbf{s}} \le 0 \right\} \tag{A4.10}$$

The **y**-space system representation is convenient because it effectively normalizes the system states. The only quantities which enter into the differential equation for **y** are the vector itself, y_R, **s**, and the set of time constants $\{\tau, \gamma_1 \ldots \gamma_m, \gamma_R\}$.

A4.2: Switching Control Theorems

The proofs to these theorems are done in the **y**-space, to simplify the mathematics. It is straight forward to show that the proofs transfer into the **x** coordinates in a manner consistent with the theorem statements in Chapter 4.

<u>THEOREM 4.1</u>: For any $\mathbf{y}_f^* \in S_{yKv}(\mathbf{s})$, design goals D1 and D2 are met by a feedback law **F** characterized by

$$\mathbf{D} = \mathbf{F}(\delta\mathbf{y}) = \mathrm{Dsat}\left(\begin{bmatrix} -y_S^*\mathbf{I} & \mathbf{y}_f^* u(-\delta y_S) \\ \mathbf{0} & y_S^* \end{bmatrix} \delta\mathbf{y} \right) \tag{A4.11}$$

where the equilibrium value of y_S satisfies $y_S^0 \ge y_S^*$. Furthermore, the transient behavior of the system satisfies

$$\|\delta\mathbf{y}_f(t)\|_2 \le e^{-t/\tau}\|\delta\mathbf{y}(0)\|_2 \tag{A4.12}$$

proof:

For design goals D1 and D2 to be met, it is sufficient to prove that conditions (4.11) and (4.13) are true. Condition (4.11) will be addressed first. Because the feedback law **F** in (4.14) is memoryless, the switching logic can be divided into two scenarios. Scenario 1 is the case where $\delta y_S<0$ while scenario 2 is where $\delta y_S\geq 0$. For convenience, these two sets in $\delta\mathbf{y}$-space will be called S_1 and S_2 respectively. To ease the notation, U_1 will be normalized as τU_1 from Chapter 4.

***Condition* (4.11)**: $\delta y \in S_1$

U_1 has the derivative

$$\begin{aligned}\frac{d}{dt}U_1 &= \delta\mathbf{y}^T\delta\dot{\mathbf{y}} \\ &= \delta\mathbf{y}^T\left(-\frac{1}{\tau}\mathbf{y}+\mathbf{B}_v\tilde{\mathbf{s}}+\mathbf{B}_D(\mathbf{y})\mathbf{D}_f+\mathbf{B}_R y_R D_R\right)\end{aligned} \tag{A4.13}$$

Eq. (A4.13) is equivalent to

$$\frac{d}{dt}U_1 = -\frac{1}{\tau}\delta\mathbf{y}^T\delta\mathbf{y}+\delta\mathbf{y}^T\left(-\frac{1}{\tau}\mathbf{y}^*+\mathbf{B}_v\tilde{\mathbf{s}}\right)+\delta\mathbf{y}^T\mathbf{B}_D(\mathbf{y}^*)\mathbf{D}_f-\frac{1}{\gamma_R}\delta y_S y_R D_R \tag{A4.14}$$

For $\delta\mathbf{y}\in S_1$, $D_R = 0$, so Eq. (A4.14) is

$$\frac{d}{dt}U_1 = -\frac{1}{\tau}\delta\mathbf{y}^T\delta\mathbf{y}+\delta\mathbf{y}^T\left(-\frac{1}{\tau}\mathbf{y}^*+\mathbf{B}_v\tilde{\mathbf{s}}+\mathbf{B}_D(\mathbf{y}^*)\mathbf{D}_f\right) \tag{A4.15}$$

Consider the following transformation and its inverse.

$$\delta\mathbf{y}=\begin{bmatrix} y_S^*\mathbf{I} & \mathbf{y}^* \\ \mathbf{0}_{1\times m} & \end{bmatrix}\begin{bmatrix}\mathbf{z}_1 \\ z_2\end{bmatrix}\ ,\ \begin{bmatrix}\mathbf{z}_1 \\ z_2\end{bmatrix}=\left(\frac{1}{y_S^*}\right)^2\begin{bmatrix}\mathbf{G}\mathbf{B}_D^T(\mathbf{y}^*) \\ \mathbf{0}_{1\times m}\ \ y_S^*\end{bmatrix}\delta\mathbf{y} \tag{A4.16}$$

In these coordinates, (A4.15) becomes

$$\frac{d}{dt}U_1 \leq y_S^*\mathbf{z}_1^T\left(-\frac{1}{\tau}\mathbf{y}_f^*-\tilde{\mathbf{s}}+y_S^*\mathbf{G}^{-1}\mathbf{D}_f\right)-z_2\left(\frac{1}{\tau}\mathbf{y}^{*T}\mathbf{y}^*+\mathbf{y}_f^{*T}\tilde{\mathbf{s}}\right) \tag{A4.17}$$

Since it is assumed that $\mathbf{y}_f^*\in S_{yKv}(\mathbf{s})$,

$$\frac{1}{\tau}\mathbf{y}^{*T}\mathbf{y}^*+\mathbf{y}_f^{*T}\tilde{\mathbf{s}}\leq 0 \tag{A4.18}$$

and since $z_2=\delta y_S/y_S^*<0$ for $\delta\mathbf{y}\in S_1$, Eq. (A4.17) implies that

$$\frac{d}{dt}U_1 \leq y_S^*\mathbf{z}_1^T\left(-\frac{1}{\tau}\mathbf{y}_f^*-\tilde{\mathbf{s}}+y_S^*\mathbf{G}^{-1}\mathbf{D}_f\right) \tag{A4.19}$$

The above derivative is minimized by the switching control logic

$$\mathbf{D}_f = \mathrm{sgn}(-\mathbf{z}_1) \tag{A4.20}$$

Using the inverse transformation in (A4.16), this switching rule can be expressed in terms of $\delta\mathbf{y}_{fs}$, as in Eq. (4.14). Because V_S^* obeys equality (4.19), the first term on the right-hand side of Eq. (A4.19) is negative-definite; i.e.,

$$\begin{aligned} &\mathbf{z}_1^T\left(-\frac{1}{\tau}\mathbf{y}_f^* - \tilde{\mathbf{s}} + y_S^*\mathbf{G}^{-1}\mathrm{sat}(\text{-}\mathbf{z}_1)\right) \le 0 \;\; \forall \mathbf{z}_1 \\ &\mathbf{z}_1^T\left(-\frac{1}{\tau}\mathbf{y}_f^* - \tilde{\mathbf{s}} + y_S^*\mathbf{G}^{-1}\mathrm{sat}(\text{-}\mathbf{z}_1)\right) = 0 \Leftrightarrow \mathbf{z}_1 = \mathbf{0} \end{aligned} \tag{A4.21}$$

giving the conclusion that

$$\delta y_S < 0 \Rightarrow \frac{d}{dt}U_1 < 0 \tag{A4.22}$$

***Condition* (4.11)**: $\delta y_{fs} \in S_2$

The time derivative of U_1 is equal to

$$\frac{d}{dt}U_1 = -\frac{1}{\tau}\delta\mathbf{y}_f^T\delta\mathbf{y}_f + \delta\mathbf{y}_f^T\left(-\frac{1}{\tau}\mathbf{y}_f^* - \tilde{\mathbf{s}} + y_S\mathbf{G}^{-1}\mathbf{D}_f\right) \tag{A4.23}$$

which is minimized by

$$\mathbf{D}_f = \mathrm{sgn}(-\delta\mathbf{y}_f) \tag{A4.24}$$

In a manner similar to the observation made in (A4.21), equality (4.19) ensures that, for $\delta y_S>0$,

$$\begin{aligned} &\delta\mathbf{y}_f^T\left(-\frac{1}{\tau}\mathbf{y}_f^* - \tilde{\mathbf{s}} + y_S\mathbf{G}^{-1}\mathrm{sat}(-\delta\mathbf{y}_f)\right) \le 0 \;\; \forall \delta\mathbf{y}_f \\ &\delta\mathbf{y}_f^T\left(-\frac{1}{\tau}\mathbf{y}_f^* - \tilde{\mathbf{s}} + y_S\mathbf{G}^{-1}\mathrm{sat}(-\delta\mathbf{y}_f)\right) = 0 \Leftrightarrow \delta\mathbf{y}_f = \mathbf{0} \end{aligned} \tag{A4.25}$$

yielding the conclusion that

$$\begin{aligned} &\delta y_S > 0, \|\delta\mathbf{y}_f\| > 0 \;\Rightarrow\; \frac{d}{dt}U_1 < 0 \\ &\delta y_S > 0, \|\delta\mathbf{y}_f\| = 0 \;\Leftrightarrow\; \frac{d}{dt}U_1 = 0 \end{aligned} \tag{A4.26}$$

This observation, together with (A4.22), yield the conclusion that condition (4.11) holds for the entire $\delta\mathbf{y}$ space. These equations also yield the inequality

$$\frac{d}{dt}U_1 \le -\frac{1}{\tau}\delta\mathbf{y}^T\delta\mathbf{y} \le -\frac{1}{\tau}U_1 \tag{A4.27}$$

it can be concluded that $U_1(t)$ has the upper bound

$$U_1(t) \le U_1(0)e^{-t/\tau} \tag{A4.28}$$

Using again the fact that $\delta\mathbf{y}_f^T\delta\mathbf{y}_f \le U_1 \le \delta\mathbf{y}^T\delta\mathbf{y}$ gives the bound in (A4.12).

***Condition* (4.13)**:

Define

$$U_2 = \mathbf{y}^T\mathbf{y} \tag{A4.29}$$

and note that

$$\frac{d}{dt}U_2\bigg|_{\delta\mathbf{y}_{fs}\in H} = \frac{d}{dt}\mathbf{y}^T\mathbf{y}\bigg|_{\delta\mathbf{y}_{fs}\in H} = 2\mathbf{y}^T\left(-\frac{1}{\tau}\mathbf{y} + \mathbf{B}_v\tilde{\mathbf{s}} + \mathbf{B}_D(\mathbf{y})\mathbf{D}_f + \mathbf{B}_R y_R D_R\right)\bigg|_{\delta\mathbf{y}_{fs}\in H} \tag{A4.30}$$

Using the orthogonality property in (A4.6), and recognizing that $\delta\mathbf{y}_f=\mathbf{0}$ on H, gives

$$\frac{d}{dt}U_2\bigg|_{\delta\mathbf{y}_{fs}\in H} = -2\mathbf{y}_f^{*T}\left(\frac{1}{\tau}\mathbf{y}_f^* + \tilde{\mathbf{s}}\right) - \frac{2}{\tau}y_S^2 - \frac{2}{\gamma_R}y_S y_R D_R \tag{A4.31}$$

Because it is assumed that $\mathbf{y}_f^* \in S_{yKv}(\mathbf{s})$, define $P^* \ge 0$ as

$$P^* = -\frac{1}{\tau}\mathbf{y}_f^{*T}\mathbf{y}_f^* - \mathbf{y}_f^{*T}\tilde{\mathbf{s}} \tag{A4.32}$$

Insertion in (A4.31) gives

$$\frac{d}{dt}U_2\bigg|_{\delta\mathbf{y}_{fs}\in H} = -\frac{2}{\tau}y_S^2 + 2P^* - \frac{2}{\gamma_R}y_S y_R D_R \tag{A4.33}$$

If $\delta\mathbf{y}\in H$ then $d\mathbf{y}_f/dt=0$ so

$$\frac{d}{dt}U_2\bigg|_{\delta\mathbf{y}_{fs}\in H} = \frac{d}{dt}y_S^2 \tag{A4.34}$$

Combining (A4.34) and (A4.31) gives

$$\frac{d}{dt}y_S^2 = -\frac{2}{\tau}y_S^2 + 2P^* - \frac{2}{\gamma_R}y_S y_R D_R \tag{A4.35}$$

For $y_S > y_S^*$ (implying $D_R=1$) Eq. (A4.35) for y_S and Eq. (A4.7) for y_R give the system

$$y_S > y_S^* \;\Rightarrow\; \frac{d}{dt}\begin{bmatrix} y_S \\ y_R \end{bmatrix} = \begin{bmatrix} -1/\tau & -1/\gamma_R \\ 1/\gamma_R & -1/\tau \end{bmatrix}\begin{bmatrix} y_S \\ y_R \end{bmatrix} + \begin{bmatrix} P^*/y_S \\ -\tilde{s}_{swR}\,\mathrm{sgn}(y_R) \end{bmatrix} \tag{A4.36}$$

This differential equation is stable, and the equilibrium point is the solution to the quadratic equation

$$\begin{bmatrix} y_S^{0\,2} \\ y_R^0 y_S^0 \end{bmatrix} = \frac{\tau^2\gamma_R^2}{\tau^2+\gamma_R^2}\begin{bmatrix} \dfrac{P^*}{\tau} + \dfrac{\tilde{s}_{swR}}{\gamma_R}\mathrm{sgn}\left(y_R^0\right)y_S^0 \\ \dfrac{P^*}{\gamma_R} - \dfrac{\tilde{s}_{swR}}{\tau}\mathrm{sgn}\left(y_R^0\right)y_S^0 \end{bmatrix} \tag{A4.37}$$

However, the differential equation is only valid for $y_S > y_S^*$. When y_S is constrained y_S^* (i.e., when $y_S = y_S^*$ and the derivative of y_S in Eq. (A4.37) is negative), the switch position D_R is undefined, and resultantly (A4.37) ceases to hold. However, note that

$$\frac{d}{dt}\left(y_S^2 + y_R^2\right) = -\frac{2}{\tau}\left(y_S^2 + y_R^2\right) + 2P^* - 2y_R\tilde{s}_{swR} \tag{A4.38}$$

Equating $y_S = y_S^*$ in Eq. (A4.38) gives the derivative of y_R in this circumstance. Thus we have that

$$y_S = y_S^* \;\Rightarrow\; \frac{d}{dt}\begin{bmatrix} y_S \\ y_R \end{bmatrix} = \begin{bmatrix} \max\left\{0, -\dfrac{1}{\tau}y_S^* - \dfrac{1}{\gamma_R}y_R + \dfrac{P^*}{y_S^*}\right\} \\ -\dfrac{1}{\tau}y_R - \tilde{s}_{swR}\,\mathrm{sgn}(y_R) + \dfrac{P^* - y_S^{*\,2}/\tau}{y_R} \end{bmatrix} \tag{A4.39}$$

It is straight forward to show that the derivative of $(y_S - y_S^0)^2 + (y_R - y_R^0)^2$ is negative-definite for both (A4.37) and (A4.39), therefore implying that the two differential equations yield a unique equilibrium point.

♦

<u>THEOREM 4.2</u>: If $\mathbf{y}_f^* \notin S_{yKv}(\mathbf{s})$ but $\mathbf{y}_f^* \in S_{yKv}(\mathbf{s}_0)$, and if the velocity uncertainty $\delta\mathbf{s}$ obeys the inequality

$$-\frac{\mathbf{y}_f^{*\,T}\,\delta\mathbf{s}}{\mathbf{y}_f^{*\,T}\,\mathbf{s}_0} < \frac{K_v - 1}{K_v} \tag{4.20A4.40}$$

then the global equilibrium for the system with the controller (4.14) is

$$\mathbf{y}^0 = \left(1 + \alpha^0\right)\mathbf{y}^* \tag{A4.41}$$

where

$$\alpha^0 = -\frac{\mathbf{y}^{*T}\mathbf{y}^* + \tau\,\mathbf{y}_f^{*T}\tilde{\mathbf{s}}}{\mathbf{y}^{*T}\mathbf{y}^*} \geq \frac{\mathbf{y}_f^{*T}\delta\mathbf{s}}{\mathbf{y}_f^{*T}\mathbf{s}_0} \tag{A4.42}$$

proof:

Define U as

$$U = \left(\delta\mathbf{y} - \alpha^0\mathbf{y}^*\right)^T\left(\delta\mathbf{y} - \alpha^0\mathbf{y}^*\right) \tag{A4.43}$$

Then

$$\begin{aligned}\frac{d}{dt}U &= \left(\delta\mathbf{y} - \alpha^0\mathbf{y}^*\right)^T\delta\dot{\mathbf{y}} \\ &= \left(\delta\mathbf{y} - \alpha^0\mathbf{y}^*\right)^T\left(-\frac{1}{\tau}\mathbf{y} + \mathbf{B}_v\tilde{\mathbf{s}} + \mathbf{B}_D(\mathbf{y})\mathbf{D}_f + \mathbf{B}_R y_R D_R\right)\end{aligned} \tag{A4.44}$$

Eq. (A4.44) is equivalent to

$$\begin{aligned}\frac{d}{dt}U = &-\frac{1}{\tau}\left(\delta\mathbf{y} - \alpha^0\mathbf{y}^*\right)^T\left(\delta\mathbf{y} + \alpha^0\mathbf{y}^*\right) \\ &+ \left(\delta\mathbf{y} - \alpha^0\mathbf{y}^*\right)^T\left(-\frac{1}{\tau}\left(1+\alpha^0\right)\mathbf{y}^* + \mathbf{B}_v\tilde{\mathbf{s}}\right) \\ &+ \left(\delta\mathbf{y} - \alpha^0\mathbf{y}^*\right)^T\mathbf{B}_D\left(\left(1+\alpha^0\right)\mathbf{y}^*\right)\mathbf{D}_f - \frac{1}{\gamma_R}\left(\delta y_S - \alpha^0 y_S^*\right)y_R D_R\end{aligned} \tag{A4.45}$$

which obeys the inequality

$$\frac{d}{dt}U < \left(\delta\mathbf{y} - \alpha^0\mathbf{y}^*\right)^T\left(-\frac{1}{\tau}\left(1+\alpha^0\right)\mathbf{y}^* + \mathbf{B}_v\tilde{\mathbf{s}} + \mathbf{B}_D\left(\left(1+\alpha^0\right)\mathbf{y}^*\right)\mathbf{D}_f\right) \tag{A4.46}$$

Using the transformation from (A4.16),

$$\delta\mathbf{y} = \begin{bmatrix} y_S^*\mathbf{I} & \mathbf{y}^* \\ \mathbf{0}_{1\times m} & \end{bmatrix}\begin{bmatrix}\mathbf{z}_1 \\ z_2\end{bmatrix}, \quad \begin{bmatrix}\mathbf{z}_1 \\ z_2\end{bmatrix} = \left(\frac{1}{y_S^*}\right)^2\begin{bmatrix}\mathbf{G}\mathbf{B}_D^T\left(\mathbf{y}^*\right) \\ \mathbf{0}_{1\times m} \quad y_S^*\end{bmatrix}\delta\mathbf{y} \tag{A4.47}$$

$$\frac{d}{dt}U < y_S^*\mathbf{z}_1^T\left(-\frac{1}{\tau}\left(1+\alpha^0\right)\mathbf{y}_f^* - \tilde{\mathbf{s}} + \left(1+\alpha^0\right)y_S^*\mathbf{G}^{-1}\mathbf{D}_f\right) - z_2\left(1-\alpha^0\right)\left(\frac{1}{\tau}\left(1+\alpha^0\right)\mathbf{y}^{*T}\mathbf{y}^* + \mathbf{y}_f^{*T}\tilde{\mathbf{s}}\right) \tag{A4.48}$$

But the second term is identically zero, by definition of α^0, so

$$\frac{d}{dt}U < y_S^*\mathbf{z}_1^T\mathbf{G}^{-1}\left(-\mathbf{G}\left(\frac{1}{\tau}\left(1+\alpha^0\right)\mathbf{y}_f^* + \tilde{\mathbf{s}}\right) + \left(1+\alpha^0\right)y_S^*\mathbf{D}_f\right) \tag{A4.49}$$

For the control law in (4.14), $\mathbf{D}_f$ is assigned such that

$$\frac{d}{dt}U < y_S^* \mathbf{z}_1^T \mathbf{G}^{-1}\left(-\mathbf{G}\left(\frac{1}{\tau}\left(1+\alpha^0\right)\mathbf{y}_f^* + \tilde{\mathbf{s}}\right) + \left(1+\alpha^0\right)y_S^* \operatorname{sgn}(\mathbf{z}_1)\right) \tag{A4.50}$$

Because $\mathbf{y}_f^* \notin S_{yKv}(\mathbf{s})$, $\alpha^0<0$. Together with the relationship between $\mathbf{s}$ and $\tilde{\mathbf{s}}$, this leads to the observation that

$$\left\|\mathbf{G}\left(\frac{1}{\tau}\left(1+\alpha^0\right)\mathbf{y}_f^* + \tilde{\mathbf{s}}\right)\right\|_\infty \le \max\left\{\|\mathbf{Gs}\|_\infty, \left\|\mathbf{G}\left(\frac{1}{\tau}\mathbf{y}_f^* + \tilde{\mathbf{s}}\right)\right\|_\infty\right\} \tag{A4.51}$$

It follows from Eq. (4.19) for the conservative assignation of V_S^* that

$$1+\alpha^0 > 1/K_v \;\;\Rightarrow\;\; dU/dt \le 0 \tag{A4.52}$$

But, because $\mathbf{y}_f^* \in S_{yKv}(\mathbf{s})$,

$$1+\alpha^0 = -\frac{\tau\,\mathbf{y}_f^{*T}\tilde{\mathbf{s}}}{\mathbf{y}^{*T}\mathbf{y}^*} \le \frac{\tau\,\mathbf{y}_f^{*T}\tilde{\mathbf{s}}}{\tau\,\mathbf{y}_f^{*T}\mathbf{s}_0} = 1 + \frac{\mathbf{y}_f^{*T}\delta\mathbf{s}}{\mathbf{y}_f^{*T}\mathbf{s}_0} \tag{A4.53}$$

Eqs. (A4.52) and (A4.53) give the expression in (A4.40) as a sufficient condition for $dU/dt < 0$

♦

<u>THEOREM 4.3</u>: If the conditions of Theorem 4.2 are met, the switching algorithm in (4.14) produces a region S_{z1} in $\delta\mathbf{y}$-space which includes $\delta\mathbf{y}^0$, in which the trajectory of $\delta\mathbf{y}(t)$ slides on the surfaces described by (A4.41). On the sliding surface, the system dynamics are described by (A4.41), in which $\alpha(t)$ is a dynamic variable, governed by the differential equation

$$\dot{\alpha} = -\frac{1}{\tau}\left(\alpha - \alpha^0\right) \tag{A4.54}$$

proof:

Consider the following coordinate transformation and its inverse.

$$\delta\mathbf{y} = \left[\mathbf{B}_D\left(\mathbf{y}^*\right)\;\mathbf{y}^*\right]\begin{bmatrix}\mathbf{z}_1\\ z_2\end{bmatrix}\;,\;\begin{bmatrix}\mathbf{z}_1\\ z_2\end{bmatrix} = \begin{bmatrix}\mathbf{B}_D^T\left(\mathbf{y}^*\right)\mathbf{B}_D\left(\mathbf{y}^*\right) & \mathbf{0}\\ \mathbf{0} & \mathbf{y}^{*T}\mathbf{y}^*\end{bmatrix}^{-1}\begin{bmatrix}\mathbf{B}_D^T\left(\mathbf{y}^*\right)\\ \mathbf{y}^{*T}\end{bmatrix}\delta\mathbf{y} \tag{A4.55}$$

In these coordinates, the differential equation of $\delta\mathbf{z}_1$ can be expressed as

$$\begin{aligned}\mathbf{B}_D^T\left(\mathbf{y}^*\right)\mathbf{B}_D\left(\mathbf{y}^*\right)\frac{d}{dt}\mathbf{z}_1 = &-\frac{1}{\tau}\mathbf{B}_D^T\left(\mathbf{y}^*\right)\mathbf{B}_D\left(\mathbf{y}^*\right)\mathbf{z}_1 + \mathbf{B}_D^T\left(\mathbf{y}^*\right)\mathbf{B}_v\tilde{\mathbf{s}}\\ &+ \mathbf{B}_D^T\left(\mathbf{y}^*\right)\left((1+z_2)\mathbf{B}_D\left(\mathbf{y}^*\right) + \mathbf{B}_D\left(\mathbf{B}_D\left(\mathbf{y}^*\right)\mathbf{z}_1\right)\right)\mathbf{D}_f\end{aligned} \tag{A4.56}$$

where D_R=0 is assumed. Define the quadratic function U_{z1} as

$$U_{z1} = \frac{1}{2}\mathbf{z}_1^T \mathbf{B}_D^T(\mathbf{y}^*)\mathbf{B}_D(\mathbf{y}^*)\mathbf{z}_1 \tag{A4.57}$$

which has the time derivative

$$\frac{d}{dt}U_{z1} = -\frac{2}{\tau}U_{z1} + \mathbf{z}_1^T \mathbf{B}_D^T(\mathbf{y}^*)\left(\mathbf{B}_v\tilde{\mathbf{s}} + (1+z_2)\mathbf{B}_D(\mathbf{y}^*)\mathbf{D}_f\right) \tag{A4.58}$$

Noting the properties

$$\begin{aligned}
\mathbf{B}_D^T(\mathbf{y}^*)\mathbf{B}_v\tilde{\mathbf{s}} &= -y_S^*\mathbf{G}^{-1}\tilde{\mathbf{s}} \\
\mathbf{B}_D^T(\mathbf{y}^*)\mathbf{B}_D(\mathbf{y}^*) &= \mathbf{G}^{-1}\left(y_S^{*2}\mathbf{I} + \mathbf{y}_f^*\mathbf{y}_f^{*T}\right)\mathbf{G}^{-1} \\
\left(\mathbf{B}_D^T(\mathbf{y}^*)\mathbf{B}_D(\mathbf{y}^*)\right)^{-1} &= \frac{1}{y_S^{*2}}\mathbf{G}\left(\mathbf{I} - \frac{\mathbf{y}_f^*\mathbf{y}_f^{*T}}{y_S^{*2} + \mathbf{y}_f^{*T}\mathbf{y}_f^*}\right)\mathbf{G}
\end{aligned} \tag{A4.59}$$

Eq. (A4.58) can be written as

$$\frac{d}{dt}U_{z1} = -\frac{2}{\tau}U_{z1} + \mathbf{z}_1^T \mathbf{B}_D^T(\mathbf{y}^*)\mathbf{B}_D(\mathbf{y}^*)\left(-\frac{1}{y_S^*}\mathbf{G}\left(\mathbf{I} - \frac{\mathbf{y}_f^*\mathbf{y}_f^{*T}}{y_S^{*2} + \mathbf{y}_f^{*T}\mathbf{y}_f^*}\right)\tilde{\mathbf{s}} + (1+z_2)\mathbf{D}_f\right) \tag{A4.60}$$

It is useful to note that the switching rule (4.14) also minimizes the derivative of U_{z1} for arbitrary $\delta\mathbf{y}\in S_1$. This implies that it minimizes the second term on the right-hand side of (A4.60).

Assume that $\delta\mathbf{y}^0\in S_{z1}$ and consider that

$$\mathbf{y}_f^{*T}\tilde{\mathbf{s}} = -\mathbf{y}_{fs}^{*T}\mathbf{B}_{fs}\tilde{\mathbf{s}} = -\frac{1+\alpha^0}{\tau}\mathbf{y}^{*T}\mathbf{y}^* \tag{A4.61}$$

Thus, Eq. (A4.60) becomes

$$\frac{d}{dt}U_{z1} = -\frac{2}{\tau}U_{z1} + \delta\mathbf{z}_1^T \mathbf{B}_{Sfs}^T(\mathbf{y}_{fs}^*)\mathbf{B}_{Sfs}(\mathbf{y}_{fs}^*)\left(-\frac{1}{y_S^*}\mathbf{G}\left(\mathbf{\Delta}_f\mathbf{v} + \frac{1+\alpha^0}{\tau}\mathbf{y}_f^*\right) + (1+\delta z_2)\mathbf{D}_f\right) \tag{A4.62}$$

But for a sliding mode to exist, Eq. (4.38) must be negative definite. The conditions for this to be true are the same as those in the proof to Theorem 4.2, yielding the result that Eq. (A4.62) is negative definite if

$$\delta z_2 > \frac{1}{K_v} - 1 \tag{A4.63}$$

which is equivalent to the inequality in (A4.42) from Theorem 4.2.

If the system is constrained as in Eq. (A4.41), then the differential equation for the constrained system can be derived by observing that

$$\begin{aligned}\frac{d}{dt}\frac{1}{2}\mathbf{y}^T\mathbf{y}\Big|_{\delta\mathbf{y}=\alpha\mathbf{y}^*} &= (1+\alpha)\mathbf{y}^{*T}\mathbf{y}^*\dot{\alpha} \\ &= (1+\alpha)\mathbf{y}^{*T}\left(-\frac{1}{\tau}(\alpha+1)\mathbf{y}^* + \mathbf{B}_v\tilde{\mathbf{s}} + \mathbf{B}_D\left((\alpha+1)\mathbf{y}^*\right)\mathbf{D}_f\right) \\ &= (1+\alpha)\left(-\frac{1}{\tau}(\alpha+1)\mathbf{y}^{*T}\mathbf{y}^* - \mathbf{y}_f^{*T}\tilde{\mathbf{s}}\right)\end{aligned} \tag{A4.64}$$

For any point other than α=–1, the differential equation for α is therefore

$$\begin{aligned}\dot{\alpha} &= -\frac{1}{\tau}(\alpha+1) - \frac{\mathbf{y}_f^{*T}\tilde{\mathbf{s}}}{\mathbf{y}^{*T}\mathbf{y}^*} \\ &= -\frac{1}{\tau}(\alpha+1) + \frac{1}{\tau}\left(\alpha^0+1\right) \\ &= -\frac{1}{\tau}\left(\alpha-\alpha^0\right)\end{aligned} \tag{A4.65}$$

thus proving Eq. (A4.54).

♦

<u>THEOREM 4.4</u>: Let the system be constrained as in (A4.41), and assume that the velocity uncertainty satisfies the upper bound in (4.18). Define the function $\bar{\mathbf{y}}_f^*(\beta,\gamma)$ as

$$\bar{\mathbf{y}}_f^* = \left[(1+\beta)\tilde{\mathbf{s}}_n^T\mathbf{y}_f^* + \beta\left\|\mathbf{y}_f^*\right\|_2\right]\tilde{\mathbf{s}}_n + \gamma\left[\mathbf{I}-\tilde{\mathbf{s}}_n\tilde{\mathbf{s}}_n^T\right]\mathbf{y}_f^* \tag{A4.66}$$

where

$$\tilde{\mathbf{s}}_n = \tilde{\mathbf{s}}_0 / \left\|\tilde{\mathbf{s}}_0\right\|_2 \tag{A4.67}$$

and where $\gamma\in[0,1]$ is related to $\beta\in[-1,0]$ through

$$\gamma = \sqrt{\frac{\mathbf{y}_f^{*T}\mathbf{y}_f^* - \left[(1+\beta)\tilde{\mathbf{s}}_n^T\mathbf{y}_f^* + \beta\left\|\mathbf{y}_f^*\right\|_2\right]^2}{\mathbf{y}_f^{*T}\mathbf{y}_f^* - \left[\tilde{\mathbf{s}}_n^T\mathbf{y}_f^*\right]^2}} \tag{A4.68}$$

Then the feedback controller

$$\beta = \max\left\{1 + \frac{\mathbf{y}_f^{*T}\tilde{\mathbf{s}}_n}{\left\|\mathbf{y}_f^*\right\|_2} - r\,,\,0\right\}\min\{0, K\alpha\} \tag{A4.69}$$

is stable for K<<1, and the differential equation for the closed-loop system for α<0 is

$$\dot{\alpha} = -\frac{1}{\tau}\left[\left(1 + \frac{\|\tilde{\mathbf{s}}_0\|_2 \|\mathbf{y}_f^*\|_2}{\|\mathbf{y}_f^*\|_2^2 + y_S^{*2}} qK\right)\alpha \; + \; \frac{\mathbf{y}_f^{*T}\mathbf{y}_f^* + y_S^{*2} + \tau \mathbf{y}_f^{*T}\tilde{\mathbf{s}}}{\mathbf{y}_f^{*T}\mathbf{y}_f^* + y_S^{*2}}\right] \tag{A4.70}$$

where q>0 is

$$q = \left[\left(1 + \frac{\mathbf{y}_f^{*T}\tilde{\mathbf{s}}_n}{\|\mathbf{y}_f^*\|_2}\right)(1 + \Delta_1 r) + \sqrt{\frac{\|\mathbf{y}_f^*\|_2 + \mathbf{y}_f^{*T}\tilde{\mathbf{s}}_n}{\|\mathbf{y}_f^*\|_2 - \mathbf{y}_f^{*T}\tilde{\mathbf{s}}_n}}\left(\frac{\mathbf{y}_f^{*T}\tilde{\mathbf{s}}_n}{\|\mathbf{y}_f^*\|_2}\right)\Delta_2 r\right]\max\left\{1 + \frac{\mathbf{y}_f^{*T}\tilde{\mathbf{s}}_n}{\|\mathbf{y}_f^*\|_2} - r \;,\; 0\right\} \tag{A4.71}$$

and where Δ_1 and $\Delta_2(\alpha)$ are uncertain constants with $|\Delta_1|\leq 1$ and $|\Delta_2|\leq 1$.

proof:

With the definitions above, the differential equation may be written

$$\dot{\alpha} = -\frac{1}{\tau}\left[\alpha + \frac{\mathbf{y}_f^{*T}\mathbf{y}_f^* + y_S^{*2} + \tau \mathbf{y}_f^{*T}\tilde{\mathbf{s}}}{\mathbf{y}_f^{*T}\mathbf{y}_f^* + y_S^{*2}}\right] - \frac{\|\mathbf{y}_f^*\|_2 + \tilde{\mathbf{s}}_n^T\mathbf{y}_f^*}{\mathbf{y}_f^{*T}\mathbf{y}_f^* + y_S^{*2}}\left(\|\tilde{\mathbf{s}}_0\|_2 + \tilde{\mathbf{s}}_n^T\delta\tilde{\mathbf{s}}\right)\beta + \frac{\mathbf{y}_f^{*T}\left[\mathbf{I} - \tilde{\mathbf{s}}_n\tilde{\mathbf{s}}_n^T\right]\delta\tilde{\mathbf{s}}}{\mathbf{y}_f^{*T}\mathbf{y}_f^* + y_S^{*2}}(1-\gamma) \tag{A4.72}$$

Using the uncertainty bound in (4.18), there exists Δ_1 with $|\Delta_1| \leq 1$ such that

$$\tilde{\mathbf{s}}_n^T\delta\tilde{\mathbf{s}} \leq \Delta_1 r\|\tilde{\mathbf{s}}_0\|_2 \tag{A4.73}$$

Furthermore, it is straight forward to show that for $-\beta$<<1

$$1 - \gamma \approx \frac{\mathbf{y}_f^{*T}\tilde{\mathbf{s}}_n}{\|\mathbf{y}_f^*\|_2 - \mathbf{y}_f^{*T}\tilde{\mathbf{s}}_n}\beta \tag{A4.74}$$

so

$$\begin{aligned}\left|\mathbf{y}_f^{*T}\left[\mathbf{I} - \tilde{\mathbf{s}}_n\tilde{\mathbf{s}}_n^T\right]\delta\tilde{\mathbf{s}}(1-\gamma)\right| &\leq \sqrt{\|\mathbf{y}_f^*\|_2^2 - \left(\mathbf{y}_f^{*T}\tilde{\mathbf{s}}_n\right)^2}\,\|\delta\tilde{\mathbf{s}}\|_2(1-\gamma) \\ &\approx \left(\|\delta\tilde{\mathbf{s}}\|_2\mathbf{y}_f^{*T}\tilde{\mathbf{s}}_n\sqrt{\frac{\|\mathbf{y}_f^*\|_2 + \mathbf{y}_f^{*T}\tilde{\mathbf{s}}_n}{\|\mathbf{y}_f^*\|_2 - \mathbf{y}_f^{*T}\tilde{\mathbf{s}}_n}}\right)\beta \\ &\leq \left(r\|\tilde{\mathbf{s}}_0\|_2\mathbf{y}_f^{*T}\tilde{\mathbf{s}}_n\sqrt{\frac{\|\mathbf{y}_f^*\|_2 + \mathbf{y}_f^{*T}\tilde{\mathbf{s}}_n}{\|\mathbf{y}_f^*\|_2 - \mathbf{y}_f^{*T}\tilde{\mathbf{s}}_n}}\right)\beta\end{aligned} \tag{A4.75}$$

So there exists Δ_2 with $|\Delta_2| \leq 1$ such that

$$\mathbf{y}_f^{*T}\left[\mathbf{I}-\widetilde{\mathbf{s}}_n\widetilde{\mathbf{s}}_n^T\right]\delta\widetilde{\mathbf{s}}(1-\gamma)=\left(\Delta_2 r\|\widetilde{\mathbf{s}}_0\|_2\,\mathbf{y}_f^{*T}\widetilde{\mathbf{s}}_n\sqrt{\frac{\|\mathbf{y}_f^*\|_2+\mathbf{y}_f^{*T}\widetilde{\mathbf{s}}_n}{\|\mathbf{y}_f^*\|_2-\mathbf{y}_f^{*T}\widetilde{\mathbf{s}}_n}}\right)\beta \tag{A4.76}$$

Thus, the control law in (A4.69) yields the closed-loop differential equation as (A4.70) for β small. To prove stability, it is sufficient to prove that $q\geq 0$. Observing that

$$\mathbf{y}_f^*\in S_{yKv}(\mathbf{s}_0)\Rightarrow\mathbf{y}_f^{*T}\widetilde{\mathbf{s}}_n<0 \tag{A4.77}$$

it follows that

$$\begin{aligned}\min(q)&\geq\left\{\left(1+\frac{\mathbf{y}_f^{*T}\widetilde{\mathbf{s}}_n}{\|\mathbf{y}_f^*\|_2}\right)(1-r)+r\frac{\mathbf{y}_f^{*T}\widetilde{\mathbf{s}}_n}{\|\mathbf{y}_f^*\|_2}\sqrt{\frac{\|\mathbf{y}_f^*\|_2+\mathbf{y}_f^{*T}\widetilde{\mathbf{s}}_n}{\|\mathbf{y}_f^*\|_2-\mathbf{y}_f^{*T}\widetilde{\mathbf{s}}_n}}\right\}\max\left\{1+\frac{\mathbf{y}_f^{*T}\widetilde{\mathbf{s}}_n}{\|\mathbf{y}_f^*\|_2}-r\ ,\ 0\right\}\\&\geq\left\{1+\frac{\mathbf{y}_f^{*T}\widetilde{\mathbf{s}}_n}{\|\mathbf{y}_f^*\|_2}-r\right\}\max\left\{1+\frac{\mathbf{y}_f^{*T}\widetilde{\mathbf{s}}_n}{\|\mathbf{y}_f^*\|_2}-r\ ,\ 0\right\}\\&=\max\left\{1+\frac{\mathbf{y}_f^{*T}\widetilde{\mathbf{s}}_n}{\|\mathbf{y}_f^*\|_2}-r\ ,\ 0\right\}^2\geq 0\end{aligned} \tag{A4.78}$$

Chapter 5. The Actuator-Structure System

In the preceding chapters, the development and characterization of RFA networks has been presented. In Chapter 2, a dynamic model for the actuation system was derived in which the switch position vector **D** is the control input. The electrical system dynamics are influenced by these control inputs and the actuation velocity vector **v**, giving the differential equation for the electrical states. In Chapter 3, the force capability of the system was characterized. This led to definition of the Region of Feasible Forces, denoted $S(\mathbf{v})$, which is the region in $\mathbf{f}_e$-space of forces which may be sustained in switching equilibrium for a given **v**. The developments in Chapter 3 also led to the maximum force limit $|\mathbf{f}_e|\leq\mathbf{f}_{\max}$, which arises because of the maximum current ratings of the electric machines. Chapter 4, dealt with the dynamics of the electrical network, and developed a way of controlling **D**, so as to bring about tracking between $\mathbf{f}_e$ and a command $\mathbf{f}_e^*$. A feedback switching rule was derived which is effective at bringing about zero-error force tracking when $\mathbf{f}_e^*\in S(\mathbf{v})$, and which is also robust to uncertainty in the boundary $\partial S(\mathbf{v})$.

With these developments, a method has been illustrated by which an RFA network such as that described in Chapter 1 might be constructed. Along the way, the characterization of the device system has led to a more realistic description of the capabilities and limitations of the these systems than that described by Eq. (1.3).

At this point, the focus is turned to the integration of an RFA network into a structure. Several specific issues are addressed. First, the physical model for the electromechanical system is presented, which includes the structural and electrical dynamics, as well as the mechanical properties of the rotor shaft and screw conversion of each machine. Next, the "nominal model" of the overall system is presented. This model is the one which will be used in the ensuing mathematical development for the purposes of system analysis and design. It is a simplified version of the physical model, which is necessary in order to permit a reasonable theoretical treatment of the control problem, while still retaining the most fundamental characteristics of the actuators.

The third section of this chapter concerns the use of the RFA network to realize an effective linear structural damping. This mode of operation falls short of utilizing the full forcing capability of the system, because it effectively constrains $\mathbf{f}_e$ to obey the linear velocity feedback law $\mathbf{f}_e=-\mathbf{C}\mathbf{v}$, with constraints on **C** to ensure that $\mathbf{f}_e\in S(\mathbf{v})$. However, this formulation is useful because that it provides some physical insight into the capabilities of RFA networks, and also

because it can, in some circumstances, be used to significantly enhance the performance of the structural response.

This chapter also contains a discussion of performance measures, and addresses the question of the degree to which a particular **C** improves the structural response. A typical performance measure would somehow weigh inter-story drifts against absolute accelerations and structural energy dissipation. In this and the following chapters, both deterministic and stochastic responses will be studied, and performance measures are thus presented for both cases.

A method is presented for the determination of the matrix **C** which yields optimal stochastic performance. This method is derived in a general framework using the nominal model. Several examples are given for different actuation systems, distributed throughout a three-story structure, subjected to stationary white-noise base excitation. Examples for three actuator configurations are presented and discussed, and together illustrate the versatility of these systems.

5.1: The Physical Model

Consider an arbitrary n-DOF base-excited shear structure equipped with an RFA system. The response of such a structure is governed by

$$\mathbf{M}_S\ddot{\mathbf{q}} + \mathbf{C}_S\dot{\mathbf{q}} + \mathbf{K}_S\mathbf{q} = -\mathbf{M}_S\mathbf{G}a_g + \mathbf{N}\mathbf{f} \tag{5.1}$$

where $\mathbf{q}$ is the structural displacement vector relative to the base, a_g is the base acceleration, and $\mathbf{f}$ is the m-vector of actuator forces.

The forces $\mathbf{f}$ are said to be *degenerate* if the matrix $\mathbf{N}$ has rank less than m (i.e., if $\mathbf{N}$ has a nontrivial null space). Here, it will be assumed that the actuation system is nondegenerate. The matrix $\mathbf{N}$ also relates the actuation velocities $\mathbf{v}$ to the structural velocities, $\dot{\mathbf{q}}$, through

$$\mathbf{v} = \mathbf{N}^T\dot{\mathbf{q}} \tag{5.2}$$

The adjoint participation of $\mathbf{N}$ in (5.1) and (5.2) is sometimes called the *reciprocity* relation.

Using Eq. (2.30), $\mathbf{f}$ is related to the electromechanical force vector $\mathbf{f}_e$, and to the structural dynamics, through

$$\mathbf{f} = \mathbf{H}(\mathbf{f},\mathbf{v})\left[\mathbf{f}_e - \mathbf{L}^{-2}\mathbf{B}_A\mathbf{N}^T\dot{\mathbf{q}} - \mathbf{L}^{-2}\mathbf{J}_A\mathbf{N}^T\ddot{\mathbf{q}}\right] \tag{5.3}$$

where

$$\mathbf{H}(\mathbf{f},\mathbf{v}) = \mathrm{diag}\{h_1(f_1v_1)\ ,\ \ldots\ ,\ h_m(f_mv_m)\} \qquad \mathbf{L} = \mathrm{diag}\{l_1\ ,\ \ldots\ ,\ l_m\}$$
$$\mathbf{B}_A = \mathrm{diag}\{B_1\ ,\ \ldots\ ,\ B_m\} \qquad \mathbf{J}_A = \mathrm{diag}\{J_1\ ,\ \ldots\ ,\ J_m\}$$

Thus, the response of the structural system can be expressed as

$$\left[\mathbf{M}_S + \mathbf{N}\mathbf{H}(\mathbf{f},\mathbf{v})\mathbf{L}^{-2}\mathbf{J}_A\mathbf{N}^T\right]\ddot{\mathbf{q}} + \left[\mathbf{C}_S + \mathbf{N}\mathbf{H}(\mathbf{f},\mathbf{v})\mathbf{L}^{-2}\mathbf{B}_A\mathbf{N}^T\right]\dot{\mathbf{q}} + \mathbf{K}_S\mathbf{q} = -\mathbf{M}_S\mathbf{G}a_g + \mathbf{N}\mathbf{H}(\mathbf{f},\mathbf{v})\mathbf{f}_e \quad (5.4)$$

This equation, together with the dynamic description of the electrical system, fully characterizes the actuator-structure model.

For the purposes of this analysis, it will be assumed that at most one flywheel exists, characterized by an angular displacement θ_{fw}, and electromechanical torque T_{efw}. The combined flywheel rotor and shaft has viscosity B_{fw} and inertia J_{fw}. The total torque applied to the flywheel shaft is thus

$$T_{fw} = T_{efw} - B_{fw}\dot{\theta}_{fw} - J_{fw}\ddot{\theta}_{fw} \quad (5.5)$$

The dynamic description in (5.4) can be augmented to include flywheel dynamics, by appending θ_{fw} to the $\mathbf{q}$ vector. Similarly, T_{fw} is appended to the $\mathbf{f}$ vector, as

$$\mathbf{q} \rightarrow \begin{bmatrix} \mathbf{q} \\ \theta_{fw} \end{bmatrix} \quad \mathbf{f} \rightarrow \begin{bmatrix} \mathbf{f} \\ T_{efs} - B_{fw}\dot{\theta}_{fw} - J_{fw}\ddot{\theta}_{fw} \end{bmatrix} \quad (5.6)$$

The system matrices in (5.4) can be extended to accommodate this new mechanical degree of freedom. Specifically, the substitutions to be made to the matrices in the system are given below.

$$\begin{gathered} \mathbf{M}_S \rightarrow \begin{bmatrix} \mathbf{M}_S & \mathbf{0} \\ \mathbf{0} & 0 \end{bmatrix}, \mathbf{C}_S \rightarrow \begin{bmatrix} \mathbf{C}_S & \mathbf{0} \\ \mathbf{0} & 0 \end{bmatrix}, \mathbf{K}_S \rightarrow \begin{bmatrix} \mathbf{K}_S & \mathbf{0} \\ \mathbf{0} & 0 \end{bmatrix}, \mathbf{B}_A \rightarrow \begin{bmatrix} \mathbf{B}_A & \mathbf{0} \\ \mathbf{0} & B_{fw} \end{bmatrix}, \mathbf{J}_A \rightarrow \begin{bmatrix} \mathbf{J}_A & \mathbf{0} \\ \mathbf{0} & J_{fw} \end{bmatrix} \\ \mathbf{N} \rightarrow \begin{bmatrix} \mathbf{N} & \mathbf{0} \\ \mathbf{0} & 1 \end{bmatrix}, \mathbf{G} \rightarrow \begin{bmatrix} \mathbf{G} \\ 0 \end{bmatrix}, \mathbf{H}(\mathbf{f},\mathbf{v}) \rightarrow \begin{bmatrix} \mathbf{H}(\mathbf{f},\mathbf{v}) \\ 1 \end{bmatrix}, \mathbf{L} \rightarrow \begin{bmatrix} \mathbf{L} & \mathbf{0} \\ \mathbf{0} & 1 \end{bmatrix} \end{gathered} \quad (5.7)$$

For the remainder of this study, the discussion is immaterial to the existence of a flywheel degree of freedom, unless otherwise mentioned.

5.2: The Nominal System Model

Eq. (5.4), together with the electrical dynamics of $\mathbf{f}_e$, constitutes the *physical model* of the system. This model, while suitable for simulation, has characteristics which make it cumbersome for the purposes of system analysis. It contains the low-frequency dynamics of the structure as well as the switching dynamics of the electronics, which occur at frequencies four or five decades higher. This results in a system model which is rather slow in simulation. The model also includes nonlinearities, some of which make dynamic system analysis unnecessarily difficult. Left unaddressed, these issues will make the analysis of RFA networks in the coming chapters significantly more complicated.

In order for an analytical treatment of RFA networks to be practical, a simplified model of the structure-actuator system must be developed which balances realism with tractability. This

will be called the *Nominal System Model* (*NSM*). It is desirable that the NSM contain the most fundamental traits of the electromechanical system, but it should be simple enough that a mathematical analysis of the system is not overly cumbersome. Toward this end, several approximations are made for the NSM:

- ***Lossless screw conversions**:* Note that $\mathbf{H}(\mathbf{f},\mathbf{v})\approx\mathbf{I}$ for high-efficiency conversions. This approximation will be made for the NSM, because it allows for the mechanical system to be represented as a linear differential equation. If this approximation is not made, then Eq. (5.3) does not, in general, have a closed-form solution for $\mathbf{f}$, due to the fact that $\mathbf{f}$ contributes to the accelerations $\ddot{\mathbf{q}}$ in (5.3).
- ***Lossless electronic switches**:* This assumption is equivalent to assuming that the semiconductor switches in the electrical system are ideal. It has been shown that the influence of semiconductor losses on $S(\mathbf{v})$ is only significant for small $\|\mathbf{v}\|$. However, the inclusion of these effects greatly complicates the expression for $S(\mathbf{v})$. If these effects are neglected, the boundary $\partial S(\mathbf{v})$ is described by a simple quadratic equation.
- ***No electrical parameter uncertainty or time delay**:* The effect of parameter uncertainty on the electronic control system's ability to track a force command was discussed at length in Chapter 4. The switching controller was designed to be robust to such uncertainties. As their inclusion would greatly complicate the NSM, such effects are ignored here.
- ***Instantaneous electrical dynamics**:* This assumption is equivalent to assuming that the electronic control system can instantaneously realize any force; i.e., $\mathbf{f}_e^*=\mathbf{f}_e$. Because the electrical time constants are explicitly designed to be much smaller than the mechanical time constants, this assumption is deemed reasonable.

It is important to emphasize that these assumptions will be used only for the purposes of system analysis and controller design. Clearly, the true physical model is a more accurate description of the system behavior. Thus, the transient simulations presented in Chapter 7 will be done using this physical model.

The simplified model resulting from these assumptions is a linear mechanical system. The viscosity and inertia of the rotor may be reflected into the structural damping and inertia, to obtain the system description

$$\mathbf{M}_{SA}\ddot{\mathbf{q}}+\mathbf{C}_{SA}\dot{\mathbf{q}}+\mathbf{K}_S\mathbf{q}=-\mathbf{M}_S\mathbf{G}a_g+\mathbf{N}\mathbf{f}_e \tag{5.8}$$

where

$$\mathbf{M}_{SA}=\mathbf{M}_S+\mathbf{N}\mathbf{L}^{-2}\mathbf{J}_A\mathbf{N}^T \qquad \mathbf{C}_{SA}=\mathbf{C}_S+\mathbf{N}\mathbf{L}^{-2}\mathbf{B}_A\mathbf{N}^T \tag{5.9}$$

The system above incorporates the mechanical dynamics of the rotor shafts with the structural dynamics, leaving $\mathbf{f}_e$ as the control input to the system. Note that the combined mass and damping matrices, $\mathbf{M}_{SA}$ and $\mathbf{C}_{SA}$, retain symmetry with the inclusion of the rotor inertia and viscosity, because $\mathbf{L}$, $\mathbf{J}_A$, and $\mathbf{B}_A$ are diagonal. However, $\mathbf{M}_{SA}$ does not in general retain diagonality.

Because the electrical dynamics are assumed to be negligible, the above equation constitutes a complete description of the dynamics of the NSM. Because there is no distinction between $\mathbf{f}_e^*$ and $\mathbf{f}_e$ in the nominal model, both will be referred to as $\mathbf{f}_e$ to ease the notation.

With the assumptions outlined above, the constraint $\mathbf{f}_e \in S(\mathbf{v})$ becomes

$$\mathbf{f}_e^T \mathbf{C}_c^{-1} \mathbf{f}_e + \mathbf{f}_e^T \mathbf{N}^T \dot{\mathbf{q}} \le 0 \tag{5.10}$$

and the constraints on maximum force are

$$|\mathbf{f}_e| \le \mathbf{f}_{\max} \tag{5.11}$$

It will be convenient in the course of this analysis to convert Eq (5.8) to a system of first-order differential equations, and to normalize the system states and forces. Introducing the coordinate vector $\mathbf{w}$ and the normalized force vector $\mathbf{u}$ as

$$\mathbf{w} = \begin{bmatrix} \mathbf{M}_{SA} & \mathbf{0} \\ \mathbf{0} & \mathbf{M}_{SA} \end{bmatrix}^{1/2} \begin{bmatrix} \mathbf{q} \\ \dot{\mathbf{q}} \end{bmatrix} \qquad \mathbf{u} = \mathbf{C}_c^{-1/2} \mathbf{f}_e \tag{5.12}$$

the system state-space description can be represented as

$$\dot{\mathbf{w}} = \mathbf{A}\mathbf{w} + \mathbf{B}_u \mathbf{u} + \mathbf{B}_a a_g \tag{5.13}$$

where

$$\begin{aligned} \mathbf{A} &= \begin{bmatrix} \mathbf{M}_{SA} & \mathbf{0} \\ \mathbf{0} & \mathbf{M}_{SA} \end{bmatrix}^{-1/2} \begin{bmatrix} \mathbf{0} & \mathbf{I} \\ -\mathbf{K}_S & -\mathbf{C}_{SA} \end{bmatrix} \begin{bmatrix} \mathbf{M}_{SA} & \mathbf{0} \\ \mathbf{0} & \mathbf{M}_{SA} \end{bmatrix}^{-1/2} \\ \mathbf{B}_u &= \begin{bmatrix} \mathbf{M}_{SA} & \mathbf{0} \\ \mathbf{0} & \mathbf{M}_{SA} \end{bmatrix}^{-1/2} \begin{bmatrix} \mathbf{0} \\ \mathbf{N}\mathbf{C}_c^{1/2} \end{bmatrix} \qquad \mathbf{B}_a = \begin{bmatrix} \mathbf{M}_{SA} & \mathbf{0} \\ \mathbf{0} & \mathbf{M}_{SA} \end{bmatrix}^{-1/2} \begin{bmatrix} \mathbf{0} \\ \mathbf{M}_S \mathbf{G} \end{bmatrix} \end{aligned} \tag{5.14}$$

The constraints on $\mathbf{u}$ are then

$$P(\mathbf{u}, \mathbf{w}) := \mathbf{u}^T \mathbf{u} + \mathbf{u}^T \mathbf{B}_u^T \mathbf{w} \le 0 \tag{5.15a}$$

$$|\mathbf{u}| \le \mathbf{u}_{\max} \tag{5.15b}$$

Together, Eqs. (5.13) and (5.15) constitute the NSM, parameterized by $\mathbf{A}$, $\mathbf{B}_u$, $\mathbf{B}_a$, and $\mathbf{u}_{\max}$.

5.3: Effective Damping of the RFA Network

Consider a feedback control regime in which **u** is related to **w** through a $m \times m$ feedback matrix **Z**, as

$$\mathbf{u} = -\mathbf{Z}\mathbf{B}_u^T\mathbf{w} \tag{5.16}$$

where the values of **Z** may be controlled. Through Eq. (5.15a), it is then clear that a constraint exists on the matrix **Z**, as

$$\mathbf{w}^T\mathbf{B}_u\left(\mathbf{Z}^T\mathbf{Z}-\mathbf{Z}\right)\mathbf{B}_u^T\mathbf{w} \le 0 \tag{5.17}$$

Assuming that the actuation system is nondegenerate, the necessary and sufficient condition for this relation to hold for all **w** is that

$$\begin{aligned} &\mathbf{Z}^T\mathbf{Z}-\mathbf{Z} \le 0 \\ &\Leftrightarrow \mathbf{Z}^T\mathbf{Z}-\tfrac{1}{2}\mathbf{Z}-\tfrac{1}{2}\mathbf{Z}^T \le 0 \end{aligned} \tag{5.18}$$

Completing the square,

$$\left(\mathbf{Z}-\tfrac{1}{2}\mathbf{I}\right)^T\left(\mathbf{Z}-\tfrac{1}{2}\mathbf{I}\right)-\tfrac{1}{4}\mathbf{I} \le 0 \tag{5.19}$$

which is true if and only if the following maximum singular value condition holds.

$$\bar{\sigma}\left(\mathbf{Z}-\tfrac{1}{2}\mathbf{I}\right) \le \tfrac{1}{2} \tag{5.20}$$

Satisfaction of Eq. (5.20) implies that **u**, as related to **v** in Eq. (5.16), satisfies constraint (5.15a).

If it can be assumed that **w** is sufficiently small, or **Z** is somehow additionally constrained such that **u** does not violate Eq. (5.15b), then this "velocity feedback" approach fully characterizes the RFA network capability for the NSM. This approach can be useful for a number of reasons. For some applications, such a formulation leads to a static feedback law (i.e., **Z** constant and pre-designed) which yields high performance in closed-loop. Such an implementation has certain advantages, in that it does not place large demands on control intelligence, and affords an implementation which requires no structural sensors. Also, if **Z** is constant then the closed-loop system is linear, which expedites an analysis of the structural response.

Equally important is the physical insight which may be gained from this approach. Let the feedback relation in (5.16) be expressed in the $\mathbf{f}_e$ coordinates, as

$$\mathbf{f}_e = -\mathbf{C}_c^{1/2}\mathbf{Z}\mathbf{C}_c^{1/2}\mathbf{v} \tag{5.21}$$

Thus, this approach establishes an effective linear structural damping relation. While it may at first seem frivolous to use such advanced technology merely to apply linear damping to a structure, several characteristics make this approach intriguing.

5.3.1: Non-local Damping

Note that, when incorporated into the NSM differential equation, the total system damping matrix becomes

$$\mathbf{C}_{SA} + \mathbf{N}\mathbf{C}_c^{1/2}\mathbf{Z}\mathbf{C}_c^{1/2}\mathbf{N}^T \tag{5.22}$$

The **Z** term above has the potential to have a very large band, even if the band of $\mathbf{C}_{SA}$ is quite small. Physically, the significance of this is that the RFA network is capable of creating the effect of viscous dampers which interface remote locations in the structure. By contrast, consider the case with the actuators removed, and replaced with mechanical viscous dampers. In this circumstance, the influence of these dampers on the structural differential equation could still be expressed in terms of **Z**, but the locally-dissipative nature of the dampers would constrain **Z** to be diagonal.

As an example, consider a structure with two actuators. Let the **Z** matrix be described as

$$\mathbf{Z} = \mathbf{C}_c^{-1/2}\begin{bmatrix} c_{11} & c_{12} \\ c_{12} & c_{22} \end{bmatrix}\mathbf{C}_c^{-1/2} \tag{5.23}$$

Let the structure be a simple n-DOF base-excited shear structure with n>2. Let actuator 1 be placed between floors p_1 and p_1+1 and actuator 2 placed between floors p_2 and p_2+1, where the floor number increases from the base and p_2>p_1+1. Then the **N** matrix is

$$\mathbf{N} = \begin{bmatrix} \cdots\ 0\ -1\ 1\ 0\ \cdots & \\ & \cdots\ 0\ -1\ 1\ 0\ \cdots \end{bmatrix}^T \tag{5.24}$$

and the contribution of the actuators to the overall structural damping matrix is therefore

$$\left[\begin{array}{c|cc|c|cc|c} \mathbf{0} & \multicolumn{2}{c|}{\mathbf{0}} & \mathbf{0} & \multicolumn{2}{c|}{\mathbf{0}} & \mathbf{0} \\ \hline \mathbf{0} & c_{11} & -c_{11} & \mathbf{0} & c_{12} & -c_{12} & \mathbf{0} \\ & -c_{11} & c_{11} & & -c_{12} & c_{12} & \\ \hline \mathbf{0} & \multicolumn{2}{c|}{\mathbf{0}} & \mathbf{0} & \multicolumn{2}{c|}{\mathbf{0}} & \mathbf{0} \\ \hline \mathbf{0} & c_{12} & -c_{12} & \mathbf{0} & c_{22} & -c_{22} & \mathbf{0} \\ & -c_{12} & c_{12} & & -c_{22} & c_{22} & \\ \hline \mathbf{0} & \multicolumn{2}{c|}{\mathbf{0}} & \mathbf{0} & \multicolumn{2}{c|}{\mathbf{0}} & \mathbf{0} \end{array}\right] \tag{5.25}$$

This damping configuration has a physical interpretation, as illustrated in Fig. 5.1. Note the distribution of *negative* damping as well as positive damping. The fact that **Z** is positive definite (as implied by (5.20)) ensures that the total supplemental damping matrix is positive definite. Furthermore, it is easy to show that if a damping matrix with a given c_{12} meets constraint (5.20), then the matrix with $-c_{12}$ also meets the constraint. The damping configuration in Fig. 5.1 illustrates that RFA networks enable not only local damping between the degrees of freedom at which each individual device is attached, but also non-local damping between remote degrees of freedom.

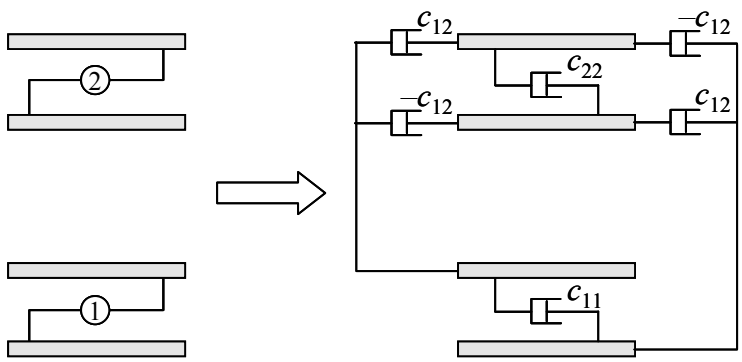

Figure 5.1: Effective damping configurations for Eq. (5.25)

5.3.2: RFA Stacks

Another interesting potential use of RFA networks involves the specific circumstance of the above characteristic, where the two actuators share a degree of freedom. In this case, again using the terminology in Eq. (5.23) for the equivalent damping, except that $p_2=p_1+1$, the overall supplemental damping is shown in Fig. 5.2. Note that if the cross-term c_{12} is small, this looks like inter-story damping. As c_{12} becomes larger, however, the structural damping becomes more interesting.

Condition (5.20) is equivalent to the conditions

$$c_{12}^2 \le c_{11}c_{22} \quad , \quad 0 \le \frac{c_{11}}{C_{c11}} + \frac{c_{22}}{C_{c22}} \le 1 \tag{5.26}$$

Note that for c_{11} and c_{22} sufficiently small, the designation of $c_{11}=c_{22}=-c_{12}=c$ is admissible. This designation results in the effective cancellation of the inter-story dampers in Fig. 5.2, leaving an effective damper c between stories 1 and 3.

This logic may be applied to stacks of more than two devices, creating the effect of dampers which connect remote degrees of freedom directly. They are therefore capable of producing so-called "Groundhook" damping (i.e., damping between the base of a structure and a degree of freedom at a level much higher in the structure.) However, it should be noted that such an implementation would require many devices, which could be rather impractical. Also, as the

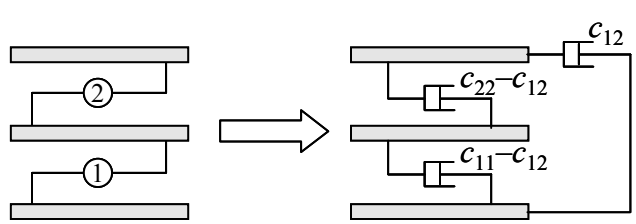

Figure 5.2: A simple stacked RFA system

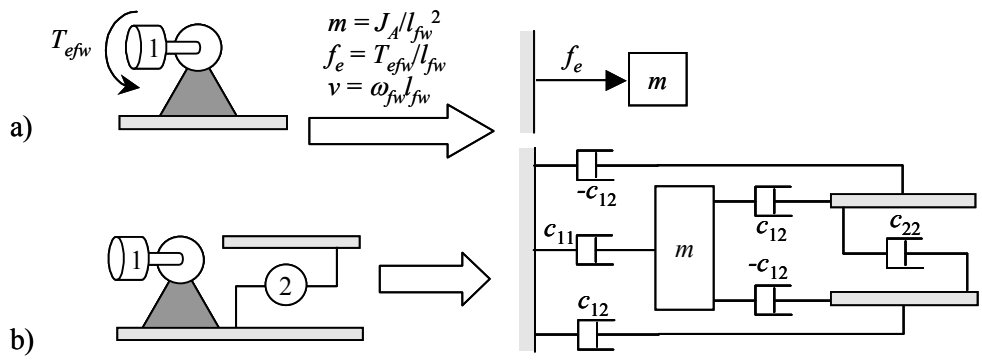

Figure 5.3: Quasi-Skyhook Damping

number of devices increases, the maximum c for which the **Z** constraint is satisfied becomes smaller, because the electrical system incurs greater transmissive power losses as the size of the network increases.

5.3.3: Quasi-Skyhook Damping

Consider that the rotational dynamics of a flywheel are mathematically equivalent to the linear dynamics of a mass, relative to the inertial reference frame. This is illustrated in Fig. 5.3a, where the screw lead l_{fw} is arbitrary. Thus, **Z** as in Eq. (5.23) couples the linear motion of a structural degree of freedom with the rotational motion of a flywheel, this is conceptually equivalent to the indirect interfacing of the structure with the inertial reference frame, as illustrated in Fig. 5.3b.

It is widely recognized that, by establishing a direct damping relationship between a base-excited structural system and the inertial reference frame, the absolute acceleration of the structure can be greatly reduced. This approach is commonly referred to as "Skyhook" damping.

For the configuration in Fig. 5.3b, the damping connection to the inertial reference frame is indirect (i.e., it interfaces an ancillary mass with the structure and the inertial reference frame, rather than providing a direct connection). This configuration will therefore be called "Quasi-Skyhook" damping. Its optimal use to reduce accelerations in civil structures is still not completely understood. An analogous concept has been recognized in the aerospace applications where a piezoelectric actuator, interfaced with a capacitive shunt, may be used to achieve the same kind of effect.

5.3.4: Skew Damping

There is an additional aspect to the velocity feedback relation in (5.16) that is worthy of discussion. Note that in the development of Eq. (5.16), **Z** is not required to be symmetric. From

Eq. (5.22), the implementation of an asymmetric **Z** results in an asymmetric structural damping matrix. Structural vibration theory with asymmetric stiffness, damping, and mass matrices has received some attention over the years (e.g. (Adhikari 1999; Caughey and Ma 1993; Inman 1983)). Asymmetric damping matrices show up in many systems with gyroscopic forces. Also, active control systems with linear velocity feedback may also be thought of as creating asymmetric (as well as possibly non-positive definite) damping matrices.

The physical meaning of "skew damping" in the context of general structural vibrations may be interpreted as a circulation of mechanical energy throughout the structure. Although this has no direct analogy in the context of traditional structural dynamics, it may nonetheless be framed in the context of passive vibrations. It corresponds to the direct transmission of energy through a structure.

Let **Z** be decomposed into symmetric and skew-symmetric components, as

$$\mathbf{Z} = \mathbf{Z}_H + \mathbf{Z}_S \quad , \quad \mathbf{Z}_H = \mathbf{Z}_H^T \quad , \quad \mathbf{Z}_S = -\mathbf{Z}_S^T \tag{5.27}$$

Then the symmetric component has a physical interpretation discussed in previous subsections, where symmetry was tacitly assumed. The skew-symmetric component of **Z** has no energy dissipation associated with it. To see this, consider that the rate of energy dissipation of the effective damping is

$$\begin{aligned} \mathbf{f}_e^T \mathbf{v} &= \mathbf{v}^T \mathbf{C}_c^{1/2} \left(\mathbf{Z}_H + \mathbf{Z}_S \right) \mathbf{C}_c^{1/2} \mathbf{v} \\ &= \mathbf{v}^T \mathbf{C}_c^{1/2} \mathbf{Z}_H \mathbf{C}_c^{1/2} \mathbf{v} \end{aligned} \tag{5.28}$$

where it has been observed that quadratic operations on skew matrices are identically zero.

The direction of the power flow for each device depends on the instantaneous structural velocity, and the choice of $\mathbf{Z}_S$. As an example, consider again a two-actuator system. Let

$$\mathbf{Z}_S = \mathbf{C}_c^{-1/2} \begin{bmatrix} 0 & c \\ -c & 0 \end{bmatrix} \mathbf{C}_c^{-1/2} \tag{5.29}$$

Then the electrical power generated by actuator 1 is cv_1v_2. Likewise, the electrical power generated by actuator 2 is $-cv_1v_2$. Thus, the circulation of mechanical energy in this system is illustrated in Fig. 5.4.

The constraint on **Z** in inequality (5.20) results in a coupling of constraints on $\mathbf{Z}_H$ and $\mathbf{Z}_S$. If $\mathbf{Z}_H=\mathbf{0}$, the only value of $\mathbf{Z}_S$ satisfying the inequality is $\mathbf{Z}_S=\mathbf{0}$. Physically, this is because the RFA network is not 100% efficient, and dissipates some electrical energy during transmission. Thus, a **Z** with a significant skew component also requires a significant symmetric component to overcome the losses in the network. However, the norm of $\mathbf{Z}-\frac{1}{2}\mathbf{I}$ is bounded, so there is a limit to how large both these matrices can be.

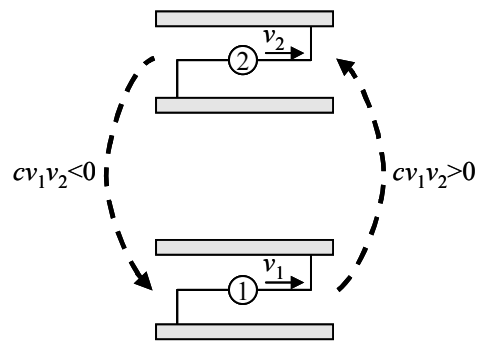

Figure 5.4: Circulation of mechanical energy due to skew damping

Skew damping matrices are particularly interesting for systems containing flywheel energy storage. In this case, the power flow between the structure and the flywheel can manifest itself in a skew damping relationship. In the design of Quasi-skyhook damping systems, for example, it will be shown that the stochastic-optimal **Z** matrix is the sum of diagonal and skew matrices.

5.4: Measures of Performance

Clearly, the characteristics of the structural response will vary with the choice of **Z**. Some responses will be more "favorable" than others. For instance, some responses will have smaller maximum inter-story drifts, structural energy dissipation, absolute accelerations, etc. It is useful to quantify this level of favorability, or *performance*, of a given **Z**. Let the functional J be this measure of performance, with the convention that lower J values denote better performance.

5.4.1: Deterministic Response

Let $\mathbf{w}(t)$ be the structural response for a given **Z** and for initial condition $\mathbf{w}_0$ and excitation $a_g(t)$, over the time interval $[0,t_f]$. Define J as

$$J\left(\mathbf{Z};a_g(.),\mathbf{w}_0\right)=\int_0^{t_f}\phi\left(\mathbf{w}(t);\mathbf{Z},a_g(t)\right)dt \tag{5.30}$$

where $\phi:\Re^{2n}\mapsto\Re$ is positive-definite and continuous. Through an appropriate definition of ϕ, such a performance measure can take on many different physical interpretations. This study concentrates on three special cases:

- ***Mean-square accelerations**:* Let $\mathbf{a}(t)$ be the vector of absolute floor accelerations at time t and consider the case

$$\begin{aligned}\phi\left(\mathbf{w}(t);\mathbf{Z},a_g(t)\right) &= \left\|\mathbf{a}(t)\right\|_2^2 \\ &= \left\|\begin{bmatrix}\mathbf{0} & \mathbf{M}_{SA}^{-1/2}\end{bmatrix}\left(\mathbf{A}-\mathbf{B}_u^T\mathbf{Z}\mathbf{B}_u\right)\mathbf{w}(t)+\left(\mathbf{I}-\mathbf{M}_{SA}^{-1}\mathbf{M}_S\right)\mathbf{G}a_g(t)\right\|_2^2\end{aligned} \tag{5.31}$$

Then J is equal to the mean-square acceleration over the duration $t\in[0,t_f]$.

- ***Maximum Drifts***: Let $\mathbf{d}(t)$ be the inter-story drift vector at time t, which is related to $\mathbf{w}(t)$ through

$$\mathbf{d}(t)=\begin{bmatrix}\begin{bmatrix}1 & & & \mathbf{0}\\ -1 & 1 & & \\ & \ddots & \ddots & \\ \mathbf{0} & & -1 & 1\end{bmatrix}\mathbf{M}_{SA}^{-1/2} & \mathbf{0}_{n\times n}\end{bmatrix}\mathbf{w}(t) \tag{5.32}$$

Suppose that "good performance" is measured by the ability of $\mathbf{Z}$ to keep each drift d_k below some threshold d_{kth}. Let

$$\phi=\sum_{k=1}^{n}\left(d_k/d_{kth}\right)^{2p} \tag{5.33}$$

where p is a positive integer. Then for p large,

$$\phi\left(\mathbf{w}(t)\right)\approx\max_{k\in\{1..n\}}\left(d_k(t)/d_{kth}\right)^{2p} \tag{5.34}$$

and consequently, J is very large if $|d_k(t)|>d_{kth}$ for $k\in\{1..n\}$, $t\in[0,t_f]$, and very small otherwise. On the other hand, if p=1, then J is a measure of the mean-square drifts.

- ***Energy Dissipation***: Let ϕ be equal to $\dot{\mathbf{q}}^T(t)\mathbf{C}_S\dot{\mathbf{q}}(t)$, i.e.,

$$\phi\left(\mathbf{w}(t)\right)=\mathbf{w}(t)^T\begin{bmatrix}\mathbf{0} & \mathbf{0}\\ \mathbf{0} & \mathbf{M}_{SA}^{-1/2}\mathbf{C}_S\mathbf{M}_{SA}^{-1/2}\end{bmatrix}\mathbf{w}(t) \tag{5.35}$$

then J is equal to the total energy dissipated by the structural elements during the time interval $t\in[0,t_f]$, and the performance of $\mathbf{Z}$ is measured by its ability to reduce this structural energy dissipation. Note that this measure of performance may also be viewed as favoring low mean-square relative velocities.

Of course, J can be taken as any linear combination of the above. For the purposes of this study, $\phi(\mathbf{w}(t);\mathbf{Z},a_g)$ will be assumed to be the weighted, linear combination

$$\phi\left(\mathbf{w};\mathbf{Z},a_g\right)=\sum_{k=1}^{n}\left[q_{ak}a_k^2+q_{dk}d_k^{2p}\right]+q_E\dot{\mathbf{q}}^T\mathbf{C}_S\dot{\mathbf{q}} \tag{5.36}$$

where q_{ak}, q_{dk}, and q_E are nonnegative weighting functions. With the matrices $\mathbf{Q}$, $\mathbf{R}$, $\mathbf{S}$, $\mathbf{Q}_a$, $\mathbf{S}_a$, and R_a properly defined, the above can be expressed as

$$\phi(\mathbf{w};\mathbf{Z},a_g)=\phi_1(\mathbf{w})+\begin{bmatrix}\mathbf{w}^T & \mathbf{u}^T & a_g\end{bmatrix}\begin{bmatrix}\mathbf{Q} & \mathbf{S} & \mathbf{Q}_a\\ \mathbf{S}^T & \mathbf{R} & \mathbf{S}_a\\ \mathbf{Q}_a^T & \mathbf{S}_a^T & R_a\end{bmatrix}\begin{bmatrix}\mathbf{w}\\ \mathbf{u}\\ a_g\end{bmatrix}$$
$$=\phi_1(\mathbf{w})+\begin{bmatrix}\mathbf{w}^T & a_g\end{bmatrix}\begin{bmatrix}\mathbf{Q}-\mathbf{B}_u\mathbf{Z}^T\mathbf{S}^T-\mathbf{S}\mathbf{Z}\mathbf{B}_u^T+\mathbf{B}_u\mathbf{Z}^T\mathbf{R}\mathbf{Z}\mathbf{B}_u^T & \mathbf{Q}_a-\mathbf{B}_u\mathbf{Z}^T\mathbf{S}_a\\ \mathbf{Q}_a^T-\mathbf{S}_a^T\mathbf{Z}\mathbf{B}_u^T & R_a\end{bmatrix}\begin{bmatrix}\mathbf{w}\\ a_g\end{bmatrix} \tag{5.37}$$

where the non-quadratic function $\phi_1(\mathbf{w})$ constitutes the drift terms in (5.34) if p>1.

The matrix **R** is equal to

$$\mathbf{R}=\mathbf{C}_c^{1/2}\mathbf{N}^T\mathbf{M}_{SA}^{-1}\begin{bmatrix}q_{a1} & & \\ & \ddots & \\ & & q_{an}\end{bmatrix}\mathbf{M}_{SA}^{-1}\mathbf{N}\mathbf{C}_c^{1/2} \tag{5.38}$$

Because the scalar weights must all be nonnegative, it follows that **R** is nonnegative-definite. It will often be convenient to assume that **R** is nonsingular. This is the case if **N** nondegenerate and each q_{ak} is nonzero. Note that if **R** is large, then values of **Z** yielding small structural accelerations are favored. This effectively assigns favorability to smaller values of **Z**. Qualitatively speaking, a larger **R** matrix results in optimal values of **Z** which produce smaller **u** values.

5.4.2: Stochastic Response

It is also useful to have measures of performance for the stationary response to stochastic excitation. In such case, define J as

$$J(\mathbf{Z})=\lim_{t_f\to\infty}\left[\frac{1}{t_f}\int_0^{t_f}\phi\big(\mathbf{w}(t);\mathbf{Z},a_g(t)\big)dt\right] \tag{5.39}$$

where a_g is modeled as white noise with power spectral density Φ_0, which is passed through a filter belonging to $\mathcal{H}_2$. Thus, a_g satisfies the state-space equation

$$\begin{aligned}\dot{\mathbf{w}}_a&=\mathbf{A}_a\mathbf{w}_a+\mathbf{B}_0a_0\\ a_g&=\mathbf{C}_a\mathbf{w}_a\end{aligned} \tag{5.40}$$

where $\mathbf{A}_a$ is asymptotically stable. For the dynamic modeling of the system, these filter states can be augmented to the **w** state space; i.e.,

$$\breve{\mathbf{w}}\to\begin{bmatrix}\mathbf{w}\\ \mathbf{w}_a\end{bmatrix} \tag{5.41}$$

where the differential equation for the system then becomes

$$\begin{aligned}\dot{\breve{\mathbf{w}}} &= \begin{bmatrix}\mathbf{A} & \mathbf{B}_a\mathbf{C}_a \\ \mathbf{0} & \mathbf{A}_a\end{bmatrix}\breve{\mathbf{w}} + \begin{bmatrix}\mathbf{B}_u \\ \mathbf{0}\end{bmatrix}\mathbf{u} + \begin{bmatrix}\mathbf{0} \\ \mathbf{B}_0\end{bmatrix}a_0 \\ &= \breve{\mathbf{A}}\breve{\mathbf{w}} + \breve{\mathbf{B}}_u\mathbf{u} + \breve{\mathbf{B}}_0 a_0\end{aligned} \tag{5.42}$$

With this terminology, Eq. (5.39) is equivalent to

$$J(\mathbf{Z};\Phi_0) = E\left[\phi(\breve{\mathbf{w}};\mathbf{Z},\Phi_0)\right] \tag{5.43}$$

In the stochastic performance assessment, it will be assumed that ϕ is quadratic (i.e., that p=1 in the drift performance function) and thus it may be expressed as

$$\begin{aligned}\phi(\breve{\mathbf{w}};\mathbf{Z},\Phi_0) &= \breve{\mathbf{w}}^T\begin{bmatrix}\mathbf{Q} - \mathbf{B}_u\mathbf{Z}^T\mathbf{S}^T - \mathbf{S}\mathbf{Z}\mathbf{B}_u^T + \mathbf{B}_u\mathbf{Z}^T\mathbf{R}\mathbf{Z}\mathbf{B}_u^T & \mathbf{Q}_a\mathbf{C}_a - \mathbf{B}_u\mathbf{Z}^T\mathbf{S}_a\mathbf{C}_a \\ \mathbf{C}_a^T\mathbf{Q}_a^T - \mathbf{C}_a^T\mathbf{S}_a^T\mathbf{Z}\mathbf{B}_u^T & R_a\mathbf{C}_a^T\mathbf{C}_a\end{bmatrix}\breve{\mathbf{w}} \\ &= \breve{\mathbf{w}}^T\left[\breve{\mathbf{Q}} - \breve{\mathbf{B}}_u\mathbf{Z}^T\breve{\mathbf{S}}^T - \breve{\mathbf{S}}\mathbf{Z}\breve{\mathbf{B}}_u^T + \breve{\mathbf{B}}_u\mathbf{Z}^T\mathbf{R}\mathbf{Z}\breve{\mathbf{B}}_u^T\right]\breve{\mathbf{w}}\end{aligned} \tag{5.44}$$

Note that cross-terms between the states and a_0 do not show up in the above expression because there are no feed-through terms in the state-space expression for a_g.

It is worth noting that for ϕ quadratic as above, the value of J is the same as that of the deterministic case, with $a_g(t)=\mathbf{C}_a\mathbf{w}_a(t)$, and where $a_0(t)=\Phi_0^{1/2}\,\delta(t)$. This is a direct consequence of Parseval's Theorem. Thus, the stochastic optimization of J also yields the optimal $\mathbf{Z}$ for the deterministic impulse response optimization, with the same ϕ. Also, note that, because the system is linear, the system differential equation is homogeneous. Thus, for ϕ quadratic, the optimal $\mathbf{Z}$ solution is invariant for any scalar multiple of $a_g(t)$ and Φ_0 for the deterministic and stochastic cases respectively.

5.5: Stochastic-Optimal Effective Damping

Consider the stochastic measure of performance. Define $\tilde{\mathbf{Q}}(\mathbf{Z})$ as

$$\tilde{\mathbf{Q}}(\mathbf{Z}) = \breve{\mathbf{Q}} - \breve{\mathbf{B}}_u\mathbf{Z}^T\breve{\mathbf{S}}^T - \breve{\mathbf{S}}\mathbf{Z}\breve{\mathbf{B}}_u^T + \breve{\mathbf{B}}_u\mathbf{Z}^T\mathbf{R}\mathbf{Z}\breve{\mathbf{B}}_u^T \tag{5.45}$$

Then the goal is to find $\mathbf{Z}$ which minimizes

$$J = E\left[\breve{\mathbf{w}}^T\tilde{\mathbf{Q}}\breve{\mathbf{w}}\right] \tag{5.46}$$

For a given $\mathbf{Z}$, the differential equation for the system is then

$$\dot{\breve{\mathbf{w}}} = \tilde{\mathbf{A}}(\mathbf{Z})\breve{\mathbf{w}} + \breve{\mathbf{B}}_0 a_0 \tag{5.47}$$

where

$$\tilde{\mathbf{A}}(\mathbf{Z}) = \breve{\mathbf{A}} - \breve{\mathbf{B}}_u\mathbf{Z}\breve{\mathbf{B}}_u^T \tag{5.48}$$

and where it has been assumed that the constraint $|\mathbf{u}|\leq\mathbf{u}_{\max}$ is not violated. The covariance matrix for the system state space is

$$\mathbf{\Phi} = E\left[\breve{\mathbf{w}}\breve{\mathbf{w}}^T\right] \tag{5.49}$$

For a_0 modeled as white noise with spectral density Φ_0, the stationary solution of $\mathbf{\Phi}$ obeys the Lyapunov equation

$$\mathbf{0} = \tilde{\mathbf{A}}\mathbf{\Phi} + \mathbf{\Phi}\tilde{\mathbf{A}}^T + \mathbf{W} \tag{5.50}$$

where

$$\mathbf{W} = \breve{\mathbf{B}}_0\breve{\mathbf{B}}_0^T\Phi_0 \tag{5.51}$$

With these definitions, J can be restated as

$$J = \mathrm{tr}\left[\tilde{\mathbf{Q}}\mathbf{\Phi}\right] \tag{5.52}$$

using the fact that compatible matrix multiplication inside the trace argument is commutative.

In order to minimize J over the set of admissible $\mathbf{Z}$, it is useful to first find an expression for the gradient of J with respect to $\mathbf{Z}$. Noting that the derivative and trace operations commute,

$$\frac{\partial J}{\partial Z_{ij}} = \mathrm{tr}\left\{\mathbf{U}^{ij}\tilde{\mathbf{Q}} + \mathbf{\Phi}\frac{\partial\tilde{\mathbf{Q}}}{\partial Z_{ij}}\right\} \tag{5.53}$$

where

$$\mathbf{U}^{ij} = \partial\mathbf{\Phi}/\partial Z_{ij} \tag{5.54}$$

Taking the derivative of (5.50), $\mathbf{U}^{ij}$ is the solution to

$$\mathbf{0} = \tilde{\mathbf{A}}\mathbf{U}^{ij} + \mathbf{U}^{ij}\tilde{\mathbf{A}}^T + \left\{\frac{\partial\tilde{\mathbf{A}}}{\partial Z_{ij}}\mathbf{\Phi} + \mathbf{\Phi}\frac{\partial\tilde{\mathbf{A}}^T}{\partial Z_{ij}}\right\} \tag{5.55}$$

Next, note that if $\mathbf{U}^{ij}$ satisfies the above, and if the matrix $\bar{\mathbf{U}}$ is defined as the solution to

$$\mathbf{0} = \tilde{\mathbf{A}}^T\bar{\mathbf{U}} + \bar{\mathbf{U}}\tilde{\mathbf{A}} + \tilde{\mathbf{Q}} \tag{5.56}$$

then it is a fact (see (Dorato et al. 1995) for proof) that

$$\mathrm{tr}\left\{\mathbf{U}^{ij}\tilde{\mathbf{Q}}\right\} = \mathrm{tr}\left\{\bar{\mathbf{U}}\left(\frac{\partial\tilde{\mathbf{A}}}{\partial Z_{ij}}\mathbf{\Phi} + \mathbf{\Phi}\frac{\partial\tilde{\mathbf{A}}^T}{\partial Z_{ij}}\right)\right\} \tag{5.57}$$

Thus,

$$\frac{\partial J}{\partial Z_{ij}} = \mathrm{tr}\left\{\bar{\mathbf{U}}\left(\frac{\partial\tilde{\mathbf{A}}}{\partial Z_{ij}}\mathbf{\Phi} + \mathbf{\Phi}\frac{\partial\tilde{\mathbf{A}}^T}{\partial Z_{ij}}\right) + \mathbf{\Phi}\frac{\partial\tilde{\mathbf{Q}}}{\partial Z_{ij}}\right\} \tag{5.58}$$

But

$$\frac{\partial \tilde{\mathbf{A}}}{\partial Z_{ij}} = -\frac{\partial}{\partial Z_{ij}} \breve{\mathbf{B}}_u \mathbf{Z} \breve{\mathbf{B}}_u^T = -\mathbf{b}_i \mathbf{b}_j^T \tag{5.59}$$

where $\mathbf{b}_i$ is the ith column of $\breve{\mathbf{B}}_u$; i.e.,

$$\breve{\mathbf{B}}_u = \left[\mathbf{b}_1 \ldots \mathbf{b}_m\right] \tag{5.60}$$

So

$$\begin{aligned}
\operatorname{tr}\left\{\bar{\mathbf{U}}\left(\frac{\partial \tilde{\mathbf{A}}}{\partial Z_{ij}}\mathbf{\Phi} + \mathbf{\Phi}\frac{\partial \tilde{\mathbf{A}}^T}{\partial Z_{ij}}\right)\right\} &= \operatorname{tr}\left\{-\bar{\mathbf{U}}\left(\mathbf{b}_i \mathbf{b}_j^T \mathbf{\Phi} + \mathbf{\Phi}\mathbf{b}_j \mathbf{b}_i^T\right)\right\} \\
&= \operatorname{tr}\left\{-\bar{\mathbf{U}}\mathbf{b}_i \mathbf{b}_j^T \mathbf{\Phi}\right\} + \operatorname{tr}\left\{-\bar{\mathbf{U}}\mathbf{\Phi}\mathbf{b}_j \mathbf{b}_i^T\right\} \\
&= -\mathbf{b}_j^T \mathbf{\Phi}\bar{\mathbf{U}}\mathbf{b}_i - \mathbf{b}_i^T \bar{\mathbf{U}}\mathbf{\Phi}\mathbf{b}_j \\
&= -2\mathbf{b}_i^T \bar{\mathbf{U}}\mathbf{\Phi}\mathbf{b}_j \\
&= -2\left\{\breve{\mathbf{B}}_u^T \bar{\mathbf{U}}\mathbf{\Phi}\breve{\mathbf{B}}_u\right\}_{ij}
\end{aligned} \tag{5.61}$$

Also, note that

$$\begin{aligned}
\frac{\partial}{\partial Z_{ij}} \operatorname{tr}\left\{\mathbf{\Phi}\tilde{\mathbf{Q}}(\mathbf{Z})\right\} &= \frac{\partial}{\partial Z_{ij}} \operatorname{tr}\left\{\mathbf{\Phi}\left(-\breve{\mathbf{B}}_u \mathbf{Z}^T \breve{\mathbf{S}}^T - \breve{\mathbf{S}}\mathbf{Z}\breve{\mathbf{B}}_u^T + \breve{\mathbf{B}}_u \mathbf{Z}^T \mathbf{R}\mathbf{Z}\breve{\mathbf{B}}_u^T\right)\right\} \\
&= -\frac{\partial}{\partial Z_{ij}} \operatorname{tr}\left\{\mathbf{\Phi}\breve{\mathbf{B}}_u \mathbf{Z}^T \breve{\mathbf{S}}^T\right\} - \frac{\partial}{\partial Z_{ij}} \operatorname{tr}\left\{\mathbf{\Phi}\breve{\mathbf{S}}\mathbf{Z}\breve{\mathbf{B}}_u^T\right\} + \frac{\partial}{\partial Z_{ij}} \operatorname{tr}\left\{\mathbf{\Phi}\breve{\mathbf{B}}_u \mathbf{Z}^T \mathbf{R}\mathbf{Z}\breve{\mathbf{B}}_u^T\right\} \\
&= -2\frac{\partial}{\partial Z_{ij}} \operatorname{tr}\left\{\breve{\mathbf{B}}_u^T \mathbf{\Phi}\breve{\mathbf{S}}\mathbf{Z}\right\} + \frac{\partial}{\partial Z_{ij}} \operatorname{tr}\left\{\mathbf{R}\mathbf{Z}\breve{\mathbf{B}}_u^T \mathbf{\Phi}\breve{\mathbf{B}}_u \mathbf{Z}^T\right\}
\end{aligned} \tag{5.62}$$

It follows that

$$\begin{aligned}
\operatorname{tr}\left\{\mathbf{\Phi}\frac{\partial \tilde{\mathbf{Q}}}{\partial Z_{ij}}\right\} &= \frac{\partial}{\partial Z_{ij}} \operatorname{tr}\left\{\mathbf{\Phi}\tilde{\mathbf{Q}}(\mathbf{Z})\right\} \\
&= -2\frac{\partial}{\partial Z_{ij}} \operatorname{tr}\left\{\breve{\mathbf{B}}_u^T \mathbf{\Phi}\breve{\mathbf{S}}\mathbf{Z}\right\} + \frac{\partial}{\partial Z_{ij}} \operatorname{tr}\left\{\mathbf{R}\mathbf{Z}\breve{\mathbf{B}}_u^T \mathbf{\Phi}\breve{\mathbf{B}}_u \mathbf{Z}^T\right\} \\
&= 2\left\{-\breve{\mathbf{S}}^T \mathbf{\Phi}\breve{\mathbf{B}}_u + \mathbf{R}\mathbf{Z}\breve{\mathbf{B}}_u^T \mathbf{\Phi}\breve{\mathbf{B}}_u\right\}_{ij}
\end{aligned} \tag{5.63}$$

Thus, inserting Eqs (5.63) and (5.61) into (5.58), the gradient of J with respect to $\mathbf{Z}$ is found through three equations:

$$\begin{aligned}
\frac{\partial J}{\partial \mathbf{Z}} &= 2\left\{-\breve{\mathbf{B}}_u^T \bar{\mathbf{U}}\mathbf{\Phi}\breve{\mathbf{B}}_u - \breve{\mathbf{S}}^T \mathbf{\Phi}\breve{\mathbf{B}}_u + \mathbf{R}\mathbf{Z}\breve{\mathbf{B}}_u^T \mathbf{\Phi}\breve{\mathbf{B}}_u\right\} \\
\mathbf{0} &= \tilde{\mathbf{A}}(\mathbf{Z})\mathbf{\Phi} + \mathbf{\Phi}\tilde{\mathbf{A}}^T(\mathbf{Z}) + \mathbf{W} \\
\mathbf{0} &= \tilde{\mathbf{A}}^T(\mathbf{Z})\bar{\mathbf{U}} + \bar{\mathbf{U}}\tilde{\mathbf{A}}(\mathbf{Z}) + \tilde{\mathbf{Q}}(\mathbf{Z})
\end{aligned} \tag{5.64}$$

If $\mathbf{Z}$ is on the interior of the admissible set given by (5.20), then the gradient (5.64) must be zero for it to be the optimal solution. If $\mathbf{Z}$ lies on the boundary of the admissible set, then at least one singular value of $\mathbf{Z}-\frac{1}{2}\mathbf{I}$ is equal to ½. Let the singular value decomposition be

$$\mathbf{Z}-\tfrac{1}{2}\mathbf{I}=\mathbf{U}\boldsymbol{\Lambda}\mathbf{V}^T \tag{5.65}$$

where $\mathbf{U}$ and $\mathbf{V}$ are unitary and $\boldsymbol{\Lambda}$ is diagonal and contains the singular values. In this case, the derivative of $J(\mathbf{Z})$, for the optimal solution, may be greater than zero in the directions of the singular values of $\mathbf{Z}-\frac{1}{2}\mathbf{I}$ equal to ½.

This observation leads to a numerical method, similar to the one proposed by (Skelton et al. 1991), which may be used to determine the optimal $\mathbf{Z}$. For a matrix $\mathbf{Z}_k$, the gradient of J is determined by solving the three equations in (5.64). Then, a matrix $\mathbf{Z}_{us}$ is found which yields a lower J through

$$\mathbf{Z}_{us}=\mathbf{Z}_k-\varepsilon\frac{\partial J}{\partial \mathbf{Z}} \tag{5.66}$$

where ε is a small constant. The singular value decomposition of the new matrix $\mathbf{Z}_{us}-\frac{1}{2}\mathbf{I}$ is then found, and the diagonal values of $\boldsymbol{\Lambda}_{us}$ are limited to ½, to get $\boldsymbol{\Lambda}_{k+1}$. Transforming back to the original basis gives $\mathbf{Z}_{k+1}$.

Repetition of this operation converges upon a value of $\mathbf{Z}$ which is a local minimum of J. It is important to note that this gradient method tacitly assumes the existence of exactly one minimum. Because the admissible set of $\mathbf{Z}$ is compact, it is known that there is at least one minimum. However, there may be several local minima, and this analysis on its own does not resolve this issue. The development of more reliable convergence algorithms for $\mathbf{Z}$ constitutes an item requiring further research. Of particular interest is the prospect of placing this problem in the context of Linear Matrix Inequality methods (Camino et al. 2003), which have yielded consistent convergence algorithms for similar structural optimization problems by breaking the problem into multiple nested convex optimizations.

5.6: Examples

5.6.1: Example 1: Tuned Mass Damper with RFA Interface

To illustrate how the concept of effective damping may be put into practice, consider the structure-actuator system in Fig. 5.5a. The machines in this example are those in the examples from Chapters 3 and 4, with Machine 1 corresponding to the inter-story actuator with a lead of

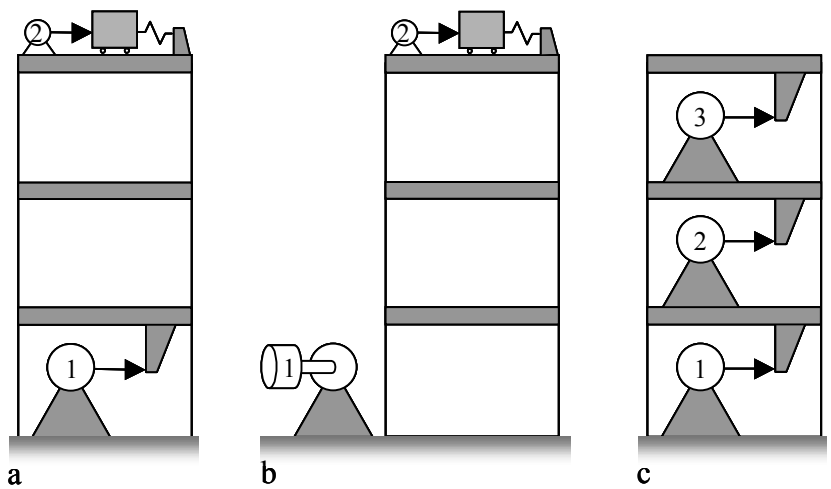

Figure 5.5: Example actuation configurations

1/650 m/rad, and Machine 2 corresponding to the mass driver with a lead of 1/70 m/rad. The $\mathbf{C}_c$ matrix for these machines is equal to

$$\mathbf{C}_c = \begin{bmatrix} 99.7 & 0 \\ 0 & 1.16 \end{bmatrix} \frac{\text{kNs}}{\text{m}} \tag{5.67}$$

The goal is to design $\mathbf{Z}$ for optimal stochastic performance.

For the structural model, a simplified version of the Benchmark Structure studied in (Spencer et al. 1998) is used. Let z_i and z_d be the displacement of story i and the mass damper, respectively, relative to the ground. The vector $\mathbf{q}$ is then

$$\mathbf{q} = \begin{bmatrix} q_1 & q_2 & q_3 & q_d \end{bmatrix}^T \tag{5.68}$$

The structural matrices (including the mass driver degree of freedom) are

$$\mathbf{C}_S = \begin{bmatrix} 175 & -50 & 0 & 0 \\ -50 & 100 & 50 & 0 \\ 0 & -50 & 50.2 & -.2 \\ 0 & 0 & -.2 & .2 \end{bmatrix} \frac{\text{Ns}}{\text{m}} \quad \mathbf{K}_S = 10^5 \begin{bmatrix} 12 & -6.84 & 0 & 0 \\ -6.84 & 13.7 & -6.84 & 0 \\ 0 & -6.84 & 6.87 & -.034 \\ 0 & 0 & -.034 & .034 \end{bmatrix} \frac{\text{N}}{\text{m}} \quad \mathbf{M}_S = 98.3 \begin{bmatrix} \mathbf{I} & \mathbf{0} \\ \mathbf{0} & .01 \end{bmatrix} \text{kg} \tag{5.69}$$

The structure is lightly damped, with damping ratios below 1% for all modes. The natural frequencies for the main structure are 5.5, 15.8, and 23.6Hz. This model represents a 158cm-high laboratory test structure, which is a scale model of a prototype building. The scaling between the model and prototype structures is 1:60 for force, 1:206 for mass, 1:5 for time, 4:29 for displacement, and 7:2 for acceleration.

The mass damper has a natural frequency and damping ratio of 5.5Hz and 0.1%, respectively. The $\mathbf{N}$ matrix for this example is

$$\mathbf{N} = \begin{bmatrix} 1 & 0 & 0 & 0 \\ 0 & 0 & -1 & 1 \end{bmatrix}^T \tag{5.70}$$

The white noise signal a_0 has spectral density Φ_0. Because the system is linear and the performance measure is a simple quadratic, the optimal value of **Z** will be the same for arbitrary values of Φ_0. Thus, this value will be normalized to unity. The spectral characteristics of the disturbance correspond to the Kanai-Tajimi spectrum (Kanai 1957; Tajiimi 1960), with

$$\mathbf{A}_a = \begin{bmatrix} 0 & 1 \\ -\omega_0^2 & -2\zeta\omega_0 \end{bmatrix} \quad \mathbf{B}_0 = \begin{bmatrix} 0 \\ 1 \end{bmatrix} \quad \mathbf{C}_a = \begin{bmatrix} \omega_0^2 & 2\zeta\omega_0 \end{bmatrix} \tag{5.71}$$

In (Housner and Jennings 1964), it was shown that ω_0=15.4rad/s and ζ=0.64 resembles a realistic earthquake spectrum. Here, these values are used, with ω_0 scaled by a factor of 5 to 77Hz, to reflect the time-scaling of the structural model.

Four measures of performance, enumerated as Cases 1 through 4, will be examined in this example. Characterized by their weights, the nonzero weights for these cases are as follows.

Case 1: $q_{d1} = q_{d2} = q_{d3} = (0.001\text{m})^{-2}$

Case 2: $q_{a1} = q_{a2} = q_{a3} = (4\text{m/s}^2)^{-2}$

Case 3: $q_E = 1$

Case 4: $q_{d1} = q_{d2} = q_{d3} = (0.001\text{m})^{-2}$, $q_{a1} = q_{a2} = q_{a3} = (4\text{m/s}^2)^{-2}$

Thus, Case 1 optimizes mean-square drifts, Case 2 the mean-square accelerations, and Case 3 the structural energy dissipation. Case 4 is a balance between Cases 1 and 2.

Results for these cases is shown in Table 5.1. For each case, three solutions were computed for **Z**. One solution is the optimal **Z**, derived using the procedure described in Section 5.5. For the second solution, **Z** is further constrained to be symmetric. A comparison between these two solutions gives some indication of the benefits of skew damping for each case. For the

Table 5.1: **Z** Optimization results for Example 1

	asymmetric solution			symmetric solution			diagonal solution		
Case	**Z**		*J*	**Z**		*J*	**Z**		*J*
1	0.224 -0.236	0.0059 0.0856	15.7	0.517 -0.396	-0.396 0.535	17.1	0.209 0	0 0.0259	18.1
2	0.0685 -0.154	0.0209 0.0837	13.5	0.0960 -0.0251	-0.0251 0.0330	15.0	0.0959 0	0 0.243	15.5
3	0.102 -0.208	0.0981 0.202	2.45	0.189 -0.0363	-0.0363 0.171	2.60	0.181 0	0 0.141	2.63
4	0.129 -0.192	0.0201 0.0781	32.1	0.173 -0.0534	-0.0534 0.123	35.5	0.149 0	0 0.0222	36.1

third solution, **Z** is constrained to be diagonal. A comparison of this solution to the other two gives some indication of the degree to which non-local damping improves the system response.

The results show a clear improvement in performance of the asymmetric and symmetric solutions over the diagonal solution. However, in all cases, the asymmetry of **Z** is responsible for the most improvement in performance. Physically, the nondiagonality of the optimal matrix solutions for all four cases makes sense, because both accelerations and drifts can be reduced by the delivery of energy from the base to the roof. However, the fact that the optimal solutions are all significantly asymmetric implies that there is benefit to be gained from the circulation of energy through the structure.

Fig. 5.6 shows the convergence of these solutions, as a function of iteration number, for cases 1 through 4. It is interesting that the asymmetric solution converges very quickly and abruptly, while the symmetric solution tends to converge more slowly, and the diagonal solution slowest. However, this makes sense in the context of the convergence algorithm, which constrains the change of **Z** by confining it to a symmetric or diagonal structure. It is also interesting to note that the symmetric and asymmetric solutions tend to start out very close to each other in the optimization, diverging later in the refinement process. This may indicate that the symmetric characteristics dominate the performance characteristics for highly sub-optimal choices of **Z**, with the skew component only becoming relevant for high-performing choices.

5.6.2: Example 2: Tuned Mass Damper with Quasi-Skyhook Damping

For the next example, consider the case where an actuator used to excite a mass damper on the roof of the three-story structure is interfaced with a remote flywheel, as shown in Fig. 5.5b. For this case, the screw lead for actuator 1 (the one on the roof) is designated to be 1/70 m/rad. Thus, the $\mathbf{C}_c$ matrix is

$$\mathbf{C}_c = \begin{bmatrix} 1157 & 0 \\ 0 & 0.236 \end{bmatrix} \frac{\text{Ns}}{\text{m}} \tag{5.72}$$

and the **N** matrix is

$$\mathbf{N} = \begin{bmatrix} 0 & 0 & -1 & 1 & 0 \\ 0 & 0 & 0 & 0 & 1 \end{bmatrix}^T \tag{5.73}$$

For this example, the optimal solutions are shown in Table 5.2. Note that in all four cases, the performance is drastically improved when **Z** is permitted to be asymmetric. The symmetric solutions are equal to the diagonal ones. Thus, this example illustrates clearly the benefit of asymmetric damping for improving the structural response. Note that the optimal **Z**

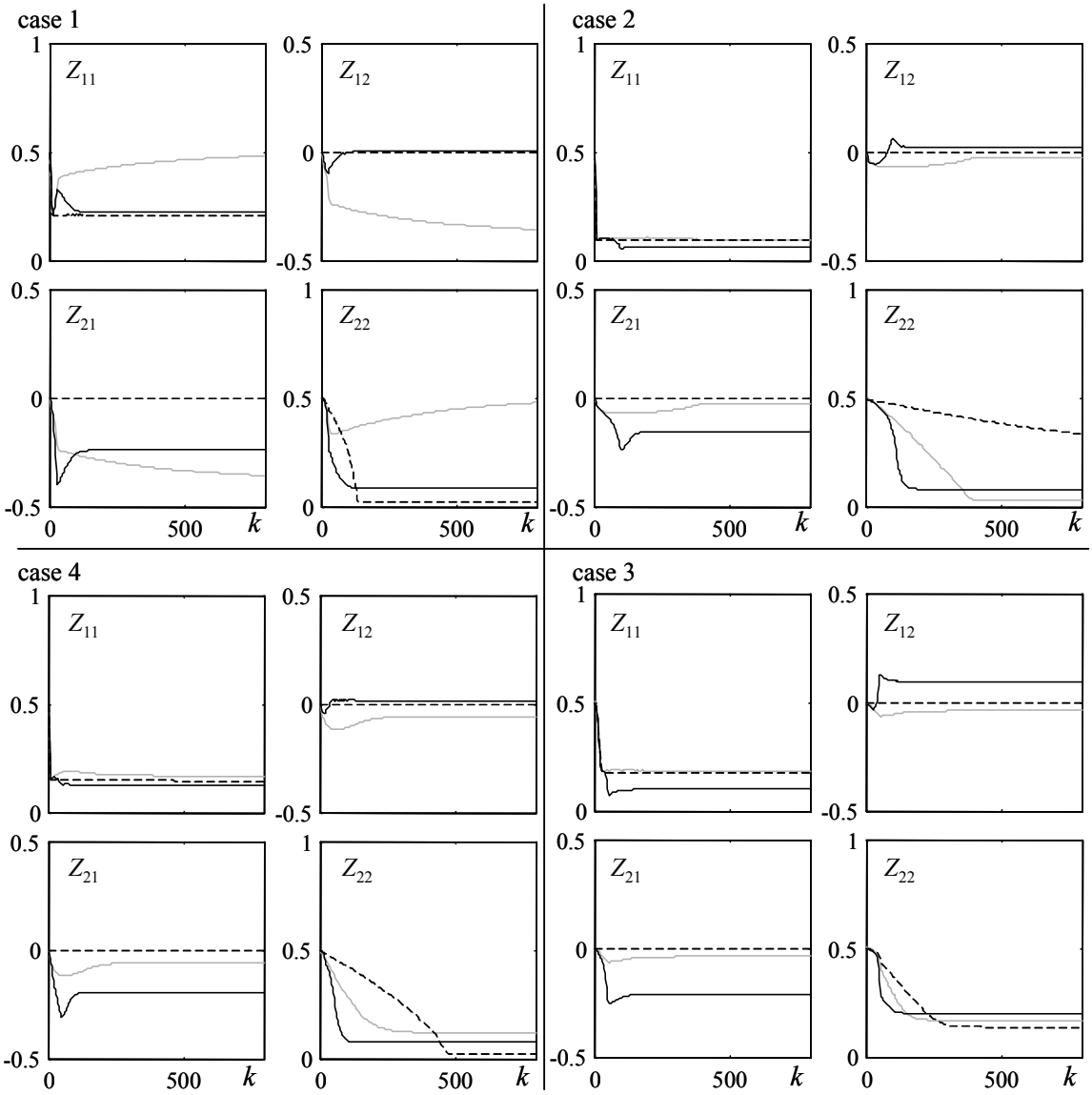

Figure 5.6: Convergence of **Z** for cases 1-4 (clockwise from top left) and for asymmetric (black), symmetric (gray) and diagonal (dotted) solutions

values are similar for the four cases. Also note that in all four cases, the symmetric solution is equal to the diagonal solution, and the asymmetric solution is a diagonal matrix plus a skew matrix.

All four cases exhibit an interesting phenomenon. For all cases, the performance J is the same for a given **Z**, and for the same value of **Z** with all the off-diagonal components negated. Thus, the optimal **Z** is always non-unique for all cases where **Z** is nondiagonal. This observation, which was found empirically, illustrates that in some circumstances J may possess multiple minima. In this particular circumstance, the problem is a moot point, because the two known

Table 5.2: **Z** Optimization results for Example 2

Case	asymmetric solution **Z**		J	symmetric solution **Z**		J	diagonal solution **Z**		J
1	0.0011 -0.0333	0.0333 0.0114	182	0.0311 0	0 ×	384	0.0311 0	0 ×	384
2	0.0012 -0.034	0.0340 0.0110	122	0.0334 0	0 ×	207	0.0334 0	0 ×	207
3	0.0012 -0.0343	0.0343 0.0128	31.8	0.0333 0	0 ×	54.5	0.0333 0	0 ×	54.5
4	0.0011 -0.0335	0.0335 0.0113	304	0.0318 0	0 ×	591	0.0318 0	0 ×	591

optimal values of **Z** produce the same J. However, this may not be the case in general, and this example motivates the need for more sophisticated global optimization routines for **Z**.

5.6.3: Example 3: Densely Actuated Structures

For the final example, consider a case where an actuator is placed in between each floor of the structure, as shown in Fig. 5.5c. Thus, m=3 for this case. The screw leads for the actuators were all chosen as 1mm/rad, and the resultant $\mathbf{C}_c$ matrix is thus

$$2.36\times10^5\,\mathbf{I}\,\frac{\text{Ns}}{\text{m}} \tag{5.74}$$

The **N** matrix is

$$\mathbf{N}=\begin{bmatrix}1 & -1 & 0\\ 0 & 1 & -1\\ 0 & 0 & 1\end{bmatrix} \tag{5.75}$$

For this configuration, Table 5.3 shows the resultant data for the four cases. Note that for Case 1 (i.e., the drift minimization case) the optimal **Z** is equal to **I**. Physically, this makes sense, because it says that the way to minimize drifts is to make the viscous damping in the structure as large as possible. For Case 2, the results are more interesting. The improvement afforded by allowing **Z** to be symmetric (but not diagonal) is slight. It is interesting, however, that an improvement of approximately 10% is achieved by allowing **Z** to be asymmetric. Thus, it is apparent that in such densely-actuated configurations, significant improvement can be gained through asymmetric damping. For Case 3, the improvements are rather slight. This, again, makes physical sense. Note that the diagonal elements of **Z** in these cases are rather large (i.e., close to 1). Because energy dissipation is proportional to mean-square relative velocities, it is reasonable that these velocities, like the drifts, can be optimally reduced with extremely large

Table 5.3: **Z** Optimization results for Example 3

Case	asymmetric solution **Z**			J	symmetric solution **Z**			J	diagonal solution **Z**			J
	1	0	0		1	0	0		1	0	0	
1	0	1	0	0.517	0	1	0	0.517	0	1	0	0.517
	0	0	1		0	0	1		0	0	1	
	0.0285	-0.132	0.0324		0.150	-0.278	-0.0731		0.0458	0	0	
2	0.0488	0.104	-0.172	5.36	-0.278	0.835	0.232	5.95	0	0.113	0	5.96
	0.0091	0.0372	0.0650		-0.0731	0.232	0.112		0	0	0.140	
	0.858	0.319	0.142		0.793	0.311	0.1382		1	0	0	
3	-0.329	0.876	-0.0134	0.0134	0.311	0.390	0.0872	0.0146	0	1	0	0.0157
	-0.116	-0.0842	0.979		0.138	0.0872	0.2979		0	0	1	
	0.354	-0.213	0.207		0.279	-0.210	0.2442		0.179	0	0	
4	0.0422	0.0915	0.0969	10.8	-0.210	0.615	-0.3675	11.0	0	0.221	0	11.0
	0.214	-0.185	0.130		0.244	-0.368	0.3253		0	0	0.317	

supplemental viscous damping. Recall that Case 4 combines the objectives of Cases 1 and 2. It is interesting to note that J for Case 4 is significantly higher than the sum of the optimal J values for Cases 1 and 2. This implies a rather severe tradeoff between minimizing drifts and accelerations.

5.7: Further Thoughts on Effective Damping

As mentioned, the approach outlined in this chapter is useful because of its convenient physical interpretation. It also yields a comparatively simple analytical solution for the response of the system. Although the approach outlined in Sections 5.5 and 5.6 involves stochastic system analysis, an equivalent analysis could be performed for the deterministic damping case. Results will be identical for the optimization of the impulse response.

There are a number of disadvantages to this approach, however, which limit its appeal. Most notably, its constraint of **Z** to a constant matrix falls short of using the full capabilities of the RFA network. Specifically, this approach, which effectively limits the structural control system design to a linear velocity feedback system, does not allow for the feedback of velocities of non-actuated degrees of freedom, or position feedback. This may limit the appeal of this approach for practical implementation.

Additionally, the constant matrix **Z** will result in a violation of the constraint $|\mathbf{f}_e|\leq\mathbf{f}_{\max}$ if the actuation velocities are sufficiently large. This problem can be resolved implicitly by making **R** larger (i.e., increasing the lowest singular value of **R**) and thus adding weight to values of **Z** that produce large forces. However, this approach does not explicitly address the maximum force constraint. Increasing **R** will depreciate the performance of the resultant **Z**. A better approach would be one that would be able to adjust **Z** in real time, to accommodate this maximum force

constraint, and in accordance with the global deformation of the structure. This is discussed in greater detail in Chapter 6, giving rise to a class of controllers called “Damping Reference” controllers.

Chapter 6. Feedback Control Algorithms

As a consequence of their physical constraints, it is clear that for open-loop-stable systems controlled by RFA networks, the closed-loop system is always stable. Therefore, the usual stability-robustness issues in control system design do not apply to these problems, and closed-loop performance is the only analytical measure by which the quality of different controllers can be compared.

In the Chapter 5, the measure of performance J was optimized over the subset of normalized forcing functions $\mathbf{u} \in \Re^m \times C[0,t_f]$ for which there exists a constant matrix $\mathbf{Z}$ such that $\mathbf{u}$ and $\mathbf{w}$ (the structural state vector) satisfy the linear relation in Eq. (5.16). By requiring $\mathbf{Z}$ to be constant, the resultant set of $\mathbf{u}$ over which the optimization was performed is a small subset of the entire set of feasible control inputs. The optimal J evaluated over the constant-$\mathbf{Z}$ domain is deceptive from this point of view, because much lower values may be physically possible with a less constrained control parameterization. In particular, a lower J may be possible if controllers are considered which relate $\mathbf{u}$ to all the system states, rather than just the actuation velocities.

This chapter concerns the development of simple, practical feedback controllers for free and forced vibration. The goal is to design controllers which require minimal computation and data storage for implementation, but which still have favorable performance characteristics. The discussion will be limited to full-information, memoryless feedback controllers; i.e.

$$\mathbf{w}(t), a_g(t) \mapsto \mathbf{u}(t) \tag{6.1}$$

and the performance measure will be considered to be quadratic, with infinite horizon.

Consider the proposition of a family of causal, nonlinear, feedback controllers parameterized by some finite-dimensional vector $\boldsymbol{\theta}$. Furthermore, suppose that the subset of *feasible* controller parameters in this family is characterized by the condition $\boldsymbol{\theta} \in \Theta$, where Θ is some convex set. Then it is straight-forward to consider the parametric optimization problem

$$\boldsymbol{\theta}_{opt} = \arg\min_{\boldsymbol{\theta} \in \Theta} \left\{ J\left(\mathbf{w}_0, a_g; \boldsymbol{\theta}\right) \right\} \tag{6.2}$$

However, even this problem is fraught with difficulty. It is nontrivial, for instance, to prove a convex relationship between $\boldsymbol{\theta}$ and J. Even more fundamentally, the nonlinear system description makes it difficult to derive explicit analytical expressions for $J(\mathbf{w}_0, a_g; \boldsymbol{\theta})$.

Due to these difficulties, the route taken here is to further relax the problem statement through the use of inequalities. Instead of seeking $\boldsymbol{\theta}\in\Theta$ which minimizes $J(\mathbf{w}_s, a_g;\boldsymbol{\theta})$, the procedure will instead be to first establish that for all $\boldsymbol{\theta}\in\Theta$, there is a guaranteed upper performance bound, i.e.,

$$J\left(\mathbf{w}_0, a_g;\boldsymbol{\theta}\right) \le J_U\left(\mathbf{w}_0, a_g;\boldsymbol{\theta}\right) \tag{6.3}$$

where J_U is a closed-form expression of the arguments. Then, the optimization problem of minimizing J_U over Θ becomes more tractable.

However, there are still lingering convexity issues for the optimization of J_U over Θ, and these issues are not completely resolved in the present analysis. Also, the tightness of bound (6.3) is in general difficult to prove, i.e., it is difficult to find $\mathbf{w}_0$, a_g, and $\boldsymbol{\theta}$ for which the equality holds in Eq. (6.3).

It should be noted that the research presented here represents a "scratching of the surface" on systematic feedback controller optimization for energy-constrained structural actuation systems, and that the ideas proposed here, unless otherwise stated, are equally relevant to RFA and semiactive systems. The analysis in this chapter makes many assumptions concerning the problem statement which simplify the problem; most notably the assumption of quadratic performance measures. There is so much more work which remains to be done in this area that it would be foolish to suggest that the work presented here constitutes the final word on the subject.

It is also important to note that there have been many ad hoc controller designs which have been proposed over the years for energy-constrained actuation systems. Yamada and Kobori (2001) provide a thorough retrospective on the current state of this subject in Earthquake Engineering. The general analysis presented here simplifies down to some of these methods for specific design choices. Most notable among these are Clipped-Optimal methods (Dyke et al. 1996; Karnopp 1983; Margolis 1983), Lyapunov-based methods (Gavin 2001; Leitmann 1994; Leitmann and Reithmeier 1993), Energy minimization approaches (Zhang and Iwan 2002), and Steepest Gradient (Tseng and Hedrick 1994) methods, all of which are ultimately based on quadratic performance measures. The attempt here has been to unify these approaches under a common umbrella, and to illustrate that in many circumstances an equivalency exists between two or more of them. It should be noted that considerable effort has been made in other control synthesis approaches for energy-constrained actuators which are not considered here; most notably Sliding Mode Control (Kim and Wang 1993; Singh et al. 1997).

Finally, it should be mentioned that the ideas discussed in this chapter, from the point of view of general control theory, are rather common. The methods employed here are similar to

"Guaranteed-Cost" quadratic control system designs, which have been investigated for many years (Chang and Peng 1972). However, while Guaranteed-Cost control concepts are usually proposed as a way of handling system uncertainty, they are here used as a way to handle actuator nonlinearities. The ideas here may also be viewed in the context of fixed-structure optimal control theory (Dorato et al. 1995). Indeed, one of the clear avenues for future research involves the application of Linear Matrix Inequality (LMI) methods, which are very useful in Fixed-Structure control optimization, to the design of control laws investigated here.

The information in this chapter is organized as follows. First, the free-vibration case (i.e. a_g=0, $\mathbf{w}_0 \neq \mathbf{0}$) is addressed. It is shown that many controllers which have been proposed for semiactive systems (and which are here extended to RFA networks) belong to a family of feedback laws which will here be called Clipped Linear controllers. For a subset of controllers in this family called Damping Reference controllers, simple expressions exist for J_U, and it is shown how the clipped-linear controller parameters can be optimized over this family to minimize J_U. This procedure is a specific application of sub-optimal, nonlinear quadratic regulator design.

Then, an analogous procedure is conducted for the forced-vibration case, for two different disturbance models. First, a_g is assumed to be white noise, and the system is assumed to be in stationary excitation. For this model, it is shown that Damping-Reference controllers yield an upper bound on the expectation of a quadratic function of the states and control. This procedure is a specific application of sub-optimal, nonlinear stochastic control. Next, the deterministic case is treated, in which it is shown again that Damping-Reference controllers can also be designed to yield a simple expression for J_U which depends only on the mean-square value of a_g and a quadratic function of $\mathbf{w}_0$. This procedure is a specific application of sub-optimal, nonlinear $\mathcal{H}_\infty$ control.

The chapter ends with some discussion concerning many ongoing and future research topics in this area.

6.1: Clipped-Linear Controllers for Free Vibration

The Nominal System Model from Chapter 5 is of the form

$$\dot{\mathbf{w}} = \mathbf{A}\mathbf{w} + \mathbf{B}_u\mathbf{u} + \mathbf{B}_a a_g \tag{6.4}$$

where $\mathbf{u} \in \mathcal{U}(\mathbf{w}(t))$; i.e.

$$P(\mathbf{u}(t), \mathbf{w}(t)) = \mathbf{u}^T(t)\mathbf{u}(t) + \mathbf{u}^T(t)\mathbf{B}_u^T\mathbf{w}(t) \leq 0 \tag{6.5a}$$

and

$$|\mathbf{u}| \le \mathbf{u}_{\max} \tag{6.5b}$$

<u>DEFINITION</u>: Define the set $\mathcal{U}(\mathbf{w}(t)) \in \Re^m$ as

$$\mathcal{U}(\mathbf{w}(t)) = \left\{ \mathbf{u}(t) \in \Re^m \;\mid\; P(\mathbf{u}(t), \mathbf{w}(t)) \le 0 \;,\; |u_k(t)| \le u_{k\max} \;\; \forall k \in \{1..m\} \right\} \tag{6.6}$$

Thus, $\mathbf{u}(t) \in \mathcal{U}(\mathbf{w}(t))$ if and only if (6.5a) and (6.5b) are satisfied.

For free vibration with quadratic performance measures, the expression from Chapter 5 for the deterministic performance $J(\mathbf{w}_0)$ is

$$J(\mathbf{w}_0) = \int_0^\infty \begin{bmatrix} \mathbf{w}^T(t) & \mathbf{u}^T(t) \end{bmatrix} \begin{bmatrix} \mathbf{Q} & \mathbf{S} \\ \mathbf{S}^T & \mathbf{R} \end{bmatrix} \begin{bmatrix} \mathbf{w}(t) \\ \mathbf{u}(t) \end{bmatrix} dt \tag{6.7}$$

6.1.1: The Generalized Clipped Linear Controller

Let $\mathbf{K}$ be an arbitrary matrix such that $\mathbf{A}+\mathbf{B}_u\mathbf{K}$ is stable, and let $\mathbf{P}=\mathbf{P}^T>0$ be the solution to the Lyapunov equation

$$(\mathbf{A} + \mathbf{B}_u\mathbf{K})^T \mathbf{P} + \mathbf{P}(\mathbf{A} + \mathbf{B}_u\mathbf{K}) + (\mathbf{Q} + \mathbf{S}\mathbf{K} + \mathbf{K}^T\mathbf{S}^T + \mathbf{K}^T\mathbf{R}\mathbf{K}) = \mathbf{0} \tag{6.8}$$

Noting that

$$\mathbf{w}_0^T\mathbf{P}\mathbf{w}_0 = -\int_0^\infty \left\{ \mathbf{w}(\tau)\left[\mathbf{A}^T\mathbf{P} + \mathbf{P}\mathbf{A}\right]\mathbf{w}(\tau) + 2\mathbf{w}^T(\tau)\mathbf{P}\mathbf{B}_u\mathbf{u}(\tau) \right\} d\tau \tag{6.9}$$

along any asymptotically stable $\{\mathbf{w},\mathbf{u}\}$ trajectory, it follows that

$$J(\mathbf{w}_0) = \mathbf{w}_0^T\mathbf{P}\mathbf{w}_0 + \int_0^\infty \left\{ \mathbf{w}^T(\tau)\left[\mathbf{A}^T\mathbf{P} + \mathbf{P}\mathbf{A} + \mathbf{Q}\right]\mathbf{w}(\tau) + 2\mathbf{w}^T(\tau)\left[\mathbf{P}\mathbf{B}_u + \mathbf{S}\right]\mathbf{u}(\tau) + \mathbf{u}^T(\tau)\mathbf{R}\mathbf{u}(\tau) \right\} d\tau \tag{6.10}$$

Combining Eqs. (6.7) and (6.10) gives

$$J(\mathbf{w}_0) = \mathbf{w}_0^T\mathbf{P}\mathbf{w}_0 + \int_0^\infty \left\{ \left\|\mathbf{u}(\tau) - \mathbf{K}_{CL}(\mathbf{P})\mathbf{w}(\tau)\right\|_{\mathbf{R}}^2 - \left\|\mathbf{K}\mathbf{w}(\tau) - \mathbf{K}_{CL}(\mathbf{P})\mathbf{w}(\tau)\right\|_{\mathbf{R}}^2 \right\} d\tau \tag{6.11}$$

where subscript "**R**" denotes the Euclidean norm with respect to weighting matrix **R**, and

$$\mathbf{K}_{CL}\left(\mathbf{P}\right)=-\mathbf{R}^{-1}\left[\mathbf{B}_u^T\mathbf{P}+\mathbf{S}^T\right] \tag{6.12}$$

The integrand in Eq. (6.11) is minimized by the feedback function

$$\mathbf{u}\left(t\right)=\underset{\tilde{\mathbf{u}}\in\mathcal{U}(\mathbf{w}(t))}{\arg\min}\left\|\tilde{\mathbf{u}}-\mathbf{K}_{CL}\left(\mathbf{P}\right)\mathbf{w}\left(t\right)\right\|_{\mathbf{R}} \tag{6.13}$$

Eq. (6.13) will be called the *Clipped-Linear* (CL) control law.

Define $\mathbf{u}_a$ as

$$\mathbf{u}_a(t)=\mathbf{K}_{CL}(\mathbf{P})\mathbf{w}(t) \tag{6.14}$$

Then, Eq. (6.13) can be restated simply as

$$\mathbf{u}(t)=\underset{\tilde{\mathbf{u}}\in\mathcal{U}(\mathbf{w}(t))}{\arg\min}\left\|\tilde{\mathbf{u}}-\mathbf{u}_a(t)\right\|_{\mathbf{R}} \tag{6.15}$$

Thus, $\mathbf{u}$ is related to $\mathbf{w}$ through two consecutive operations. The first step consists of the linear feedback function $\mathbf{u}_a$, while the second consists of "clipping" $\mathbf{u}_a$ to accommodate the constraints of the feasible force region. These two steps will be called the *active feedback signal* and the *clipping action* respectively.

It turns out that several of the popular control algorithms which are used for energy-constrained systems are variants of Eq. (6.13). They differ by the choice of $\mathbf{Q}$, $\mathbf{R}$, and $\mathbf{S}$ performance matrices, as well as the $\mathbf{K}$ matrix chosen. Of course, different choices result in different closed-loop system characteristics. There are some special cases for the choice of $\mathbf{K}$ which have some physical and practical significance.

***Circumstances Arising from Singular* R**

The development of the CL control law above assumed that $\mathbf{R}$ was nonsingular. However, this may not be the case for some performance measures. In particular, the case where $\mathbf{S}=\mathbf{0}$ and $\mathbf{R}=\mathbf{0}$ simplifies Eq. (6.8) for $\mathbf{P}$ to

$$\left(\mathbf{A}+\mathbf{B}_u\mathbf{K}\right)^T\mathbf{P}+\mathbf{P}\left(\mathbf{A}+\mathbf{B}_u\mathbf{K}\right)+\mathbf{Q}=\mathbf{0} \tag{6.16}$$

and the control law in Eq. (6.13) to

$$\mathbf{u}=\underset{\tilde{\mathbf{u}}\in\mathcal{U}(\mathbf{w}(t))}{\arg\min}\left\{\tilde{\mathbf{u}}^T\mathbf{B}_u^T\mathbf{P}\mathbf{w}\left(t\right)\right\} \tag{6.17}$$

This expression is equivalent to a control law which minimizes the derivative of $\mathbf{w}^T(t)\mathbf{P}\mathbf{w}(t)$ at each time t. Such controllers are common in Lyapunov-based and sliding-mode approaches.

6.1.2: Clipped-Optimal Control

Consider the case where $\mathbf{K}$ is chosen to be equal to $\mathbf{K}_{CL}(\mathbf{P})$. Insertion of the above into Eq. (6.8) gives an algebraic Riccati equation for $\mathbf{P}$, the solution of which will be denoted $\mathbf{P}_o$; i.e.

$$\left(\mathbf{Q}-\mathbf{S}\mathbf{R}^{-1}\mathbf{S}^T\right)+\left(\mathbf{A}-\mathbf{B}_u\mathbf{R}^{-1}\mathbf{S}^T\right)^T\mathbf{P}_o+\mathbf{P}_o\left(\mathbf{A}-\mathbf{B}_u\mathbf{R}^{-1}\mathbf{S}^T\right)-\mathbf{P}_o\mathbf{B}_u\mathbf{R}^{-1}\mathbf{B}_u^T\mathbf{P}_o=\mathbf{0} \tag{6.18}$$

The resultant solution for $\mathbf{K}=\mathbf{K}_{CL}(\mathbf{P}_o)$ will be denoted $\mathbf{K}_o$. Equating $\mathbf{K}=\mathbf{K}_o$ results in a simplification of Eq. (6.11) to

$$J\left(\mathbf{w}_0\right)=\mathbf{w}_0^T\mathbf{P}_a\mathbf{w}_0+\int_0^\infty\left\|\tilde{\mathbf{u}}-\mathbf{K}_o\mathbf{w}\left(\tau\right)\right\|_{\mathbf{R}}^2 d\tau \tag{6.19}$$

Note that the integrand is positive definite. If $\mathbf{u}(t)$ were not constrained $\mathcal{U}(\mathbf{w}(t))$ (i.e. if the control force were fully active) then the integrand would be minimized uniquely to zero by equating $\mathbf{u}(t)=\mathbf{K}_o\mathbf{w}(t)$. This is the classical result for the active optimal full-information LQR controller. The optimization with $\mathbf{u}(t)$ constrained to $\mathcal{U}(\mathbf{w}(t))$ must yield a higher value for J than the unconstrained optimization, yielding the lower bound

$$J(\mathbf{w}_0)\big|_{\mathbf{u}(t)\in\mathcal{U}(\mathbf{w}(t))}\geq\mathbf{w}_0^T\mathbf{P}_o\mathbf{w}_0 \tag{6.20}$$

As expected, this lower bound says that no controller will perform better than the unconstrained optimal controller.

A popular design technique for energy-constrained controllers, called *Clipped-Optimal* (*CO*) control, implements the CL control law with $\mathbf{P}=\mathbf{P}_o$; i.e.

$$\mathbf{u}\left(t\right)=\underset{\tilde{\mathbf{u}}\in\mathcal{U}(\mathbf{w}(t))}{\arg\min}\left\|\tilde{\mathbf{u}}-\mathbf{K}_o\mathbf{w}\left(t\right)\right\|_{\mathbf{R}} \tag{6.21}$$

As such, the clipped-optimal controller attempts to approximate the active lower bound of J, through the point-by-point minimization of the integrand in Eq. (6.19). This lower bound can be matched if and only if $\mathbf{K}_o\mathbf{w}(t)\in\mathcal{U}(\mathbf{w}(t))$ at all times. Because the force constraints were not incorporated into the derivation of $\mathbf{K}_o$, there is in general no reason to expect that this will be the case.

The appeal of clipped-optimal control lies in its simplicity and intuitiveness. By replicating as closely as possible the optimal active feedback control law at all times, subject to the forcing constraint $\mathbf{u}(t)\in\mathcal{U}(\mathbf{w}(t))$, the performance of the resultant constrained control system should hopefully resemble the active controller's performance. The difficulty with clipped-optimal control is the fact that it does not possess a useful upper bound for J, as in Eq. (6.3).

Thus, although it is known that clipped-optimal controllers deviate from the unconstrained optimal performance, it is unclear how large that deviation can theoretically be, without explicitly solving for the response trajectory for a given $\mathbf{w}_0$.

The standard practice with Clipped-Optimal control design is one of trial-and-error. A common design technique would be to start with **Q**, **R**, and **S** matrices which correspond to some desired performance (i.e. accelerations, drifts, etc.). Typically, these matrices will yield bad performance for the Clipped-Optimal controller, because they will require the controller to produce forces which require external power. So then, the controller is modified by changing **K** directly, or by modifying the **Q**, **S**, and **R** matrices to somehow favor more dissipative forces.

6.1.3: Damping-Reference Control

Suppose constraint (6.5b) is disregarded, as has been done on occasion in previous chapters, due to assumptions that **u** is regulated implicitly either through the size of **R** or through assumptions of small **w**. In this case, any **K** which can be described by

$$\mathbf{K} = -\mathbf{Z}\mathbf{B}_u^T \quad , \quad \bar{\sigma}\left(\mathbf{Z} - \tfrac{1}{2}\mathbf{I}\right) \le \tfrac{1}{2} \tag{6.22}$$

will result in $\mathbf{K}\mathbf{w}(t) \in \mathcal{U}(\mathbf{w}(t))$, $\forall \mathbf{w}(t)$. Using the above parameterization, a choice for **Z** gives a solution for **P**, which will be called $\mathbf{P}_z$, found through

$$\left(\mathbf{A} - \mathbf{B}_u\mathbf{Z}\mathbf{B}_u^T\right)^T \mathbf{P}_z + \mathbf{P}_z\left(\mathbf{A} - \mathbf{B}_u\mathbf{Z}\mathbf{B}_u^T\right) + \left(\mathbf{Q} - \mathbf{S}\mathbf{Z}\mathbf{B}_u^T - \mathbf{B}_u\mathbf{Z}^T\mathbf{S}^T + \mathbf{B}_u\mathbf{Z}^T\mathbf{R}\mathbf{Z}\mathbf{B}_u^T\right) = \mathbf{0} \tag{6.23}$$

The solution for $\mathbf{P}_z$ is such that $\mathbf{w}_0{}^T\mathbf{P}_z\mathbf{w}_0$ is the performance for $\mathbf{u}(t) = \mathbf{K}\mathbf{w}(t)$; i.e. the application of the constant damping matrix **Z**. The CL control law with $\mathbf{P} = \mathbf{P}_z$ gives the expression

$$J\left(\mathbf{w}_0\right) = \mathbf{w}_0^T\mathbf{P}_z\mathbf{w}_0 + \int_0^\infty \left\{ \min_{\tilde{\mathbf{u}} \in \mathcal{U}(\mathbf{w}(\tau))} \left\|\tilde{\mathbf{u}} - \mathbf{K}_{CL}\left(\mathbf{P}_z\right)\mathbf{w}(\tau)\right\|_{\mathbf{R}}^2 - \left\|-\mathbf{Z}\mathbf{B}_u^T\mathbf{w}(\tau) - \mathbf{K}_{CL}\left(\mathbf{P}_z\right)\mathbf{w}(\tau)\right\|_{\mathbf{R}}^2 \right\} d\tau \tag{6.24}$$

But, because **K** as defined in Eq. (6.22) always results in a feasible **u**, the integrand in the above equation is always less than zero. Thus,

$$\mathbf{P} = \mathbf{P}_z \quad \Rightarrow \quad J\left(\mathbf{w}_0\right) \le \mathbf{w}_0^T\mathbf{P}_z\mathbf{w}_0 \tag{6.25}$$

It is therefore clear that a given choice of **K**, as parameterized by **Z** in Eq. (6.22), results in an upper bound on performance in Eq. (6.24), equal to the performance with linear damping matrix **Z**. Thus, this control algorithm is called *Damping-Reference* (*DR*) control.

Recalling the discussion in introduction to this chapter, the set of **Z** obeying the constraint in Eq. (6.22) constitutes a family of control laws (i.e. for a given performance metric, **Z**

fully characterizes the CL control law). In the terminology of the introduction, the parameter vector $\boldsymbol{\theta}$ contains the elements of $\mathbf{Z}$, and the parameter set Θ constitutes those $\boldsymbol{\theta}$ vectors for which $\mathbf{Z}$ is feasible.

***Optimization of* Z**

The next step is to find the $\mathbf{Z}$ which optimizes (i.e. minimizes) the upper bound for a particular initial condition $\mathbf{w}_0$. Here, this will be done for $\mathbf{w}_0$ resulting from an impulsive disturbance. The optimization at hand is the deterministic analog of the stochastic optimization of $\mathbf{Z}$ performed in Chapter 5.

An impulsive acceleration $a_g = \delta(t)$, results in an initial condition $\mathbf{w}_0 = \mathbf{B}_a$. We wish to minimize the quantity

$$\mathbf{B}_a^T \mathbf{P}_z \mathbf{B}_a = tr\left\{\mathbf{P}_z \mathbf{B}_a \mathbf{B}_a^T\right\} \tag{6.26}$$

over the admissible $\mathbf{Z}$ domain, subject to the constraint that $\mathbf{Z}$ and $\mathbf{P}_z$ be related by Eq. (6.23). But

$$tr\left\{\mathbf{P}_z \mathbf{B}_a \mathbf{B}_a^T\right\} = tr\left\{\boldsymbol{\Phi}\left(\mathbf{Q} - \mathbf{S}\mathbf{Z}\mathbf{B}_u^T - \mathbf{B}_u \mathbf{Z}\mathbf{S}^T + \mathbf{B}_u \mathbf{Z}^T \mathbf{R}\mathbf{Z}\mathbf{B}_u\right)\right\} \tag{6.27}$$

where $\boldsymbol{\Phi}$ satisfies the Lyapunov equation

$$\boldsymbol{\Phi}\left(\mathbf{A} - \mathbf{B}_u \mathbf{Z}\mathbf{B}_u^T\right)^T + \left(\mathbf{A} - \mathbf{B}_u \mathbf{Z}\mathbf{B}_u^T\right)\boldsymbol{\Phi} + \mathbf{B}_a \mathbf{B}_a^T = \mathbf{0} \tag{6.28}$$

The procedure described in Chapter 5 optimizes the quantity on the right-hand side of Eq. (6.27), subject to Lyapunov equations (6.23) and (6.28) for $\mathbf{P}_z$ and $\boldsymbol{\Phi}$ respectively. Here, the optimization is the same problem statement, and therefore the result will be identical.

The gradient of the performance, with respect to $\mathbf{Z}$, was found as Eq. (5.64), repeated here as

$$\frac{\partial}{\partial \mathbf{Z}}\left(\mathbf{B}_a^T \mathbf{P}_z \mathbf{B}_a\right) = 2\left(-\mathbf{B}_u^T \mathbf{P}_z - \mathbf{S}^T + \mathbf{R}\mathbf{Z}\mathbf{B}_u^T\right)\boldsymbol{\Phi}\mathbf{B}_u \tag{6.29}$$

Thus, using the same numerical procedure employed in Chapter 5, $\mathbf{Z}$ (and therefore $\mathbf{P}_z$) can be optimized. Then, through implementation of the clipped-linear control algorithm with $\mathbf{P} = \mathbf{P}_z$, the closed-loop system will have optimized upper bound on performance.

Relation to Steepest-Gradient Control

In a semiactive context, DR controllers can be implemented in a manner similar to that described above. However, for semiactive devices, the feasible region analogous to $\mathcal{U}(\mathbf{w})$ is more restrictive. Consequently the **Z** domain, over which the upper performance bound is optimized, would be constrained to diagonal **Z** matrices satisfying the singular value constraint in Eq. (6.22).

This kind of approach was implemented for a semiactive suspension system by (Tseng and Hedrick 1994), and given the name "Steepest-Gradient" control. The name is derived from the fact that the control algorithm makes the integrand in Eq. (6.24) as negative as possible, thus maximizing the rate of descent of the quantity $J(\mathbf{w}(t))-\mathbf{w}^T(t)\mathbf{P}_z\mathbf{w}(t)$. Here, this idea has been generalized to arbitrarily-large systems, and extended to RFA constraints.

Relation to Maximum-Dissipation and Free Reference Control

The special circumstance of DR controllers with $\mathbf{Z} = \mathbf{0}$ reduces to a control system which is guaranteed to perform better than the structural system in the absence of control. This approach has been investigated in various forms by many researchers, and is here called "Free-Reference" control. This method reduces to maximum energy dissipation controller design, with certain choices for **Q**, **S**, and **R**.

Free-Reference control has an appealing trait, in that its guaranteed performance is still valid in the presence of constraint (6.5b), which was ignored in the development of the DR controller above. The specifics of this controller design are discussed in the appendix to this chapter. However, it was found that in general the performance of this controller was not competitive with DR and CO controllers.

6.1.4: Relationship to Lyapunov-Based Controllers

Define $V(\mathbf{w}(t),t)$, evaluated along a given $\{\mathbf{w},\mathbf{u}\}$ trajectory, as

$$V\left(\mathbf{w}(t),t\right)=\int_t^{\infty}\begin{bmatrix}\mathbf{w}^T(\tau) & \mathbf{u}^T(\tau)\end{bmatrix}\begin{bmatrix}\mathbf{Q} & \mathbf{S}\\ \mathbf{S}^T & \mathbf{R}\end{bmatrix}\begin{bmatrix}\mathbf{w}(\tau)\\ \mathbf{u}(\tau)\end{bmatrix}d\tau \tag{6.30}$$

Note that $V(\mathbf{w}(0),0)=J(\mathbf{w}_0)$, and that $V(\mathbf{w}(t),t)$ is in general equal to the performance of the closed-loop system for initial condition $\mathbf{w}(t)$. Clearly, V is a Lyapunov function for the closed-loop system, and therefore $\dot{V}\left(\mathbf{w}(t),t\right)\le 0$.

For any of the CL controllers discussed in the previous sections, it is true that

$$\frac{d}{dt}\left(\mathbf{w}^T(t)\mathbf{P}\mathbf{w}(t)\right)=\dot{V}\left(\mathbf{w}(t),t\right)+\left\|\mathbf{u}(t)-\mathbf{K}_{CL}(\mathbf{P})\mathbf{w}(t)\right\|_{\mathbf{R}}^2-\left\|\mathbf{K}\mathbf{w}(t)-\mathbf{K}_{CL}(\mathbf{P})\mathbf{w}(t)\right\|_{\mathbf{R}}^2 \quad (6.31)$$

But for DR controllers, the right-hand side is always negative-definite (assuming constraint (6.5b) is ignored) so for these controllers,

$$\frac{d}{dt}\left(\mathbf{w}^T(t)\mathbf{P}_z\mathbf{w}(t)\right)\le\dot{V}\left(\mathbf{w}(t),t\right)\le 0 \quad (6.32)$$

$$\mathbf{w}^T(t)\mathbf{P}_z\mathbf{w}(t)\ge V\left(\mathbf{w}(t),t\right) \quad (6.33)$$

Thus, these controllers provide an upper bound for $V(\mathbf{w}(t),t)$, and yield a quadratic Lyapunov function for the closed-loop system. As such, these controllers are equivalent to Lyapunov-based controller designs.

Recall from Section 6.1.2 that the matrix $\mathbf{P}_o$ establishes a lower bound for $J(\mathbf{w}_0)$ equal to $\mathbf{w}_0{}^T\mathbf{P}_o\mathbf{w}_0$. Thus, for $V(\mathbf{w}(t),t)$, it follows that

$$V\left(\mathbf{w}(t),t\right)\ge\mathbf{w}^T(t)\mathbf{P}_o\mathbf{w}(t) \quad (6.34)$$

Thus, the matrix $\mathbf{P}_o$ establishes a lower bound for $V(\mathbf{w}(t),t)$. While the upper bound in Eq. (6.33) only exists for DR controllers, the lower bound in Eq. (6.33) exists for any CL controller.

6.1.5: Characteristics of the Clipping Action

The clipping action in Eq. (6.15) is equivalent to the variational statement

$$\delta\left\{\mathbf{u}^T\mathbf{R}\mathbf{u}-2\mathbf{u}^T\mathbf{R}\mathbf{u}_a+\mathbf{u}_a^T\mathbf{R}\mathbf{u}_a+\boldsymbol{\lambda}^T(|\mathbf{u}|-\mathbf{u}_{\max})+\lambda_R\left(\mathbf{u}^T\mathbf{u}+\mathbf{u}^T\mathbf{B}_u^T\mathbf{w}\right)\right\}=0 \quad (6.35)$$

where Lagrange multiplier λ_R is constrained by

$$\left(\mathbf{u}^T\mathbf{u}+\mathbf{u}^T\mathbf{B}_u^T\mathbf{w}\right)\lambda_R=0 \quad , \quad \lambda_R\ge 0 \quad , \quad \mathbf{u}^T\mathbf{u}+\mathbf{u}^T\mathbf{B}_u^T\mathbf{w}\le 0 \quad (6.36)$$

and Lagrange multiplier vector $\boldsymbol{\lambda}$ is constrained by

$$\lambda_i\left(|u_i|-u_{i\max}\right)=0 \quad , \quad \lambda_i\ge 0 \quad , \quad |u_i|-u_{i\max}\le 0 \quad (6.37)$$

But evaluation of the variational statement in Eq. (6.35) gives

$$(\mathbf{R}+\lambda_R\mathbf{I})\mathbf{u}+\tfrac{1}{2}\lambda_R\mathbf{B}_u^T\mathbf{w}+\tfrac{1}{2}\boldsymbol{\lambda}'-\mathbf{R}\mathbf{u}_a=\mathbf{0} \quad (6.38)$$

where $\lambda'_i=\mathrm{sgn}(\mathbf{u}_i)\lambda_i$.

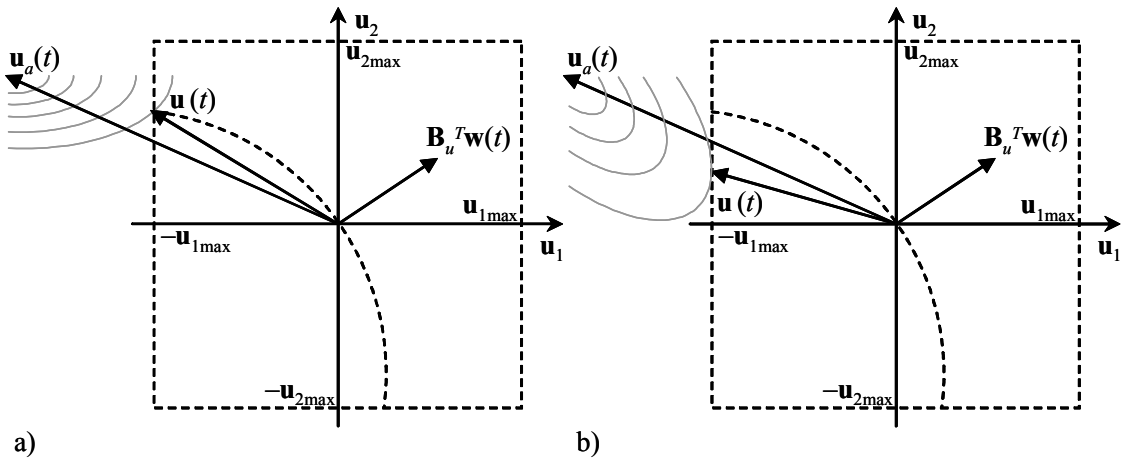

Figure 6.1: Clipping actions for diagonal (a) and nondiagonal (b) **R** matrices

Implications of* R *diagonal

To determine which configurations yield a diagonal **R** matrix, recall the expression for **R** in Eq. (5.38). It is nondiagonal for this formulation only if multiple columns of **N** have nonzero entries on the same row. This corresponds to actuator configurations where two or more actuators share a common degree of freedom, such as stacked actuation systems. In cases where actuators do not share degrees of freedom, it is reasonable to assume that **R** is diagonal for measures of performance that weigh accelerations against drifts.

If **R** is diagonal, Eq. (6.38) can be rewritten as

$$\mathbf{u}(t) = -\underset{\mathbf{u}_{\max}}{\text{sat}}\left\{(\mathbf{R} + 2\lambda_R\mathbf{I})^{-1}\left[\lambda_R\mathbf{B}_u^T\mathbf{w}(t) - \mathbf{R}\mathbf{u}_a(t)\right]\right\} \tag{6.39}$$

where sat(.) is the element-by-element saturation function with bounds at $\pm\mathbf{u}_{\max}$. Otherwise, the clipping action can take on a somewhat non-intuitive role in the modification of $\mathbf{u}_a$. This is illustrated in Fig. 6.1, where the lighter lines represent surfaces of equal $\|\mathbf{u}(t)\text{-}\mathbf{u}_a(t)\|_{\mathbf{R}}$ values. For diagonal **R**, the clipping action behaves like a saturation function, whereas for nondiagonal **R**, it can give more complicated results. This observation is relevant to both RFA and semiactive systems.

***Implications of* R=*r*I**

The case **R**=*r***I**, where *r* is a positive scalar, is not an unreasonable outcome of the acceleration weighting scheme if no two actuators share a degree of freedom. Then the expression for the optimal control in Eq. (6.38) simplifies to

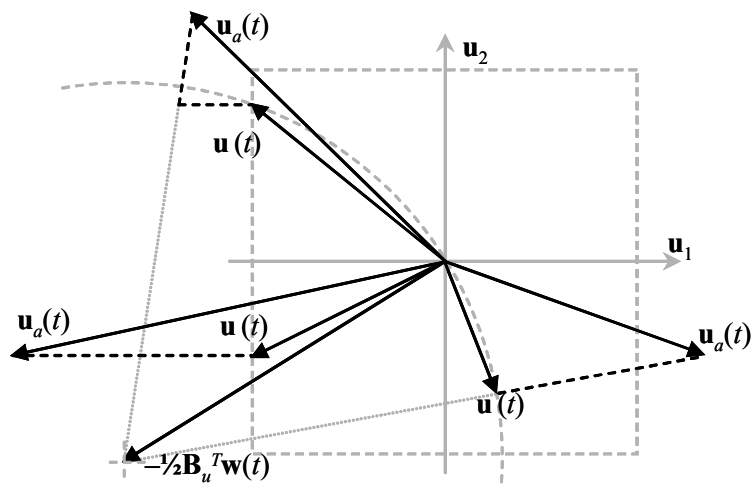

Figure 6.2: Clipping action for $\mathbf{R} = r\mathbf{I}$, for several different $\mathbf{u}_a(t)$

$$\mathbf{u}(t) = \underset{\mathbf{u}_{\max}}{\mathrm{sat}}\left\{\frac{r}{r+2\lambda_R}\mathbf{u}_a(t) - \frac{2\lambda_R}{r+2\lambda_R}\tfrac{1}{2}\mathbf{B}_u^T\mathbf{w}(t)\right\} \tag{6.40}$$

Using the definition

$$\alpha = \frac{2\lambda_R}{r+2\lambda_R} \tag{6.41}$$

Eq. (6.40) becomes

$$\mathbf{u}(t) = \underset{\mathbf{u}_{\max}}{\mathrm{sat}}\left\{(1-\alpha)\mathbf{u}_a(t) - \alpha\tfrac{1}{2}\mathbf{B}_u^T\mathbf{w}(t)\right\} \tag{6.42}$$

The value of $\alpha(t)$ can be found as

$$\alpha = \max\{\tilde{\alpha}, 0\} \tag{6.43}$$

where $\tilde{\alpha}$ is a solution to

$$\left\|\underset{\mathbf{u}_{\max}}{\mathrm{sat}}\left\{(1-\tilde{\alpha})\mathbf{u}_a(t) - \tilde{\alpha}\tfrac{1}{2}\mathbf{B}_u^T\mathbf{w}(t)\right\}\right\|_2^2 + \underset{\mathbf{u}_{\max}}{\mathrm{sat}}\left\{(1-\tilde{\alpha})\mathbf{u}_a(t) - \tilde{\alpha}\tfrac{1}{2}\mathbf{B}_u^T\mathbf{w}(t)\right\}^T\mathbf{B}_u^T\mathbf{w}(t) = 0 \tag{6.44}$$

It is straight-forward to show that Eqs. (6.43) and (6.44) yield at least one solution $\alpha(t) \in [0,1]$ for all $\mathbf{w}(t)$ and $\mathbf{u}_a(t)$, and that the solution is unique for almost all $\mathbf{w}(t)$ and $\mathbf{u}_a(t)$.

Eq. (6.42) has a useful graphical interpretation, because in this case the clipping action simplifies to a kind of nested saturation process. Consider Fig. 6.2, which shows several different values of $\mathbf{u}_a(t)$ for a given $\mathbf{w}(t)$, and the resultant clipped inputs $\mathbf{u}(t)$. In each case, note that the clipping action consists of the saturation of a line segment starting at $\mathbf{u}_a(t)$ and ending at

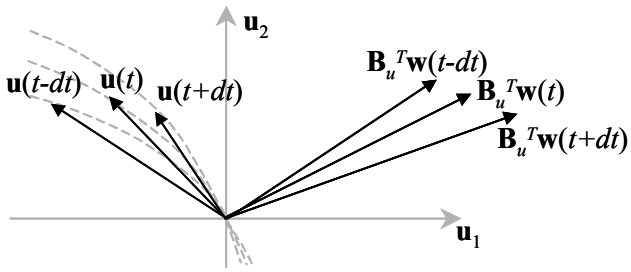

Figure 6.3: Succession of optimal $\mathbf{u}(t)$ values for singular control case

$-\frac{1}{2}\mathbf{B}_u^T\mathbf{w}(t)$ (i.e. the center of $S(\mathbf{v}(t))$ when mapped into $\mathbf{u}(t)$-space). The saturation of this end point is always feasible. Thus, the clipping action consists of the following steps. If the saturation of $\mathbf{u}_a(t)$ is inside $\mathcal{U}(\mathbf{w}(t))$ (such as the example in quadrant 3 in the figure) then this saturated vector is $\mathbf{u}(t)$. If not, then the point of minimum distance along the line from $\mathbf{u}_a(t)$ to $-\frac{1}{2}\mathbf{B}_u^T\mathbf{w}(t)$ (i.e. the minimal $\alpha(t)$ coordinate) is found for which the saturated vector lies on the feasible boundary (such as the examples in quadrants 2 and 4), and this vector is $\mathbf{u}(t)$.

***Implications of* $\mathbf{R}\rightarrow\mathbf{0}$**

It is also interesting to observe the effects of a choice of optimization weights resulting in an $\mathbf{R}$ matrix which is very small (e.g. a case where the drifts are weighed much more heavily than the accelerations). In the limit as $\mathbf{R}\rightarrow\mathbf{0}$, this leads to a phenomenon which is generally called "singular" optimal control. For such a weighting scheme, Eq. (6.38) becomes Eq. (6.17). Because this is an optimization of a linear function, there is no minimum on the interior of $\mathcal{U}(\mathbf{w}(t))$, and the resultant $\mathbf{u}(t)$ will always lie on the boundary of $\mathcal{U}(\mathbf{w}(t))$. Thus, $\mathbf{u}$ becomes reminiscent of a "bang-bang" type of signal in the absence of explicit acceleration regulation. However, unlike bang-bang controllers, the time derivative of $\mathbf{u}(t)$ is finite and nonzero during periods when $\mathbf{u}(t)$ is on the boundary $P(\mathbf{u}(t),\mathbf{w}(t)) = 0$, as illustrated in Fig. 6.3. Here, dt is some small increment in time, and the figure shows relevant vectors at t-dt, t, and t+dt. The $\mathbf{u}(t)$ vector varies continuously in this case, lying on the boundary corresponding to $P(\mathbf{u}(t),\mathbf{w}(t))=0$ at each time.

Computational Issues

For CL controllers to be of any practical use, they have to be computationally-tractable. But the control law in Eq. (6.13) consists of a minimization over the domain $\mathcal{U}(\mathbf{w}(t))$. It is important to investigate the practicality of performing this minimization; i.e., to determine if it can at least be performed in a computationally-finite number of steps. In the appendix to this

chapter, an algorithm is proposed for resolving the clipping action for arbitrary positive-definite **R**. For clipping actions involving singular **R** matrices, the proposed routine can be applied with the augmented weighting matrix $\mathbf{R}+\varepsilon\mathbf{I}$, for $\varepsilon>0$ arbitrarily small. It may also be generalized to explicitly accommodate the singular case, although that is not done here.

In the literature, the clipping action has almost universally been treated as a simple element-by-element saturation at the minimum and maximum feasible force values; a much less computationally-intensive procedure. For semiactive systems, where $\mathcal{U}(\mathbf{w}(t))$ has a prismatic boundary, this corresponds to the clipping action of the CL control law in Eq. (6.13) if and only if **R** is diagonal. In the case of RFA networks, the concept of element-by-element saturation does not really make sense, because $\mathcal{U}(\mathbf{w}(t))$ has ellipsoidal as well as planar boundaries.

6.1.6: Examples

For the purpose of illustration, a simple demonstration of CL controller synthesis techniques will now be given. The structural model and actuation configurations from Example 1 of Chapter 5 will be used again here. This example concerns the three-story shear structure, with two actuators; one between the base and the first story, and the other between the third story and a hybrid mass damper. It should be mentioned that for these simulations, the Nominal System Model will be used.

It will be assumed that $a_g(t) = A_0\delta(t)$, where A_0=0.01m/s^2. The strength of this impulse is small enough that constraint (6.5b) is effectively irrelevant, because the regenerative constraint (6.5a) will typically not produce a boundary large enough to intersect with the maximum force boundaries. As such, the simulation results will be homogeneous for A_0 below that value for which **u** violates Eq. (6.5b).

Two performance measurement cases will be considered, which measure mean-square drift and mean-square acceleration respectively. As in Chapter 5, the quadratic performance measures are constructed through scalar weights q_{dk}, q_{ak}, and q_E. For each of the clipped-linear control synthesis techniques, the controller is fully determined from the **Q**, **R**, **S**, and **K** matrices. For a given weighting scheme, **Q**, **R**, and **S** follow directly from Eq. (5.36). Different synthesis methods (i.e. CO and DR) will result in different choices for **K**. However, these methods arrive at **K** through systematic means, as described in the previous subsections.

At the risk of creating confusion, the data pertaining to these examples will be presented in terms of the *physical* quantities (i.e. the force vector $\mathbf{f}_e$, structural positions **q**, and so on) with the tacit understanding that these quantities relate to the normalized quantities of the Nominal System Model (i.e. normalized force vector **u**, state vector **w**, and so on) through the Eq (5.12).

Example 1: Drift Regulation

For the drift minimization case, the weights q_{ak}, and q_E are equal to zero. The drift weights are assigned such that the performance measure is

$$J = 10^6 \int_0^\infty \left\{ 0.5\left(d_1(t)\right)^2 + 1.5\left(d_2(t)\right)^2 + 2\left(d_3(t)\right)^2 \right\} dt \tag{6.45}$$

Thus, priority is given to minimization of the second- and third-story drifts, over the first-story. There is no weight given to the drift of the mass damper.

From these weights, the appropriate **Q**, **S**, and **R** matrices can be found. In this case, **R** and **S** will be zero, because these matrices depend only on acceleration weights. However, the **R** matrix will be adjusted to

$$\mathbf{R} = \varepsilon \begin{bmatrix} f_{1\max}^{-2} & \\ & f_{2\max}^{-2} \end{bmatrix} \tag{6.46}$$

where $\varepsilon = 10^{-2}$. This value of ε is small enough to have only a negligible impact on the evaluation of J. However, it does make the problem computationally more straight-forward because it establishes a clipping action which is continuous in its arguments.

From these matrices, the **P** matrices corresponding to CO and DR control designs (i.e. $\mathbf{P}_o$ and $\mathbf{P}_z$) are found from Eqs. (6.18) and (6.23) respectively. For the DR controller, $\mathbf{P}_z$ is optimized as described in the previous section. The computation of the **P** matrices completes the synthesis of the CL control law. In addition to these two control laws, the optimal constant-**Z** (CZ) case will also be examined. All three control implementations are compared to the uncontrolled case (i.e. $\mathbf{u} = \mathbf{0}$).

Response data is shown in Table 6.1. The table shows not only the performance metric J, but also the maximum quantities for drift, acceleration, and force magnitudes for all controllers. From this data, the most interesting fact is that the controllers perform almost equally, even though their maximum drift data is quite different. In the case of the DR controller, the maximum drifts have a pattern which roughly corresponds to the q_{dk} weights; i.e. the drifts with higher weights had lower responses. However, the CO controller does not exhibit this effect at all. Also, note the large accelerations for the first story, and the mass damper, in comparison to the uncontrolled case. Clearly, because the controllers were not designed to regulate accelerations, they take liberties with extremely large forces (and thus accelerations) in order to reduce the drifts. In the CZ case, however, the forces and accelerations are more comparable

with the uncontrolled case, suggesting that the high quantities arising in the CO and DR cases are from the implementation of the clipping action.

Transient plots are shown in Figs. 6.4 through 6.12 for impulse responses with these controllers. For each controller, transient plots are shown for the drifts and accelerations, as well as the actuator velocity vector **v** and force vector $\mathbf{f}_e$. The CO and DR controllers yield similar shapes for the drift responses, but the DR controller manages to obtain slightly better suppression characteristics for drifts 2 and 3 during the first few oscillations of the system. Despite the somewhat similar shapes for the three story drifts, the mass damper drift is drastically different for the CO and DR controllers, with the CO controller resulting in almost twice the maximum drift of the DR controller. Although the drift of the mass damper was not weighed in the performance expression, these different drift histories are indicative of the way in which the RFA network is being utilized by the different control algorithms. In the CO and DR cases, the mass damper is excited a great deal, but the DR case obtains better performance with much less motion of the mass.

Consider the responses for the CZ controller, shown in Fig. 6.10. By contrast with the other two controller cases, the responses here show a strong, undamped presence of the third structural mode. The implementation with constant **Z** does not yield a great deal of suppression in the third mode. This fact will become even more apparent in the forced vibration examples discussed in the next section.

The actuation power flows P_1 and P_2, as well as the total power P_T, are shown in Figs. 6.5, 6.8, and 6.11. All controllers exhibit a pronounced power-sharing behavior, to one degree or another.

Table 6.1: Impulse Response Data for Drift Regulation

	CO	DR	CZ	No control
d_1 (mm)	0.094	0.135	0.113	0.192
d_2 (mm)	0.114	0.0932	0.0953	0.0827
d_3 (mm)	0.102	0.082	0.0858	0.0706
d_4 (mm)	1.58	0.857	1.14	0.469
a_1 (m/s^2)	2.19	2.56	0.280	0.223
a_2 (m/s^2)	0.558	0.423	0.446	0.447
a_3 (m/s^2)	0.709	0.554	0.585	0.485
a_4 (m/s^2)	5.96	6.05	1.52	0.279
f_1 (N)	493	578	62.8	–
f_2 (N)	46.6	49.1	12.5	–
J	0.00145	0.00141	0.00152	0.0573

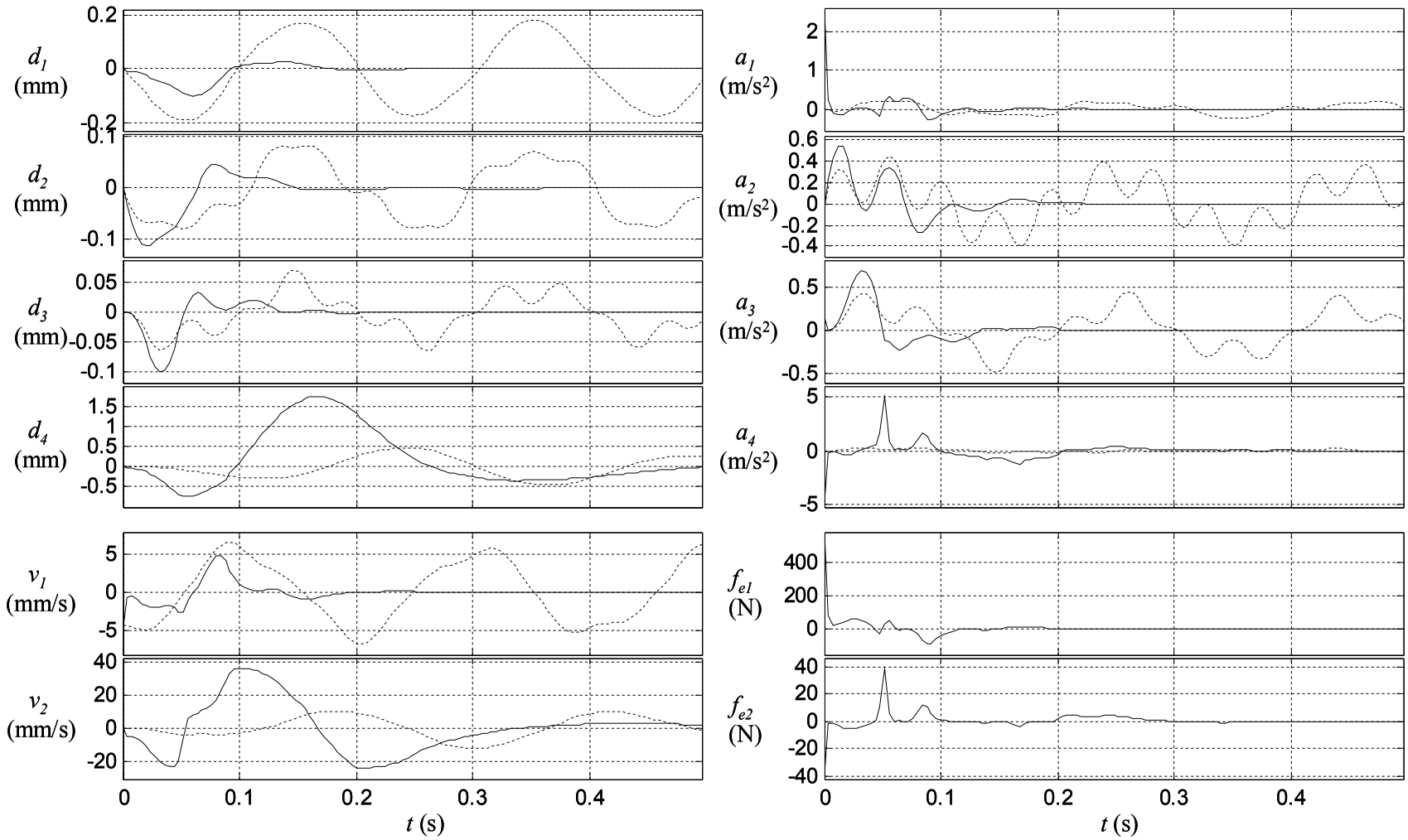

Figure 6.4: Transient plots for Example 1, with Clipped-Optimal controller (solid) and uncontrolled case (dotted)

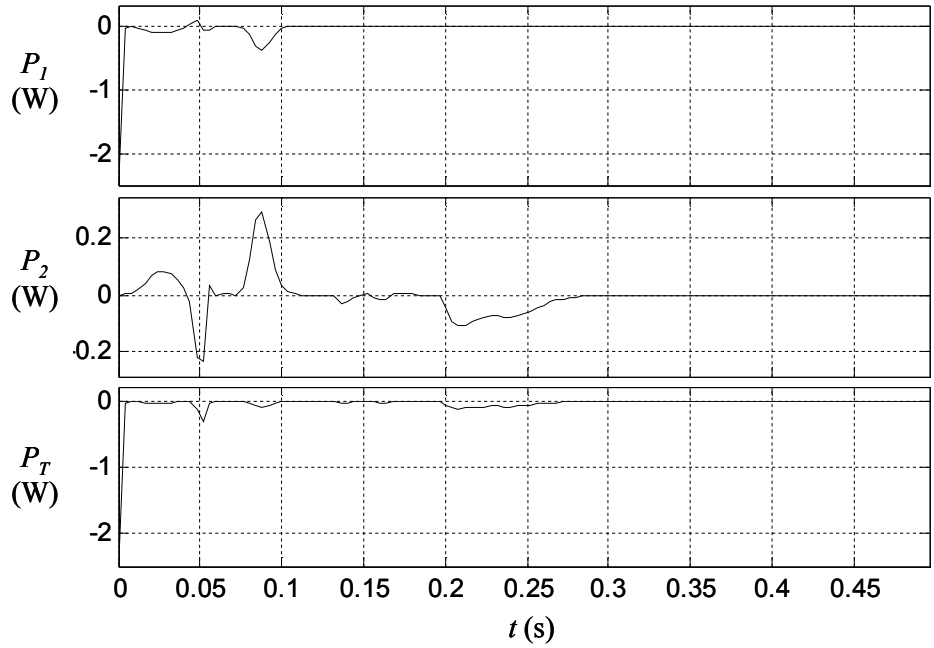

Figure 6.5: Power flows for Example 1, with CO controller

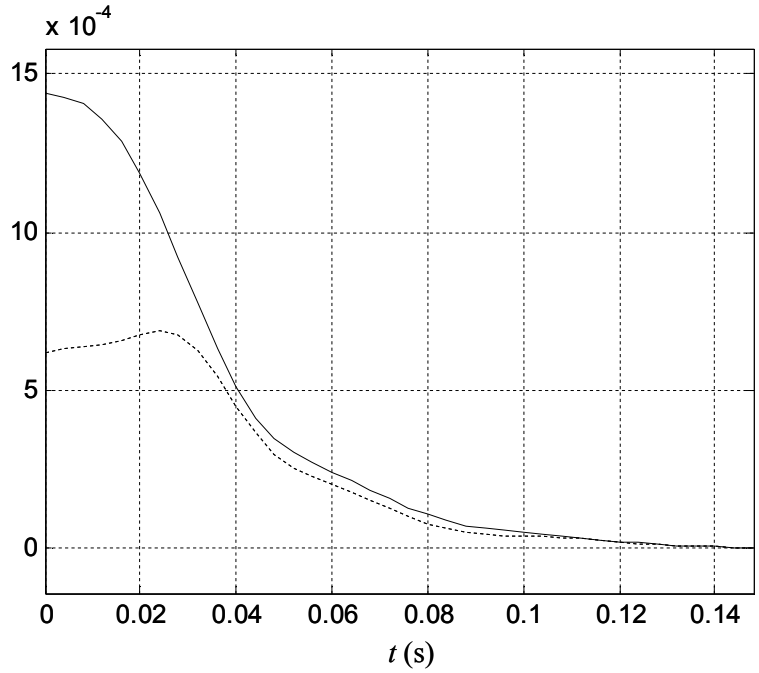

Figure 6.6: $V(\mathbf{w}(t))$ (dark) and its lower bound (light) for Example 1 with CO control

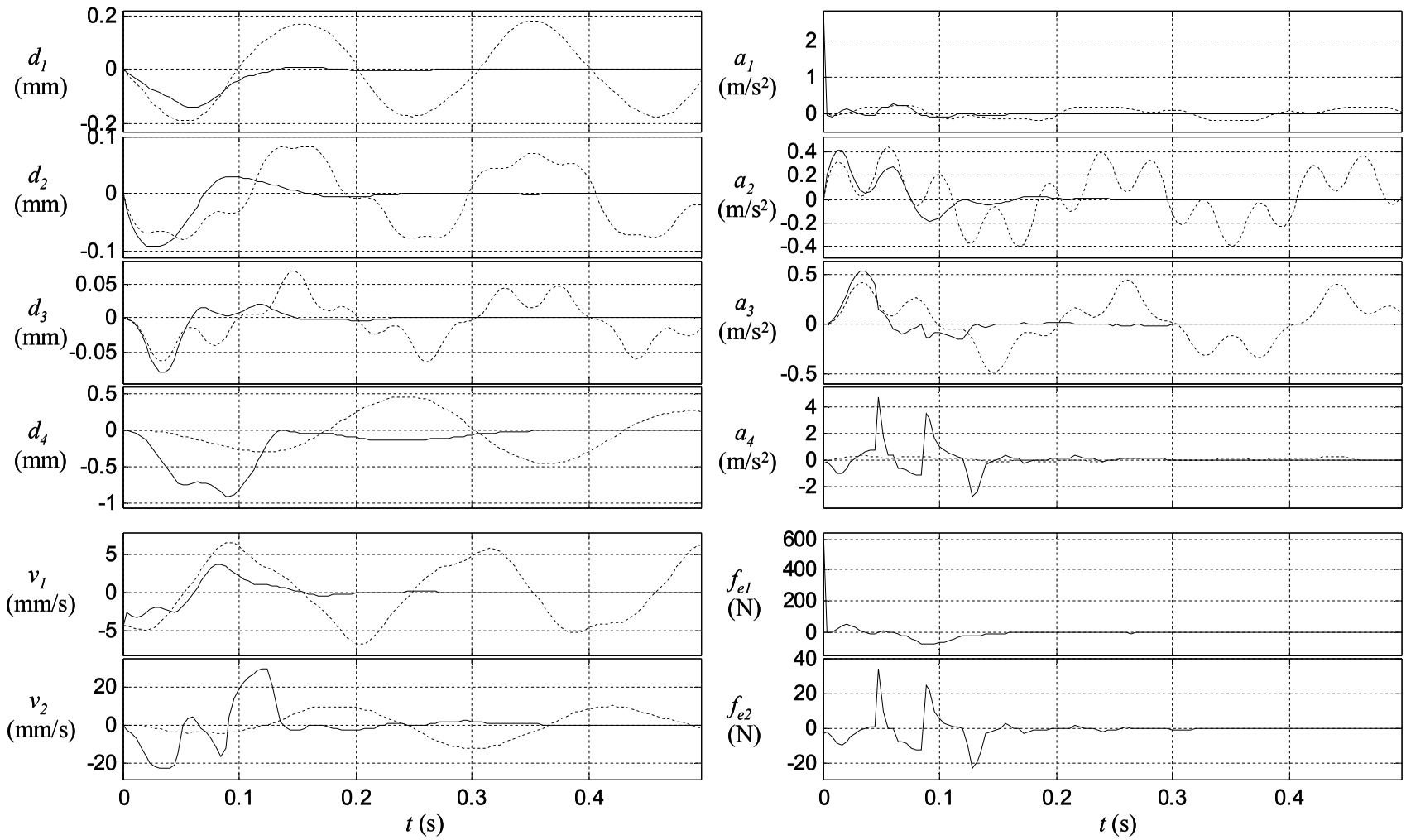

Figure 6.7: Transient plots for Example 1, with Damping-Reference controller (solid) and uncontrolled case (dotted)

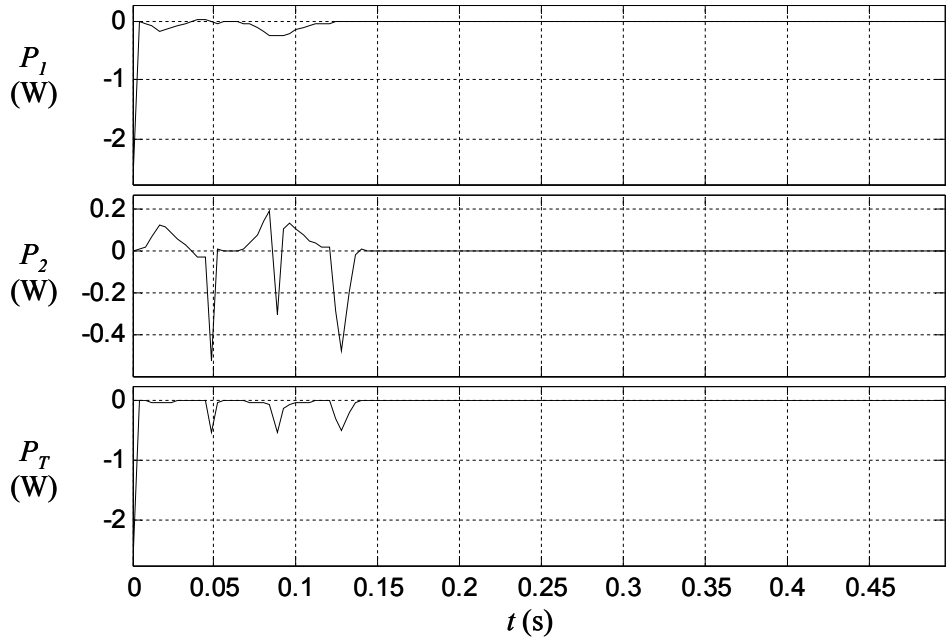

Figure 6.8: Power flows for Example 1, with DR controller

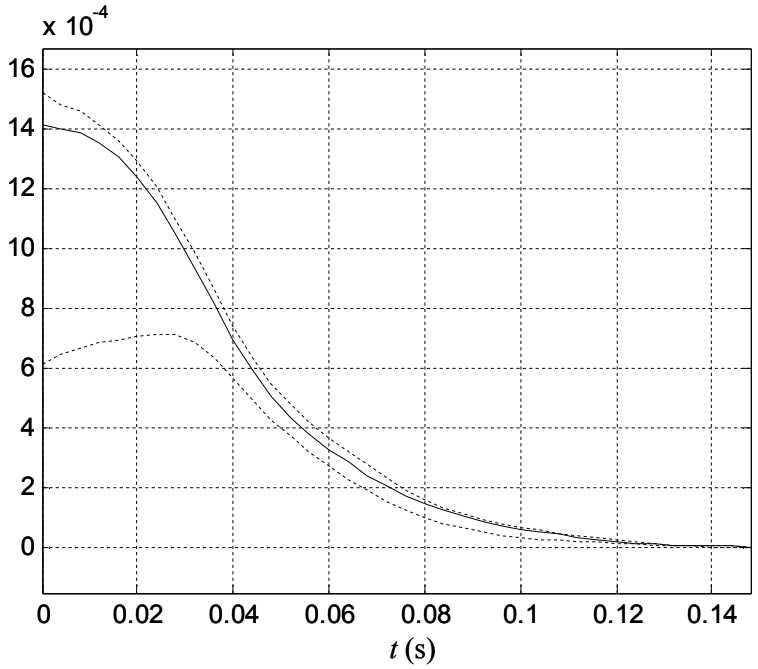

Figure 6.9: $V(\mathbf{w}(t))$ (dark) and its bounds (light) for Example 1 with DR controller

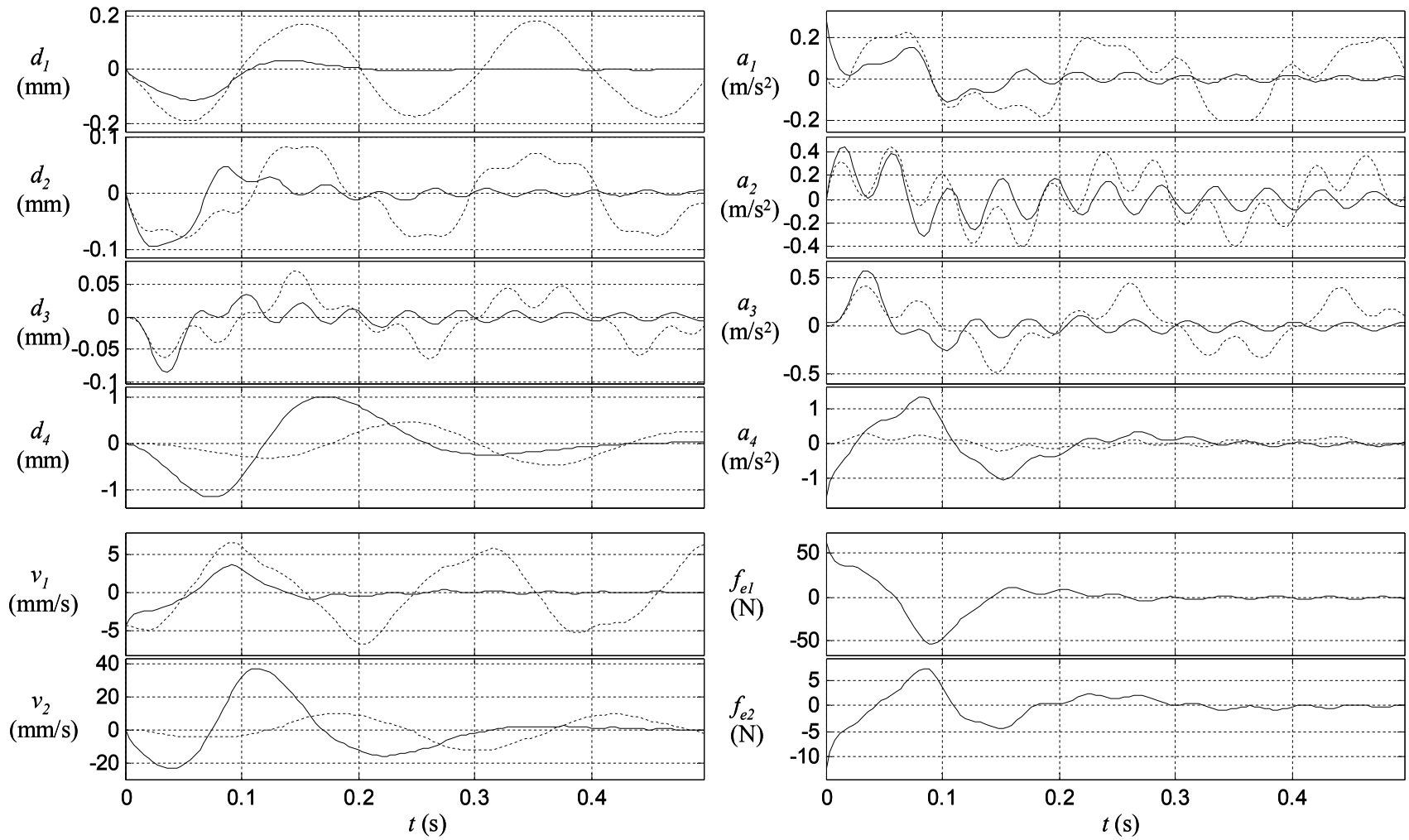

Figure 6.10: Transient plots for Example 1, with Constant-**Z** controller (solid) and uncontrolled case (dotted)

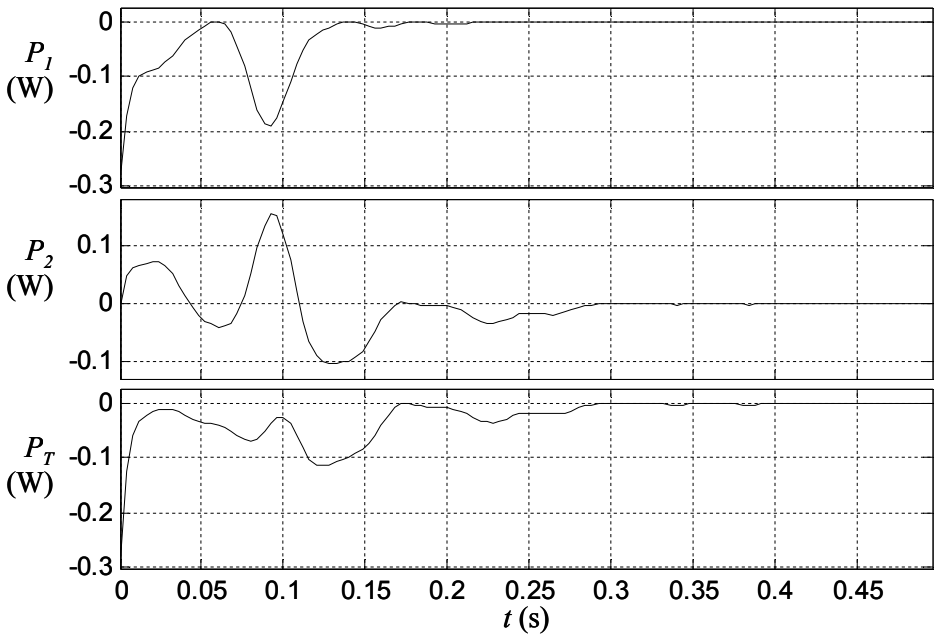

Figure 6.11: Power flows for Example 1, with constant **Z**

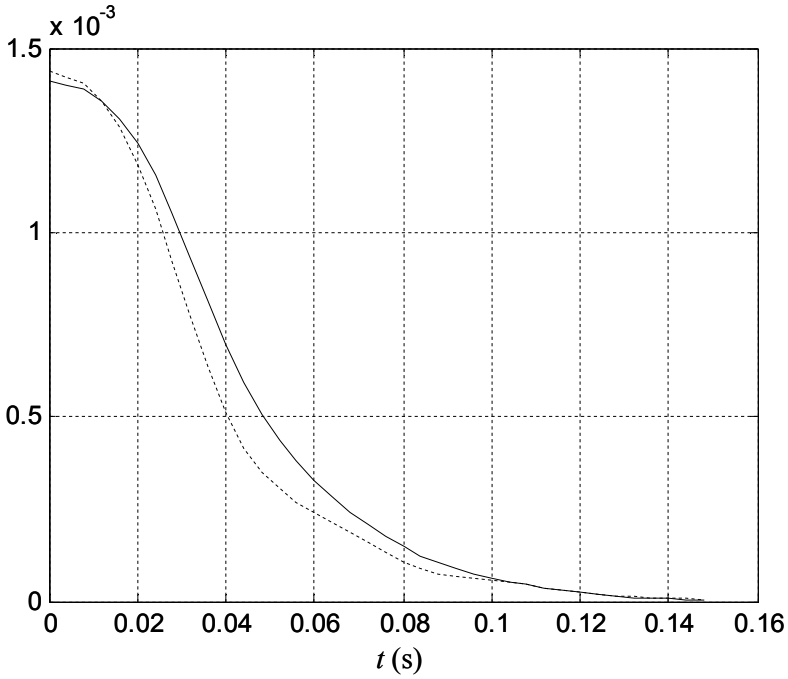

Figure 6.12: Comparison of $V(\mathbf{w}(t))$ for CO (dashed) and DR (solid) controllers for Example 1

Table 6.2: Impulse Response Data for Acceleration Regulation

	CO	DR	CZ	No control
d_1 (mm)	0.186	0.170	0.130	0.192
d_2 (mm)	0.0805	0.107	0.0950	0.0827
d_3 (mm)	0.0686	0.0782	0.0826	0.0706
d_4 (mm)	0.857	0.4578	0.277	0.469
a_1 (m/s^2)	0.213	0.297	0.185	0.223
a_2 (m/s^2)	0.389	0.338	0.381	0.447
a_3 (m/s^2)	0.482	0.532	0.564	0.485
a_4 (m/s^2)	2.50	3.88	1.36	0.279
f_1 (N)	87.6	79.7	55.2	–
f_2 (N)	17.4	31.8	11.1	–
J	0.0143	0.0159	0.0186	0.362

For each controller, the Lyapunov function $V(\mathbf{w}(t))$ discussed in Section 6.1.4 is also shown. Recall that $V(\mathbf{w}(0)) = J(\mathbf{w}_0)$. The lower bound for V in Eq. (6.34) is shown and, in the case of the DR controller, the upper bound in Eq. (6.32). These plots are similar for the two controllers, which are compared in Fig. 6.12. Note that although $J(\mathbf{w}_0)$ is smaller for the DR controller, this comes at the price of a slower decay for $V(\mathbf{w}(t))$. Thus, DR control achieves a lower J by reducing the drifts early in the response, in exchange for larger drifts later.

Example 2: Acceleration Regulation

For acceleration regulation, a similar analysis can be performed. For this example, weights q_{dk} and q_E are zero, and weights q_{ak} are assigned such that

$$J = \int_0^\infty \left\{ a_1^2(t) + a_2^2(t) + a_3^2(t) \right\} dt \tag{6.47}$$

Thus, the accelerations for the three main stories are weighed equally in the performance assessment, and the acceleration of the mass driver is not weighed at all. For this case, the appropriate **Q**, **R**, and **S** matrices are nonzero and **R** is nonsingular.

Response data for the controllers is shown in Table 6.2. The CO and DR controllers perform comparably with each other, although in this case the CO controller yields superior performance. This brings about an important point concerning these controllers. The appeal of the DR controller synthesis is that it yields a guaranteed upper bound on performance. However, the theory leading to the controller design does not prohibit the possibility that, for a given set of circumstances, there may be many other CL feedback control laws which will out-perform it.

However, as will be shown in the next section, the same CO control law performs less favorably in other circumstances.

Comparisons of the controllers' abilities to produce low maximum accelerations yield mixed conclusions. The DR controller does better for story 2, while the CO controller does better for stories 1 and 3. Both controllers result in similar maximum forces. The maximum of $|f_{e1}(t)|$ is higher for the CO case, while the maximum of $|f_{e2}(t)|$ is higher for the DR case. However, as the design objective was to minimize mean-square acceleration quantities, the maximum accelerations shown in Table 6.2 do not give an adequate illustration of the behavior of different controllers.

Consider the transient response plots for this example, shown in Figs. 6.13-6.21. From these plots, the disparity between the performances of the DR and CO controllers becomes more understandable. Following the impulse, the two controllers respond very differently during the first oscillation of the structure, and the DR controller incurs much larger initial accelerations in the first story. Alternatively, the CO controller yields a response in which the higher modes are much more evident in the accelerations, and this behavior works to the benefit of the controller in this circumstance. It is interesting to note that, while the CO controller does out-perform the DR controller, the response quantities for the DR controller die out much more quickly. In particular, note the decay of the accelerations for the CO controller, which exhibit a large amount of high-frequency oscillation, especially in the motion of the first story.

This observation is reflected in the $V(\mathbf{w}(t))$ functions for the CO and DR controllers, compared in Fig. 6.21. It is clear from this plot that, although the DR controller yields a higher value of $J(\mathbf{w}_0)$ $(=V(\mathbf{w}_0,0))$, the value of $V(\mathbf{w}(t),t)$ decays much more quickly, indicating that the accelerations die out much more rapidly. Thus, the DR controller yields higher accelerations at the outset of the disturbance, in exchange for lower accelerations later.

Conclusions

As with many nonlinear systems, it is difficult to make generalized conclusions about the merit of different controllers by examination of a few examples. However, there are some general observations which do follow from the two examples above. First of all, it is clear that it is not difficult to find examples where other controllers (notably, the CO controller) produce somewhat better performance in comparison to the DR controller. However, the appeal of DR control is *consistency*. Because there are guaranteed upper bounds on performance, it can be stated with full confidence that for any example, DR control performs better than a certain quadratic bound.

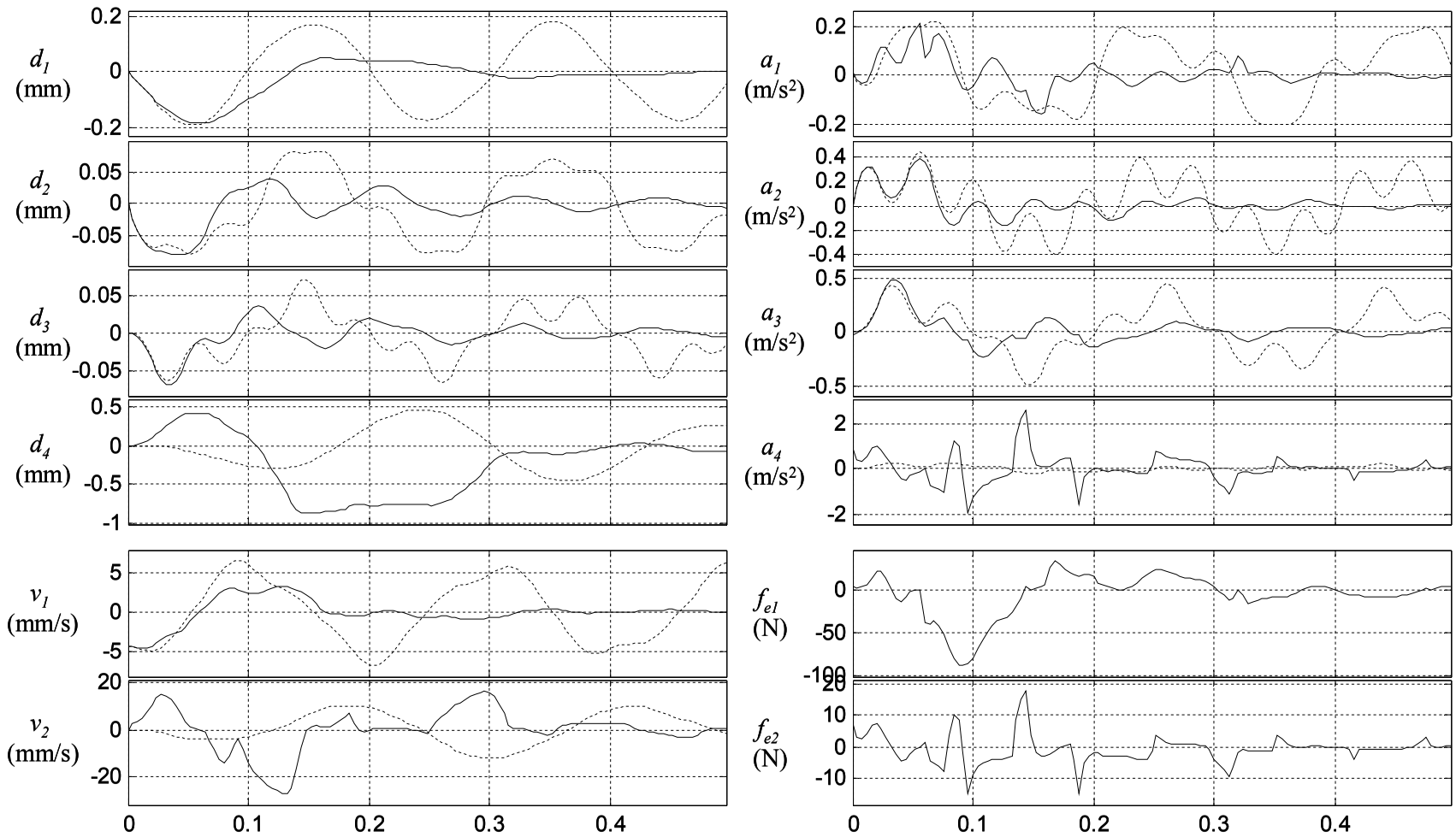

Figure 6.13: Transient plots for Example 2, with Clipped-Optimal controller (solid) and uncontrolled case (dotted)

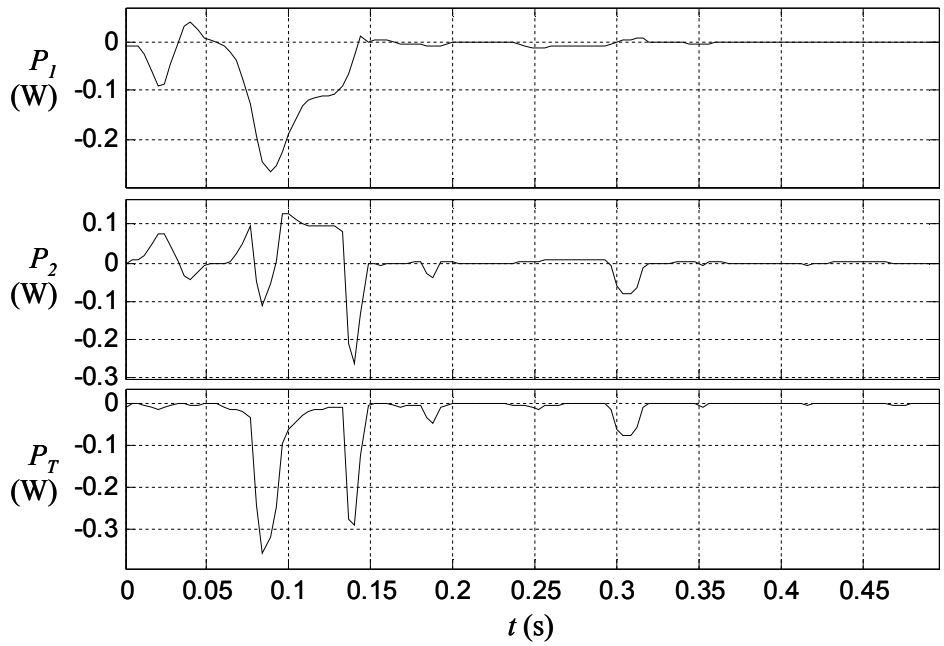

Figure 6.14: Power flows for Example 2, with CO controller

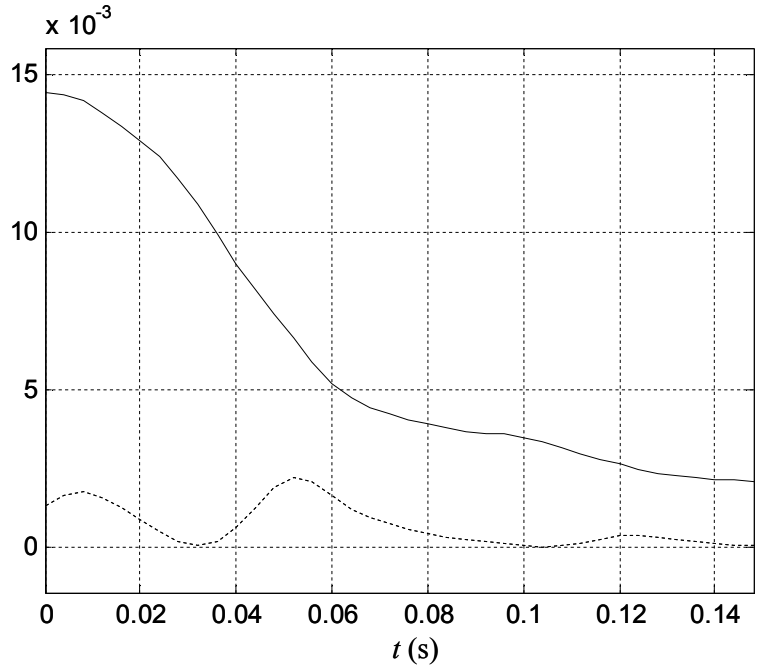

Figure 6.15: $V(\mathbf{w}(t))$ (dark) and its bounds (light) for Example 2 with CO control

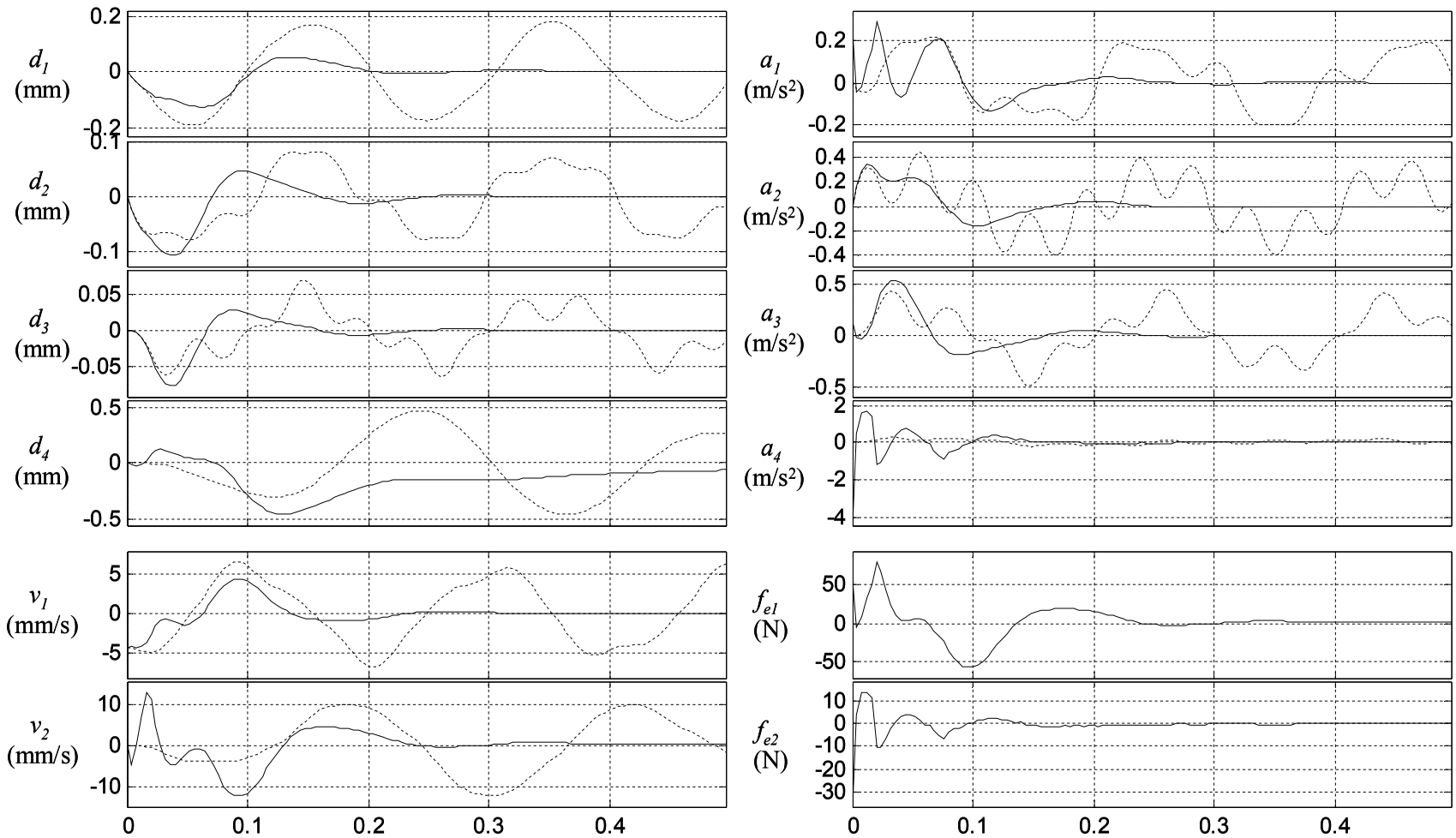

Figure 6.16: Transient plots for Example 2, with Damping-Reference controller (solid) and uncontrolled case (dotted)

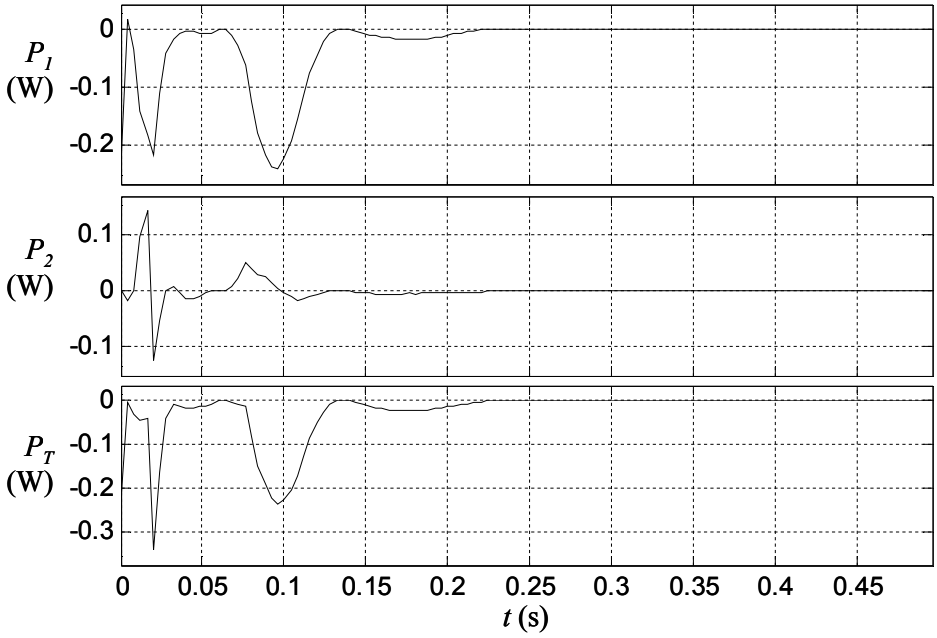

Figure 6.17: Power flows for Example 2, with DR controller

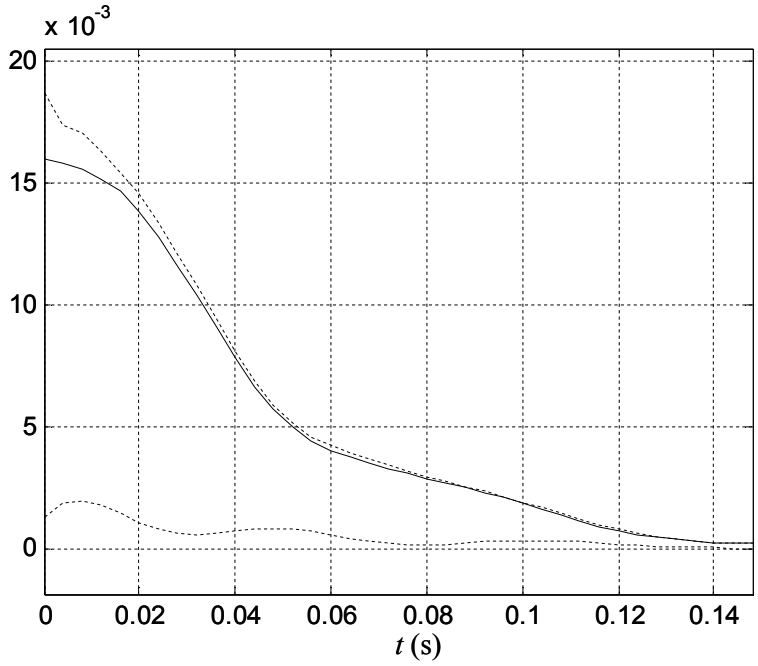

Figure 6.18: $V(\mathbf{w}(t))$ (dark) and its bounds (light) for Example 2 with DR control

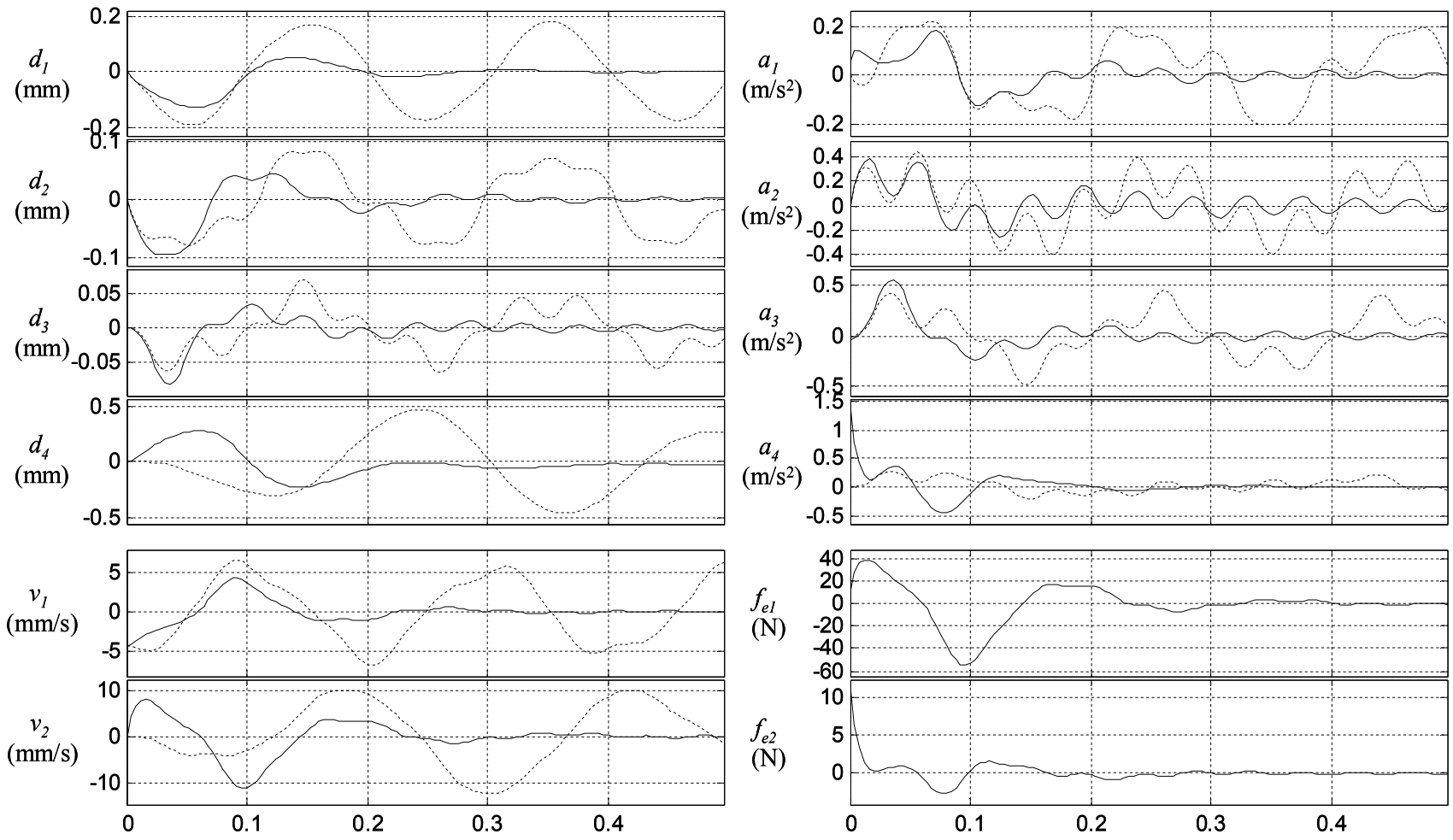

Figure 6.19: Transient plots for Example 2, with Constant-**Z** controller (solid) and uncontrolled case (dotted)

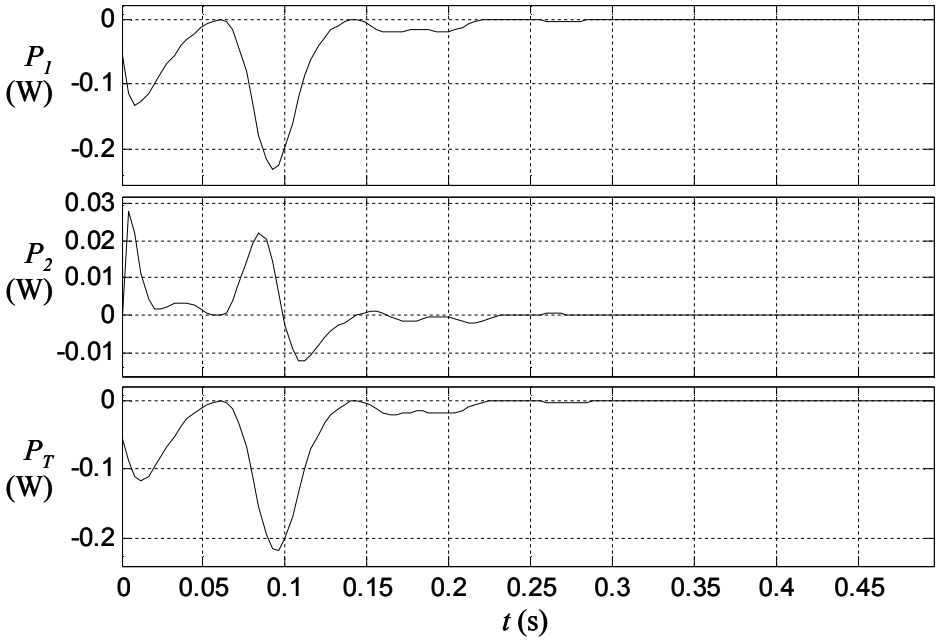

Figure 6.20: Power flows for Example 2, with constant **Z**

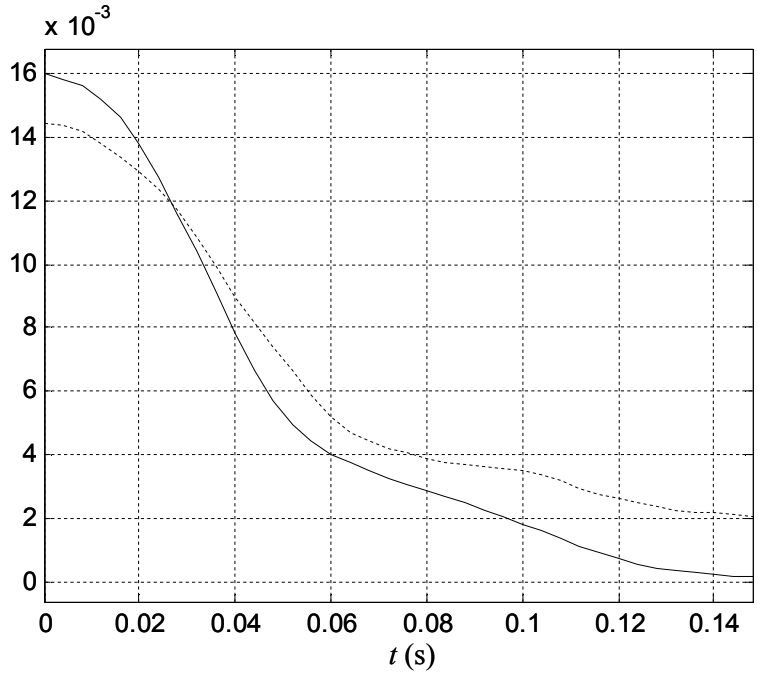

Figure 6.21: Comparison of $V(\mathbf{w}(t))$ for CO (dashed) and DR (solid) controllers for Example 2

6.2: Clipped-Linear Controllers for Forced Response

Many control system design methods have been proposed for reducing the forced response of structures using semiactive devices. However, by far the most common method is Clipped-Optimal stochastic (CO-S) control.

This method is similar to the free-response CO controller discussed in the previous section, but is applied to systems in stationary stochastic excitation. For full-information noiseless feedback, the control synthesis yields the same feedback law. The general approach is to design a stochastic-optimal linear active feedback law, and then clip the control signal to the admissible space $\mathcal{U}(\mathbf{w}(t))$. As with the CO controller for free response, CO-S control system design is largely an ad-hoc method, in which the original **Q**, **S**, and **R** matrices used in the design are adjusted until the linear stochastic controller produces forces which tend to be dissipative.

For many applications, CO-S control tends to yield favorable performance, and is a useful tool for the design of simple controllers. However, it has a disadvantage in that there are no *guaranteed* performance bounds.

In this section, it is shown that, as with the free-vibration case, there exist Damping-Reference control synthesis methods which yield control laws which are similar to those for CO-S control, but which *do* have quadratic bounds on performance. However, naturally, the bounds of the response will be functions of the input characteristics.

Performance Measures

In the free-vibration case, the performance metric J was defined as in Eq. (6.7). In the forced response case, the measure of performance will be treated in two different ways, depending on the nature of the input disturbance. Different performance measures will be proposed for stationary white-noise excitation and for deterministic excitation (with $a_g \in \mathcal{L}_2[0,\infty)$). These two cases are addressed in Sections 6.2.1 and 6.2.2. The former development is an application of nonlinear stochastic LQ control, while the latter is an application of nonlinear $\mathcal{H}_\infty$ control.

Both performance measures involve a measure of the "smallness" of the quadratic quantity

$$\phi(t) = \begin{bmatrix} \mathbf{w}^T(t) & \mathbf{u}^T(t) & a_g(t) \end{bmatrix} \begin{bmatrix} \mathbf{Q} & \mathbf{S} & \mathbf{Q}_a \\ \mathbf{S}^T & \mathbf{R} & \mathbf{S}_a \\ \mathbf{Q}_a^T & \mathbf{S}_a^T & R_a \end{bmatrix} \begin{bmatrix} \mathbf{w}(t) \\ \mathbf{u}(t) \\ a_g(t) \end{bmatrix} \tag{6.48}$$

However, it is necessary that this measure be treated differently for the two cases.

Case 1: Controller Designs for Stochastic Excitation

Consider the case where a_g is white noise with intensity Φ_a. For this case, controllers are sought which yield a low expectation for ϕ. However, ϕ must first be modified such that this problem is well-posed.

It will be assumed that the feedback controller does not contain feed-through terms for a_g (i.e. that $\mathbf{u}(t)$ and $a_g(t)$ are uncorrelated at time t). Consequently, the following expectations are true for stationary excitation:

$$E\left[\mathbf{u}a_g\right]=\mathbf{0} \quad , \quad E\left[\mathbf{w}a_g\right]=\mathbf{0} \quad , \quad E\left[a_g^2\right]\rightarrow\infty \tag{6.49}$$

The fact that $E[a_g^2] = \infty$ implies that the design of controllers for the minimization of $E[\phi]$ is an ill-posed problem for $R_a \neq 0$. But consider that, because $a_g(t)$ is uncorrelated with $\mathbf{u}(t)$ and $\mathbf{w}(t)$, the a_g terms are effectively decoupled from the $\mathbf{u}$ and $\mathbf{w}$ terms in the expectation of Eq. (6.48). The quadratic terms involving $\mathbf{Q}_a$, $\mathbf{S}_a$, and R_a may therefore be ignored in the synthesis of the controller, because they do not influence the controller parameters. Thus, controllers are sought which yield good performance based on the metric

$$J=E\left[\bar{\phi}\right]=E\left\{\begin{bmatrix}\mathbf{w}^T & \mathbf{u}^T\end{bmatrix}\begin{bmatrix}\mathbf{Q} & \mathbf{S}\\ \mathbf{S}^T & \mathbf{R}\end{bmatrix}\begin{bmatrix}\mathbf{w}\\ \mathbf{u}\end{bmatrix}\right\} \tag{6.50}$$

It will be shown that Damping-Reference stochastic (DR-S) controllers yield an upper bound on performance of the form

$$J \leq v_a \Phi_a \tag{6.51}$$

where v_a is a function of the controller parameters. Furthermore, it will be shown that v_a can be optimized over the set of all DR-S controllers, to tighten the bound above.

Case 2: Controller Designs for Deterministic Excitation

In this case, the measure of performance is simply an extension of the performance measure from Section 6.1; i.e.

$$J\left(\mathbf{w}_0, a_g\right)=\int_0^\infty \phi\left(t\right)dt \tag{6.52}$$

For this case, DR controllers will be designed which yield a worst-case upper bound on performance of the form

$$J\left(\mathbf{w}_0, a_g\right) \le \mathbf{w}_0^T \mathbf{P}_U \mathbf{w}_0 + v_a \int_0^\infty a_g^2\left(t\right) dt \tag{6.53}$$

Because this problem is essentially a simple nonlinear application of $\mathcal{H}_\infty$ methods, these controllers will be called DR-$\mathcal{H}_\infty$ controllers. The optimization of v_a over all DR-$\mathcal{H}_\infty$ controllers remains an item for future work.

Stochastic vs. Deterministic Design

DR-$\mathcal{H}_\infty$ controllers are appealing because they provide a simple quadratic upper bound on the worst-case performance in forced excitation. However, the acceleration input producing this worst-case scenario may not be very probable. For instance, earthquake excitations are almost invariably broadband signals which resemble filtered noise, with time-varying filter parameters. Thus, as with linear systems, $\mathcal{H}_\infty$-based designs may produce overly-conservative controllers. Consequently, they may yield less-favorable performance "on average," as compared with stochastic controllers.

On the other hand, stochastic controller designs have the opposite problem. By assigning controllers based only on the *expected* value of ϕ in stationary response, there is no explicit attention given to the size of the tails of the distribution of ϕ. Thus, some controllers which yield favorable values for $E[\phi]$ may yield unfavorable higher moments in the response distribution. In some applications, this may not be an issue. However, in the design of controllers for structural engineering, where the focus is on reducing the probability of failure, the tails of the distribution for ϕ may be of great importance, and DR-S controllers are not well-equipped to handle this.

6.2.1: Clipped-Linear Stochastic Control

In this section, the performance of controllers is measured by Eq. (6.50). The development of the Clipped-Linear control law for the stochastic case closely mirrors that of the free-vibration case. Thus, the equations below are analogous to Eqs. (6.4) through (6.13).

Define

$$\mathbf{\Phi}_u = E\left[\mathbf{u}\mathbf{u}^T\right] \quad , \quad \mathbf{\Phi}_{uw} = E\left[\mathbf{u}\mathbf{w}^T\right] \quad , \quad \mathbf{\Phi}_w = E\left[\mathbf{w}\mathbf{w}^T\right] \tag{6.54}$$

Then stationary excitation implies that

$$\mathbf{A}\mathbf{\Phi}_w + \mathbf{\Phi}_w\mathbf{A}^T + \mathbf{B}_u\mathbf{\Phi}_{uw} + \mathbf{\Phi}_{uw}^T\mathbf{B}_u^T + \mathbf{B}_a\mathbf{B}_a^T\Phi_a = \mathbf{0} \tag{6.55}$$

and the optimization of Eq. (6.50) is equivalent to the minimization of

$$J = tr\left\{\mathbf{Q}\mathbf{\Phi}_w + 2\mathbf{S}\mathbf{\Phi}_{uw} + \mathbf{R}\mathbf{\Phi}_u\right\} \tag{6.56}$$

Let arbitrary matrix $\mathbf{K}$ be such that $\mathbf{A}+\mathbf{B}_u\mathbf{K}$ is stable, and let $\mathbf{P}$ be related to $\mathbf{K}$ by Eq. (6.8), repeated here as

$$\mathbf{0} = \left(\mathbf{A}+\mathbf{B}_u\mathbf{K}\right)^T\mathbf{P} + \mathbf{P}\left(\mathbf{A}+\mathbf{B}_u\mathbf{K}\right) + \left(\mathbf{Q}+\mathbf{K}^T\mathbf{S}^T + \mathbf{S}\mathbf{K} + \mathbf{K}^T\mathbf{R}\mathbf{K}\right) \tag{6.57}$$

It follows that

$$0 = tr\left\{\mathbf{\Phi}_w\left(\mathbf{A}+\mathbf{B}_u\mathbf{K}\right)^T\mathbf{P} + \mathbf{P}\left(\mathbf{A}+\mathbf{B}_u\mathbf{K}\right)\mathbf{\Phi}_w + \left(\mathbf{Q}+\mathbf{K}^T\mathbf{S}^T + \mathbf{S}\mathbf{K} + \mathbf{K}^T\mathbf{R}\mathbf{K}\right)\mathbf{\Phi}_w\right\} \tag{6.58}$$

Combining Eqs. (6.58) and (6.55) gives

$$0 = tr\left\{\mathbf{P}\mathbf{B}_u\mathbf{\Phi}_{uw} + \mathbf{\Phi}_{uw}^T\mathbf{B}_u^T\mathbf{P} + \mathbf{P}\mathbf{B}_a\mathbf{B}_a^T\Phi_a - \mathbf{\Phi}_w\mathbf{K}^T\mathbf{B}_u^T\mathbf{P} - \mathbf{P}\mathbf{B}_u\mathbf{K}\mathbf{\Phi}_w - \mathbf{\Phi}_w\left(\mathbf{Q}+\mathbf{K}^T\mathbf{S}^T + \mathbf{S}\mathbf{K} + \mathbf{K}^T\mathbf{R}\mathbf{K}\right)\right\} \tag{6.59}$$

which is equivalent to

$$J = E\left\|\mathbf{u} - \mathbf{K}_{CL}\left(\mathbf{P}\right)\mathbf{w}\right\|_{\mathbf{R}}^2 - E\left\|\mathbf{K}\mathbf{w} - \mathbf{K}_{CL}\left(\mathbf{P}\right)\mathbf{w}\right\|_{\mathbf{R}}^2 + \mathbf{B}_a^T\mathbf{P}\mathbf{B}_a\Phi_a \tag{6.60}$$

where $\mathbf{K}_{CL}(\mathbf{P})$ is defined as in Eq. (6.12), repeated here as

$$\mathbf{K}_{CL}\left(\mathbf{P}\right) = -\mathbf{R}^{-1}\left[\mathbf{B}_u^T\mathbf{P} + \mathbf{S}^T\right] \tag{6.61}$$

The generalized Clipped-Linear stochastic (CL-S) controller attempts to make the first norm in Eq. (6.60) small through point-by-point minimization in time, resulting in the same control law as in Eq. (6.13), repeated here as

$$\mathbf{u}\left(t\right) = \underset{\tilde{\mathbf{u}}\in\mathcal{U}\left(\mathbf{w}(t)\right)}{\arg\min}\left\|\tilde{\mathbf{u}} - \mathbf{K}_{CL}\left(\mathbf{P}\right)\mathbf{w}\left(t\right)\right\|_{\mathbf{R}} \tag{6.62}$$

Thus, for a given choice of $\mathbf{K}$, the CL control laws for the impulse response and stochastic forced response case are the same. There is also an equivalence for Clipped-Optimal and Damping Reference control methods in these two cases as well, as discussed below.

Clipped-Optimal Stochastic Control

Consider the case where **u** is unconstrained and where $\mathbf{K}=\mathbf{K}_{CL}(\mathbf{P})$, giving rise to the same Riccati equation in Eq. (6.18) with solution $\mathbf{P} = \mathbf{P}_o$. As with the free-vibration case, Eq. (6.60) would be minimized uniquely through the assignation $\mathbf{u}=\mathbf{K}_{CL}(\mathbf{P}_o)\mathbf{w}$, giving the full-information optimal unconstrained stochastic controller.

Now, consider the case where **u** is constrained such that $\mathbf{u}(t)\in\mathcal{U}(\mathbf{w}(t))$. If the CL-S control law is implemented with $\mathbf{P} = \mathbf{P}_o$ then Eq. (6.60) yields a lower bound on the expected performance; i.e.

$$J = E\left\|\mathbf{u} - \mathbf{K}_{CL}\left(\mathbf{P}_o\right)\mathbf{w}\right\|_{\mathbf{R}}^2 + \mathbf{B}_a^T\mathbf{P}_o\mathbf{B}_a\Phi_a \tag{6.63}$$

As with the free-vibration case, it is in general difficult to find a closed-form upper bound for the norm in the above expression.

Damping Reference Stochastic Control

As in the free-vibration case, if the CL-S control law is implemented with **K** assigned as in Eq. (6.22) with **Z** chosen such that **Kw** is guaranteed to be feasible and with $\mathbf{P} = \mathbf{P}_z$ as found from Eq. (6.23), then the inequality

$$\left\|\mathbf{u}(t) - \mathbf{K}_{CL}\left(\mathbf{P}_z\right)\mathbf{w}(t)\right\|_{\mathbf{R}}^2 \le \left\|\mathbf{K}_z\mathbf{w}(t) - \mathbf{K}_{CL}\left(\mathbf{P}_z\right)\mathbf{w}(t)\right\|_{\mathbf{R}}^2 \tag{6.64}$$

holds at all times. Consequently, taking the expectation of both sides and inserting in Eq. (6.60), it follows that

$$J \le \mathbf{B}_a^T\mathbf{P}_z\mathbf{B}_a\Phi_a \tag{6.65}$$

So the DR-S control provides a quadratic upper bound on the expected performance in stationary excitation. In reference to Eq. (6.51), $v_a = \mathbf{B}_a^T\mathbf{P}\mathbf{B}_a$.

As with the free-vibration DR controller, **Z** can be optimized to tighten the bound in Eq. (6.65); i.e. to minimize $\mathbf{B}_a^T\mathbf{P}_z\mathbf{B}_a$. This minimization is identical to the optimization process discussed in Section 6.1.4, as well as in Chapter 5. In fact, the upper bound in Eq. (6.65) is identical to the stochastic performance for a constant **Z** matrix, as studied in the examples of Chapter 5. Thus, this control synthesis guarantees improvement over the constant-**Z** solutions, in stationary response.

Conclusions

It is a well-known fact that for linear controllers, there is a duality between their impulsive and stochastic behavior. From the above analysis it is clear that this duality extends to the performance bounds of CL controllers. Furthermore, it is clear that the optimal **Z** matrices for the DR impulsive and stochastic controllers are identical.

6.2.2: Clipped-Linear $\mathcal{H}_\infty$ Control

Now, consider the measure of performance in Eq. (6.52). For any **P**>0, it is true that

$$\mathbf{w}_0^T\mathbf{P}\mathbf{w}_0 = -\int_0^\infty \left\{\mathbf{w}^T(\tau)\left[\mathbf{A}^T\mathbf{P}+\mathbf{P}\mathbf{A}\right]\mathbf{w}(\tau) + 2\mathbf{w}^T(\tau)\mathbf{P}\mathbf{B}_u\mathbf{u}(\tau) + 2\mathbf{w}^T(\tau)\mathbf{P}\mathbf{B}_a a_g(\tau)\right\} d\tau \quad (6.66)$$

along any stable $\{\mathbf{w},\mathbf{u},a_g\}$ trajectory. Subtracting Eq. (6.66) form Eq. (6.52) gives

$$\begin{aligned} J(\mathbf{w}_0, a_g) &= \mathbf{w}_0^T\mathbf{P}\mathbf{w}_0 \\ &+\int_0^\infty \begin{bmatrix}\mathbf{w}^T(\tau) & \mathbf{u}^T(\tau) & a_g(\tau)\end{bmatrix}\begin{bmatrix}\mathbf{Q}+\mathbf{A}^T\mathbf{P}+\mathbf{P}\mathbf{A} & \mathbf{P}\mathbf{B}_u+\mathbf{S} & \mathbf{P}\mathbf{B}_a+\mathbf{Q}_a \\ \mathbf{S}^T+\mathbf{B}_u^T\mathbf{P} & \mathbf{R} & \mathbf{S}_a \\ \mathbf{Q}_a^T+\mathbf{B}_a^T\mathbf{P} & \mathbf{S}_a^T & R_a\end{bmatrix}\begin{bmatrix}\mathbf{w}(\tau) \\ \mathbf{u}(\tau) \\ a_g(\tau)\end{bmatrix} d\tau \end{aligned} \quad (6.67)$$

Define $\mathbf{K}_{CL}$ and $\mathbf{K}_{CLa}$ as

$$\mathbf{K}_{CL}(\mathbf{P}) = -\mathbf{R}^{-1}\left[\mathbf{B}_u^T\mathbf{P}+\mathbf{S}^T\right] \quad (6.68)$$

$$\mathbf{K}_{CLa} = -\mathbf{R}^{-1}\mathbf{S}_a \quad (6.69)$$

Then Eq. (6.67) can be expressed as

$$\begin{aligned} J(\mathbf{w}_0, a_g) = \mathbf{w}_0^T\mathbf{P}\mathbf{w}_0 + \int_0^\infty \Big\{ & \mathbf{w}^T(\tau)\left[\mathbf{Q}+\mathbf{A}^T\mathbf{P}+\mathbf{P}\mathbf{A}\right]\mathbf{w}(\tau) \\ & + 2\mathbf{w}^T(\tau)\left[\mathbf{P}\mathbf{B}_a+\mathbf{Q}_a\right]a_g(\tau) + R_a a_g^2(\tau) \\ & + \left\|\mathbf{u}(\tau)-\mathbf{K}_{CL}(\mathbf{P})\mathbf{w}(\tau)-\mathbf{K}_{CLa}a_g(\tau)\right\|_{\mathbf{R}}^2 \\ & - \left\|\mathbf{K}_{CL}(\mathbf{P})\mathbf{w}(\tau)+\mathbf{K}_{CLa}a_g(\tau)\right\|_{\mathbf{R}}^2 \Big\} d\tau \end{aligned} \quad (6.70)$$

For arbitrary **K** and $\mathbf{K}_a$ with $\mathbf{A}+\mathbf{B}_u\mathbf{K}$ stable, Eq. (6.70) is equivalent to

$$J\left(\mathbf{w}_0, a_g\right) = \mathbf{w}_0^T \mathbf{P} \mathbf{w}_0 + \int_0^\infty \left\{ \begin{bmatrix} \mathbf{w}^T(\tau) & a_g(\tau) \end{bmatrix} \begin{bmatrix} \tilde{\mathbf{Q}}_{11} & \tilde{\mathbf{Q}}_{12} \\ \tilde{\mathbf{Q}}_{12}^T & \tilde{Q}_{22} \end{bmatrix} \begin{bmatrix} \mathbf{w}(\tau) \\ a_g(\tau) \end{bmatrix} \right.$$
$$+ \left\| \mathbf{u}(\tau) - \mathbf{K}_{CL}(\mathbf{P})\mathbf{w}(\tau) - \mathbf{K}_{CLa} a_g(\tau) \right\|_{\mathbf{R}}^2 \tag{6.71}$$
$$\left. - \left\| \left(\mathbf{K} - \mathbf{K}_{CL}(\mathbf{P})\right)\mathbf{w}(\tau) + \left(\mathbf{K}_a - \mathbf{K}_{CLa}\right) a_g(\tau) \right\|_{\mathbf{R}}^2 \right\} d\tau$$

where

$$\tilde{\mathbf{Q}}_{11} = \left(\mathbf{A} + \mathbf{B}_u \mathbf{K}\right)^T \mathbf{P} + \mathbf{P}\left(\mathbf{A} + \mathbf{B}_u \mathbf{K}\right) + \left(\mathbf{Q} + \mathbf{K}^T \mathbf{S}^T + \mathbf{S}\mathbf{K} + \mathbf{K}^T \mathbf{R}\mathbf{K}\right) \tag{6.72a}$$

$$\tilde{\mathbf{Q}}_{12} = \left(\mathbf{K}^T \mathbf{R}\mathbf{K}_a + \mathbf{K}^T \mathbf{S}_a + \mathbf{S}\mathbf{K}_a + \mathbf{Q}_a\right) + \mathbf{P}\left(\mathbf{B}_u \mathbf{K}_a + \mathbf{B}_a\right) \tag{6.72b}$$

$$\tilde{Q}_{22} = R_a + \mathbf{K}_a^T \mathbf{R}\mathbf{K}_a + \mathbf{K}_a^T \mathbf{S}_a + \mathbf{S}_a^T \mathbf{K}_a \tag{6.72c}$$

If $\mathbf{u}$ is chosen so as to instantaneously minimize the integrand in Eq. (6.71), the result is the Clipped-Linear control law for forced vibration, given as

$$\mathbf{u}(t) = \underset{\tilde{\mathbf{u}} \in \mathcal{U}(\mathbf{w}(t))}{\arg\min} \left\| \tilde{\mathbf{u}} - \mathbf{K}_{CL}(\mathbf{P})\mathbf{w}(t) - \mathbf{K}_{CLa} a_g(t) \right\|_{\mathbf{R}}^2 \tag{6.73}$$

The CL control law above is the same as that for the free-vibration case except that it contains an additional term in the norm which is proportional to the input a_g. This feed-forward term represents an instantaneous opposition to a_g by the controller. As with the free-vibration case, different choices of $\mathbf{K}$ (along with $\mathbf{K}_a$) will result in different closed-loop behavior.

Combining Eqs. (6.71) and (6.73) gives J as

$$J\left(\mathbf{w}_0, a_g\right) = \mathbf{w}_0^T \mathbf{P} \mathbf{w}_0 + \int_0^\infty \left\{ \begin{bmatrix} \mathbf{w}^T(\tau) & a_g(\tau) \end{bmatrix} \begin{bmatrix} \tilde{\mathbf{Q}}_{11} & \tilde{\mathbf{Q}}_{12} \\ \tilde{\mathbf{Q}}_{12}^T & \tilde{Q}_{22} \end{bmatrix} \begin{bmatrix} \mathbf{w}(\tau) \\ a_g(\tau) \end{bmatrix} \right.$$
$$+ \min_{\tilde{\mathbf{u}} \in \mathcal{U}(\mathbf{w}(\tau))} \left\| \tilde{\mathbf{u}} - \mathbf{K}_{CL}(\mathbf{P})\mathbf{w}(\tau) - \mathbf{K}_{CLa} a_g(\tau) \right\|_{\mathbf{R}}^2 \tag{6.74}$$
$$\left. - \left\| \left(\mathbf{K} - \mathbf{K}_{CL}(\mathbf{P})\right)\mathbf{w}(\tau) + \left(\mathbf{K}_a - \mathbf{K}_{CLa}\right) a_g(\tau) \right\|_{\mathbf{R}}^2 \right\} d\tau$$

We are interested in designing the controller parameters (i.e. $\mathbf{K}$ and $\mathbf{K}_a$) such that the above has an upper bound which is a function only of $\mathbf{w}_0$ and a_g, as in Eq. (6.53).

To do this, first consider that if $\mathbf{P}$ is chosen such that

$$\tilde{\mathbf{Q}}_{11} = -\gamma^{-2} \tilde{\mathbf{Q}}_{12} \tilde{\mathbf{Q}}_{12}^T \tag{6.75}$$

for some $\gamma > 0$, then Eq. (6.74) becomes

$$J\left(\mathbf{w}_0,a_g\right)=\mathbf{w}_0^T\mathbf{P}\mathbf{w}_0+\int_0^\infty\Big\{-\left\|\gamma^{-1}\tilde{\mathbf{Q}}_{12}^T\mathbf{w}(\tau)-\gamma a_g(\tau)\right\|_2^2+\left(\tilde{Q}_{22}+\gamma^2\right)a_g^2(\tau)$$
$$+\min_{\tilde{\mathbf{u}}\in\mathcal{U}(\mathbf{w}(\tau))}\left\|\tilde{\mathbf{u}}-\mathbf{K}_{CL}(\mathbf{P})\mathbf{w}(\tau)-\mathbf{K}_{CLa}a_g(\tau)\right\|_{\mathbf{R}}^2 \tag{6.76}$$
$$-\left\|\left(\mathbf{K}-\mathbf{K}_{CL}(\mathbf{P})\right)\mathbf{w}(\tau)+\left(\mathbf{K}_a-\mathbf{K}_{CLa}\right)a_g(\tau)\right\|_{\mathbf{R}}^2\Big\}d\tau$$

Because the first term is negative-semidefinite, J has the upper bound

$$J\left(\mathbf{w}_0,a_g\right)\le\mathbf{w}_0^T\mathbf{P}\mathbf{w}_0+\int_0^\infty\Big\{\left(\tilde{Q}_{22}+\gamma^2\right)a_g^2(\tau)$$
$$+\min_{\tilde{\mathbf{u}}\in\mathcal{U}(\mathbf{w}(\tau))}\left\|\tilde{\mathbf{u}}-\mathbf{K}_{CL}(\mathbf{P})\mathbf{w}(\tau)-\mathbf{K}_{CLa}a_g(\tau)\right\|_{\mathbf{R}}^2 \tag{6.77}$$
$$-\left\|\left(\mathbf{K}-\mathbf{K}_{CL}(\mathbf{P})\right)\mathbf{w}(\tau)+\left(\mathbf{K}_a-\mathbf{K}_{CLa}\right)a_g(\tau)\right\|_{\mathbf{R}}^2\Big\}d\tau$$

To convert Eq. (6.77) into the form of Eq. (6.53), it is necessary that $\mathbf{K}$ be chosen such that

$$\min_{\tilde{\mathbf{u}}\in\mathcal{U}(\mathbf{w}(t))}\left\|\tilde{\mathbf{u}}-\mathbf{K}_{CL}(\mathbf{P})\mathbf{w}(t)-\mathbf{K}_{CLa}a_g(t)\right\|_{\mathbf{R}}^2\le\left\|\left(\mathbf{K}-\mathbf{K}_{CL}(\mathbf{P})\right)\mathbf{w}(t)-\left(\mathbf{K}_a-\mathbf{K}_{CLa}\right)a_g(t)\right\|_{\mathbf{R}}^2 \tag{6.78}$$

Through a similar process to that described in Section 6.1.4, DR-$\mathcal{H}_\infty$ controllers may be constructed which yield the inequality in Eq. (6.78), assuming that constraint (6.5b) is not violated.

Supposing again that constraint (6.5b) can be taken for granted, let $\mathbf{K}$ and $\mathbf{K}_a$ be

$$\mathbf{K}=-\mathbf{Z}\mathbf{B}_u^T\quad,\quad\bar{\sigma}\left(\mathbf{Z}-\tfrac{1}{2}\mathbf{I}\right)\le\tfrac{1}{2} \tag{6.79a}$$

$$\mathbf{K}_a=\mathbf{0} \tag{6.79b}$$

Then $\mathbf{K}\mathbf{w}(t)+\mathbf{K}_a a_g(t)\in\mathcal{U}(\mathbf{w}(t))$ for all t. In this circumstance, Eq. (6.82) may be used to find the $\mathbf{P}$ corresponding to Eq. (6.79). Specifically, the equation for this value of $\mathbf{P}$, which will be called $\mathbf{P}_z$, is

$$\begin{aligned}\mathbf{0}=&\left[\mathbf{Q}+\gamma^{-2}\mathbf{Q}_a\mathbf{Q}_a^T\right]-\mathbf{B}_u\mathbf{Z}^T\left[\mathbf{S}^T+\gamma^{-2}\mathbf{S}_a\mathbf{Q}_a^T\right]-\left[\mathbf{S}+\gamma^{-2}\mathbf{Q}_a\mathbf{S}_a^T\right]\mathbf{Z}\mathbf{B}_u^T+\mathbf{B}_u\mathbf{Z}^T\left[\mathbf{R}+\gamma^{-2}\mathbf{S}_a\mathbf{S}_a^T\right]\mathbf{Z}\mathbf{B}_u^T\\&+\left\{\left[\mathbf{A}+\gamma^{-2}\mathbf{B}_a\mathbf{Q}_a^T\right]-\left[\mathbf{B}_u+\gamma^{-2}\mathbf{B}_a\mathbf{S}_a^T\right]\mathbf{Z}\mathbf{B}_u^T\right\}^T\mathbf{P}_z\\&+\mathbf{P}_z\left\{\left[\mathbf{A}+\gamma^{-2}\mathbf{B}_a\mathbf{Q}_a^T\right]-\left[\mathbf{B}_u+\gamma^{-2}\mathbf{B}_a\mathbf{S}_a^T\right]\mathbf{Z}\mathbf{B}_u^T\right\}\\&+\mathbf{P}_z\left[\gamma^{-2}\mathbf{B}_a\mathbf{B}_a^T\right]\mathbf{P}_z\end{aligned} \tag{6.80}$$

If the CL control law is implemented, then this implies that

$$J\left(\mathbf{w}_0, a_g\right) \le \mathbf{w}_0^T \mathbf{P}_z \mathbf{w}_0 + \left(R_a + \gamma^2\right) \int_0^\infty a_g^2(\tau) d\tau \tag{6.81}$$

Thus, the DR-$\mathcal{H}_\infty$ controller ensures a worst-case upper bound on J, as a function only of $\mathbf{w}_0$ and the norm of a_g. In this sense, it yields a kind of robust performance. Referring to Eq. (6.53), we have the desired performance bounds, with $\mathbf{P}_U = \mathbf{P}_z$, and $v_a = R_a + \gamma^2$.

Optimizing γ, given Z

Consider the case where $\mathbf{w}_0 = \mathbf{0}$. In this circumstance, Eq. (6.81) is only an expression of a_g, and γ reflects the magnification of a_g in the upper bound. As γ is decreased this bound is tightened However, γ cannot be assigned to be arbitrarily small. Rather, a minimum $\gamma = \gamma_{opt}$ exists for which Eq. (6.75) has a solution $\mathbf{P}$ for which $\mathbf{P} = \mathbf{P}^T > 0$.

Eq. (6.75) can be expanded to give the algebraic Riccati equation

$$\left(\tilde{\mathbf{Q}} + \gamma^{-2}\tilde{\mathbf{K}}\tilde{\mathbf{K}}^T\right) + \left(\tilde{\mathbf{A}} + \gamma^{-2}\tilde{\mathbf{B}}\tilde{\mathbf{K}}^T\right)^T \mathbf{P} + \mathbf{P}\left(\tilde{\mathbf{A}} + \gamma^{-2}\tilde{\mathbf{B}}\tilde{\mathbf{K}}^T\right) + \mathbf{P}\left(\gamma^{-2}\tilde{\mathbf{B}}\tilde{\mathbf{B}}^T\right)\mathbf{P} = \mathbf{0} \tag{6.82}$$

where

$$\tilde{\mathbf{Q}} = \mathbf{Q} + \mathbf{K}^T\mathbf{S}^T + \mathbf{S}\mathbf{K} + \mathbf{K}^T\mathbf{R}\mathbf{K} \quad , \quad \tilde{\mathbf{A}} = \mathbf{A} + \mathbf{B}_u\mathbf{K}$$

$$\tilde{\mathbf{K}} = \mathbf{K}^T\mathbf{R}\mathbf{K}_a + \mathbf{K}^T\mathbf{S}_a + \mathbf{S}\mathbf{K}_a + \mathbf{Q}_a \quad , \quad \tilde{\mathbf{B}} = \mathbf{B}_u\mathbf{K}_a + \mathbf{B}_a$$

One of the many results of the Bounded-Real Lemma (Green and Limebeer 1995) is that Eq. (6.82) has a solution $\mathbf{P} = \mathbf{P}^T > 0$ if and only if the matrix

$$H = \begin{bmatrix} \tilde{\mathbf{A}} & \mathbf{0} \\ -\tilde{\mathbf{Q}} & -\tilde{\mathbf{A}}^T \end{bmatrix} + \gamma^{-2} \begin{bmatrix} \tilde{\mathbf{B}} \\ -\tilde{\mathbf{K}} \end{bmatrix} \begin{bmatrix} \tilde{\mathbf{K}}^T & \tilde{\mathbf{B}}^T \end{bmatrix} \tag{6.83}$$

has no eigenvalues on the imaginary axis. It is worth noting a few traits of H. However, the discussion will be kept brief and qualitative.

The matrix H has the Hamiltonian property, such that if λ is an eigenvalue then so is $-\lambda^*$. Thus, the eigenvalues of H are symmetric across the imaginary axis in the complex plane. It is instructive to think about the loci formed by the paths of these eigenvalues in the complex plane, as γ is varied. Note that the first matrix in the summation, on its own, has negative-real eigenvalues if $\tilde{\mathbf{A}}$ is stable. But the second matrix in the summation has nonzero eigenvalues equal to those of $\tilde{\mathbf{K}}^T\tilde{\mathbf{B}} - \tilde{\mathbf{B}}^T\tilde{\mathbf{K}}$; a skew-symmetric matrix. Thus, the second term has purely imaginary eigenvalues. It follows that as the value of γ is decreased there will come a point

where the corresponding loci of eigenvalues for H will reach the imaginary axis. The critical value of γ at this point is the minimum γ for which a solution exists. Thus, there is an optimal γ_{opt} for which Eq. (6.75) is a valid expression for $\mathbf{P}=\mathbf{P}^T>0$, and therefore an optimal (i.e. minimal) amplification of a_g in Eq. (6.77), resulting in a minimally-conservative approximation for J. This optimal value may be found through a standard numerical root-finding algorithm, such as the bisection algorithm.

***Optimizing γ and* Z**

A lingering issue is the optimization of **Z**. The above development was for general feasible **Z**. But clearly some choices for **Z** will yield lower values of γ_{opt} than others. There is therefore some benefit to finding the **Z** for which γ_{opt} is minimum. The DR-$\mathcal{H}_\infty$ controller, implemented with $\mathbf{Z}=\mathbf{Z}_{opt}$, could therefore yield the tightest quadratic performance bound. The optimization of **Z** is a problem requiring further work, and is currently being investigated in an LMI framework.

Clipped-Optimal $\mathcal{H}_\infty$ Control?

In the impulse and stochastic response cases, CO controllers were presented. As a final thought on $\mathcal{H}_\infty$ methods, we consider the question of whether a useful analogy exists for CO-$\mathcal{H}_\infty$ control. It general, the answer is "no." The usefulness of $\mathcal{H}_\infty$ methods lies in the worst-case upper bound for the gain of a closed-loop system, and CO-$\mathcal{H}_\infty$ methods cannot ensure any worst-case upper bound. Thus, the main appeal of $\mathcal{H}_\infty$ methods is lost when the clipping action is imposed on the linear active $\mathcal{H}_\infty$ control law.

6.2.3: Stochastic Forced Response Examples

The structural system studied in the examples in Section 6.1.6 was subjected to an impulsive acceleration. In this example, we examine the same system subjected to a stationary white-noise excitation. For this excitation, a_g will be assumed to have intensity $\Phi_a = 10^{-4}$ m^2/s^3. This intensity is small enough that in stationary response, for all controllers, constraint (6.5b) is seldom violated, because constraint (6.5a) is dominant. Thus, as for the free-vibration example, constraint (6.5b) can be ignored.

As in section 6.1.6, two examples will be presented, corresponding to drift and acceleration reduction. For both examples, simulations were conducted which calculate the

stationary response of the nominal system to uncorrelated noise, with a time duration of 500s. From this data, distribution functions for system response quantities were approximated.

However, the most revealing analysis for the stationary response of these controllers lies in their spectral characteristics. Consider $\mathbf{y}(t)$, a vector function of the response described by

$$\mathbf{y}(t) = \mathbf{C}_y \mathbf{w}(t) + \mathbf{D}_{uy}\mathbf{u}(t) + \mathbf{D}_{ay} a_g(t) \tag{6.84}$$

With appropriate definitions of $\mathbf{C}_y$, $\mathbf{D}_{uy}$, and $\mathbf{D}_{ay}$, $\mathbf{y}(t)$ can be related to Eq. (6.48) through

$$\bar{\phi} = \mathbf{y}^T(t)\mathbf{y}(t) - \mathbf{D}_{ay}^T \mathbf{D}_{ay} a_g(t) \tag{6.85}$$

Let the power spectral density matrix of $\mathbf{y}$ be denoted $\mathbf{S}_{\mathbf{yy}}(\omega)$. Then it follows that for stochastic performance assessment,

$$E\left[\bar{\phi}\right] = \int_{-\infty}^{\infty} \left\{ tr\left(\mathbf{S}_{\mathbf{yy}}(\omega)\right) - \mathbf{D}_{ay}^T \mathbf{D}_{ay} \Phi_a \right\} d\omega \tag{6.86}$$

Thus, the optimization of Eq. (6.50) can be interpreted as an average reduction in the PSD of $\mathbf{y}$. This context turns out to be the most convenient for revealing the differences between different controllers.

The simulation data was used to approximate the PSD $\mathbf{S}_{\mathbf{yy}}$. This approximation was performed in MATLAB, through a built-in routine which employs Welch's averaged periodogram method.

For these examples, four feedback controllers are compared; DR-$\mathcal{H}_\infty$, DR-S, and CO-S, and CZ control. For the CZ and DR-S controllers, the $\mathbf{Z}$ matrix was optimized to minimize the bound in Eq. (6.65). For the DR-S controller, this optimized $\mathbf{Z}$ gives the corresponding $\mathbf{P}_z$ matrix through Eq. (6.23). With the $\mathbf{P}_z$ matrix found, the CL control law is fully parameterized for the DR-S controller. This same $\mathbf{Z}$ was used for the DR-$\mathcal{H}_\infty$ controller design. For this particular $\mathbf{Z}$, the optimal (i.e. minimum) γ was found and the corresponding $\mathbf{P}_z$ was found through Eq. (6.80). However the $\mathbf{Z}$ matrix itself was not optimized to yield a global minimum γ (i.e. over the set of admissible $\mathbf{Z}$). As mentioned, the reason for this is that the optimization of $\mathbf{Z}$ for the absolute minimization of γ is an item requiring further research. Note that, although the DR-$\mathcal{H}_\infty$ controller is not optimized, it does minimize the upper bound on performance *with reference to a given* $\mathbf{Z}$.

Example 1: Drift Reduction

Simulation data for $E[\bar{\phi}]$ is shown Table 6.3, for all controllers as well as the uncontrolled case. Corresponding distributions for $\bar{\phi}$ are shown in Fig. 6.22. Note that the CO-S and DR-S controllers perform very comparably, with a difference of about 1.5% in performance. The stochastic performance of the DR-$\mathcal{H}_\infty$ controller is much higher, but this is to be expected because the controller was optimized for an upper bound on worst-case, not stochastic, performance. For this example, all three of these controllers perform better than the constant-damping case.

Fig. 6.23 shows distributions for power flows P_1, P_2, as well as the distribution for the total power flow P_T, for the controllers. While these distributions are very close for the CO-S, DR-S, and DR-$\mathcal{H}_\infty$ cases, it is evident that the DR-$\mathcal{H}_\infty$ controller exhibits a great deal more power flow for the second actuator (the one corresponding to the mass driver on the top story). Also, note that the distribution for P_2 is skewed slightly to the left of the origin for the DR-$\mathcal{H}_\infty$ controller, indicating that on average, this actuator is removing energy from the structure. By contrast, the CO-S and DR-S distributions for P_2 are skewed slightly to the right, indicating that they are, on average, injecting energy into the structure.

The spectral densities for the controllers are shown in Fig. 6.24. First, consider the comparison of the DR-S and CO-S controllers. The CO-S controller tends to improve on the CZ case by reducing the spectral content of **y** for frequencies below the first mode. This comes at the expense of increased spectral content in the frequency range of the second and third mode. The DR-S controller, on the other hand, does better at suppressing the spectral content for the higher modes, but at the expense of larger spectral content below the first mode. The spectral content of the system response with the DR-$\mathcal{H}_\infty$ controller is reminiscent of linear $\mathcal{H}_\infty$ controllers. The controller does better at reducing the maximum frequency response of the entire spectrum, but does not yield favorable suppression uniformly. In particular, it leads to a pronounced increase in the spectral content near the higher mode, in comparison to the DR-S and CO-S controllers.

Table 6.3: Evaluations of $E[\bar{\phi}]$ for Various Controller Designs

	CO-S	DR-S	DR-$\mathcal{H}_\infty$	CD	No control
Ex. 1 ($\times 10^{-3}$)	1.34	1.35	1.50	1.51	57.6
Ex. 2 ($\times 10^{-3}$)	18.2	15.1	16.0	18.6	364

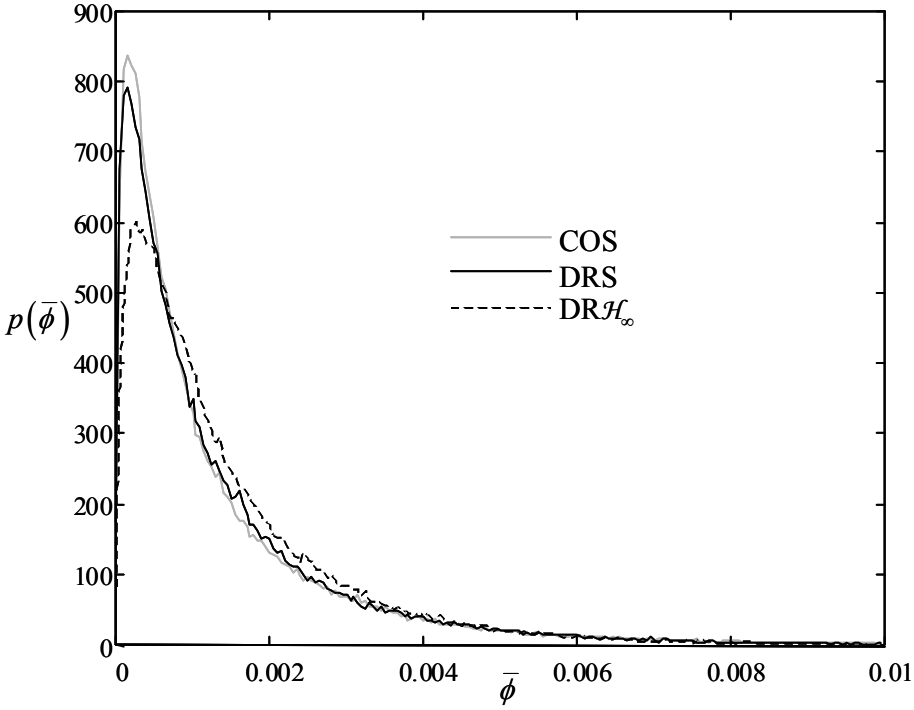

Figure 6.22: Distributions for $\bar{\phi}$ for Example 1

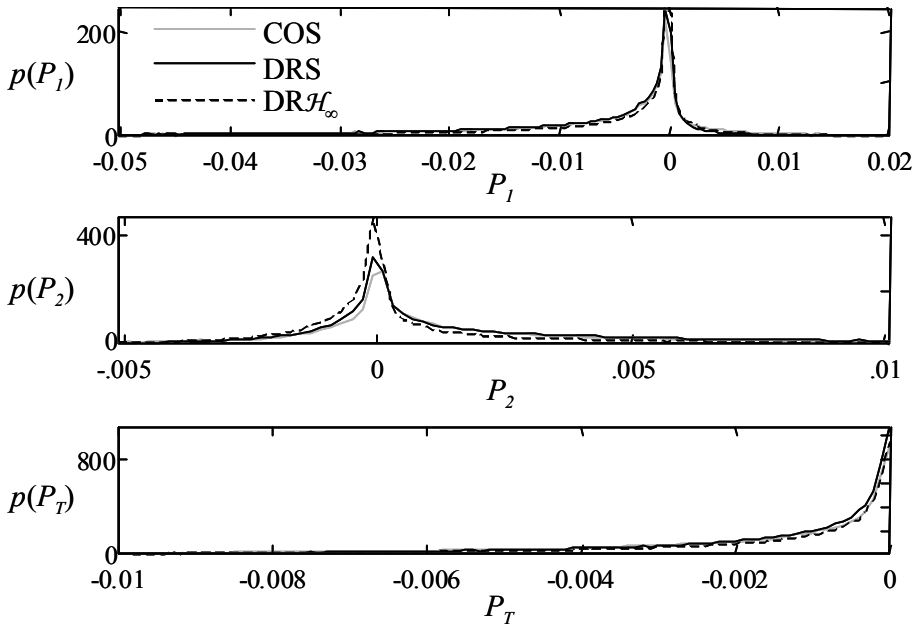

Figure 6.23: Distributions for power flow quantities for Example 1

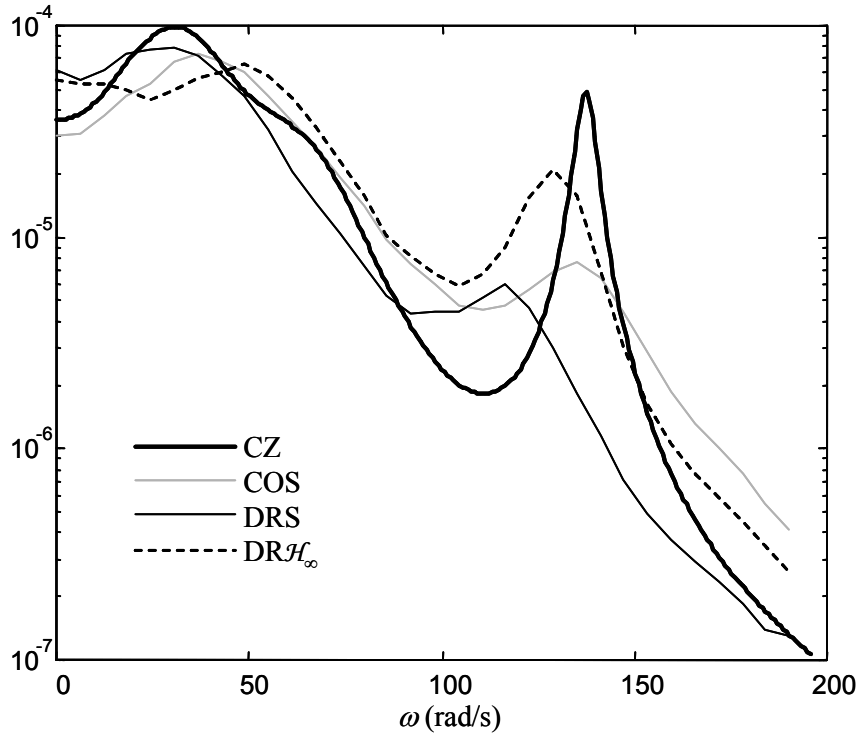

Figure 6.24: Spectral densities for Example 1

Example 2: Acceleration Reduction

Now, consider the case where mean-square accelerations are used as the performance measure. From Table 6.3 the DR-S controller out-performs the CO-S controller by about 20%. This is also illustrated in Fig. 6.25, which shows the performance distributions for the various controllers. It is interesting that these same controllers, in the impulse response case, yielded the opposite conclusions. The performance of the DR-$\mathcal{H}_\infty$ controller is above the DR-S, but well below the CO-S and CZ cases.

The power flow distributions, shown in Fig. 6.26, show that for all controllers, P_1 is skewed to the left, indicating that the actuator between the base and first story is extracting more energy from the structure than it is injecting. However P_2 is fairly even, indicating that on average, the actuator exciting the hybrid mass damper delivers just as much energy to the structure as it extracts. Thus, as in Example 1, the control systems all take advantage of the power-sharing nature of RFA networks.

The spectral density of **y**, shown in Fig. 6.27, provides more information concerning the discrepancy in the performances of the different controllers. In the first mode, the CO-S controller actually performs better than the other controllers. However its performance for the second and third modes is comparably poor, and this inadequacy at higher frequencies leads to

its unfavorable performance. These qualitative observations are harmonious with those made for the free-vibration case, where it was noted that for acceleration reduction, the CO-S controller yields responses with more significant high-frequency content. The spectral content of the DR-$\mathcal{H}_\infty$ controller yields a maximum response magnitude, near the first mode, which is higher than that of the DR-S controller. Clearly, this would not be the case for a linear system, because in that circumstance, the $\mathcal{H}_\infty$ controller should optimize this maximum response.

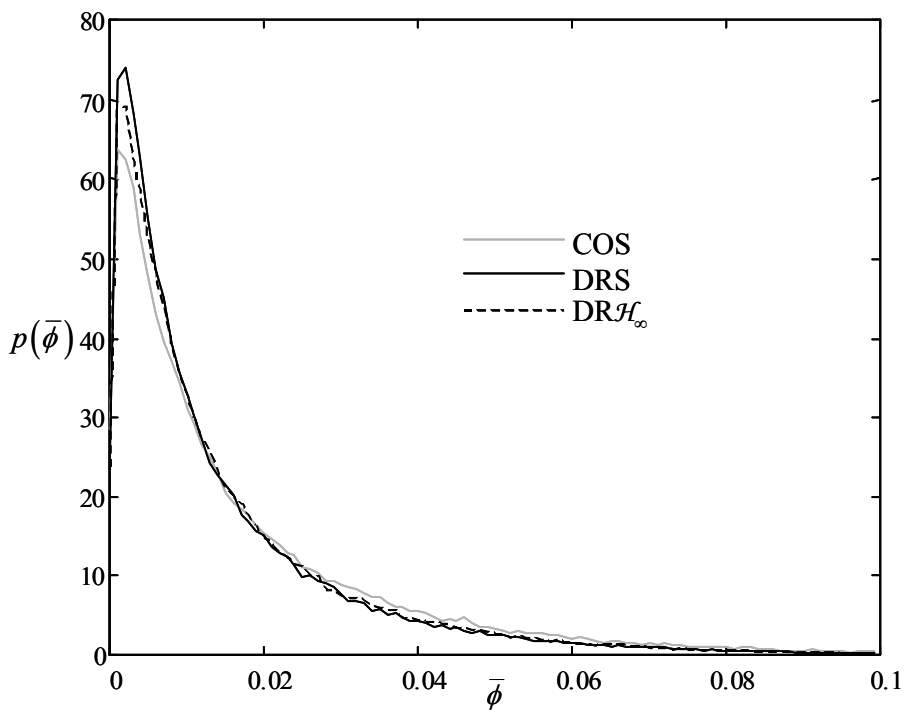

Figure 6.25: Distributions for $\bar{\phi}$ for Example 2

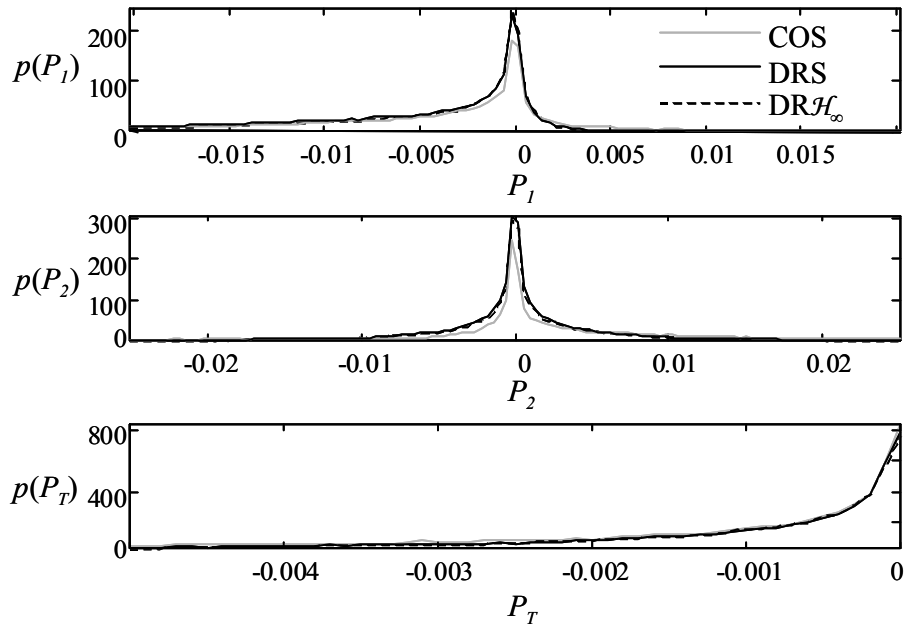

Figure 6.26: Distributions for power flow quantities for Example 2

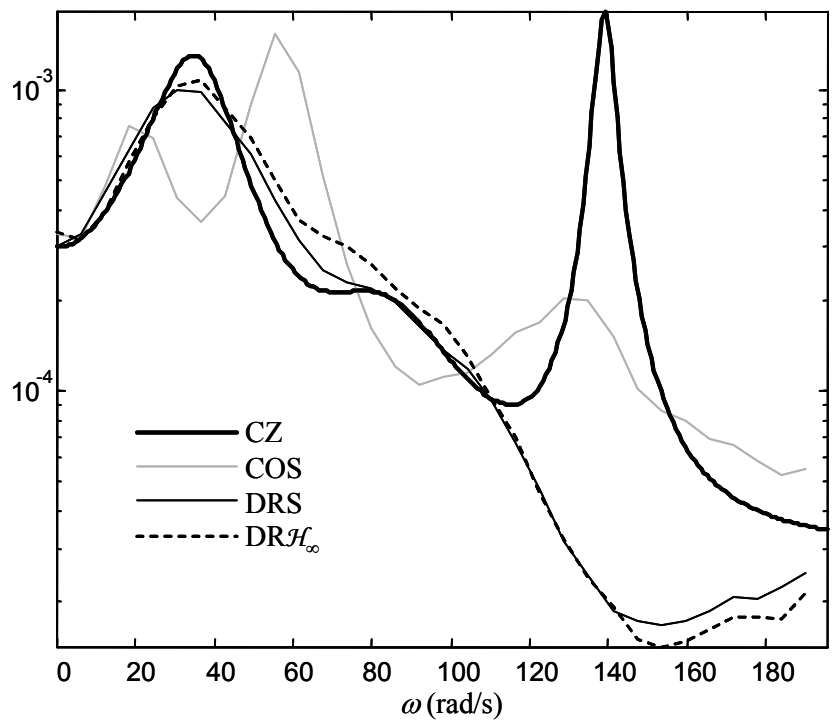

Figure 6.27: Spectral densities for Example 2

6.3: Further Comments

The research reported in this chapter had several motivations. Originally, the goal was simply to unify many of the methods of semiactive control system design under a common approach, and to extend them to accommodate the constraints of RFA networks. Clipped-Optimal and Damping-Reference controllers have both been studied elsewhere, in various equivalent forms, for semiactive systems. The general consensus is that they are both reasonable techniques for the design of simple controllers for energy-constrained systems. In the extension of these ideas to RFA networks, the examples shown in this chapter also imply this. In general, they both "tend" to yield favorable performance.

However, in some applications, it is desirable to work with controller designs which yield some guarantees on performance. Thus, the motivation for this research became the development of control synthesis methods for energy-constrained actuation systems which guarantee a certain level of performance, and yield a simple control law. For RFA networks as well as semiactive systems, Damping Reference Controllers accomplish this. It has been shown that these methods can be used in both a stochastic and deterministic setting.

However, as mentioned in the introduction, the work presented here is hardly the "final word" on this subject. Rather it is merely the simplest approach to the design of RFA and semiactive systems with guaranteed quadratic cost. There are a great many avenues which can be explored, toward the development of controllers which guarantee an even tighter bound on quadratic performance, or which generalize the measure of "performance" to a broader class of functionals. In Chapter 9, some specific areas of possible further research are discussed in greater detail.

Appendix A6

A6.1: An Algorithm for Resolving the Clipping Action

We wish to minimize the quantity

$$\|\mathbf{u}+\mathbf{b}\|_{\mathbf{R}}^{2} \tag{A6.1}$$

over all u satisfying the constraints

$$P(\mathbf{u},\mathbf{s}) = \mathbf{u}^{T}\mathbf{u} + \mathbf{u}^{T}\mathbf{s} \le 0 \tag{A6.2}$$

$$|\mathbf{u}| \le \mathbf{u}_{\max} \tag{A6.3}$$

If $\mathbf{u}=-\mathbf{b}$ satisfies constraints (A6.2) and (A6.3), then it is the only solution. In the circumstance that this value of $\mathbf{u}$ does not meet the constraints, the clipping action must be characterized. The algorithm detailed below assumes that $\mathbf{u}=-\mathbf{b}$ violates either Eq. (A6.2) or (A6.3), or both. Equivalently, we wish to solve Eq. (6.38) for feasible $\mathbf{u}$, $\boldsymbol{\lambda}$, and λ_R values.

Vector $\mathbf{u}$ is said to belong to a particular *saturation state*, N_s, depending on which of its forces are maximized at $\pm\mathbf{u}_{\max}$. For each u_i, it has three saturation states; lower saturation (i.e. $u_i = -u_{i\max}$), no saturation (i.e. $-u_{i\max}<u_i<u_{i\max}$) and upper saturation (i.e. $u_i = u_{i\max}$). Thus, if $\mathbf{u}\in\Re^m$ then there are 3^m saturation states N_s.

The proposed algorithm works by systematically considering each saturation state until it finds one which yields a solution. Thus, it consists of a loop which could repeat from 1 to 3^m times, depending on how many N_s states are tried before the correct one is reached. Each time through the loop, the algorithm assumes N_s to be true, and then checks for consequential violations in the necessary conditions. Because it is known that Eq. (6.38) has a unique minimum in the feasible $\mathbf{u}$-space (given that $\mathbf{R}$ is nonsingular), Eqs. (6.36), (6.37) and (6.38) are necessary and sufficient conditions for $\mathbf{u}$ to be the solution. Thus, the algorithm stops as soon as it finds a saturation state in which Eqs. (6.36), (6.37) and (6.38) are harmonious. Because it is known that a solution exists, the algorithm is guaranteed to find the solution (eventually).

More computationally-efficient algorithms exist if $\mathbf{R}$ is diagonal or scalar. First, the general algorithm is presented. Then, simplifications to the algorithm for diagonal and scalar $\mathbf{R}$ are discussed.

1. Case for General R:

The steps below are repeated for different N_s, until a solution is reached.

Step 1: N_s, $\mathbf{b}$, $\mathbf{s}$, $\lambda_R \mapsto \mathbf{u}'$, $\boldsymbol{\lambda}^o$

Let the number of unsaturated forces for N_s be $p \leq m$. Then $\mathbf{u}$ can be expressed as

$$\mathbf{u} = \mathbf{D}_{us}\mathbf{u}' + \mathbf{D}_s\mathbf{u}^o_{\max} \tag{A6.4}$$

where $\mathbf{u}'$ is the vector of unsaturated forces (i.e. forces for which $|\mathbf{u}_i| < \mathbf{u}_{i\max}$) and $\mathbf{u}^o_{\max}$ contains only those maximum force levels corresponding to the saturated forces. For this parameterization, the matrices $\mathbf{D}_{us}$ and $\mathbf{D}_s$ have exactly one nonzero component in each column, and have the characteristic that

$$\mathbf{D}_{us}^T\mathbf{D}_{us} = \mathbf{I} \quad , \quad \mathbf{D}_s^T\mathbf{D}_s = \mathbf{I} \tag{A6.5}$$

For a given scenario, the Lagrange multiplier vector $\boldsymbol{\lambda}$ may be expressed as

$$\boldsymbol{\lambda}' = \mathbf{D}_s\boldsymbol{\lambda}^o \tag{A6.6}$$

where $\boldsymbol{\lambda}^o$ is the vector of absolute-valued Lagrange multipliers for the saturated forces only. Substitution of the above quantities into Eq. (6.38) gives

$$\begin{bmatrix} \lambda_R\mathbf{I} + \mathbf{D}_{us}^T\mathbf{R}\mathbf{D}_{us} & \mathbf{0} \\ \mathbf{D}_s^T\mathbf{R}\mathbf{D}_{us} & \mathbf{I} \end{bmatrix} \begin{bmatrix} \mathbf{u}' \\ \boldsymbol{\lambda}^o \end{bmatrix} = -\begin{bmatrix} \mathbf{D}_{us}^T \\ \mathbf{D}_s^T \end{bmatrix} \left[\mathbf{R}\mathbf{b} + \mathbf{R}\mathbf{D}_s\mathbf{u}^o_{\max}\right] - \lambda_R \begin{bmatrix} \frac{1}{2}\mathbf{D}_{us}^T\mathbf{s} \\ \mathbf{u}^o_{\max} + \frac{1}{2}\mathbf{D}_s^T\mathbf{s} \end{bmatrix} \tag{A6.7}$$

There are two general possibilities for this equation to result in a feasible $\mathbf{u}$ for a given N_s. Either λ_R=0 and $P(\mathbf{u},\mathbf{s}) \leq 0$, or else $\lambda_R \geq 0$ and $P(\mathbf{u},\mathbf{s})$=0. Steps 2 and 3 check these cases, respectively.

Step 2: N_s, $\mathbf{b}$, $\mathbf{s}$, λ_R=0 $\mapsto$ Feasible $\mathbf{u}$?

Assuming λ_R=0, solutions to $\mathbf{u}'$ and $\boldsymbol{\lambda}^o$ can be found directly from Eq. (A6.7) as

$$\begin{bmatrix} \mathbf{u}' \\ \boldsymbol{\lambda}^o \end{bmatrix} = -\begin{bmatrix} \left(\mathbf{D}_{us}^T\mathbf{R}\mathbf{D}_{us}\right)^{-1}\mathbf{D}_{us}^T\mathbf{R} \\ 2\mathbf{D}_s^T\mathbf{R}\left(\mathbf{I} - \mathbf{D}_{us}\left(\mathbf{D}_{us}^T\mathbf{R}\mathbf{D}_{us}\right)^{-1}\mathbf{D}_{us}^T\mathbf{R}\right) \end{bmatrix} \left(\mathbf{b} + \mathbf{D}_s\mathbf{u}^o_{\max}\right) \tag{A6.8}$$

If these solutions result in satisfaction of the constraints then case N_s is the valid case, and the solution has been found. Specifically, the three conditions to check are

$$\mathbf{u}' \text{ feasible} \Leftrightarrow \left|\left(\mathbf{D}_{us}^T\mathbf{R}\mathbf{D}_{us}\right)^{-1}\mathbf{D}_{us}^T\mathbf{R}\left(\mathbf{b} + \mathbf{D}_s\mathbf{u}^o_{\max}\right)\right| \leq \left|\mathbf{D}_{us}^T\mathbf{u}_{\max}\right| \tag{A6.9}$$

$$P(\mathbf{u},\mathbf{s})\text{ feasible} \Leftrightarrow \left(\left(\mathbf{D}_{us}^T\mathbf{R}\mathbf{D}_{us}\right)^{-1}\mathbf{D}_{us}^T\mathbf{R}\left(\mathbf{b}+\mathbf{D}_s\mathbf{u}_{\max}^o\right)+\mathbf{D}_{us}^T\mathbf{s}\right)^T\left(\mathbf{D}_{us}^T\mathbf{R}\mathbf{D}_{us}\right)^{-1}\mathbf{D}_{us}^T\mathbf{R}\left(\mathbf{b}+\mathbf{D}_s\mathbf{u}_{\max}^o\right) + \mathbf{u}_{\max}^{oT}\mathbf{u}_{\max}^o + \mathbf{u}_{\max}^{oT}\mathbf{D}_s^T\mathbf{s} \le 0 \tag{A6.10}$$

$$\boldsymbol{\lambda}^o \text{ feasible} \Leftrightarrow \left\{-2\mathbf{D}_s^T\mathbf{R}\left(\mathbf{I}-\mathbf{D}_{us}\left(\mathbf{D}_{us}^T\mathbf{R}\mathbf{D}_{us}\right)^{-1}\mathbf{D}_{us}^T\mathbf{R}\right)\left(\mathbf{b}+\mathbf{D}_s\mathbf{u}_{\max}^o\right)\right\}_i \ge 0\,, i\in\{1..m-p\} \tag{A6.11}$$

Otherwise, saturation state N_s, with λ_R=0, cannot yield the solution.

Step 3: N_s, **b**, **s**, P(**u**,**s**)=0 $\mapsto$ Feasible **u**?

Now, we replace the assumption that λ_R=0 with the assumption that **u**′ is feasible, i.e.,

$$\left(\mathbf{u}_{\max}^{oT}\mathbf{u}_{\max}^o + \mathbf{u}_{\max}^{oT}\mathbf{D}_s^T\mathbf{s}\right)+\left(\mathbf{s}^T\mathbf{D}_{us}\right)\mathbf{u}' + \mathbf{u}'^T\mathbf{u}' = 0 \tag{A6.12}$$

Let **T** be the diagonalizing similarity transformation such that

$$\mathbf{T}^T\mathbf{D}_{us}^T\mathbf{R}\mathbf{D}_{us}\mathbf{T} = \mathbf{R}_\Delta = \begin{bmatrix}\mathbf{R}_{\Delta 11} & & \\ & \ddots & \\ & & \mathbf{R}_{\Delta pp}\end{bmatrix} \tag{A6.13}$$

Then Eq. (A6.7) can be expressed as

$$\begin{aligned}\mathbf{u}' &= -\mathbf{T}\mathbf{B}(\lambda_R)\mathbf{T}^T\left(\mathbf{D}_{us}^T\mathbf{R}\mathbf{D}_{us}\right)^{-1}\mathbf{D}_{us}^T\mathbf{R}\left[\mathbf{b}+\mathbf{D}_s\mathbf{u}_{\max}^o\right]-\tfrac{1}{2}\mathbf{T}\left[\mathbf{I}-\mathbf{B}(\lambda_R)\right]\mathbf{T}^T\mathbf{D}_{us}^T\mathbf{s}\\ \boldsymbol{\lambda}^o &= -2\mathbf{D}_s^T\left[\mathbf{R}\mathbf{b}+\mathbf{R}\mathbf{D}_s\mathbf{u}_{\max}^o\right]-2\lambda_R\left[\mathbf{u}_{\max}^o+\tfrac{1}{2}\mathbf{D}_s^T\mathbf{s}\right]-2\mathbf{D}_s^T\mathbf{R}\mathbf{D}_{us}\mathbf{u}'\end{aligned} \tag{A6.14}$$

where

$$\mathbf{B}(\lambda_R) = diag\left\{\beta_1(\lambda_R),\ldots,\beta_p(\lambda_R)\right\} \tag{A6.15}$$

and

$$\beta_i(\lambda_R) = \frac{R_{\Delta ii}}{R_{\Delta ii}+\lambda_R} \tag{A6.16}$$

Note that $\beta_i \in [0,1]$. Define

$$\boldsymbol{\varphi}(\mathbf{s},\mathbf{b},N_s) = \mathbf{T}^T\left(\left(\mathbf{D}_{us}^T\mathbf{R}\mathbf{D}_{us}\right)^{-1}\mathbf{D}_{us}^T\mathbf{R}\left(\mathbf{b}+\mathbf{D}_s\mathbf{u}_{\max}^o\right)-\tfrac{1}{2}\mathbf{D}_{us}^T\mathbf{s}\right) \tag{A6.17}$$

and

$$\theta(\mathbf{s},N_s) = \mathbf{u}_{\max}^{oT}\mathbf{u}_{\max}^o + \mathbf{u}_{\max}^{oT}\mathbf{D}_s^T\mathbf{s} - \tfrac{1}{4}\mathbf{s}^T\mathbf{D}_{us}\mathbf{D}_{us}^T\mathbf{s} \tag{A6.18}$$

and Eq. (A6.12) can be expressed as

$$\boldsymbol{\varphi}^T \mathbf{B}^2(\lambda_R)\boldsymbol{\varphi} + \theta = 0 \tag{A6.19}$$

which is equivalent to the polynomial expression

$$\sum_{i=1}^{p}\left\{\varphi_i^2 R_{\Delta ii}^2 \prod_{j=1\neq i}^{p}\left(R_{\Delta ii}+\lambda_R\right)^2\right\} + \theta\prod_{j=1}^{p}\left(R_{\Delta ii}+\lambda_R\right)^2 = 0 \tag{A6.20}$$

The above root equation must be solved to get λ_R. Note that only positive solutions are valid, so if there is no positive root, the case N_s cannot be valid. By inspection of Eq. (A6.16), we see that for λ_R positive, each element in **B** decreases uniformly with λ_R. Thus, there can be at most one positive root. Furthermore, it follows that exactly one positive root exists if and only if $-\boldsymbol{\varphi}^T\boldsymbol{\varphi}<\theta$. If the positive root exists, then λ_R can be found uniquely, and $\boldsymbol{\lambda}^o$ can in turn be found from Eq. (A6.7).

If the resultant λ_R root, when inserted in Eq. (A6.7), results in **u** feasible, then the solution has been found. The items to check are

$$\lambda_R \text{ feasible} \Leftrightarrow -\boldsymbol{\varphi}^T\boldsymbol{\varphi} \le \theta < 0 \tag{A6.21}$$

$$\mathbf{u}' \text{ feasible} \Leftrightarrow \left|\left(\mathbf{D}_{us}^T\mathbf{R}\mathbf{D}_{us}+\lambda_R\mathbf{I}\right)^{-1}\mathbf{D}_{us}^T\left(\mathbf{R}\left(\mathbf{b}+\mathbf{D}_s\mathbf{u}_{\max}^o\right)+\lambda_R\,\tfrac{1}{2}\mathbf{s}\right)\right| \le \left|\mathbf{D}_{us}^T\mathbf{u}_{\max}\right| \tag{A6.22}$$

$$\boldsymbol{\lambda}^o \text{ feasible} \Leftrightarrow \left\{-2\mathbf{D}_s^T\mathbf{R}\left(\mathbf{b}+\mathbf{D}_s\mathbf{u}_{\max}^o\right)-2\lambda_R\left(\mathbf{u}_{\max}^o+\tfrac{1}{2}\mathbf{D}_{us}^T\mathbf{s}\right)-2\mathbf{D}_s^T\mathbf{R}\mathbf{D}_{us}\mathbf{u}'\right\}_i \ge 0\,, i\in\{1..m-p\} \tag{A6.23}$$

where λ_R and $\mathbf{u}'$ are found through Eqs. (A6.20) and (A6.14) respectively. If any one of these conditions is violated, then $P(\mathbf{u},\mathbf{s})=0$ cannot be the case for saturation state N_s.

Step 4: Is N_s the correct saturation state?

If Steps 2 and 3 did not yield feasible **u**, then N_s cannot be the correct saturation state. In this circumstance, the algorithm is repeated for the next N_s. If either Steps 2 or 3 yield a solution, then this is the *only* solution, and the algorithm can be aborted, without trying the remaining N_s.

2. Simplifications for Diagonal R:

For **R** diagonal, the above can be simplified somewhat. Equation (A6.7) becomes

$$\begin{aligned}\mathbf{u}' &= -\mathbf{B}(\lambda_R)\mathbf{D}_{us}^T\mathbf{b} - \tfrac{1}{2}\left[\mathbf{I}-\mathbf{B}(\lambda_R)\right]\mathbf{D}_{us}^T\mathbf{s}\\ \boldsymbol{\lambda}^o &= -2\left[\mathbf{D}_s^T\mathbf{R}\mathbf{b}+\mathbf{D}_s^T\mathbf{R}\mathbf{D}_s\mathbf{u}_{\max}^o\right]-2\lambda_R\left[\mathbf{u}_{\max}^o+\tfrac{1}{2}\mathbf{D}_s^T\mathbf{s}\right]\end{aligned} \tag{A6.24}$$

Note that in the case of $\lambda_R = 0$, these equations become

$$\begin{aligned} \mathbf{u}' &= -\mathbf{D}_{us}^T \mathbf{b} \\ \boldsymbol{\lambda}^o &= -2\left[\mathbf{D}_s^T \mathbf{R}\mathbf{b} + \mathbf{D}_s^T \mathbf{R}\mathbf{D}_s \mathbf{u}_{\max}^o\right] \end{aligned} \tag{A6.25}$$

implying that for $\lambda_R = 0$, force saturation occurs element-by-element, as

$$\lambda_R = 0 \quad \Rightarrow \quad \mathbf{u} = \underset{\mathbf{u}_{\max}}{\operatorname{sat}}\{-\mathbf{b}\} \tag{A6.26}$$

So the case with λ_R=0 (i.e. Step 2) can be checked only once at the outset of the algorithm, because the saturation state N_s implied by λ_R=0 can be inferred directly from Eq. (A6.26).

Also note that for diagonal **R**, $\boldsymbol{\varphi}$ in Step 3 is simplified to

$$\boldsymbol{\varphi}(\mathbf{s}, \mathbf{b}, N_s) = \mathbf{D}_{us}^T \left(\mathbf{b} - \tfrac{1}{2}\mathbf{s}\right) \tag{A6.27}$$

However, the roots of the 2p-order polynomial in Eq. (A6.20) must still be solved in order to get the solution for λ_R.

3. Simplifications for R = rI:

In this circumstance, in addition to the simplifications in Step 2 for diagonal **R**, things simplify considerably for Step 3, because the β_i factors all become equal, for any λ_R. Thus, $\mathbf{B}(\lambda_R) = \beta(\lambda_R)\mathbf{I}$, and the polynomial in Eq. (A6.20) simplifies to the simple quadratic

$$\left(\boldsymbol{\varphi}^T \boldsymbol{\varphi} + \theta\right) + 2\theta \frac{\lambda_R}{r} + \theta\left(\frac{\lambda_R}{r}\right)^2 = 0 \tag{A6.28}$$

and the solution may be found readily in closed-form as

$$\lambda_R = r\left(-1 + \sqrt{-\frac{\boldsymbol{\varphi}^T \boldsymbol{\varphi}}{\theta}}\right) \tag{A6.29}$$

Also note that, if $\alpha = 1-\beta$, then $\mathbf{u}'$ may be expressed as

$$\mathbf{u}' = -(1-\alpha)\mathbf{D}_{us}^T \mathbf{b} - \alpha \tfrac{1}{2} \mathbf{D}_{us}^T \mathbf{s} \tag{A6.30}$$

Resultantly, **u** can be expressed for arbitrary α as

$$\mathbf{u} = -\underset{\mathbf{u}_{\max}}{\operatorname{sat}}\left\{(1-\alpha)\mathbf{b} + \alpha \tfrac{1}{2}\mathbf{s}\right\} \tag{A6.31}$$

Thus, the solution to **u** is such that the term in the brackets of Eq. (A6.31) lies on a line between **b** and ½**s**.